Kasper Hancke

Photosynthetic responses as a function of light and temperature: Field and laboratory studies on marine microalgae

Thesis for the degree philosophiae doctor

Trondheim, May 2007

Norwegian University of Science and Technology
Faculty of Natural Sciences and Technology
Department of Biology
Trondhjem Biological Station

NTNU

UNIS

NTNU
Norwegian University of Science and Technology

Thesis for the degree philosophiae doctor

Faculty of Natural Sciences and Technology
Department of Biology

Evaluating committee:

First opponent:	Assoc. Prof. Mark Moline California Polytechnic State University San Luis Obispo, CA USA
Second opponent:	Prof. Stiig Markager National Environmental Research Institute Roskilde, Denmark
Committee administrator:	Prof. Jarle Mork Norwegian University of Science and Technology Trondheim, Norway

ISBN 978-82-471-2436-9 (printed version)
ISBN 978-82-471-2453-6 (electronic version)
ISSN 1503-8181

Doctoral theses at NTNU, 2007:111

Printed by NTNU-trykk

Preface and acknowledgements

My thesis is focused on light attenuation in the water column, light absorption by phytoplankton and photosynthesis in microalgae, as a function of temperature. It has been a great challenge and a valuable experience trying to grasp such a wide subject and put it into text with a clear structure. I have learnt a lot along the way and owe a thank you to a lot of skilled colleagues and kind friends.

I will like to sincerely thank my two supervisors Prof. Geir Johnsen and Prof. Egil Sakshaug for the opportunity to fulfil my PhD work at Trondhjem Biological Station (TBS) and for skilful guiding through the stormy waters of science. Geir deserves a dedicated thank you for his endless enthusiasm, countless ideas and significant inputs to my work and wonders. Egil, is especially thanked for his scientific questioning, and lectures on miscellaneous topics. It has been a pleasure (most of the time).

My PhD has been a part of the project 'Carbon flux and ecosystem feedback in the northern Barents Sea in an era of climate change' (CABANERA), headed by Prof. Paul Wassmann at the Norwegian College of Fishery Science, University of Tromsø. I will like to address a sincere gratitude to Paul and everybody involved in CABANERA for three educational cruises to the Barents Sea and for fruitful collaborations. My fellow PhD candidates involved in CABANERA deserves a special appreciation for the many discussions, workshop sessions and social activities that have served as an important source of inspiration and motivation during the project period.

Thanks are due to my co-authors for their interest in the work and for the rewarding collaboration. Especially, I will like to express my gratitude to Prof. Ronnie Glud at the Marine Biological Laboratory (University of Copenhagen, Denmark) for his long-distance supervision and considerable contribution to my achievements. At TBS especially Nils Tokle, Johanna Järnegren, Lasse Olsen, Jussi Evertsen, Mathilde Chauton and Sten Karlsson are thanked for numerous educational discussions on a range of subjects including scientific matters and the challenge of working within a

scientific environment. Nils Tokle, additionally, deserves dedicated thanks for introducing me to the secrets of after-dark cross-country skiing and for being a devoted skiing companion through countless trips, on all kinds of skis. Kjersti Andresen is thanked for HPLC analyses. Colleagues, staff and students at TBS are acknowledged for creating a pleasurable working environment at TBS.

At last I want to thank my family and friends for understanding and support, in particular my father for many fruitful discussions of the scientific process and comprehension.

Outstanding all others I want to thank my dear and wonderful wife, colleague and co-author Torunn B. Hancke. It has been a fantastic inspiring and great experience to work with you on both experimental work and through the writing of our two joint papers. More importantly, I want to thank you deeply for the patience and support you have offered during the entire, and especially final stages, of my PhD writing. Thea Emilie, my daughter of 19 month, you are simply wonderful and inspire me daily, never missing a change to amuse and cheer me up in a moody moment.

Funding for this study was provided by the Norwegian Research Council through CABANERA to the Norwegian University of Science and Technology (NTNU) and The University Centre in Svalbard (UNIS). The support is greatly acknowledged.

It is my hope that I through this thesis can contribute to our understanding of aquatic photosynthesis and to the comprehension of the important processes of primary production and its relevance in the Barents Sea. In light of the increased human activity in the Arctic region, an understanding of the ecosystem is becoming increasingly important.

Trondheim, March 2007 *Kasper Hancke*

List of papers

This thesis is based on the following papers, referred to by their respective numbers:

1. **Hancke K**, Johnsen G, Sakshaug E (submitted) Spectral light attenuation in the Barents Sea: Impact of pigment signature and relevance for optical depth and primary production. *Deep-Sea Research Part II*

2. Hancke TB, **Hancke K**, Johnsen G, Sakshaug E (submitted) Rate of O_2 production derived from PAM fluorescence: Testing three bio-optical approaches against measured O_2 production rate. *Journal of Phycology*

3. **Hancke K**, Hancke TB, Olsen LM, Johnsen G, Glud RN (submitted) Temperature effects on microalgae photosynthesis-light responses measured by O_2-production, Pulse Amplitude Modulated (PAM) fluorescence and ^{14}C-assimilation. *Journal of Phycology*

4. **Hancke K**, Glud RN (2004) Temperature effects on respiration and photosynthesis in three diatom-dominated benthic communities. *Aquatic Microbial Ecology 37:265-281*

Table of contents

1. Introduction

Photosynthesis has been of scientific interest since the mid eighteenth century (J. Priestly). Since then several Nobel Prizes have been given in photosynthesis-related research, from H. Fischer in 1930 (porphyrins and leaf pigments), M. Calvin (and his student A. Benson, CO_2-assimilation in photosynthesis) in 1961, and R. Marcus for his contribution to the theory of electron transfer reactions in photosynthesis in 1992.

Photosynthesis supports the bulk of life on Earth and thereby underpins the biomass and biodiversity of the planet. Approximately 45 % of the photosynthesis each year occurs in aquatic environments (Falkowski 1994, Field et al. 1998). The Arctic region contributes considerably to the global primary production. The annual production of the Barents Sea is estimated to ~90 g C m^{-2} (Sakshaug 2004). In comparison the average for the world oceans is ~140 g C m^{-2} y^{-1} (Field et al. 1998). Irradiance and temperature are important variables controlling the rates of photosynthesis. This also pertains for respiration, which can be considered the opposite process. In temperate and arctic seas (including coastal shallow waters) both variables show marked seasonal and diurnal variation (Papers 1 & 4, Cahoon 1999, Glud et al. 2002, Sakshaug 2004).

Primary production is typically measured as O_2-evolution or ^{14}C-assimilation, but can also be estimated using variable fluorescence as a proxy (Marra 2002). The techniques, however, measure different physiological processes with potentially different response to environmental variables such as light and temperature (Paper 3, Geider & Osborne 1992, Morris & Kromkamp 2003). Accurate estimation of the marine primary production is important on both local and global scale because primary production is a 'cornerstone' in marine food webs and in the ecosystem carbon budget. Primary production will inevitably be affected by climate change which is likely to alter sea temperature and irradiance (cloudiness and ice cover). Possible changes are suspected to be amplified in the Arctic (Sakshaug 2004, Holland et al. 2006).

My thesis focuses on the flux of photons, i.e. irradiance[1] originating from the Sun, as it 'travels' down the water column, being absorbed by microalgae fuelling photosynthesis (Fig. 1.1). Each of the sections in this thesis presents an introduction to the subject in question, followed by a brief presentation of the relevant underlying theory, concluding with a review of my most important findings. The theory part is meant to review the underlying theories on which the papers are based, and to provide assistance in interpreting the results.

[1] Irradiance (denoted E, μmol photons m^{-2} s^{-1}) is the flux of radiant energy on a (small) surface, divided by the area of the surface, per time unit.

2. Scope of my thesis

The aim of my thesis is to elucidate the different pathways of light in the marine environment, from underwater irradiance to the absorption of photons in microalgae[2]. The pathway is followed through light harvesting and the subsequent electron transfer, to the fuelling of the photosynthetic process (Fig. 1.1, Papers 1, 2 & 3). In addition, the effect of temperature on photosynthesis and respiration in pelagic and benthic microalgae has been investigated (Papers 3 & 4). A novel approach to estimate the light absorption in Photosystem II (PSII) is evaluated in combination with Pulse Amplitude Modulated (PAM) fluorescence measurements, to calculate the rate of photosynthetic oxygen production (Paper 2). The approach was evaluated against measured rates of oxygen production and ^{14}C-assimilation, as a function of temperature (Papers 2 & 3).

Paper 1 is an *in situ* study of water column processes in the Marginal Ice zone (MIZ) of the Barents Sea, Paper 2 & 3 are laboratory studies on culture-grown phytoplankton species, and Paper 4 is a comparison study of intact temperate and arctic diatom-dominated benthic communities from shallow-water sites.

The aims of the papers were:

1) to analyse the significance of spectral composition of irradiance in relation to the concentration and vertical distribution of chl *a*, dissolved oxygen and phytoplankton productivity in the water column. *Spectral attenuation is related to optical depth and discussed in a photo-physiological context, including the concentration and composition of phytoplankton pigments and productivity*

2) to determine the absolute rates of photosynthetic O_2 production from variable fluorescence (PAM) measurements by testing three bio-optical approaches to

[2] Throughout the thesis, the term 'microalgae' is used referring to both pelagic and benthic microalgae. 'Phytoplankton' or 'microphytobenthos' are used referring to pelagic or benthic microalgae, specifically.

estimate the light absorption in PSII, against measured O_2 production rates. *A spectral-related approach using PSII-specific light absorption is recommended.*

3) to investigate the relationship between temperature and photosynthetic parameters derived from measurements of 1) O_2-production by O_2-microsensors, 2) calculated rates of O_2-production based on variable fluorescence combined with bio-optical determined PSII absorption, and 3) measured rates of ^{14}C-assimilation. *The temperature influence on photosynthetic parameters is discussed in a physiological context.*

4) to evaluate possible differences in the temperature adaptation strategy between arctic and temperate benthic microalgae-dominated communities, during short-term temperature incubation studies. *The study includes rate measurements of the sediment community respiration, gross photosynthesis and net photosynthesis as determined from O_2 microsensor measurements in intact sediments.*

3. Light regime in water columns and sediments

Sunlight is essential to primary producers being the energy source driving photosynthesis (Falkowski & Raven 1997). Light available for photosynthesis is referred to as photosynthetically active radiation (PAR) and includes radiation at wavelengths from 400 to 700 nm (Kirk 1994). The underwater light regime ultimately determines the vertical distribution, abundance and photosynthetic activity of phototrophic microalgae in the water column (phytoplankton) and in the benthic sediments (microphytobenthos) beneath. The Arctic light regime offers extreme seasonal variation, from midnight sun to winter darkness. Moreover, phytoplankton in the water column are subject to a strong vertical light gradient, which is amplified in the MIZ by the sea ice cover. The focus on light regime in the present thesis begins immediately beneath the sea surface. The variables that affect the light regime above the sea surface will, thus, not be treated further than mentioning that day length, zenith sun angle, cloud cover, albedo (i.e. the reflection of light) and ice cover in the Arctic and Antarctic, are major key variables (Sakshaug et al. 1989, Sakshaug & Slagstad 1992, Kirk 1994).

3.1. Downwelling irradiance and attenuation

Downwelling irradiance[3], E_d (in this work termed E, since only downwelling irradiance is considered), in a water column diminishes in an approximately exponential manner with depth (Kirk 1994). This can be described as

$$E_z = E_0 e^{-K_d z} \qquad (3.1)$$

where E_z and E_0 are the values of downwelling irradiance at depth z m and just below the surface, respectively, and K_d (m^{-1}) is the vertical diffuse attenuation coefficient for downwelling irradiance.

[3] Downwelling irradiance (E_d) is defined as the flux of photons received by a flat collector with a cosine response, facing upwards (Kirk 1994).

The attenuation of light in water is wavelength specific, having the highest attenuation in the long-waved red spectrum, subsequently decreasing with wavelength. Pure seawater is transparent mainly to blue light (clearest at 475 nm), followed by green light, and is nearly opaque to red light and UVB (Paper 1, Kirk 1994). With focus on K_d, the spectral attenuation for downwelling irradiance can be rewritten from equation 3.1 as

$$K_{d(\lambda)} = \frac{-\ln\left(E_{0(\lambda)} / E_{z(\lambda)}\right)}{z} \qquad (3.2)$$

where $E_{0(\lambda)}$, $E_{z(\lambda)}$ and $K_{d(\lambda)}$ have a spectral distribution. Light is attenuated in the water column as a consequence of both absorption and scattering. The attenuation coefficient $K_{d(\lambda)}$ is thus related to the absorption and scattering by water molecules, chromophoric dissolved organic matter (cDOM), particulate organic and inorganic material, and the living plankton themselves (Sathyendranath et al. 2000). In clear oceanic water masses, $K_{d(\lambda)}$ is mainly influenced by the absorption and scattering of phytoplankton, by the sea water itself, and in some cases by marine cDOM (Case I waters), while terrigenous cDOM and suspended matter additionally influence the optical properties in coastal water masses and fjords (Case II waters, Jerlov 1976, Sathyendranath et al. 2000).

In the strictest sense, $K_{d(\lambda)}$ (as an apparent[4] optical property) is dependent on the angular distribution of the light field and lacks the additive quality of inherent[3] optical properties. Nonetheless, $K_{d(\lambda)}$ is often considered to be a 'quasi-inherent' optical property and treated as such, and is therefore commonly considered independent of the solar zenith angle (Smith & Baker 1978, Kirk 1994, Sosik in press), which is the case in this work (Paper 1).

In oceanic waters, typical K_d values for PAR, $K_{d(PAR)}$, are in the range of 0.03 to 0.10 m^{-1} measured during low chl *a* concentrations (<0.1 mg m^{-3}), e.g. in the Sargasso Sea

[4] The optical properties that govern the underwater irradiance regime are divided into so-called 'inherent' and 'apparent' properties. The former is independent of the solar zenith angle and includes properties of absorption and attenuation. The latter is dependent on solar angle, and includes backscatter and reflectance (Mobley 1994, Light and Water).

column, a given optical depth will correspond to a much shallower physical depth than in a chl *a*-poor water column.

Profiles of chl *a*, dissolved oxygen and primary production showed large natural variations in the Barents Sea. Yet the variables showed a trend of aligning by forming profiles with comparable curvatures when plotted as a function of optical depth for PAR, $\xi_{(PAR)}$, instead of physical depth. If plotted as a function of the attenuation at 490 nm, $\xi_{(490)}$ (blue light), uniformity in the curvature became increasingly clear (Paper 1, Behrenfeld & Falkowski 1997). *Conclusion, optical depth proved to be valuable in the attempt to describe the dynamics of chl a, dissolved oxygen and primary production in the water column of the MIZ in the Barents Sea (Paper 1).*

3.3. Spectral irradiance *versus* PAR: the relationship to primary production

Paper 1 shows that the accumulated[5] chl *a* concentration in the water column during bloom conditions in the Barents Sea is correlated with the optical depth, $\xi_{(PAR)}$. Furthermore, I found that when the optical depth was calculated from a single wavelength at 490 nm, the coefficient of determination (r^2) increased from 0.41 to 0.50 (entire data set, Fig 3.2). Focusing on only the chl *a*-rich peak-bloom stations with [chl *a*] >9 mg m^{-3}, the correlation between accumulated chl *a* and optical depth was close to 100 % (r^2 = 0.99, insert in Fig 3.2). *This shows that chl a, representing the phytoplankton biomass, correlates to the total light absorption down to an optical depth of ~9, corresponding to ~0.01 % of the surface irradiance at 490 nm (Paper 1).* These results are consistent with findings in the North Water Polynya, where chl *a* and particulate organic carbon (POC) were the components that most influenced $K_{d(\lambda)}$, accounting for 36 to 83 % of the variance in light attenuation (Vasseur et al. 2003).

[5] The accumulated chl *a* concentration (mg m^{-2}) was calculated from accumulating (summarising) trapezoidal integrated volumetric values for each measuring interval from the surface and down through the water column.

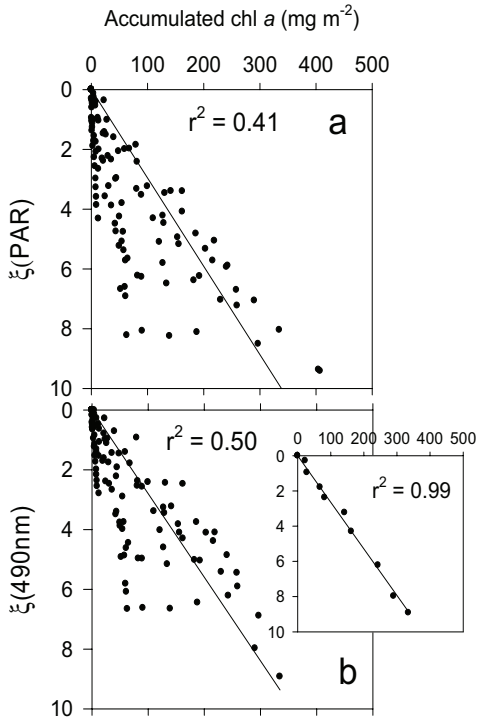

Fig. 3.2. Optical depth as a function of the accumulated chl *a* concentration down through the water column, calculated for a) PAR, $\xi_{(PAR)}$, and b) 490 nm, $\xi_{(490)}$, for 12 stations visited during summer months 2003-5 in the Barents Sea. The insert in b) shows data collected exclusively during chl *a*-rich, >9 mg m^{-3}, peak-bloom conditions (stations XIV and XVI). Lines are linear regressions and the coefficient of determination (r^2) is given.

It is important to note that chl *a* is a biomass estimate and is therefore not directly correlated to rates of production. Hence, I analysed the relationship between downwelling irradiance and the chl *a*-normalised primary production rates. The results showed that the primary production was strongly related to optical depth, and hence the water column light regime. *I concluded that the chl a-normalised primary production was closer related to the irradiance at 490 nm (blue light) than to PAR (Paper 1).* The conclusion was supported when all data of chl *a*-normalised production rates were plotted as a function of downwelling irradiance for PAR, $E_{z(PAR)}$, and at 490 nm, $E_{z(490)}$, respectively (Fig. 3.3). The compiled data showed that 66 % (r^2 = 0.66) of the variance

in the normalised production could be explained by PAR (Fig 3.3a), while 81 % (r^2 = 0.81) could be explained from the downwelling irradiance at 490 nm (Fig 3.3b). A strong correlation between the irradiance at 490 nm and primary production is consistent with the average absorption spectrum for the identified dominating phytoplankton groups (Paper 1, Johnsen & Sakshaug in press) and illustrate that the phytoplankton community of the MIZ respond spectrally equivalent to temperate and tropical phytoplankton ecosystems (Bouman et al. 2000, Bricaud et al. 2004). *In conclusion, by fitting chl a-normalised production rates to downwelling irradiance at 490 nm, instead of PAR, improved the correlation ~15 % (Paper 1). It follows, as mentioned in 3.1, that shading of the water column by phytoplankton is considerably more pronounced in blue light than for PAR. This is of relevance for modelling the 1 % irradiance depth and critical depth (see Paper 1 for details).*

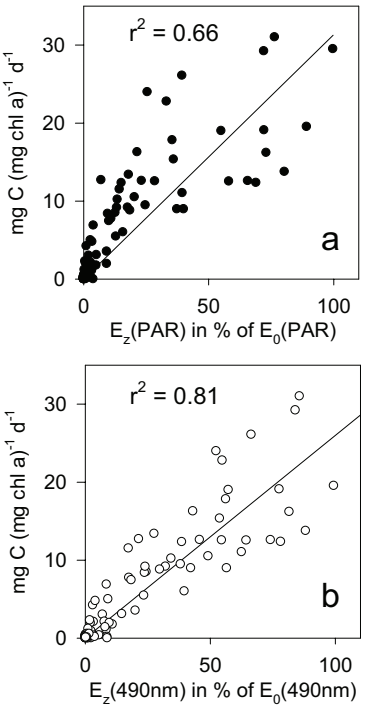

Fig. 3.3. Chl *a*-normalised primary production rates plotted as a function of available irradiance as a) PAR and b) at 490 nm in per cent of the immediate sub-surface irradiance. Data are compiled from 12 stations visited during summer months 2003-5 in the Barents Sea. Lines are linear regressions and the coefficient of determination (r^2) is given. Regression lines are forced through origo.

4. Light absorption in microalgae and Photosystem II (PSII)

This section includes a presentation of the absorption properties of microalgae and their light-harvesting and photo-protective pigments. The presentation includes the absorption properties of PSII and an evaluation of three bio-optical approaches to quantify the PSII-specific light absorption in microalgae.

4.1 Light absorption in microalgae

The rate of light absorption sets an upper limit for algal productivity, i.e. photosynthetic activity. The photosynthetic unit is composed of PSII, PSI and their respective light-harvesting complexes (LHC II and I, Green et al. 2003). The different pigments in LHC II and I, both chlorophylls and carotenoids (see section 4.2), have different absorption properties, and the bulk properties reflects a composite spectrum of the summed contributions from all absorbing molecules presented, i.e. $a^*_\varphi(\lambda)$. The absorption properties of single-isolated pigments is generally well described and understood and can be used to identify and model microalgae absorption under both laboratory and field conditions (Johnsen et al. 1994a, Jeffrey et al. 1997a, Jeffrey et al. 1997b).

As mentioned earlier, light absorption in a water column is characterised as an inherent optical property, and as such holds properties of being additive. This means that, for a water sample containing a mixture of constituents, the absorption and scattering coefficients of the various constituents are independent. Thus, the total coefficient can be determined by summation. The total absorption, $a_t(\lambda)$ can then be calculated from the summarised absorption by sea water, $a_w(\lambda)$, phytoplankton $a_\varphi(\lambda)$, cDOM, $a_{cDOM}(\lambda)$, and non-algal particles, $a_{nap}(\lambda)$ (Prieur & Sathyendranath 1981). The non-algal particles essentially include virus, heterotrophic bacteria and other heterotrophs, as well as debris from these organisms. In the open ocean, far from terrestrial influence, phytoplankton are generally the principle agents responsible for the optical properties of a water column (Morel & Prieur 1977, Morel 2006).

In the present study I measured absorption in laboratory-grown monocultures of phytoplankton to obtain the *in vivo* chl *a*-specific absorption coefficient, $a^*_\varphi(\lambda)$ (m^2 (mg chl $a)^{-1}$). The i*n vivo* absorption coefficient yields information about total absorption of photosynthetic and photo-protective pigments and reflects the photo-acclimation status of the algae (Paper 2 & 3, Johnsen & Sakshaug 1993).

4.2. Light harvesting and photo-protective pigments

The three main pigment classes that determine the bio-optical properties of algae are the chlorophylls (chl's), the carotenoids and the phycobiliproteins (Johnsen et al. 1994b, Jeffrey et al. 1997b). The two major functions of microalgae pigments are light harvesting and photo-protection (Scheer 2003).

The chl's and phycobiliproteins are involved mainly in light harvesting. The carotenoids play an import role both in light harvesting and in photo protection for degrading potentially damaging excess excitation energy to (mostly) harmless heat (Scheer 2003). The major light-harvesting carotenoids are fucoxanthin and the 19'-acyloxy-fucoxanthins, along with peridinin (specific for some dinophytes) and prasinoxanthin (specific for some Prasinophytes) (Sathyendranath et al. 1987, e.g. Johnsen et al. 1994b, Jeffrey et al. 1997b).

The major *in vivo* absorption signature caused by the chlorophylls (chl *a*, *b* and *c*) is in the blue (400 – 500 nm) and in the red (580 – 700 nm) regions of the PAR spectra. The major light-harvesting carotenoids absorb *in vivo* mainly at 450 – 550 nm (Johnsen & Sakshaug in press, and references herein). Figure 4.1 illustrates the absorption of individual pigments and the effect of the photoprotective carotenoid diadinoxanthin in high and low light adapted cells of *Prorocentrum minimum*. The general absorption maxima for light-harvesting and photo-protective carotenoids at 490 nm motivated the choice of 490 nm when relating primary production to a single wavelength (section 3.3, Paper 1, see also Fig. 4.2 and Paper 2) (Johnsen et al. 1994a, Johnsen et al. 1994b).

The composition and ratio of pigments and carotenoids can be used as chemotaxonomic markers for microalgae identification, and to elucidate the photo-acclimation status of algal cells (Johnsen et al. 1994b, Jeffrey et al. 1997b). This can be studied with HPLC (High Performance Liquid Chromatography) techniques, and important pigment-group markers can be used to differentiate between major phytoplankton groups since chlorophyll c_3 and 19′-acyl-oxy-fucoxanthins are major pigment markers for Haptophytes, chl *b* and prasinoxanthin for prasinoxanthin-containing Prasinophytes, while a high fucoxanthin to chl *a* ratio (w:w) indicates the presence of diatoms (Paper 1, Jeffrey et al. 1997a). As mentioned above, the different chl's and carotenoids have absorption maxima at different wavelengths and thus K_d (in Case I waters with low cDOM) will reflect the concentration and composition of phytoplankton pigment groups (Bricaud et al. 1988, Bricaud et al. 1998).

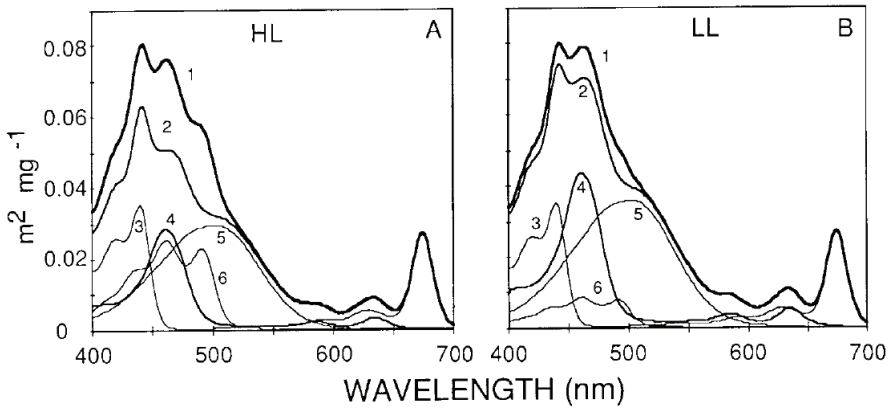

Fig. 4.1. Fractional unpacked absorption (obtained from a pigment model) of individual pigments and the effect of the photoprotective carotenoid diadinoxanthin in (A) high light- and (B) low light-adapted cells of *Prorocentrum minimum*. 1: total pigments; 2: photosynthetic pigments (total pigments minus diadinoxanthin); 3: chl *a*; 4: chl *c*2; 5: peridinin; 6: diadinoxanthin (From Johnsen et al 1994a, MEPS 114:245-258, with permission).

4.3. Absorption in Photosystem II

During photosynthesis ~20 % of the absorbed light is utilised in the photochemical process, while ~75 - 77 % is lost as heat (thermal decay), and 3 - 5 % is emitted as chl *a* fluorescence of which about 95 % arises from PSII (Owens 1991, Kirk 1994).

Fluorescence emission intensity (at a fixed wavelength) is dependent on the wavelength of the excitation light. By measuring fluorescence emission at 730 nm against a wavelength-specific excitation light, a fluorescence excitation spectrum[6] can be obtained (Blankenship 2002). The shape of the fluorescence excitation spectrum resembles that of the corresponding action spectrum for oxygen, as well as arises from PSII, and thus represents the fraction of light received by PSII (Haxo 1985, Neori et al. 1988). The distribution of light absorption between PSII and PSI is pigment-group specific; this is also the case for the fluorescence excitation spectrum caused by the cell composition of chl's and carotenoids (Johnsen & Sakshaug in press).

From a theoretical viewpoint, Johnsen et al. (1997) suggested that the PSII-specific light absorption for photosynthesis can be calculated by scaling the *in vivo* fluorescence excitation spectrum to the *in vivo* absorption spectrum, $a^*_\varphi(\lambda)$, by the 'no-overshoot' procedure (Fig 4.2, Paper 2). By matching the fluorescence spectra to $a^*_\varphi(\lambda)$ between 540 and 650 nm, assuming a 100 % energy conversion efficiency, the obtained spectrum equals the PSII absorption spectrum, $F^*_{PSII}(\lambda)$ (Johnsen et al. 1997). In contrast to $a^*_\varphi(\lambda)$, the $F^*_{PSII}(\lambda)$ does not include the signatures from photo-protective carotenoids and PSI (Johnsen & Sakshaug 1993, in press).

[6] A plot of the intensity of fluorescence emission at a fixed wavelength versus the wavelength of excitation is called a fluorescence excitation spectrum (Haxo 1985).

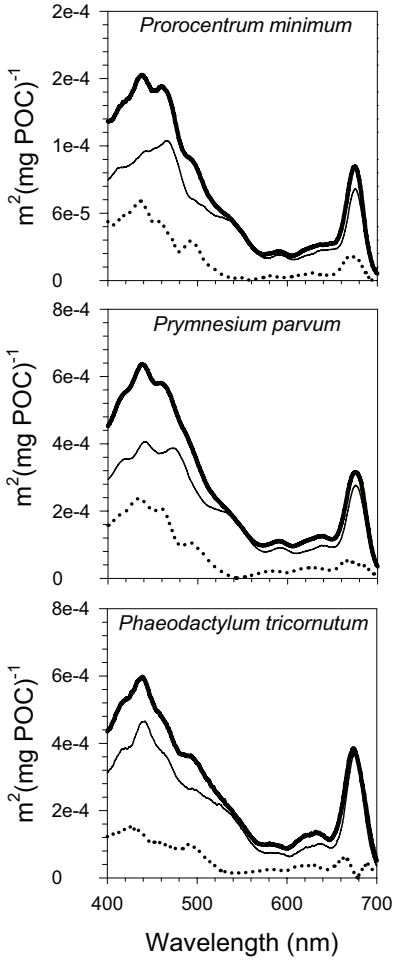

Fig. 4.2. *In vivo* absorption (thick line) and PSII-scaled fluorescence excitation (thin line) spectra for the dinoflagellate *P. minimum* (upper panel), the haptophyte *P. parvum* (middle panel) and the diatom *P. tricornutum* (lower panel). The fluorescence excitation spectrum was scaled to the absorption spectrum by the 'no-overshoot' procedure, to estimate the light absorption by PSII. The difference spectra (dotted line) were obtained by subtracting the excitation from the absorption spectra and hence denote the light absorption by PSI and photoprotective pigments.

The amount of photons absorbed by PSII, $\bar{a}^{*}_{PSII}$, was computed by spectrally weighting $F^{*}_{PSII}(\lambda)$ against the incubator light source according to eq. 4.1, as illustrated in Fig. 4.3

$$\bar{a}^{*}_{PSII} = \frac{\left[\sum_{400}^{700} F^{*}_{PSII}(\lambda) \cdot E(\lambda)\, d\lambda\right]}{E(PAR)} \qquad (4.1)$$

where $E(\lambda)$ is the spectral irradiance of the incubator light source and E(PAR) is the integrated irradiance from 400 to 700 nm (Paper 2 & 3).

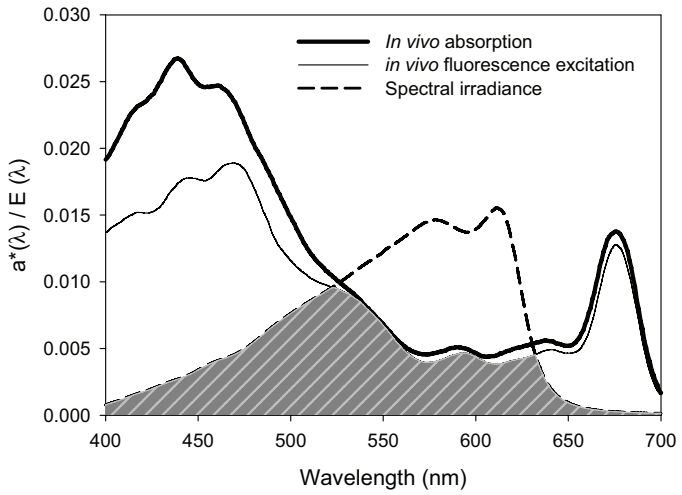

Fig. 4.3. An illustration of the calculation of the light absorption by PSII, $\bar{a}^{*}_{PSII}$. The *in vivo* fluorescence excitation spectrum was scaled to match the *in vivo* absorption spectrum by the 'no-overshoot' procedure (as in Fig. 4.2). The light absorption by PSII equals the shaded area, which is obtained by spectrally weighting (eq. 4.1) the scaled excitation spectrum against the spectral irradiance of the incubator light source ($E_{(PAR)}$ = 2 µmol photons m^{-2} s^{-1}). Data are from Papers 2 & 3.

Most studies dealing with PSII absorption for measurements of photosynthesis assume that the light absorption by PSII and PSI, respectively, is divided equally giving a ratio of 0.5 (e.g. Schreiber et al. 1986, Kolber & Falkowski 1993, Gilbert et al. 2000). However, this imposes an error as the distribution of chl *a* between PSII and PSI has a

ratio >0.5 in most microalgae[7]. The distribution of chl *a* between PSII and PSI is pigment-group specific and related to the light-harvesting complex and the distribution of chl *a* and pigments within the cell (Johnsen & Sakshaug in press). Chromophytes, the algae class I worked with, has an average PSII to PSI ratio of 0.72, as recently found by Johnsen & Sakshaug (in press). This is in agreement with the PSII to PSI ratio of 0.75 to 0.82 reported in Paper 2.

In Paper 2, we tested the 'no-overshoot' approach to calculate the fraction of light received by PSII in absolute units. To evaluate the practical implications of this theoretical approach, the outcome was tested along with two other commonly applied bio-optical approaches for estimating light absorption in PSII (Paper 2, Kromkamp & Forster 2003, Johnsen & Sakshaug in press). The results were then applied in combination with measurements of the quantum yield for PSII to obtain rates of photosynthetic O_2 production from PAM measurements.

4.4. Evaluating three bio-optical approaches to estimate the light absorption in PSII

In Paper 2, we tested three bio-optical approaches to estimate the fraction of light absorbed by PSII. These estimates were to be used in combination with the operational quantum yield for PSII, derived from PAM measurements, to calculate rates of O_2 production. The three approaches were: 1) the factor 0.5 which implies that absorbed light is equally distributed among PSI and PSII, 2) the fraction of chl *a* in PSII, determined as the ratio between the red-peak ratios between PSII-scaled fluorescence excitation and the corresponding absorption spectrum (Fig. 4.3) and 3) the measure of light absorbed by PSII, determined from the scaling of fluorescence excitation spectra to absorption spectra by the 'no-overshoot' procedure (Fig. 4.2). By calculating photosynthesis *vs.* irradiance (P *vs*. E, see box 5.1) parameters using the three approaches, we compared the results against simultaneously measured rates of oxygen

[7] Cyanobacteria, however not microalgae, represent an important group of phototrophs with the major part of chl *a* associated with PSI, giving a ratio between PSII and PSI of ~0.12 (Johnsen & Sakshaug 1996).

production. Generally, approach 1) underestimated while approach 2) overestimated the gross O_2 production rate. *In conclusion, approach 3 gave the best approximation to estimate quanta absorbed by PSII. Hence, we recommend approach 3) for estimation of gross O_2 production rates based on PAM fluorescence measurements (Paper 2).*

5. Photosynthesis and respiration

This section includes a brief presentation of the fundamental theories in photosynthesis and respiration underlying my initial interest for studying these processes by applying different methodological approaches. The introduction is meant to provide essential information on the subject and to assist the understanding of the papers included in this thesis. The most important findings from the comparison of variable fluorescence measurements and O_2 production measurements for studying photosynthesis are presented towards the end of the section. Section 6 reviews the achieved results concerning temperature effects on photosynthesis and respiration.

5.1. Photosynthesis

Photosynthesis is the process of capturing radiation energy from the sun and transforming it into chemically bound energy (Fig. 1.1). The processes of photosynthesis are responsible for the energy supply in the formation of organic carbon compounds and for the metabolism in primary producers. The overall oxygenic[8] photosynthetic process can be represented as (Falkowski & Raven 1997):

$$2H_2O + CO_2 \xrightarrow{sunlight} (CH_2O) + H_2O + O_2 \qquad (5.1)$$

The photosynthesis process within the chloroplasts can be divided into two parts: the 'light reactions' and the 'dark reactions'.

The light reactions can be described by the formula:

$$2H_2O + Light \xrightarrow{LHP+Chla} 4H^+ + 4e^- + O_2 \qquad (5.2)$$

and is the process in which light energy, via chl *a*, is used to withdraw hydrogen from water to generate electrons, and liberate oxygen. In this process, chl *a* fluorescence is emitted when the excited electrons decay to the ground state. The reactions drive the ATPase and take place in the thylakoid membranes.

---

[8] The photosynthetic process can, additionally to oxygenic, be carried out during anoxic condition by exchanging the oxygen in eq. 5.1 by e.g. an atom of sulphur to run anoxic photosynthesis. Most photosynthetic bacteria, with exception of cyanobacteria and prochlorophytes, are obligate anaerobes. In the present thesis, the term photosynthesis will address only the oxygenic process.

5.2. Respiration

The reverse reaction of photosynthesis is oxidative respiration[9]. This process is the breaking of the high-energy bonds of carbohydrates in an oxidative reaction, supplying energy for metabolism. Both phototrophic and heterotrophic organisms carry out respiration. Whereas photosynthesis proceeds only during periods with sufficient irradiation, respiration is carried out during both light and dark conditions (Raven & Beardall 1981, Hall & Rao 1999).

The respiration rate in phototrophs can be divided into two parts: 1) 'dark respiration' which is the metabolic respiration of a cell, phototroph or heterotroph, independent of the electron transport of photosynthesis. Dark respiration is thus, in principle, independent of photosynthetic activity. However, even uncoupled from photosynthetic activity it might be enhanced by the rate of photosynthesis, as a response to a generally enhanced metabolism (Markager et al. 1992, Epping & Jørgensen 1996). Experimentally, dark respiration is very difficult to isolate from the photorespiration under illumination (Raven & Beardall 1981). 2) 'Photorespiration' is the 'extra' oxidative respiration, in addition to dark respiration, and is closely linked to photosynthetic activity. Photorespiration is divided into two reactions, the Mehler[10] reaction and the oxygenase reaction of RuBPc (ribulose 1,5-bisphosphate carboxylase) (Raven & Beardall 1981, Falkowski & Raven 1997).

5.3. Measuring photosynthesis: three methodological approaches

As seen from the theory above, photosynthesis can be estimated from the variable fluorescence kinetics of PSII, from the rate of O_2 production and from the rate of ^{14}C-assimilation (Paper 3). Each of these methods has its advantages and disadvantages and

---

[9] As with photosynthesis, respiration can also be anoxic. In anoxic respiration, organic molecules are oxidised by an electron accepter other than O_2, e.g. nitrate or sulphate. In this thesis, the term respiration refers to the oxygenic process only.

[10] The Mehler reaction, also called pseudocyclic electron transport, involves an electron transport sequence where the O_2 produced at PSII is reduced again at PSI. Consequently, there is no net production of O_2. The process leads to formation of ATP, but not $NADPH_2$.

have all been applied to access the ecosystem primary production in various environments. The techniques, however, measure different products of the photosynthetic pathway and reflect different physiological processes with potentially different responses to environmental variables, such as temperature (Paper 2 & 3, Geider & Osborne 1992, Geel et al. 1997, Morris & Kromkamp 2003).

Below is a brief presentation of the three measuring techniques, ordered downstream according to the electron flux of the photosynthetic pathway. In the following section, the outcome of the three techniques will be compared.

Variable fluorescence measurements

Variable fluorescence from PSII can be measured by e.g. Pulse Amplitude Modulated (PAM) fluorometry and can be used to estimate the operational quantum yield[11] of PSII, Φ_{PSII} (Schreiber et al. 1986). The electron transfer rate (ETR, from PS II to PS I) can be quantified from Φ_{PSII} times the absorbed quanta in PSII, as a proxy for the gross photosynthetic rate (Paper 2 & 3, Genty et al. 1989, Kroon et al. 1993). The electrons generated in PSII are closely coupled to the O_2-evolution, and subsequently follow several pathways, among those the reduction of CO_2 via NADP(H) production (Falkowski & Raven 1997). The PAM technique is fast and non-invasive and can thus yield measurements of photosynthesis with a high temporal and spatial resolution.

In this study, the operational quantum yield of PSII, Φ_{PSII}, was calculated from steady-state fluorescence before (F_s) and after exposing the sample to a saturating light pulse (F_m'), during actinic illumination by the PAM technique (Eq. 5.4, Genty et al. 1989).

---

[11] The quantum yield is defined as the ratio of moles of product to the moles of photons absorbed in a photochemical reaction (Falkowski & Raven 1997). Thus, the operational quantum yield of PSII, Φ_{PSII}, is mol electrons generated in PSII to mol photons absorbed. Likewise, is the quantum yield for O_2, Φ_{O2}, mol O_2 produced to mol photons absorbed. The inverse of the quantum yield ($1/\Phi$) is called the 'quantum requirement', i.e. mol photons absorbed per mol product formed. Because of an inevitable energy loss in the photochemical reactions, the quantum yield is always <1, while the quantum requirement is >1.

The maximum quantum yield, Φ_{PSII_max}, was calculated in a similar way on dark acclimated (~15 min) cells. See Papers 2 & 3 for a detailed methodological description.

$$\Phi_{PSII} = \Delta F/F_m' = \frac{F_m' - F_s}{F_m'} \qquad (5.4)$$

In combination with knowledge of the chl *a*-specific light absorption in PSII (section 4.3), measurements of Φ_{PSII} can be used to estimate the photosynthetic rate of gross O_2 production, P_{PSII}, as from eq. 5.5 (Kroon et al. 1993);

$$P_{PSII} = \Phi_{PSII} \cdot E \cdot \Gamma \cdot \bar{a}^*_{PSII} \qquad (5.5)$$

where Γ is the stoichiometric ratio of oxygen evolved per electron generated at PSII. Usually, according to theory of the standard Z-scheme of photosynthesis, Γ is assumed to equal 0.25 O_2 electrons^{-1} (for PSII, Kroon et al. 1993, Gilbert et al. 2000). However, a lower ratio is usually found when studied empirically (Paper 2 & 3, Kromkamp et al. 2001, Longstaff et al. 2002). For simplicity, I initially assumed Γ to be 0.25 in the present study (see section 6.1 and Paper 3 for a discussion on the divergence between the theoretical and empirical ratio).

Dissolved oxygen measurements

Measuring the rate of photosynthesis in phytoplankton using concentration changes of dissolved O_2 was first proposed by Gaarder & Gran (1927), who invented the light-dark bottle technique. They calculated the concentration of dissolved O_2 using the Winkler titration technique (Strickland & Parsons 1968). With the development of the O_2-electrode, measurements of dissolved O_2 have become faster and possible to apply during incubation experiments. The fast responding and signal-stable Clark type O_2-microelectrode (Revsbech 1989) has been widely applied in aquatic science, and allows for continuous measurements of net O_2-production in the light, and O_2-respiration in the dark (for a review see Glud et al. 2000).

In oxygenic photosynthesis, the term 'gross photosynthesis' refers to the rate of oxygen evolution equivalent to the photochemically generated electron flux produced from the oxidation of water, excluding any respiratory losses (Sakshaug et al. 1997). 'Net photosynthesis' in the present work is defined as the net evolution of oxygen following

all respiratory losses within the investigated system (i.e. both autotrophic and heterotrophic respiratory oxygen consumption).

All measurements of O_2 production and consumption rates in this study were performed using Clark-type O_2 microelectrodes (Revsbech 1989) with a fast response (90 % response in <10 s for net production/consumption and <0.5 s for gross production measurements), small tip size (external diameter <1 mm) and low stirring sensitivity (<3 %).

Photosynthetic gross O_2 production can be measured in benthic sediments by the light/dark shift method (Paper 4, Revsbech & Jørgensen 1983, Glud et al. 1992). However, because of a much lower biomass per volume, this method has not yet been successfully applied on water samples. In sea water, gross O_2 production can be measured by spiking the water samples with ^{18}O-labelled water and measuring the amount of ^{18}O-labelled O_2 produced photosynthetically (Bender et al. 1987). Alternatively, gross production can be estimated from correcting the net O_2 production rates for respiration. The ^{18}O-labelling method unequivocally measures gross primary production (i.e. there are no respiratory losses of the labelled O_2), while the latter method will lead to gross production being underestimated if respiration in the light is significantly different from respiration in the dark. In the present study, gross O_2 production was measured by the light/dark shift technique in sediments (P_{gross}, Paper 4) and estimated from the net production and dark respiration rates in the studied phytoplankton cultures (P_{O2}, Paper 2 & 3). Net O_2 production was measured from concentration profiles (P_n, Paper 4) and from net changes of the O_2 concentration over time in phytoplankton samples (Paper 2 & 3).

^{14}C-assimilation measurements

The ^{14}C technique was developed by Steemann-Nielsen (1952) and has probably been the most widely used method in aquatic science for estimating primary production, because of its high sensitivity allowing measurements on low biomass. The method quantifies the rate of ^{14}C-assimilation and hence the conversion of inorganic C into cell biomass. It reflects an activity intermediate to net and gross photosynthesis, dependent

on the incubation time (Lewis & Smith 1983, Falkowski & Raven 1997, MacIntyre et al. 2002). For 1 hour incubations, the technique is, for convenience, commonly assumed to indicate gross rates (P_{14C}). This method, however, is labour-intensive and the quantum yield of carbon fixation varies according to the intermediate steps in photosynthesis, environmental variables and growth phase of the cells (Paper 3, Kroon et al. 1993). As a consequence, models of primary production based on the ^{14}C method can be inaccurate (Prézelin et al. 1991, Schofield et al. 1993, Kroon et al. 1993).

5.4. Comparing PSII fluorescence and oxygen production

Photosynthetic O_2-production, Φ_{PSII} and/or ^{14}C-assimilation have been compared in a number of studies of macroalgae, microphytobenthos, and marine phytoplankton (e.g. Geel et al. 1997, Barranguet & Kromkamp 2000, Longstaff et al. 2002). Although the investigations have been conducted under a variety of experimental conditions, a preponderance of the studies on microalgae find a linear relationship between O_2-evolution and Φ_{PSII} under moderate irradiance, sometimes with deviation at very low or very high irradiance conditions (e.g. Schreiber et al. 1995, Flameling & Kromkamp 1998). Different explanations for the deviation have been proposed: spectral difference in PAR sources, changes in O_2-consumption in the light, cyclic electron transport around PSII and Mehler-type reactions, see Flameling and Kromkamp (1998) for an overview.

In my studies at moderate irradiances below the photoinhibited levels, the relationship between rates of measured (P_{O2}) and calculated O_2 production (P_{PSII}, from PAM and PSII absorption, eq. 5.5) showed approximately linear responses (r^2 = 0.7–0.97, Fig. 5.2, Paper 2). As seen from Fig. 5.2, the linear response of P_{PSII} versus P_{O2} showed species-specific slope coefficients for the three microalgae species investigated. Where the diatom (*P. tricornutum*) tended to show a slope coefficient close to unity, P_{PSII} tended to underestimate the O_2 production, compared to $P_{O2,}$ for the dinoflagellate (*P. minimum*) and overestimate P_{PSII} for the haptophyte (*P. parvum*). The divergence in the slope coefficient was presumably caused by a lower quantum yield for O_2, Φ_{O2}, and hence a stoichiometric ratio lower than the 0.25 theoretically assumed for the calculation of P_{PSII}

(eq. 5.4) of oxygen evolved per electron generated at PSII. A careful discussion of this subject is found in Paper 2 & 3.

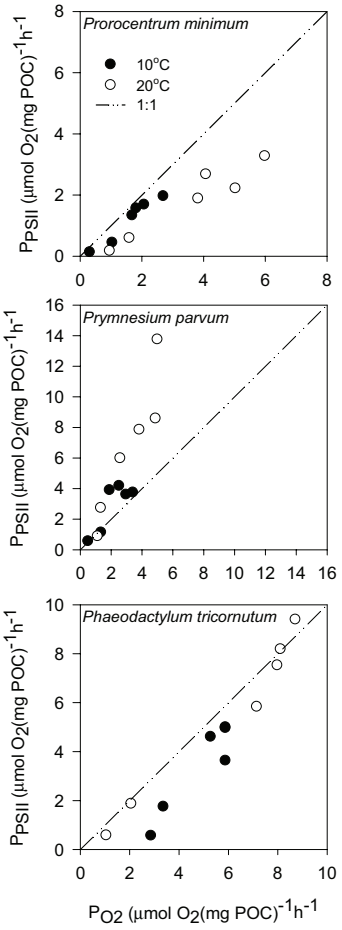

Fig. 5.2. Rates of O_2 production calculated from Φ_{PSII} in combination with $\overline{a}^{*}_{PSII}$, P_{PSII}, as a function of measured O_2 production, P_{O2}, for *P. minimum*, *P. parvum* and *P. tricornutum*. The dashed line represents x = y (Paper 2).

The PAM and the O_2-microelectrode techniques have their limitations and strengths in terms of sensitivity and noise. In low lights ($E < E_k$), the electron transfer rate (ETR) is relatively robust and thus the estimation of α from the PAM technique. Conversely, the microelectrode technique is working near the detection limit, thus yielding a low

accuracy for α. In high light ($E > E_k$), the accuracy of the results from the PAM and the O_2-microsensor technique, respectively, are the opposite of that for low light ($E < E_k$). As the ratio of Φ_{PSII} to E decreases with increasing irradiance the accuracy becomes weak. In contrast, the signal-to-noise ratio of the O_2-microsensor increases with increasing irradiance, yielding more reliable results under high light conditions.

6. Temperature effects on photosynthesis and respiration

The present thesis contains two distinctly different approaches to studying temperature effects on processes of photosynthesis and respiration. Paper 3 is a study on laboratory-grown monocultures of pelagic phytoplankton, and Paper 4 is a study on intact diatom-dominated benthic communities, sampled at shallow water. However, both papers are based on physiological response studies in microalgae, and the associated heterotrophic community, imposed by short-term (minutes to hours) temperature experiments. Laboratory-grown cultures of phytoplankton allow for detailed investigations of temperature-imposed responses on light-saturated and light-limited rates of photosynthesis (P *vs.* E relationship), where intact sediment samples with microphytobenthos allow for ecological relevant, intact-community temperature-response studies. This section contains a review of the achieved results on temperature effects on light-saturated and light-limited photosynthesis, followed by an introduction to the results of the benthic community study. Section 6.4 summarises the ecosystem implications of the obtained results.

6.1. Temperature effects on light-saturated photosynthesis

Calculated and measured O_2-production rates along with ^{14}C-assimilation rates showed overall the same *relative* response to a short-term temperature change for all the three phytoplankton species studied (Paper 3). The maximum photosynthetic rate, P^C_{max}[12], increased with temperature, resulting in an average Q_{10} of 2.1 ± 0.2 (mean ± S.E.). The Q_{10} values showed only small variance between methods and species. This demonstrated that Φ_{PSII} from intact algae cells responded similarly to the rate of O_2-evolution and ^{14}C-assimilation, to a short-term temperature change. This is consistent with the hypothesis that the overall rate-limiting reaction for light-saturated photosynthesis is carbon fixation rather than electron transport, as suggested by Sukenik et al. (1987). For the present data, this implies that Φ_{PSII} as well as the O_2-production

[12] The '^{C}' on P^C_{max} denotes that the parameter was normalised to the particulate organic carbon (POC) content of the sample investigated. Likewise, '*' denotes normalisation to the chl *a* content.

Box 6.1 : Temperature and Q_{10} (temperature coefficient)

Temperature in an important environment variable for understanding the physiological ecology of microalgae in nature, as it affect key biological processes, including photosynthesis, enzymatic activity and respiration (Davison 1991).

Calculation of Q_{10}

Temperature-imposed activity changes are often quantified by the so-called 'Q_{10} factor', describing the relative rate of increase for a temperature increase of 10 °C. The temperature response of a given process can be calculated from the apparent activation energy (E_a, $kJ \cdot mol^{-1}$) and Q_{10} then from E_a. E_a can be calculated from the initial linear slope of an Arrhenius plot where ln(k) is plotted as a function of temperature $(R \cdot T)^{-1}$, according to Raven and Geider (1988) as:

$$\ln(k) = \ln(A) + \left[-E_a (RT)^{-1}\right]$$

where k is the rate of the reaction, A is the Arrhenius constant, R is the gas constant ($8.3144\ J^{-1} \cdot mol^{-1}$) and T is the absolute temperature (K).

Q_{10} is then calculated for a given temperature interval of interest as (Berry & Bjorkman 1980):

$$Q_{10} = \exp\left(Ea \cdot 10\left(RT(T+10)\right)^{-1}\right)$$

All Q_{10} values in the present study are calculated from Arrhenius plots, according to the above equation. In the literature, Q_{10} is sometimes alternatively calculated from a more simple equation, which is strictly exponential, as:

$$Q_{10} = \left(r_2 / r_1\right)^{(10/(t_2 - t_1))}$$

where t_1 and t_2 are the lower and upper temperatures of the range of consideration, and r_1 and r_2 are the metabolic rates corresponding to t_1 and t_2, respectively (Davis & McIntire 1983).

Acclimation versus adaptation

Temperature *acclimation* usually describes phenotypic changes in a community as a response to short-term temperature change, whereas temperature *adaptation* involves genetic differences in metabolism between communities from different thermal environments (Berry & Bjorkman 1980, Davison 1991)

may be limited by carbon-fixing enzyme activity, i.e. the Rubisco-complex. In addition, the data suggest that rates of Φ_{PSII} and O_2-production driven by the light reactions were not different from rates of ^{14}C-fixation, driven by the dark reaction, as a function of short-term temperature changes (Paper 3). *Conclusively, the PAM technique, analogous*

to O_2-production and ^{14}C-assimilation measurements, can be applied to study relative temperature responses of light-saturated photosynthesis.

Overall, the *absolute* rates of calculated O_2-production, P_{PSII} (based on Φ_{PSII}, Eq. 5.5), showed a species-specific correlation to and overestimated the measured O_2-production rates of ~1 to 3 times, for light-saturated photosynthesis (Fig. 6.1). As I have shown, $\bar{a}^*_{PSII}$ is a good measure for the light absorption in PSII (section 4.3 & 4.4, Papers 2 & 3). *Hence, I suggest that the off-set of the Φ_{PSII} based measurements (P_{PSII}) is caused by a lower quantum yield for O_2-production than the theoretical maximum, and thus the amount of O_2 evolved per electron generated in PSII (Γ) is lower than the commonly assumed 0.25 (Paper 3, e.g. Kroon et al. 1993, Suggett et al. 2004). The lower quantum yield for O_2-production can possibly be ascribed to irradiance induced cyclic electron transport around PSII, Mehler reactions (Flameling & Kromkamp 1998, Longstaff et al. 2002), and to the difference between the rates of metabolic respiration ('dark' respiration) during light and dark conditions, respectively (section 5.2). The off-set of the Φ_{PSII} based measurements seemed to be insensitive to temperature (Paper 3).*

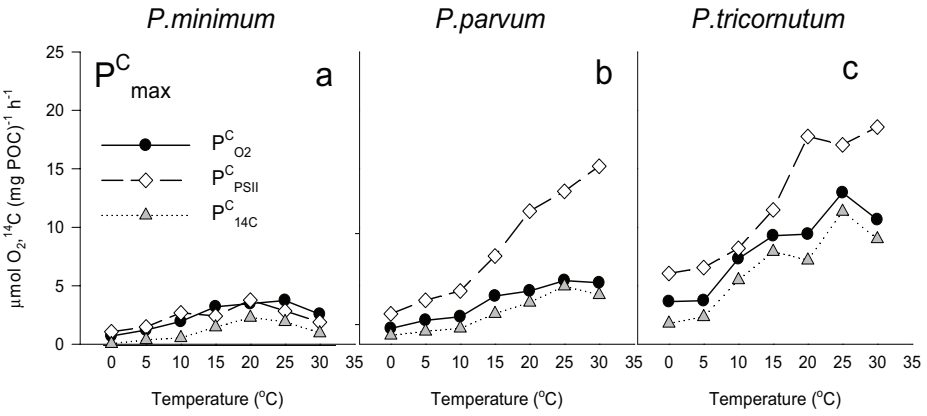

Fig. 6.1. Effect of temperature on the absolute values for the maximum photosynthetic rate (P^C_{max}). The photosynthetic parameters were calculated from rates of measured O_2-production (P^C_{O2}, filled circles), Φ_{PSII} (P^C_{PSII}, eq. 5.5, open diamonds), and ^{14}C-assimilation (P^C_{14C}, grey triangles). The three pelagic algae species were grown at 15 °C and 80 µmol photons m^{-2} s^{-1} (Paper 3).

6.2 Temperature effects on light-limited photosynthesis

The *relative* and *absolute* values of α^C showed an analogous response to a short-term temperature change and showed itself to be insensitive to (*P. minimum*), or possibly slightly decreasing (*P. parvum* and *P. tricornutum*), with increasing temperature resulting in average Q_{10} of 1.0 ± 0.2 (mean ± S.E.). Based on a statistical test of covariance (ANCOVA) I concluded that the temperature response for the three methods was the same for all three species (Fig 6.2, Paper 3). *The absolute values of α^C demonstrated an off-set of α^C_{PSII} compared to α^C_{O2} and α^C_{14C} which was constant for the entire temperature range, arguing for a linear temperature-insensitive relationship between rates obtained from the three methods, in the light limited part of the P vs. E curve. The off-set in the light-limited region was similar to the off-set of P_{PSII} in the light-saturated region (Fig. 6.1) and hence I concluded that the off-set was general for the Φ_{PSII} based O_2-production rates (P^C_{PSII}), for the entire irradiance range (Paper 3).* The possible decrease of α^C with temperature for *P. tricornutum* is explained by an apparent decrease of the chl *a* to C ratio, as α^C (carbon-specific) is often correlated to this ratio because light absorption is correlated with chl *a* (MacIntyre et al. 2002).

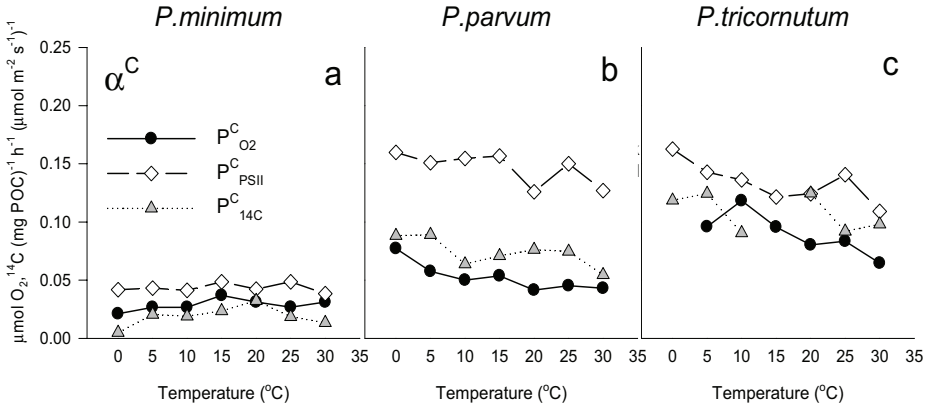

Fig 6.2. Effect of temperature on the absolute values for the maximum light utilization coefficient (α^C). Symbols and calculations as in Fig 6.1 (Paper 3).

6.3 Temperature effects on intact benthic microphyte communities

Studies at subtidal and intertidal sites have shown that temperature can exert tight control on benthic photosynthetic rates, and can lead to seasonal temperature acclimation and/or change in the microphyte community composition (e.g. Grant 1986, Barranguet et al. 1998). In Paper 4, I studied the short-term temperature effects on respiration and photosynthesis in intact diatom-dominated benthic communities collected at two temperate and one high-arctic subtidal sites, to resolve a potential adaptation strategy (Fig. 6.3). Areal rates of both total (TOE) and diffusive (DOE) O_2 exchange were determined from O_2-microsensor measurements in darkness and at 140 μmol photons m^{-2} s^{-1}. In darkness, the O_2 consumption increased exponentially with increasing temperature for both TOE and DOE with Q_{10} ranging between 1.7 and 3.3. Overall, Q_{10} was not correlated to the *in situ* water temperature or geographical position. Accordingly, no difference in the temperature acclimation or adaptation strategy of the microbial community was observed (see Paper 4 for details). Gross photosynthetic rates increased with temperature yielding Q_{10} in the range of 2.2 to 2.6. However, no temperature adaptation was observed between the sites. The present study shows that increasing temperature stimulates the heterotrophic activity more than gross photosynthesis does. *Consequently, the typically mixed benthic community of heterotrophic and phototrophic microbes gradually turns heterotrophic with increasing temperature. In conclusion, no difference in the temperature acclimation response between the sites was observed, suggesting that the temperature adaptation strategy for the benthic microbial communities was similar for the arctic and the temperate communities.*

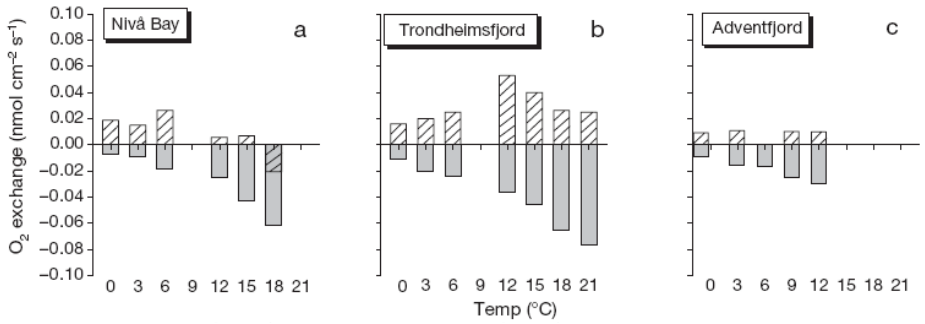

Fig. 6.3. Areal rates of total oxygen exchange as a function of temperature, measured from whole core incubations in darkness (dark columns) and at 140 µmol photons m^{-2} s^{-1} (open columns) in (a) Denmark, (b) Norway and (c) Svalbard. Negative values indicate net O_2 consumption and positive values net O_2 production (Paper 4).

6.4. Phototrophic *versus* heterotrophic temperature responses (ecosystem implications)

The results of Paper 3 demonstrate that P^C_{max} increased and α^C was more or less insensitive to increasing temperature for all the three investigated species, consistent with most eukaryote algae (Davison 1991). Generally, the light-limited photosynthesis, represented by α^C, is a function of photochemical light reactions (not enzyme-dependent), whereas the light-saturated part, represented by P^C_{max}, is limited by enzyme activity associated with the carbon metabolism of the dark reactions (Paper 3, Davison 1991, Sakshaug et al. 1997). Intact community responses to temperature, as in benthic microphyte communities, are confounded by both light-saturated and light-limited processes, as the irradiance regime within the sediment is distributed gradiently, and is further complicated by the simultaneous impact on physical, chemical and biological controls (Paper 4, Epping & Jørgensen 1996, Fenchel & Glud 2000). Based on the laboratory results showing that the light-limited part of photosynthesis is temperature insensitive (Paper 3), it is presumed that the temperature response of the intact benthic microphyte communities (quantified from Q_{10}) is controlled by the light-saturated temperature response. *Thus the light-saturated temperature response on photosynthesis is responsible for the temperature response of the net community in the sediments*

(Paper 4). This is consistent with the obtained Q_{10} values, see Papers 3 and 4 for details.

A dataset extracted from Paper 3, allowed isolation of the effect of temperature on rates of net O_2 production, measured on the laboratory-grown culture of *Prorocentrum minimum*, at five irradiances and in darkness (Fig. 6.4). The data shows that the net O_2 production rate as a function of temperature decreases with decreasing irradiance in a manner so that the temperature of maximum production (not to be confused with the temperature optimum) decreases. This phenomenon illustrates the balance between the phototrophic *versus* the heterotrophic temperature response, and leads me to conclude that the heterotrophic activity increased more than the gross O_2 production, with increasing temperature, in laboratory-grown culture. *In conclusion, the phytoplankton and the intact microphytobenthic community responded similarly, demonstrating a gradual transition from a phototrophic to a heterotrophic dominated community with increasing temperature. This has implications for the carbon cycling in both pelagic and benthic microalgae-dominated communities that experience seasonal and diel temperature fluctuations.*

Similar observations have previously been reported for intertidal sediments (Davis & McIntire 1983) and in temperate planktonic communities (Lefevre et al. 1994, Robinson 2000). The observations have generally been explained by a stronger and more rapid physiological acclimation of heterotrophic compared to phototrophic activity, to temperature changes. *I therefore suggest that the stronger heterotrophic temperature response as observed in my studies is a general rather than exceptional phenomenon*.

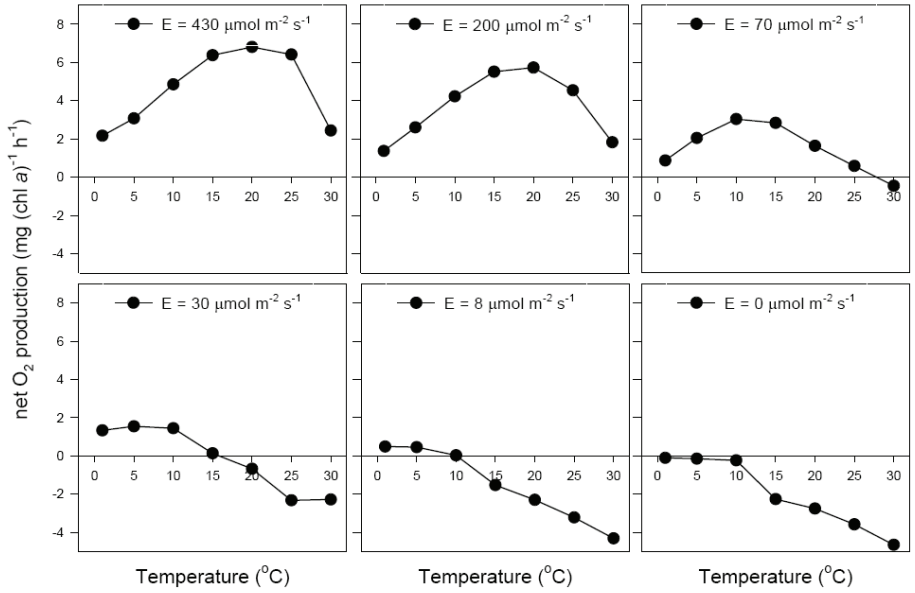

Fig. 6.4. Effects of temperature on rates of the net O_2 production (which is the sum of the gross O_2 production and the respiration) in a laboratory-grown culture of *P. minimum*. Each of the six panels represents different irradiances, from 430 µmol m^{-2} s^{-1} (upper left) to darkness (lower right) (based on the dataset of Paper 3).

7. Conclusions

- Profiles of chl *a*, dissolved oxygen and primary production showed large natural variations in the Barents Sea. Yet the profiles correlated closely to optical depth, i.e. a certain irradiance regime defined from the attenuation coefficient. The chl *a*-normalised primary production correlate stronger to the light regime in the blue-green region, at 490 nm, than to PAR, improving the correlation between irradiance and primary production by ~15 %. Hence, I suggest using 490 nm instead of PAR when relating phytoplankton production to a single wavelength band.

- An accurate estimation of light absorption in PSII is essential for calculating rates of photosynthetic O_2 production from the operational quantum yield in PSII, Φ_{PSII}, derived from PAM measurements. Three bio-optical approaches to estimate the fraction of light absorbed by PSII were tested. The best estimate was obtained from a spectrally weighted approach based on the PSII-scaled fluorescence excitation spectrum, by the so-called 'no-overshoot' procedure. The approach was evaluated by comparing calculated rates of photosynthetic O_2 production based on Φ_{PSII} and the PSII absorption, against simultaneously measured rates of O_2 production. This approach is hence recommended for estimation of gross O_2 production rates from PAM fluorescence recordings.

- Both calculated and measured O_2-production rates along with ^{14}C-assimilation rates showed the same relative response to a short-term temperature change, (for the three studied microalgae species.) This implies that the PAM technique analogous to O_2-production and ^{14}C-assimilation measurements can be applied to study relative temperature responses of photosynthesis *versus* irradiance relationships. Absolute rates of calculated O_2-production based on Φ_{PSII} showed a species-specific correlation and overestimated the measured O_2-production rates of ~1 to 3 times during both light-limited (α^C) and light-saturated (P^C_{max}) photosynthesis. The off-set of the Φ_{PSII} based measurements was due to a lower

quantum yield for O_2-production than the theoretical maximum and seemed to be insensitive to temperature. In conclusion, the PAM technique can be used to study temperature responses of photosynthesis in microalgae when attention is paid to the absorption properties in PSII.

- No difference in the temperature acclimation response was observed between the investigated arctic and temperate diatom-dominated benthic communities. This was observed from similar Q_{10} values, arguing for a similar temperature adaptation strategy between the sites. Overall, temperature stimulated the heterotrophic activity more than the gross photosynthesis, gradually turning the benthic communities heterotrophic with increasing temperature.

8. Some thoughts on photosynthesis and algorithms of primary production

Bio-optical models developed for the estimation of marine primary production P, and often used with remotely sensed ocean colour data (often determined as g C m^{-3} s^{-1}), can be written on the general form (e.g. Platt & Sathyendranath 1988, Claustre et al. 2005)

$$P = PAR[chla]a_{\varphi}^{*}\Phi_{C} \qquad (8.1)$$

where a_{φ}^{*} is the chl *a*-specific absorption coefficient and Φ_C is the quantum yield for carbon fixation. Equation 8.1 is in units of moles, which by multiplying with a factor of 12 can be converted into grams of carbon. The estimation of PAR and [chl*a*] is generally not an issue, and these variables can be estimated with a good accuracy, even at a global scale from remotely sensed data or models. Estimation of the product of a_{φ}^{*} and Φ_C is in general considered more challenging (e.g. Claustre et al. 2005). Statistical relationships that relate $a_{\varphi}^{*}\Phi_C$ to [chl *a*] have been described, however, these only reproduce average trends and remain limited in accounting for natural variability (e.g. Bricaud et al. 1995).

Three major findings in the thesis have inspired me to propose some improvements to eq. 8.1, with the aim of estimating P from natural ecosystems. First, Paper 1 demonstrates that from a simple approach exchanging PAR with the irradiance at 490 nm the correlation of irradiance to measured primary production can be improved by ~15 % (Fig. 3.3 and section 3.3). Secondly, Paper 2 shows that replacing a_{φ}^{*} with the PSII-specific absorption coefficient, F_{PSII}^{*}, gives a more accurate estimate of the light absorption for oxygenic photosynthesis (origin in PSII), as it corrects for absorption by photo-protective carotenoids (and PSI). Thirdly, Paper 3 quantifies the (maximum) quantum yield of O_2 production based on the light absorption in PSII, ${}^{PSII}\Phi_{O2}$. Using ${}^{PSII}\Phi_{O2}$ instead of Φ_C is in principle not better, however, by applying the bio-optical approach for quantification of the PSII absorption (Paper 2) it is possible to quantify

${}^{PSII}\Phi_{O2}$ with a better accuracy than usually applied for Φ_C. Consequently, incorporating these improvements into equation 8.1, it can be rewritten as

$$P_{O2} = kE_{490}\left[chla\right]F^{*}_{PSII}\,{}^{PSII}\Phi_{O2} \qquad (8.2)$$

where k is a factor correcting the irradiance at 490 nm to the 400 - 700 nm waveband. The outcome of eq. 8.2 is an estimate of the photosynthetic (gross) O_2 production in units of mole, and summaries the finding in this thesis synthesised in a single equation. This approached offers improvement to the mentioned uncertainties included in eq. 8.1.

As ${}^{PSII}\Phi_{O2}$ in this study is based on culture-grown phytoplankton it is not necessarily representative under *in situ* conditions. Obviously, there exists a challenge in obtaining accurate and reliable measurements of ${}^{PSII}\Phi_{O2}$ (and similar bio-optical parameters) under natural conditions in phytoplankton and microphytobenthic communities. This task is still recognised as a major challenge (Behrenfeld & Falkowski 1997, Claustre et al. 2005).

Conclusively, to improve models for marine primary production, not least for the Arctic region, further field investigations are required. From simultaneously measurements of photophysiological parameters (P *vs.* E curves), phytoplankton absorption and taxonomic composition (e.g. HPLC) knowledge of the *in situ* variability of the bio-optical parameters (e.g. the quantum yield for photosynthesis) can be obtained (Claustre et al. 2005, Johnsen & Sakshaug in press). Such studies would be extremely valuable for future improvement of primary production estimates: perhaps especially in the Arctic with present climate change scenarios predicting a decreasing ice cover and thus increased light availability in the water column (Holland et al. 2006).

References

Barranguet C, Kromkamp J (2000) Estimating primary production rates from photosynthetic electron transport in estuarine microphytobenthos. Marine Ecology-Progress Series 204:39-52

Behrenfeld MJ, Falkowski PG (1997) A consumer's guide to phytoplankton primary productivity models. Limnology and Oceanography 42:1479-1491

Bender M, Grande K, Johnson K, Marra J, Williams PJL, Sieburth J, Pilson M, Langdon C, Hitchcock G, Orchardo J, Hunt C, Donaghay P, Heinemann K (1987) A Comparison of 4 Methods for Determining Planktonic Community Production. Limnology and Oceanography 32:1085-1098

Berry J, Bjorkman O (1980) Photosynthetic Response and Adaptation to Temperature in Higher-Plants. Annual Review of Plant Physiology and Plant Molecular Biology 31:491-543

Blankenship RE (2002) Molecular mechanisms of photosynthesis. Blackwell Science

Bouman HA, Platt T, Sathyendranath S, Irwin BD, Wernand MR, Kraay GW (2000) Bio-optical properties of the subtropical North Atlantic. II. Relevance to models of primary production. Marine Ecology-Progress Series 200:19-34

Bricaud A, Babin M, Morel A, Claustre H (1995) Variability in the Chlorophyll-Specific Absorption-Coefficients of Natural Phytoplankton - Analysis and Parameterization. Journal of Geophysical Research-Oceans 100:13321-13332

Bricaud A, Bedhomme AL, Morel A (1988) Optical-Properties of Diverse Phytoplanktonic Species - Experimental Results and Theoretical Interpretation. Journal of Plankton Research 10:851-873

Bricaud A, Claustre H, Ras J, Oubelkheir K (2004) Natural variability of phytoplanktonic absorption in oceanic waters: Influence of the size structure of algal populations. Journal of Geophysical Research-Oceans 109

Bricaud A, Morel A (1986) Light Attenuation and Scattering by Phytoplanktonic Cells - a Theoretical Modeling. Applied Optics 25:571-580

Bricaud A, Morel A, Babin M, Allali K, Claustre H (1998) Variations of light absorption by suspended particles with chlorophyll a concentration in oceanic

(case 1) waters: Analysis and implications for bio-optical models. Journal of Geophysical Research-Oceans 103:31033-31044

Cahoon LB (1999) The role of benthic microalgae in neritic ecosystems. In: Oceanography and Marine Biology, Vol 37, Vol 37, p 47-86

Claustre H, Babin M, Merien D, Ras J, Prieur L, Dallot S, Prasil O, Dousova H, Moutin T (2005) Toward a taxon-specific parameterization of bio-optical models of primary production: A case study in the North Atlantic. Journal of Geophysical Research-Oceans 110

Dalløkken R, Sandvik R, Sakshaug E (1995) Seasonal variations in the vertical light attenuation coefficient in the Greenland Sea: effect of phytoplankton light absoption. In: Skjoldal HR, Hopkins CCE, Erikstad KE, Leinaas HP (eds) Ecology of Fjords and Coastal Waters. Elsevier Science, Amsterdam

Davis MW, McIntire CD (1983) Effects of Physical Gradients on the Production Dynamics of Sediment-Associated Algae. Marine Ecology-Progress Series 13:103-114

Davison IR (1991) Environmental-Effects on Algal Photosynthesis - Temperature. Journal of Phycology 27:2-8

Emerson R, Arnold W (1932) The photochemical reaction in photosynthesis. Journal of General Physiology 16:191-205

Epping EHG, Jørgensen BB (1996) Light-enhanced oxygen respiration in benthic phototrophic communities. Marine Ecology-Progress Series 139:193-203

Falkowski PG (1994) The Role of Phytoplankton Photosynthesis in Global Biogeochemical Cycles. Photosynthesis Research 39:235-258

Falkowski PG, Raven JA (1997) Aquatic photosynthesis. Blackwell Science

Fenchel T, Glud RN (2000) Benthic primary production and O-2-CO2 dynamics in a shallow-water sediment: Spatial and temporal heterogeneity. Ophelia 53:159-171

Field CB, Behrenfeld MJ, Randerson JT, Falkowski P (1998) Primary production of the biosphere: Integrating terrestrial and oceanic components. Science 281:237-240

Flameling IA, Kromkamp J (1998) Light dependence of quantum yields for PSII charge separation and oxygen evolution in eucaryotic algae. Limnology and Oceanography 43:284-297

Geel C, Versluis W, Snel JFH (1997) Estimation of oxygen evolution by marine phytoplankton from measurement of the efficiency of Photosystem II electron flow. Photosynthesis Research 51:61-70

Geider RJ, Osborne BA (1992) Algal Photosynthesis. Chapman & Hall, New York

Genty B, Briantais JM, Baker NR (1989) The Relationship between the Quantum Yield of Photosynthetic Electron-Transport and Quenching of Chlorophyll Fluorescence. Biochimica Et Biophysica Acta 990:87-92

Gilbert M, Domin A, Becker A, Wilhelm C (2000) Estimation of primary productivity by chlorophyll a in vivo fluorescence in freshwater phytoplankton. Photosynthetica 38:111-126

Glud RN, Gundersen JK, Ramsing NB (2000) Electrochemical and optical oxygen microsensors for in situ measurements. In: Buffle J, Horvai G (eds) In situ monitoring of aquatic systems: Chemical analysis and speciation. John Wiley & Sons Ltd., p 20-73

Glud RN, Kuhl M, Wenzhofer F, Rysgaard S (2002) Benthic diatoms of a high Arctic fjord (Young Sound, NE Greenland): importance for ecosystem primary production. Marine Ecology-Progress Series 238:15-29

Glud RN, Ramsing NB, Revsbech NP (1992) Photosynthesis and Photosynthesis-Coupled Respiration in Natural Biofilms Quantified with Oxygen Microsensors. Journal of Phycology 28:51-60

Green BR, Anderson JM, Parson WW (2003) Photosynthetic membranes and their light-harvesting antennas. In: Green BR, Parson WW (eds) Light-harvesting antennas in photosynthesis. Kluwer Academic Publishers, Dordrecht, The Netherlands, p 1-28

Gaarder T, Gran HH (1927) Investigations of the production of plankton in the Oslo fjord. Rapp Proc-Verb Cons Int Expl Mer 42:3-48

Hall DO, Rao KK (1999) Photosynthesis. Cambridge University Press

Haxo FT (1985) Photosynthetic Action Spectrum of the Coccolithophorid, Emiliania-Huxleyi (Haptophyceae) - 19'hexanoyloxyfucoxanthin as Antenna Pigment. Journal of Phycology 21:282-287

Holland MM, Bitz CM, Tremblay B (2006) Future abrupt reductions in the summer Arctic sea ice. Geophysical Research Letters 33

Jassby AD, Platt T (1976) Mathematical formulation of the relationship between photosynthesis and light for phytoplankton. Limnology and Oceanography 21:540-547

Jeffrey SW, Mantoura RFC, Bjørnland T (1997a) Data for the identification of 47 key phytoplankton pigments. In: Jeffrey SW, Mantoura RFC, Wright SW (eds) Phytoplankton pigments in oceanography: guidelines to modern methods. UNESCO, Paris, p 449-559

Jeffrey SW, Vesk M, Mantoura RFC (1997b) Phytoplankton pigments: windows into the pastures of the sea. Nature & Resources 33:14-29

Jerlov NG (1976) Marine optics. Report No. 0-444-41490-8, Elsevier, Amsterdam

Johnsen G, Nelson NB, Jovine RVM, Prezelin BB (1994a) Chromoprotein-Dependent and Pigment-Dependent Modeling of Spectral Light-Absorption in 2 Dinoflagellates, Prorocentrum-Minimum and Heterocapsa-Pygmaea. Marine Ecology-Progress Series 114:245-258

Johnsen G, Prezelin BB, Jovine RVM (1997) Fluorescence excitation spectra and light utilization in two red tide dinoflagellates. Limnology and Oceanography 42:1166-1177

Johnsen G, Sakshaug E (1993) Biooptical Characteristics and Photoadaptive Responses in the Toxic and Bloom-Forming Dinoflagellates *Gyrodinium-Aureolum*, *Gymnodinium-Galatheanum*, and two strains on *Prorocentrum minimum*. Journal of Phycology 29:627-642

Johnsen G, Sakshaug E (in press) Bio-optical characteristics of PSII and PSI in 33 species (13 pigment groups) of marine phytoplankton, and the relevance for PAM and FRR fluorometry. Journal of Phycology

Johnsen G, Samset O, Granskog L, Sakshaug E (1994b) In-Vivo Absorption Characteristics in 10 Classes of Bloom-Forming Phytoplankton - Taxonomic Characteristics and Responses to Photoadaptation by Means of Discriminant and Hplc Analysis. Marine Ecology-Progress Series 105:149-157

Kirk JTO (1994) Light and Photosynthesis in Aquatic Ecosystems. Cambridge University Press, Bristol

Kolber Z, Falkowski PG (1993) Use of Active Fluorescence to Estimate Phytoplankton Photosynthesis in-Situ. Limnology and Oceanography 38:1646-1665

Kromkamp JC, Domin A, Dubinsky Z, Lehmann C, Schanz F (2001) Changes in photosynthetic properties measured by oxygen evolution and variable chlorophyll fluorescence in a simulated entrainment experiment with the cyanobacterium Planktothrix rubescens. Aquatic Sciences 63:363-382

Kromkamp JC, Forster RM (2003) The use of variable fluorescence measurements in aquatic ecosystems: differences between multiple and single turnover measuring protocols and suggested terminology. European Journal of Phycology 38:103-112

Kroon B, Prezelin BB, Schofield O (1993) Chromatic Regulation of Quantum Yields for Photosystem-Ii Charge Separation, Oxygen Evolution, and Carbon Fixation in Heterocapsa-Pygmaea (Pyrrophyta). Journal of Phycology 29:453-462

Kühl M, Lassen C, Jørgensen BB (1994) Light Penetration and Light-Intensity in Sandy Marine-Sediments Measured with Irradiance and Scalar Irradiance Fiberoptic Microprobes. Marine Ecology-Progress Series 105:139-148

Lefevre D, Bentley TL, Robinson C, Blight SP, Williams PJL (1994) The Temperature Response of Gross and Net Community Production and Respiration in Time-Varying Assemblages of Temperate Marine Micro-Plankton. Journal of Experimental Marine Biology and Ecology 184:201-215

Lewis MR, Smith JC (1983) A Small Volume, Short-Incubation-Time Method for Measurement of Photosynthesis as a Function of Incident Irradiance. Marine Ecology-Progress Series 13:99-102

Longstaff BJ, Kildea T, Runcie JW, Cheshire A, Dennison WC, Hurd C, Kana T, Raven JA, Larkum AWD (2002) An *in situ* study of photosynthetic oxygen exchange and electron transport rate in the marine macroalga *Ulva lactuca* (Chlorophyta). Photosynthesis Research 74:281-293

MacIntyre HL, Kana TM, Anning T, Geider RJ (2002) Photoacclimation of photosynthesis irradiance response curves and photosynthetic pigments in microalgae and cyanobacteria. Journal of Phycology 38:17-38

Markager S, Jespersen AM, Madsen TV, Berdalet E, Weisburd R (1992) Diel Changes in Dark Respiration in a Plankton Community. Hydrobiologia 238:119-130

Marra J (2002) Approaches to the measurement of plankton production. In: Williams PJL, Thomas DN, Reynolds CS (eds) Phytoplankton Productivity:Carbon Assimilation in Marine and Freshwater Ecosystems. Blackwell, Oxford

Morel A (1988) Optical Modeling of the Upper Ocean in Relation to Its Biogenous Matter Content (Case-I Waters). Journal of Geophysical Research-Oceans 93:10749-10768

Morel A (2006) Meeting the challenge of monitoring chlorophyll in the ocean from outer space. In: Grimm B, Porra RJ, Rüdiger W, Scheer H (eds) Chlorophylls and Bacteriophylls, Vol 25. Springer, p 521-533

Morel A, Prieur L (1977) Analysis of Variations in Ocean Color. Limnology and Oceanography 22:709-722

Morris EP, Kromkamp JC (2003) Influence of temperature on the relationship between oxygen- and fluorescence-based estimates of photosynthetic parameters in a marine benthic diatom (*Cylindrotheca closterium*). European Journal of Phycology 38:133-142

Nelson NB, Prezelin BB, Bidigare RR (1993) Phytoplankton Light-Absorption and the Package Effect in California Coastal Waters. Marine Ecology-Progress Series 94:217-227

Neori A, Vernet M, Holm-Hansen O, Haxo FT (1988) Comparison of chlorophyll far-red and red fluorescence excitation-spectra with photosynthetic oxygen action spectra for Photosystem-II in algae. Marine Ecology-Progress Series 44:297-302

Owens TG (1991) Energy transformation and fluorescence in photosynthesis. In: Demers S (ed) Particle analysis in oceanography, Vol NATO ASI series G. Springer Verlag, Berlin, p 101-137

Platt T, Gallegos CL, Harrison WG (1980) Photoinhibition of photosynthesis in natural assemblages of marine phytoplankton. J Mar Res 38:687-701

Platt T, Sathyendranath S (1988) Oceanic Primary Production - Estimation by Remote-Sensing at Local and Regional Scales. Science 241:1613-1620

Prieur L, Sathyendranath S (1981) An Optical Classification of Coastal and Oceanic Waters Based on the Specific Spectral Absorption Curves of Phytoplankton Pigments, Dissolved Organic-Matter, and Other Particulate Materials. Limnology and Oceanography 26:671-689

Raven JA, Beardall J (1981) Respiration and photorespiration. In: Platt T (ed) Physiological Bases of Phytoplankton Ecology, Vol 210. Canadian Bulletin of Fisheries and Aquatic Sciences, p 55-82

Raven JA, Geider RJ (1988) Temperature and Algal Growth. New Phytologist 110:441-461

Revsbech NP (1989) An Oxygen Microsensor with a Guard Cathode. Limnology and Oceanography 34:474-478

Revsbech NP, Jørgensen BB (1983) Photosynthesis of Benthic Microflora Measured with High Spatial-Resolution by the Oxygen Microprofile Method - Capabilities and Limitations of the Method. Limnology and Oceanography 28:749-756

Robinson C (2000) Plankton gross production and respiration in the shallow water hydrothermal systems of Miles, Aegean Sea. Journal of Plankton Research 22:887-906

Sakshaug E (2004) Primary and secondary production in the Arctic Seas. In: Stein R, Macdonald RW (eds) The organic carbon cycle in the Arctic Ocean. Springer-Verlag, Berlin Heidelberg, p 57-81

Sakshaug E, Andresen K, Kiefer DA (1989) A Steady-State Description of Growth and Light-Absorption in the Marine Planktonic Diatom Skeletonema-Costatum. Limnology and Oceanography 34:198-205

Sakshaug E, Bricaud A, Dandonneau Y, Falkowski PG, Kiefer DA, Legendre L, Morel A, Parslow J, Takahashi M (1997) Parameters of photosynthesis: definitions, theory and interpretation of results. Journal of Plankton Research 19:1637-1670

Sakshaug E, Slagstad D (1992) Sea-Ice and Wind - Effects on Primary Productivity in the Barents Sea. Atmosphere-Ocean 30:579-591

Sathyendranath S, Bukata RP, Arnone R, Dowell MD, Davis CO, Babin M, Berthon JF, Kopelevich OV, Campbell JW (2000) Remote Sensing of Ocean Colour in Coastal, and Other Optically Complex Waters, IOCCC, Dartmouth, Canada

Sathyendranath S, Lazzara L, Prieur L (1987) Variations in the Spectral Values of Specific Absorption of Phytoplankton. Limnology and Oceanography 32:403-415

Scheer H (2003) The pigments. In: Green BR, Parson WW (eds) Light-harvesting antennas in Photosynthesis, Vol 13. Kluwer Academic Publishers, p 29-81

Schreiber U, Hormann H, Neubauer C, Klughammer C (1995) Assessment of Photosystem-II Photochemical Quantum Yield by Chlorophyll Fluorescence Quenching Analysis. Australian Journal of Plant Physiology 22:209-220

Schreiber U, Schliwa U, Bilger W (1986) Continuous Recording of Photochemical and Nonphotochemical Chlorophyll Fluorescence Quenching with a New Type of Modulation Fluorometer. Photosynthesis Research 10:51-62

Siegel DA, Dickey TD (1987) On the Parameterization of Irradiance for Open Ocean Photoprocesses. Journal of Geophysical Research-Oceans 92:14648-14662

Smith RC, Baker KS (1978) Optical classification of natural waters. Limnology and Oceanography 23:260-267

Smith RC, Marra J, Perry MJ, Baker KS, Swift E, Buskey E, Kiefer DA (1989) Estimation of a Photon Budget for the Upper Ocean in the Sargasso Sea. Limnology and Oceanography 34:1673-1693

Sosik HM (in press) Characterizing seawater constituents from optical properties. In: Babin M, Roesler CS, Cullen JJ (eds) Real Time Coastal Observing systems for ecosystem dynamics and harmful algal bloom. UNESCO publishing

Steemann-Nielsen E (1952) The use of radio-active carbon (^{14}C) for measuring organic production in the sea. J Cons Int Explor Mer 18:177-140

Strickland JDH, Parsons TR (1968) A practical handbook of seawater analysis. Can Bull Fish Res 167

Suggett DJ, MacIntyre HL, Geider RJ (2004) Evaluation of biophysical and optical determinations of light absorption by photosystem II in phytoplankton. Limnology and Oceanography-Methods 2:316-332

Sukenik A, Bennett J, Falkowski P (1987) Light-Saturated Photosynthesis - Limitation by Electron-Transport or Carbon Fixation. Biochimica Et Biophysica Acta 891:205-215

Vasseur C, Mostajir B, Nozais C, Denis M, Fouilland E, Klein B, Demers S (2003) Effects of bio-optical factors on the attenuation of ultraviolet and photosynthetically available radiation in the North Water Polynya, northern Baffin Bay: ecological implications. Marine Ecology-Progress Series 252:1-13

Webb WL, Newton M, Starr D (1974) Carbon-Dioxide Exchange of Alnus-Rubra - Mathematical-Model. Oecologia 17:281-291

Paper 1

Hancke K, Johnsen G, Sakshaug E (submitted) Spectral light attenuation in the Barents Sea: Impact of pigment signature and relevance for optical depth and primary production.

Deep-Sea Research II

Research article for Deep Sea Research II (CABANERA Special Issue)

SPECTRAL LIGHT ATTENUATION IN THE BARENTS SEA: IMPACT OF PIGMENT SIGNATURE AND RELEVANCE FOR OPTICAL DEPTH AND PRIMARY PRODUCTIVITY

Kasper Hancke*, Geir Johnsen and Egil Sakshaug

Trondhjem Biological Station, Dept. of Biology, Norwegian University of Science and Technology (NTNU), Norway
Postal address: Trondhjem Biological Station, Bynesveien 46, 7018 Trondheim, Norway

* Author of correspondence. E-mail: kasper.hancke@bio.ntnu.no, phone +47 73550841, fax +47 73591595

Running title: Spectral attenuation in relevance to primary production

Abstract

Surface incident irradiance and spectral downwelling irradiance ($E_{z(\lambda)}$) were measured to obtain the spectral attenuation coefficients ($K_{d(\lambda)}$) and optical depth ($\xi_{(\lambda)}$) at twelve stations in the Marginal Ice Zone (MIZ) of the Barents Sea, as part of the Norwegian CABANERA programme. The stations were sorted according to their bloom stage; early, peak and late, based on multidisciplinary data analysis. Profiles of the concentration of chl *a*, dissolved oxygen and primary production (PP) exhibited large variations yet were visually clustered similarly as a function of $\xi_{(PAR)}$, showing close correlations. As a function of $\xi_{(490)}$, the chl *a*-normalised production (PP*) profiles clustered largely above the 10 % $E_{z(490)}$ depth, and the shape of the profiles became more uniform. The optical depth for PAR, $\xi_{(PAR)}$, was correlated to the chl *a* concentration at an r^2 of 0.41, whereas $\xi_{(490)}$ yielded an improved correlation of 0.50. The relationship between downwelling irradiance and PP* showed the highest coefficient of determination in the blue-green region, $E_{z(490)}$ ($r^2 = 0.81$) compared to PAR ($r^2 = 0.66$) and green-orange $E_{z(585)}$ ($r^2 = 0.59$). As phytoplankton related more closely to blue-green irradiance (490 nm) than to PAR and green-orange (585 nm), we therefore suggest using 490 nm when relating phytoplankton production to a single wavelength. Photosynthetic pigment analyses (HPLC) showed that diatoms were predominant during peak phases of blooms whereas smaller cells of Haptophytes (e.g. *Phaeocystis* sp.) and chl *b*-containing algae (e.g. Chlorophytes and Prasinophytes) dominated during early- and late bloom stages. The presented results emphasise the importance of a spectral approach when relating phytoplankton chl *a* and primary production to underwater irradiance. This has implications for improving of primary productivity models and application of remote sensing techniques in the Barents Sea.

Key Words: Spectral attenuation, PAR, Photosynthetic pigments, Marine phytoplankton, Primary production, Barents Sea, Marginal Ice Zone

1. Introduction

The Barents Sea is the westernmost of the Siberian shelf seas and a transition sea between the Arctic Ocean and the Nordic seas. It boundaries to the north and west by steep continental slopes and its average depth is 230 m (Loeng, 1991). The Barents Sea is partly ice covered, primarily by seasonal ice, with a maximal extension in March-April depending on the inflow and temperature of Atlantic water masses (Vinje and Kvambekk, 1991). The latter impose large annual variations, which affect the heat flux into the Barents Sea and causing large variations in the ice cover. The northern and the southern parts of the Barents Sea are divided by the Polar Front, separating the Arctic waters of the north from the Atlantic waters from the south. Close to, and north of the Polar Front, which is most distinct in the western parts at 75 - 76° N, the spring bloom starts in early May induced by the thermally created stratification in the upper 20 - 30 m by the melting of ice (Sakshaug and Slagstad, 1992). As the ice melts, and the ice edge retreats northward, the phytoplankton bloom is triggered in the upper nutrient-rich layer as it becomes gradually more exposed to light. As a result, the intensity of the primary productivity is closely related to ice-edge region, the Marginal Ice Zone (MIZ), and limited by the availability of light (Sakshaug, 1997). The intensive fluctuating physical conditions and horizontal gradients within the MIZ causes pronounced variations in the phytoplankton abundance, pigment concentration, species composition and evidently the primary productivity of the pelagic Barents Sea ecosystem.

The vertical diffuse attenuation coefficient (K_d) of light in a water column is related to the absorption and scattering by phytoplankton, coloured dissolved organic matter (cDOM), and suspended matter (Sathyendranath *et al.*, 2000). In clear oceanic water masses, K_d is mainly influenced by the absorption and scattering of phytoplankton, by sea water itself and in some cases by marine cDOM (Case I waters), while terrigenous cDOM and suspended matter additionally influence the optical properties in coastal waters masses and fjords (Case II waters, Jerlov, 1976; Sathyendranath *et al.*, 2000). The 'optical depth' in a water column is defined as the vertical diffuse attenuation coefficient, spectral or PAR, multiplied by physical depth (Morel, 1988). The optical

depth differs from the physical depth and is independent of this. Thus, a given optical depth will correspond to different physical depths, in waters of different optical properties, yet to the same overall diminution of irradiance (Kirk, 1994). Thus in chl *a*-rich water column, a given optical depth will correspond to a much shallower physical depth than in a chl *a*-poor water column. Phytoplankton biomass (e.g. chl *a*) and productivity are related to optical depth, and can be calculated for PAR or with a spectral resolution.

Pure seawater is transparent mainly to blue light (clearest at 475 nm), followed by green light, and is nearly opaque to red light and UVB (Kirk, 1994). The clearest pre-bloom arctic waters have a vertical attenuation coefficient (K_d) of 0.07 m^{-1} implying that 1% of the surface light reaches a depth of 66 m and 0.1 % of the surface light reaches > 130 m (Dalløkken *et al.*, 1995). Algae, in contrasts to pure seawater, absorb mainly blue to blue-green and red light while being virtually transparent in the green-orange wavelength band. Thus, when a phytoplankton bloom develops, the 1 % light penetration depth decreases more rapidly for blue light than for green-orange light, turning the water greenish. Self-shading by phytoplankton in the water column is therefore considerably more pronounced than apparent from the commonly measured PAR depth (Bricaud and Morel, 1986; Nelson *et al.*, 1993; Sakshaug, 2004). The 1 % irradiance depth (PAR) often is used as an approximation for the euphotic zone (Falkowski and Raven, 1997). However, considering the spectral properties of absorption and of the water itself, this is a rough estimate.

Phytoplankton pigments, chlorophylls (chl's) and carotenoids, can be used as chemotaxonomic markers and to elucidate photo-physiological functionality through knowledge about the ratio between light-harvesting pigments and photo-protective carotenoids (Jeffrey *et al.*, 1997b; Johnsen *et al.*, 1994). The qualitative and quantitative abundance of phytoplankton pigments can be studies by HPLC (High Performance Liquid Chromatography) techniques. Important pigment-group markers can be used to differentiate between major phytoplankton groups; as chlorophyll c_3 and 19´-acyl-oxy-fucoxanthins are major pigment markers for Haptophytes, chl *b* and prasinoxanthin for prasinoxanthin-containing Prasinophytes, while a high fucoxanthin to chl *a* ratio (w:w)

indicate the presence of diatoms (Jeffrey *et al.*, 1997a). Different chl's and carotenoids have absorption maxima at different wavelengths and thus will K_d, in Case I waters with low cDOM, content reflect the concentration and composition of phytoplankton pigment groups (Bricaud *et al.*, 1988; Bricaud *et al.*, 1998).

The aim of the present paper was to evaluate the relationship between the concentration and vertical distribution of chl *a*, dissolved oxygen and primary production to the irradiance field in the water column. Moreover, we wanted to analyse the significance of a spectral resolution compared to PAR of the relationship between irradiance field and the phytoplankton productivity in the water column. The analyses are based on *in situ* data from 12 stations in the MIZ of the northern Barents Sea, sampled during the Norwegian research program 'CABANERA' (Wassmann, this issue). The spectral attenuation is related to optical depth and discussed in a photo-physiological context, including the concentration and composition of phytoplankton pigments and productivity. The present study is relevant for our understanding of the dynamics of the primary producers in the Barents Sea as the productivity by phytoplankton is little related to the day of the year or the physical depths, but instead to the light field as determined by latitude and ice cover and the optical properties, as attenuation and scattering, in the water column.

2. Materials and Methods

2.1. Study area

Sampling was conducted in the Marginal Ice Zone (MIZ) of the northern Barents Sea and across the shelf break into the Polar Ocean during three cruises with research vessel R/V Jan Mayen (University of Tromsø, Norway). The field data in this study were collected as part of the Norwegian research program 'CABANERA'. A total of twelve pelagic stations, of which eleven were partly ice covered, were visited in July 2003 and 2004, and May 2005, respectively. Stations were chosen to represent different bloom-development stages within the MIZ. The stations were sampled in numerical order and numbered by their Roman numbers (Fig. 1). Bloom-development stage, sampling date and position, and ice cover are given in Table 1.

2.2. Sampling

In situ profiles of conductivity, temperature, depth (CTD) and chlorophyll *a* fluorescence were measured using a Sea-Bird CTD (SBE9 system, Sea-Bird Electronic, US) equipped with a Seapoint fluorometer (Chlorophyll Fluorometer, Seapoint Sensors, US). Water was collected from 12 fixed depths (1, 5, 10, 20, 30, 40, 50, 60, 90, 120, 150 and 200 m) and one additional depth in the chl *a*-max layer (defined from the fluorescence profile) if not covered by one of the fixed depths. Water samples for dissolved oxygen measurements and for nutrients were collected using Niskin bottles (5 L, model 1010C), mounted on the CTD rack, from the first cast. Sea water for other analyses was subsequently sampled using Go-Flow bottles (20 and 30 L, General Oceanics) and Niskin bottles (5 L), from the eight upper depths and the four lower depths, respectively.

Water samples for pigment composition analysis (HPLC) were collected at the depth of 1 m "surface" and at chl *a*-max. The *in situ* fluorescence-determined chl *a*-max layer and the *in vitro* measured chl *a*-max layer mismatched at some stations and, thus, did the samples for pigment composition analysis from chl *a*-max not always match the depth of the chl *a*-peak. Volumes of 1000 - 3000 mL, depending on the chl *a*

concentration, were filtered onto Whatman GF/F glass fibre filters <15 h after sampling (stored in the dark at 2 ^{o}C in 15 L plastic containers until filtered). Two to four replicates were filtered when possible. Filters were frozen immediately at –20 ^{o}C and subsequently transported and stored in liquid nitrogen (–196 ^{o}C) or in a bio-freezer (–80 ^{o}C) until analysed in the laboratory at Trondhjem Biological Station (Trondheim, Norway) within three months from sampling.

2.3. Pigment analysis

Pigment composition analysis was performed using a Hewlett-Packard HPLC 1100 Series system, equipped with a quaternary pump system and diode array detector. Pigments were separated is a Waters Symmetry C8 column (150 × 4.6 mm, 3.5 µm particle size) using the method described by Zapata et al. (2000), as modified by Rodriguez et al. (2006). The frozen filters with algae were extracted, in Teflon-lined screw-capped tubes, in 1.5 mL of methanol overnight at –20 °C. The extract was re-filtered (Millipore 0.2 µm) to remove debris, and 154 µL of the final extract was injected in to the HPLC system, using an automatic injection system. Chlorophylls and carotenoids were quantified by their absorbance at 440 nm and identified by a diode array detector (λ = 350-750 nm, 1.3 nm spectral resolution). Calibration of the HPLC system was performed using standards for chl *a* from Sigma (C6144, Aldrich, UK) and custom isolated standards for carotenoids and chl *c*, made using a preparative column on the same HPLC instrument (Rodriguez *et al.*, 2006, K. Andresen unpub.). Identification of pigments and specific extinction coefficients for quantification followed procedures recommended by Jeffrey et al. (1997a).

2.4. Measurements of nutrients, chl *a*, dissolved oxygen and primary production

Sea water samples for nitrate and phosphate analyses were drained directly from the Niskin bottles and subsequently frozen and stored for later analysis. The nutrients were analysed on a Scalar Autoanalyser (Scan Plussystem, Netherlands) by the National Environmental Research Institute in Roskilde, Denmark (Kivimäe, Pers. Comm.). Chl *a* was measured from sea water samples filtered on GF/F filters, extracted overnight in pure methanol. The concentrations of chl *a* and phaeophytin were determined before

and after acidification (Holm-Hansen *et al.*, 1965) using a calibrated fluorometer (Turner Designs) by (Hodal and Kristiansen, this issue).

Sea water for dissolved oxygen concentration measurements were cautiously drained directly from the Niskin bottles into 125 mL dark glass bottles (Winkler type), which were closed immediately with a gas-tight lid. The oxygen concentration was measured on-board within an hour using an O_2-microelectrode (Clark type, Unisense, Denmark) calibrated against an atmosphere-saturated and an oxygen-depleted sample. The samples and the calibration solutions were temperature-stabilised prior to measurements, in a water bath at 1 ^{o}C for 20 min, due to the temperature sensitivity of the oxygen sensor. The oxygen sensor was connected to a picoammeter (Unisense) and the output was read from a flatbed recorder (Kipp & Zonen, The Netherlands).The atmospheric saturation of oxygen in each sample was calculated as a function of temperature and salinity according to Li and Gregory (1974).

Primary production rates were obtained from 24 h *in situ* incubations using the ^{14}C-incorporation technique (Steemann-Nielsen, 1952) by Hodal and Kristiansen (this issue). Water from the eight upper depth and for chl *a*-max were enriched with ^{14}C-labeled bicarbonate and incubated at the respective depths in light and dark bottles. Subsequently, the water samples were filtered after which the filters were frozen for later analysis on a scintillation counter ashore.

2.5. Irradiance measurements

Surface incident irradiance and repeated downward irradiance profiles were measured with a spectral resolution of 1 nm, from 380 to 800 nm, using an underwater spectroradiometer (RAMSES 101, TRIOS, Germany). Profiles were conducted lowering the instrument 'by hand', and irradiance was measured with a vertical resolution of 1 m in the upper 10 m, and 5 to 10 m below the 10 m depth (depending on the attenuation) down to <0.1 % incident irradiance depth (max 90 m). Profiles were preferably measured from nearby ice flows in order to representative *in situ* conditions (and avoid shading by the ship) at approximately solar noon and midnight at each station. Data were collected on a PC and the instrument pack was power-supplied from a 12V car battery, through a 12-200 V converter, when running on ice flows.

2.6. Calculations

The vertical attenuation of light, which is a consequence of both absorption and scattering of light, is spectrally dependent. The vertical attenuation coefficient for a specific wavelength ($K_{d(\lambda)}$, m^{-1}) for downwelling irradiance was calculated as Eq. 1 (Kirk, 1994)

$$K_{d(\lambda)} = \frac{-\ln\left(E_{0(\lambda)} / E_{z(\lambda)}\right)}{z} \qquad (1)$$

where $E_{0(\lambda)}$ and $E_{z(\lambda)}$ are the values of downwelling irradiance at a specific wavelength just below the surface, and at z m depth, respectively. The spectral-specific optical depth, $\xi_{(\lambda)}$, was then calculated for the same wavelength, from Eq. 2 (Kirk, 1994; Morel, 1988)

$$\xi_{(\lambda)} = K_{d(\lambda)} z \qquad (2)$$

In the present study we have calculated $K_{d(\lambda)}$ and $\xi_{(\lambda)}$ for 490 and 585 nm to represent the blue-green and green-orange wavelength bands, respectively. The spectrally-averaged (4-700 nm) attenuation coefficient, $K_{d\,(PAR)}$, was calculated using Eq.1, replacing $E_{0(\lambda)}$ and $E_{z(\lambda)}$ with downwelling PAR just below the surface, $E_{0(PAR)}$, and at z m depth, $E_{z(PAR)}$, respectively. Similarly, the spectrally-averaged optical depth, $\xi_{(PAR)}$, was calculated from Eq. 2, replacing $K_{d(\lambda)}$ with $K_{d(PAR)}$. $E_{0(PAR)}$ and $E_{z(PAR)}$ were calculated by integrating the spectral irradiance data from 400 to 700 nm. As a consequence of the logarithmic relationship in Eq. 1, the 1% attenuation depth for a certain water column will correspond to an optical depth of 2.3 (Eq. 2). Similarly, did the 0.1% attenuation depth corresponds to an optical depth of 4.6.

3. Results

3.1. Position and bloom-development stage of sampling stations

The twelve sampling stations were geographically positioned in different regions of the Northern Barents Sea (Fig. 1) and were divided into northern shelf-break stations (VII and XIV), interior stations (II, III, X, XI, XIII) and southern MIZ stations (I, IV, XVI, XVII, XVIII) (Sundfjord *et al.*, this issue). The northern and the interior stations were located north of the Polar Front, where the southernmost stations were at the Polar Front. The hydrographical characteristics and the prevalence of water masses differed markedly between stations. The northernmost stations were strongly influenced by Arctic Water (temperature $<-1^{o}$C and salinity between 34.4 and 34.7 (Pfirman *et al.*, 1994)) and the southernmost by Atlantic Water (temperature $>3^{o}$C and salinity >34.95 (Carmack, 1990)), with the two water masses mixed intensively in the interior (Sundfjord *et al.*, this issue). Station XIII and XVIII were strongly influenced by tidal and wind-driven mixing, respectively (Sundfjord *et al.*, this issue). Station XVIII was the only station which was not covered by sea ice during sampling, and the station was exposed to storm conditions immediately prior to sampling.

The sampling stations were grouped into three bloom-development stages; early, peak and late bloom, as none of the stations represented pre- or post-bloom situations (Table 1). The grouping of the stations were achieved from multidisciplinary data analysis; including profiles of CTD data, nutrients (Kivimäe *et al.*, submitted to J. Mar. Res.), dissolved oxygen (this study), chl *a* and ^{14}C-assimilation (Hodal and Kristiansen, this issue), and vertical transport of particulate organic matter (POM) (Reigstad, this issue). The optical properties of the water column were not considered when stations were grouped and can therefore be related independently to the development stage of the bloom at each station.

3.2. Pigment composition

The phytoplankton pigment composition in the water column was analysed at each station. Ratios of light-harvesting carotenoids (LHC), chl's, photo-protective carotenoids (PPC) and degraded pigments (deg.pig.) to chl *a* were calculated to

elucidate the pigment signature and physiological state of phytoplankton cells at different bloom stages (Table 2). Replicate samples from 1 m and chl *a*-max, respectively, were pooled for each station.

The overall dominating light-harvesting carotenoid was fucoxanthin (fuco), which was found at all stations at ratios to chl *a* of 10 to 54 % (w:w, Table 2). Fucoxanthin is a major chemotaxonomic marker for Chromophytes (with exception of Cryptophytes and Dinophytes). Peridinin and *cis*-peridinin (a degradation product of peridinin) specific marker for Dinophytes, were found only at the early-bloom stations XVII and IV, with ratios of 7 and 4 %, respectively. At the early- and late-bloom stations, a relatively high ratio to chl *a* was observed of 19'-butanoyl-oxy-fucoxanthin (19'But, 1-5 %) and 19'-hexanoyl-oxy-fucoxanthin (19'Hex, 1-12 %). This co-varied with a high chl c_3 to chl *a* ratio (4-9 %) indicating the presence of Haptophytes (e.g. *Phaeocystis* sp.). These group-specific pigments are relatively stable chemotaxonomic markers and show little variance (< 25 %) as a function of photo-acclimation status (Rodriguez *et al.*, 2006). The peak-bloom stations showed the highest ratios of fucoxanthin to chl *a* (23-54 %) and relatively low ratios of other group-specific markers to chl *a*, indicating a dominance of diatoms. Station XVI, for example, showed to be diatom dominated (~ 90 % of biomass) indicated by a high fuco:chl *a* ratio (54 %), chl c_{1+2}:chl *a* ratio (26 %), low chl c_3:chl *a* ratio (3.5 %) and absence of other group-specific pigment markers (Table 2).

The ratio of the pooled PPC, the sum of diadinoxanthin (diadino) and diatoxanthin (diato) to chl *a*, was higher for the surface samples (5-25 %) than for the chl *a*-max samples (12-16 %, Table 3), indicating a ample light regime in the surface waters at all the stations.

Chl *b* was present at most stations with ratios to chl *a* of 1-20 %, indicating the presence of Chlorophytes, Euglenophytes and/or Prasinophytes. The highest ratios tented to be associated with the early- and late-bloom stations (and the peak-bloom station X) and support the importance of chl *b*-containing phytoplankton during these bloom conditions (Egeland *et al.*, 1995, Table 2 and 3). The co-existence of chl *b* with prasinoxanthin (prasino) at station XVIII emphasise the presence of prasinoxanthin-

containing Prasinophytes. The apparent high ratio of chl *b* to chl *a* at station X was found in the surface waters and associated with a low chl *a* concentration (0.3 mg m^{-3}), and was consequently linked to a low signal to noise ratio (data not shown).

3.3. Downwelling irradiance and spectral attenuation

Vertical profiles of $E_{z(PAR)}$, in per cent of the immediate sub-surface irradiance, $E_{0(PAR)}$, is a function of the total attenuation of light in the water column, and is shown for all early-, peak- and late bloom stations (Fig 2a-c). Absolute values of incident irradiance, E_{PAR} (µmol photons m^{-2} s^{-1}), $E_{0(PAR)}$ and the 10 % and 1 % attenuation depths (the depth at which $E_{z(PAR)}$ equalled 1 % and 10 % of $E_{0(PAR)}$) are given in Table 4. The shape of the $E_{z(PAR)}$ profiles and the 1% attenuation depth for each station illustrate the overall optical properties for the three bloom-development stages.

The early-bloom stations were characterised by a deep PAR penetration, as clearly observed from the deep 1 % attenuation depth (especially at station VII, Fig 2a). In contrast, the peak-bloom stations were characterised by shallower attenuation depths, especially at station XIV and XVI (Fig 2b), resulting from strong light attenuation due to high pigment concentrations. The late-bloom stations showed a deeper PAR penetration than the peak-bloom stations and hence a deeper 1% depth, which corresponded to lower pigment concentrations, as typically during late-bloom conditions.

Station VII, XVI and I were selected to represent each of the bloom-development stages as examples for the early- peak- and late-bloom stage conditions, respectively, and profiles of the downwelling irradiance at 490 nm, 585 nm and PAR are shown (Fig 3a-c). The early-bloom station VII was characterised by "clear blue waters" as seen from the deep penetration of blue light (490 nm) and a relatively shallower penetration of green-orange light (585 nm). The attenuation of green-orange light by the water itself is stronger than for blue light, and the deep blue-light penetration observed at this station is characteristic for waters containing <1 mg chl *a* per m^3 (Morel, 1988). The peak-bloom station XVI was characterised by greenish water as seen from similar attenuation of 490 nm, 585 nm and PAR, as the high algae biomass ([chl *a*] >10 mg m^{-3}) effectively absorbed the light at 490 nm (primarily by fuco, Johnsen *et al.*, 1992). The irradiance at

585 nm, however, was only weakly attenuated compared to the clear waters of the early bloom demonstrating a neglectable phytoplankton absorption at 585 nm, even though chl c_3 absorb efficiently at this wavelength band (Johnsen *et al.*, 1992). At the late-bloom station I, the water (again) turned blue, showing a deeper light penetration at 490 than at 585 nm, and a 1 % attenuation depth at 490 nm >70 m. The chl *a* concentration of station I was <1 mg m^{-3} (Fig 3c).

Spectral attenuation coefficients, $K_{d(\lambda)}$, at 490 nm, 585 nm and PAR, as a function of depth, are shown for station VII, XVI, and I (Fig 4a-c). The attenuation coefficient was up to 6 times higher at the peak-bloom station (XVI) than for the early- and late-bloom stations (VII and I), mainly due to a strong light absorption by phytoplankton pigments, leading to a shallow light penetration depth. This observation was emphasised by the higher attenuation at 490 nm than at 585 nm (and PAR) for the peak-bloom station and opposite for the early- and late-bloom stations, respectively. For station XVI the 490 and 585 nm irradiance were attenuated beyond the sensitivity of the spectroradiometer (<0.0001 µmol photons m^{-2} s^{-1} $wavelength^{-1}$) at >20 m depth. The relationship between the optical and the physical depth at 490 nm, 585 nm and PAR is shown for station VII, XVI and I as examples (Fig 4d-e).

3.4. Optical *versus* physical depth

Vertical profiles of chl *a* concentration, concentration of dissolved oxygen and primary production rate were related to physical depth, optical depth for PAR and for 490nm, and analysed according to bloom development stage (Fig. 5-7). At the early-bloom stations the chl *a* concentration was <3.4 mg m^{-3} and associated with the upper surface waters showing chl *a*-max depths shallower than 10 m, as typical for early bloom conditions. Station VII, representing the earliest registered stage of a bloom, showed a chl *a*-max of only 0.9 mg m^{-3} at 1 m depth (Fig. 5a). The peak-bloom station chl *a*-max was related to depth between 10 and 30 m, with values of 3.0 to 12.8 mg chl *a* m^{-3} (Fig 5b). At the peak-bloom stations the chl *a* concentration was diminished in the surface waters as compared to the chl *a*-max, except at station XIV and XVI where the chl *a* concentration was high (>9 mg m^{-3}) from the surface down to the chl *a*-max and further below to 30m (fig. 5b). Station XIV and XVI represented the two bloom stations with

highest chl *a* concentration. At the only true late-bloom station (I) chl *a* showed a deep maximum at 37 m and was absent (<0.1 mg m^{-3}) at the surface (<10 m, Fig 5c).
The vertical distribution of chl *a* as a function of the optical depth, $\xi_{(PAR)}$, showed that the chl *a*-max correlated to an optical depth between the 10 % and 1 % attenuation depth (equal to $\xi_{(PAR)}$ between 2.3 and 4.6), at most of the stations (Fig 5d-f). Two exceptions were found at station XIV and XVI, where the chl *a* concentration showed no clear correlation with $\xi_{(PAR)}$. This was caused by the high $K_{d(PAR)}$ and shallow light penetration depth observed at these two stations. Then the chl *a* distribution was analysed as a function of $\xi_{(490nm)}$ the maximum chl *a* concentration (and shape of the profiles) largely moved 'up-ward' and correlated closely to the 10 % depth (where the irradiance at 490 nm equalled 10 % of the immediate sub-surface irradiance at 490 nm, Fig 5g-i).

The distribution of dissolved oxygen in a water column reflects the net result of biological activity and physical transport mechanisms as advection (mixing) and molecular diffusion. In a stratified water column, the biological activity will govern the distribution of dissolved oxygen, as advection is minimal and the importance of molecular diffusion is restricted to a mm scale. The net biological activity is thus the result of biological oxygen consumption (respiration) and production (photosynthesis) rates.
The *in situ* distribution of oxygen at the visited stations varied from 87 to 122 % of the atmospheric oxygen saturation (Fig. 6). The oxygen distribution was by large sub-saturated (<100 % saturation) throughout the water column at the early-bloom stations (Fig. 6a), and super-saturated (>100 %) in the upper waters of the peak-bloom stations (Fig. 6b). At the peak-bloom stations the oxygen distribution showed distinct profiles with maximum levels in the upper 20 m and sub-saturated oxygen levels below 30 to 50 m (Fig. 6b). At the late-bloom station I, the oxygen level was weakly super-saturated in the upper ~40 meters and sub-saturated below, suggesting that the oxygen consumption rate exceeded the production rate (resulting in a net consumption) at this station, which led to the reduction of the oxygen peak as observed predominate at the peak-bloom stations (Fig. 6c). The vertical oxygen distributions as a function of $\xi_{(PAR)}$ tended to show peak values that correlated at the 10 % irradiance depth, again, with exception for

station XIV and XVI and the mixed station XVIII (Fig. 6d-f). As a function of $\xi_{(490nm)}$ the oxygen profiles 'compressed' to a shallower optical depth and the oxygen level tented to be at equilibrium (~100 % atmospheric saturation) at the 10 % attenuation depth, for both the peak- and late-bloom stations (Fig. 6g-i).

The primary production was associated with the surface waters (<20 m) at the early-bloom stations overall descending deeper and deeper in the water column, as the bloom stage developed, towards the deep (30-40 m) primary production observed at the late-bloom station (Fig. 7a-c). Re-analysed, as a function of optical depth, revealed that the primary production were related to the region in the water column with an irradiance regime between 10 and 1 % of $E_{0(PAR)}$ and above 10 % of $E_{0(490)}$, most pronounced at the deep-production stations (I, III and X, Fig. 7d-i). These results indicate that the primary production is related not to the depth in metres but to optical depth. A more detailed description of the primary production rates and the chl *a* distribution can be found in (Hodal and Kristiansen, this issue).

Chl *a*-normalised primary production rates illustrate the light-dependent production as the implication of the chl *a* concentration is neutralised (Fig 8). Consequently, the profiles illustrate the light-harvesting characteristics and capacity of the phytoplankton community, reflecting the light availability for photosynthesis throughout the water column. The chl *a*-normalised production ranged from ~9 to 30 mg C (mg chl *a*)$^{-1}$ d^{-1} in the surface and decreased rapidly approaching zero between 10 and 50 meters (Fig 8a-c). The shape of the normalised primary production profiles was generally alike for the different stations, but reach zero at different depths. When the profiles were analysed as function of $\xi_{(PAR)}$ the profiles were more tightly clustered (than as a function of physical depth) and decreased to values below 0.5 mg C (mg chl *a*)$^{-1}$ d^{-1} near the 1% depth, with a few exceptions (Fig. 8d-f). As a function of $\xi_{(490nm)}$, the profiles clustered even closer with the majority of stations reaching a chl *a*-normalised production rate below 2 mg C (mg chl *a*)$^{-1}$ d^{-1} at the 10% depth and below 0.5 mg C (mg chl *a*)$^{-1}$ d^{-1} above the 1% depth (Fig 8g-i). The exceptions will be discussed (in section 4.3).

4. Discussion

In the Marginal Ice Zone of the Barents Sea, phytoplankton blooms are triggered by the melting of sea ice, creating stratification, which leaves phytoplankton suddenly exposed to strong light (Sakshaug and Slagstad, 1992). The intensive fluctuating physical conditions and horizontal gradients within the MIZ causes pronounced variations in the phytoplankton abundance, pigment concentration, species composition and evidently the primary productivity. In the Barents Sea, $K_{d(\lambda)}$ and $\xi_{(\lambda)}$ are mainly influenced by the absorption and scattering of phytoplankton and by sea water itself, as we assumed marine cDOM concentrations to be low (Sathyendranath *et al.*, 2000; Vasseur *et al.*, 2003) and terrigenous cDOM to be neglectable, even though cDOM is little studied in the Arctic (Sakshaug, 2004).

4.1. Pigment concentration and composition

The chl *a* concentration profiles generally reflected the bloom stage of the phytoplankton community (Fig 5). The chl *a* varied from low concentrations at the early-bloom station VII, to high concentrations at the chl *a*-dense bloom station XVI. The station representing the latest stage of a bloom, station I, showed a deep, low chl *a* concentration with maximum at 37 m (the deepest observed of all stations). The water-column integrated chl *a* concentration ranged from 12 to 588 mg chl *a* m^{-2} as the integrated values at the earliest to the peak bloom stations, VII and XVI, respectively, was almost 50 fold (Hodal and Kristiansen, this issue).

The peak-bloom stations were generally dominated by diatoms, as identified from the fuco to chl *a* ratios of 23 to 54 % and low abundance of other major pigment markers for phytoplankton (Table 2 and 3); such as for Haptophytes (19'But, 19'Hex, chl c_3), Dinophytes (peridinin, chl c_2) and prasinoxanthin-containing Prasinophytes (prasinoxanthin, chl *b*). A general diatom dominance at the peak-bloom stations were supported by Hodal and Kristiansen (this issue); they found larger cells (>10 μm) to account for 50 to 97 % of the chl *a* concentration and responsible for 35 to 100 % of the

primary production. A diatom dominance is commonly observed during peak bloom conditions in the Barents Sea (von Quillfeldt, 2000).

Isolation of chl *b* from the peak bloom stations and absence of prasino, 19'Hex and 19'But (except at station III), lead us to conclude that the chl *b* originated from Chlorophytes (Jeffrey *et al.*, 1997a), presumable abundant at most of the peak bloom stations (Table 2). An exception among the mostly diatom-dominated peak-bloom stations, were indicated at station X were Hodal and Kristiansen (this issue) found a large fraction of small-celled (<10 μm) phytoplankton, accounting for 52-61 % of the chl *a* biomass and 71-91 % of the production, atypical for the peak bloom stations. This observation concurred with the highest ratio of chl *b* that we isolated from the peak-bloom stations (Table 2), and suggests an importance of a picophytoplankton community (cells <3 μm). Picophytoplankton are not distinguishable in light microscopes and are often overlooked in classical studies of algae composition. Thus, we know little about their contribution to the primary production and importance for the ecosystem in the Barents Sea (Not *et al.*, 2005), though they have been reported to be numerous occasionally (Throndsen and Kristiansen, 1991). A resent study indicates that Prasinophytes can be a major component in truly Arctic waters while Haptophytes are prominent in more Atlantic waters (Not *et al.*, 2005). These observations support our findings. HPLC signature studies of distinct phytoplankton pigment marker may be of great taxonomic and ecological significance for future studies of picophytoplankton and their importance for the primary production in the Barents Sea.

The pigment signature for the early- and late-bloom stations suggested larger phytoplankton diversity than at the peak-bloom stations and an increased importance by small-cell phytoplankton groups during early and late bloom conditions seemed likely. This, we concluded from high ratios of chl c_3:chl *a* and the coherence of 19'But, 19'Hex and chl c_3 proposing the presence of Haptophytes especially in the surface waters at the early-bloom stations and at chl *a*-max at the late-bloom stations (Table 2 and 3). The presence of prasinoxanthin in combination with chl *b* in the samples from chl *a*-max argues for a significance of prasinoxanthin-containing Prasinophytes during early- and late-bloom conditions. A higher ratio of PPC to chl *a* in the surface samples than at chl

a-max demonstrated a ample light regime in the surface waters (Moline, 1998), pronounced at the peak- and late-bloom stations (Table 3). At late bloom scenarios, high PPC ratios are typically observed in relation to nutrient starvation and correlated within our data of a high abundance of degraded pigments during late bloom (Table 2 and 3). The major phytoplankton pigment groups have absorption maximum at different wavelength (Johnsen *et al.*, 1994). This implies that the spectral attenuation is dependent on both the composition and the concentration of phytoplankton pigments.

4.2. Chl *a* and dissolved oxygen as a function of optical *versus* physical depth

Profiles of chl *a* concentration and the dissolved oxygen concentration showed a natural large variability when plotted as a function of depth in metres, during both early-, peak- and late-bloom conditions (Fig. 5-6a-c). However, the variables showed a trend of aligning in comparable curvatures when plotted as a function of optical depth calculated for PAR, $\xi_{(PAR)}$, instead of physical depth (Fig 5-6d-f). When data were plotted as a function of optical depth, calculated from the attenuation at 490 nm ($\xi_{(490)}$) uniformity in the shape of the profiles became increasingly clear (Fig 5-7g-i).

Station XIV and XVI were apparently divagating to the above described uniformity in shape as a function of optical depth, which was observed as a deep chl *a* distribution exceeding the light penetration depth (Fig. 5e+h). This was observed from a high chl *a* concentration (>9 mg m^{-3}) at optical depths below 8. This phenomenon can be explained as chl *a* biomass being 'build up' during an earlier stage of the bloom holding lower chl *a* concentration and deeper light penetration (e.g. as at station XVII). As the biomass and the chl *a* concentration has increased in the well-illuminated surface waters, absorption and inter- and intra cellular shading by the phytoplankton in the water column has become increasingly pronounced (Mitchell and Kiefer, 1988; Sakshaug and Slagstad, 1991), causing the irradiance to decrease to less than 0.1 % of E_0 at 20 m depth (Fig. 2b). Thus did the chl *a* distribution at station XIV and XVI not correlate directly with optical depth (Fig 5e+h). A chl *a* accumulation in the surface layer of the MIZ is a typical event during the few weeks of ice melting, particularly in the strongly stratified waters north of the Polar Front (Wassmann, 2002).

Analysing the accumulated chl *a* concentration down through the water column at all the stations, as a function of optical depth showed that PAR explained 41 % ($r^2 = 0.41$, Fig 9a) of the variance in the total chl *a* distribution. As a function of $\xi_{(490)}$ the correlation improved to 50 % ($r^2 = 0.50$, Fig 9b). The accumulated data showed, that during early- and late-bloom conditions, characterised by a low chl *a* concentration and deep light penetration, $k_{d(\lambda)}$ of water itself is more important than $k_{d(\lambda)}$ of phytoplankton. Such conditions resulted in data points 'below' the regression line of Fig 9. Contrary, the relationship between the accumulated chl *a* concentration and $\xi_{(490)}$ exclusively for the chl *a*-rich stations XIV and XVI, [chl *a*] >9 mg m^{-3}, showed a near 100 % correlation ($r^2 = 0.99$, inlet in Fig. 9b). This showed that chl *a*, representing the phytoplankton biomass, correlated to the total light absorption down to an optical depth of ~9, corresponding to ~0.01 % of the surface irradiance at 490 nm (Fig. 3). The optical depth at 585 nm only explained 9 % of the total variance in the accumulated chl *a* concentration (Fig.9c). These results are consistent with findings in the North Water Polynya by Vasseur *et al.* (2003). They found chl *a* and particulate organic carbon (POC) to be the most influencing components on $K_{d(\lambda)}$ and to account for 36 to 83 % of the variance in light attenuation (Vasseur *et al.*, 2003).

The concentration and distribution of dissolved oxygen supported the ordering of the stations into the particular development stages, reflecting sub saturated concentration at the early-bloom stations and super saturation in the light exposed surface waters at the peak-bloom station (Fig. 6). The fact, that the oxygen profiles correlated closely to the light attenuation, especially at 490 nm, implies that the oxygen production by phytoplankton is easily recognised in the water column. The oxygen concentration reflects the net result of the oxygen production and the oxygen consumption within a water column. Accordingly, do oxygen profiles store information of the community production (Pomeroy, 1997). As for chl *a*, the close correlation between the dissolved oxygen profile and the optical depth divagated at station XIV and XVI (Fig. 6e+h). The explanation is parallel to that for chl *a*, as the 'build up' of chl *a* by an efficient photosynthetic activity, as well 'builded up' a super saturation of oxygen, which at time of sampling were below the 1 % attenuation depth. We suspect, however, that this must

have happened recently as the dissolved oxygen concentration, at sampling, still was super saturated.

4.3. Primary production as a function of optical *versus* physical depth

The two main controlling factors for primary production in a water column are the light regime and the nutrients (Sakshaug, 1997). At sufficient surface irradiance, nutrients become limited in the surface waters and are depleted with increasing photosynthetic activity, as during bloom conditions (Falkowski and Raven, 1997; Sakshaug *et al.*, 1994). Our data are in agreement with such a scenario, as the biomass (as chl *a*) and the primary production descended as a function of physical depth (Fig. 7), leaving the surface waters relative clear to light penetration (Fig. 2), in accordance with Kirk (1994) and Sakshaug and Slagstad (1991). As a result, did the phytoplankton decent in the water column but remained positioned in water masses of similar optical properties, resulting in uniform profiles when plotted as a function of optical depth (Fig. 7+8).

The chl *a* normalised primary production (Fig. 8) showed a strong correlation when rates were plotted as a function of $\xi_{(PAR)}$ and an even more uniform profile shapes as a function of $\xi_{(490)}$. As seen from Fig. 8d-f, the majority of the normalised production decreased and approached zero near the 1 % attenuation depth as a function of $\xi_{(PAR)}$. As a function of $\xi_{(490)}$ the profiles clustered even closer and approached zero higher up in the water column near the 10 % depth. These results illustrated that the primary production was strongly related to optical depth and the water column light regime. Based on these findings we concluded, that the chl *a* normalised primary production related stronger to the blue irradiance regime, at 490nm, than to PAR (Fig. 8g-i). The conclusion was supported when all data of chl *a*-normalised production rates were plotted as a function of the $E_{z(PAR)}$ and $E_{z(490)}$, respectively (Fig. 10). The compiled data showed that 66% ($r^2 = 0.66$) of the variance in the normalised production could be explained by PAR (Fig. 10a), while 81 % ($r^2 = 0.81$) could be explained from the downwelling irradiance at 490 nm (Fig. 10b). A strong correlation between the irradiance at 490 nm and primary production is consistent with the average absorption spectrum for the identified dominating phytoplankton groups (Johnsen *et al.*, 1992) and illustrate that the phytoplankton community of the MIZ respond spectrally equivalent to

temperate and tropical phytoplankton ecosystems (Bouman *et al.*, 2000; Bricaud *et al.*, 2004). The irradiance at 585nm (green-orange light) showed a coefficient of determination (r^2) to normalised primary production of 0.59 and verified at weak importance of green-orange light for photosynthesis (Fig. 10c). Additionally to PAR, 490 nm and 585nm we tested the relationship between 440 nm and the normalised production. The data showed a weaker relationship than for 490 nm, giving an $r^2 = 0.77$ for the relationship between $E_{z(440)}$ and the normalised primary production (data not shown).

An apparent exception to the trend of uniformity for the profile shape was observed at station XIV (Fig. 8) where the chl *a* normalised production was higher below the 10 and 1% attenuation depth, than at the remaining stations. This optical deeper production lead to a >3 times higher integrated primary production at station XIV (1475 mg C m^{-2} d^{-1}) than for instance at station XVI (405 mg C m^{-2} d^{-1}, Hodal and Kristiansen, this issue), having a similar chl *a* concentration and distribution, as well as light attenuation properties (Fig. 2b and 5). The high production efficiency observed at station XIV could have several explanations. First, the phytoplankton community at station XIV could be stronger low-light acclimated than compared to station XVI, resulting in increased photosynthetic efficiency per chl *a* (Behrenfeld and Falkowski, 1997; Johnsen and Sakshaug, 1996) caused by a higher quantum yield for C-fixation (Hancke *et al.*, submitted). Secondly, the nutrient concentrations were markedly higher at station XIV (>0.8 µmol NO_3/kg at 0 to 20 m) compared to station XVI (<<0.1 µmol/kg at 0 to 20 m) stimulating a higher and longer-lasting primary production. This kept the phytoplankton cells at an exponential growth phase at station XIV compared to a more stationary-phase at station XVI. The higher nutrient input at station XIV was primary imposed by vertical mixing, constrained by the hydrodynamic conditions of the continental slope zone, were the station was located (Fig. 1, Sundfjord *et al.*, this issue). Thirdly, a difference in the species composition of the dominating diatoms were observed between the two stations, from microscope analyses (T. Ratkova, pers. comm.), even through the composition of the major phytoplankton pigments did not differ, as observed from pigment analyses (Table 3). At station XIV typically early bloom species as Bacterosira spp. (typical in Atlantic waters) seemed to be dominating, while more typical late bloom

species as Thalassiosira spp. and Chaetoceros spp. seemed to dominate at station XVI (Reigstad, this issue, and T. Ratkova pers. comm.).

4.4 Conclusions

In the present study we have evaluated the downwelling irradiance and the spectral attenuation coefficients in relation to concentration and vertical distribution of chl *a*, dissolved oxygen and primary production. Concentration profiles of these variables showed large natural variations but clustered into similar shapes as a function of $\xi_{(PAR)}$, showing close correlations. As a function of $\xi_{(490)}$ the correlation became more clear and the shape of the profiles more uniform (Fig. 5-8). The optical depth for PAR, $\xi_{(PAR)}$, explained 41 % ($r^2 = 0.41$, Fig 9a) of the variance in the accumulated chl *a* concentration down through the water column, while $\xi_{(490)}$ improved this correlation to 50 % ($r^2 = 0.50$, Fig 9b). The downwelling irradiance and the chl *a*-normalised primary production showed a closer relationship in the blue region, at 490 nm, than for PAR, as the normalised production as a function of $E_{z(490)}$ gave an $r^2 = 0.81$ and of $E_{z(PAR)}$ gave $r^2 = 0.66$ (Fig. 10). Based on these findings we concluded that phytoplankton related stronger to blue-green irradiance at 490 nm than to PAR and 585 nm, and we hence suggest using 490 nm instead of PAR when relating phytoplankton production to a single wavelength band, in agreement with Kyewalyanga *et al.* (1992). This will according to our data, improve the correlation to measured primary production of ~15 % (Fig 10). Our results reflect that phytoplankton essentially absorb blue light in natural water columns. It follows that inter- and intra cellular shading by phytoplankton is much stronger in blue light than in PAR and green light, of relevance for calculating the critical depth. Diatoms seemed to be predominant during peak bloom whereas smaller cells of Haptophytes (e.g. Phaeocystis sp.) and chl *b*-containing algae (e.g. Chlorophytes and Prasinophytes) seemed dominating during early- and late bloom. The present study is relevant for our understanding of the dynamics of the primary production in the Barents Sea. Improved understanding of the spectral attenuation and phytoplankton composition during bloom stages in the MIZ is important for advancement of primary productivity models and application of remote sensing techniques in the Barents Sea.

Acknowledgements

We sincerely thank P. Wassmann and his ‘right-hand’ group for arrangement and logistics of three successful cruises in the Barents Sea. The captain and crew of R/V Jan Mayen (UiT) and the CABANERA participants are thanked for an always enjoyable working climate and miscellaneous assistance during field work. K. Andresen is thanked for HPLC analyses. This study is part of the project "Carbon flux and ecosystem feed back in the Northern Barents Sea in an era of climate change" (CABANERA) financed by the Norwegian Research Council (project number: 155936/700).

References

Behrenfeld, M.J., Falkowski, P.G., 1997. A consumer's guide to phytoplankton primary productivity models. Limnology and Oceanography 42 (7), 1479-1491.

Bouman, H.A., Platt, T., Sathyendranath, S., Irwin, B.D., Wernand, M.R., Kraay, G.W., 2000. Bio-optical properties of the subtropical North Atlantic. II. Relevance to models of primary production. Marine Ecology-Progress Series 200, 19-34.

Bricaud, A., Bedhomme, A.L., Morel, A., 1988. Optical-Properties of Diverse Phytoplanktonic Species - Experimental Results and Theoretical Interpretation. Journal of Plankton Research 10 (5), 851-873.

Bricaud, A., Claustre, H., Ras, J., Oubelkheir, K., 2004. Natural variability of phytoplanktonic absorption in oceanic waters: Influence of the size structure of algal populations. Journal of Geophysical Research-Oceans 109 (C11).

Bricaud, A., Morel, A., 1986. Light Attenuation and Scattering by Phytoplanktonic Cells - a Theoretical Modeling. Applied Optics 25 (4), 571-580.

Bricaud, A., Morel, A., Babin, M., Allali, K., Claustre, H., 1998. Variations of light absorption by suspended particles with chlorophyll a concentration in oceanic (case 1) waters: Analysis and implications for bio-optical models. Journal of Geophysical Research-Oceans 103 (C13), 31033-31044.

Carmack, E., 1990. Large scale physical oceanography of polar oceans. In: Smith, W.O. (Ed.), Polar oceanography, part A: Physical Science. Academic Press, New York, pp. 171-222.

Dalløkken, R., Sandvik, R., Sakshaug, E., 1995. Seasonal variations in the vertical light attenuation coefficient in the Greenland Sea: effect of phytoplankton light absoption. In:

Skjoldal, H.R., Hopkins, C.C.E., Erikstad, K.E., Leinaas, H.P. (Eds.), Ecology of Fjords and Coastal Waters. Elsevier Science, Amsterdam.

Egeland, E.S., Johnsen, G., Eikrem, W., Throndsen, J., Liaaen-Jensen, S., 1995. Pigments of *Bathycoccus Prasinos* (Prosinophyceae): Methodological and chemosystematic implications. J. Phycology 31, 554-561.

Falkowski, P.G., Raven, J.A., 1997. Aquatic photosynthesis. Blackwell Science.

Hancke, K., Hancke, T.B., Olsen, L.M., Johnsen, G., Glud, R.N., submitted. Temperature effects on microalgae photosynthesis-light responses measured by O2-production, Pulse Amplitude Modulated (PAM) fluorescence and 14-C assimilation. Journal of Phycology.

Hodal, H., Kristiansen, S., this issue. The importance of small cell phytoplankton in spring blooms at the mariginal ice zone in the northern Barents Sea. Deep-Sea Research Part II.

Holm-Hansen, O., Lorenzen, C.J., Holmes, R.W., Strickland, J.D.H., 1965. Fluorometric determination of chlarophyll. Journal du Conseil International pour l' Exploration de la Mer 30, 3-15.

Jeffrey, S.W., Mantoura, R.F.C., Bjørnland, T., 1997a. Data for the identification of 47 key phytoplankton pigments. In: Jeffrey, S.W., Mantoura, R.F.C., Wright, S.W. (Eds.), Phytoplankton pigments in oceanography: guidelines to modern methods. UNESCO, Paris, pp. 449-559.

Jeffrey, S.W., Vesk, M., Mantoura, R.F.C., 1997b. Phytoplankton pigments: windows into the pastures of the sea. Nature & Resources 33 (2), 14-29.

Jerlov, N.G., 1976. Marine optics. Oceanography Series 14. Elsevier, Amsterdam, pp. 1-231.

Johnsen, G., Sakshaug, E., 1996. Light Harvesting in bloom-forming marine phytoplankton: Species-specificity and photoacclimation. Scientia Marina 60, 47-56.

Johnsen, G., Sakshaug, E., Vernet, M., 1992. Pigment Composition, Spectral Characterization and Photosynthetic Parameters in Chrysochromulina-Polylepis. Marine Ecology-Progress Series 83 (2-3), 241-249.

Johnsen, G., Samset, O., Granskog, L., Sakshaug, E., 1994. In-Vivo Absorption Characteristics in 10 Classes of Bloom-Forming Phytoplankton - Taxonomic Characteristics and Responses to Photoadaptation by Means of Discriminant and Hplc Analysis. Marine Ecology-Progress Series 105 (1-2), 149-157.

Kirk, J.T.O., 1994. Light and Photosynthesis in Aquatic Ecosystems. Cambridge University Press, Bristol.

Kivimäe, C., Bellerby, R., Sundfjord, A., Omar, A., submitted to J. Mar. Res. Variability of new production and CO2 air-sea exchange in the northwestern Barents Sea in relation to sea ice cover.

Kyewalyanga, M., Platt, T., Sathyendranath, S., 1992. Ocean Primary Production Calculated by Spectral and Broad-Band Models. Marine Ecology-Progress Series 85 (1-2), 171-185.

Li, Y.H., Gregory, S., 1974. Diffusion of ions in sea water and in deep-sea sediments. Geochem Cosmochim Acta 38 (703-714).

Loeng, H., 1991. Features of the physical oceanographic conditions of the Barents Sea. Polar Research 10, 5-18.

Mitchell, B.G., Kiefer, D.A., 1988. Chlorophyll *a* specific absorption and fluorescence excitation spectra for light-limited phytoplankton. Deep-Sea Research Part I 35 (5), 639-663.

Moline, M.A., 1998. Photoadaptive response during the development of a coastal Antarctic diatom bloom and relationship to water column stability. Limnology and Oceanography 43 (1), 146-153.

Morel, A., 1988. Optical Modeling of the Upper Ocean in Relation to Its Biogenous Matter Content (Case-I Waters). Journal of Geophysical Research-Oceans 93 (C9), 10749-10768.

Nelson, N.B., Prezelin, B.B., Bidigare, R.R., 1993. Phytoplankton Light-Absorption and the Package Effect in California Coastal Waters. Marine Ecology-Progress Series 94 (3), 217-227.

Not, F., Massana, R., Latasa, M., Marie, D., Colson, C., Eikrem, W., Pedros-Alio, C., Vaulot, D., Simon, N., 2005. Late summer community composition and abundance of photosynthetic picoeukaryotes in Norwegian and Barents Seas. Limnology and Oceanography 50 (5), 1677-1686.

Pfirman, S.L., Bauch, D., Gammelsrød, T., 1994. The Northern Barents Sea: Water mass dristibution and modification. In: Johannesen, O.M., Muench, R.D., Overland, J.E. (Eds.), The polar oceans and their role in shaping the global environment: The Nansen Centennial Volume. AGU, Washington DC., pp. 77-94.

Pomeroy, L.R., 1997. Primary production in the Arctiv Ocean estimated from dissolved oxygen. Journal of Marine Systems 10, 1-8.

Reigstad, M., this issue.

Rodriguez, F., Chauton, M., Johnsen, G., Andresen, K., Olsen, L.M., Zapata, M., 2006. Photoacclimation in phytoplankton: implications for biomass estimates, pigment functionality and chemotaxonomy. Marine Biology 148 (5), 963-971.

Sakshaug, E., 1997. Biomass and productivity distributions and their variability in the Barents Sea. Ices Journal of Marine Science 54 (3), 341-350.

Sakshaug, E., 2004. Primary and secondary production in the Arctic Seas. In: Stein, R., Macdonald, R.W. (Eds.), The organic carbon cycle in the Arctic Ocean. Springer-Verlag, Berlin Heidelberg, pp. 57-81.

Sakshaug, E., Bjorge, A., Gulliksen, B., Loeng, H., Mehlum, F., 1994. Structure, Biomass Distribution, and Energetics of the Pelagic Ecosystem in the Barents Sea - a Synopsis. Polar Biology 14 (6), 405-411.

Sakshaug, E., Slagstad, D., 1991. Light and Productivity of Phytoplankton in Polar Marine Ecosystems - a Physiological View. Polar Research 10 (1), 69-85.

Sakshaug, E., Slagstad, D., 1992. Sea-Ice and Wind - Effects on Primary Productivity in the Barents Sea. Atmosphere-Ocean 30 (4), 579-591.

Sathyendranath, S., Bukata, R.P., Arnone, R., Dowell, M.D., Davis, C.O., Babin, M., Berthon, J.F., Kopelevich, O.V., Campbell, J.W., 2000. Remote Sensing of Ocean Colour in Coastal, and Other Optically Complex Waters. In: Sathyendranath, S. (Ed.), Reports of the International Ocean-colour Coordinating Group. IOCCC, Dartmouth, Canada, pp. 23-46.

Steemann-Nielsen, E., 1952. The use of radio-active carbon (^{14}C) for measuring organic production in the sea. J Cons Int Explor Mer 18, 177-140.

Sundfjord, A., Fer, I., Kasajima, Y., Svendsen, H., this issue. Observations of turbulent mixing and hydrography in the marginal ice zone of the Barents Sea.

Throndsen, J., Kristiansen, S., 1991. Micromonas-Pusilla (Prasinophyceae) as Part of Picoplankton and Nanoplankton Communities of the Barents Sea. Polar Research 10 (1), 201-207.

Vasseur, C., Mostajir, B., Nozais, C., Denis, M., Fouilland, E., Klein, B., Demers, S., 2003. Effects of bio-optical factors on the attenuation of ultraviolet and

photosynthetically available radiation in the North Water Polynya, northern Baffin Bay: ecological implications. Marine Ecology-Progress Series 252, 1-13.

Vinje, T., Kvambekk, Å.S., 1991. Barents Sea drift ice characteristics. Polar Research 10, 59-68.

von Quillfeldt, C.H., 2000. Common diatom species in arctic spring blooms: Their distribution and abundance. Botanica Marina 43 (6), 499-516.

Wassmann, P., 2002. Seasonal C-cycling variability in the open and ice-covered waters of the Barents Sea: an introduction. Journal of Marine Systems 38, 1-7.

Wassmann, P., this issue. Introduction.

Zapata, M., Rodriguez, F., Garrido, J.L., 2000. Separation of chlorophylls and carotenoids from marine phytoplankton: a new HPLC method using a reversed phase C-8 column and pyridine-containing mobile phases. Marine Ecology-Progress Series 195, 29-45.

Table 1: Sampling stations ordered after bloom developing stage, including sampling date, position, ice cover and ice thickness at the beginning of each station

Bloom stage	Station	Date of sampling	Latitude (N)	Longitude (E)	Ice cover (%)	Ice thickness (m)
Early	IV	18.07.2003	77° 03.4	29° 09.7	50-60	0-2
Early	VII	23.07.2004	82° 24.9	29° 26.2	80	0.5
Early	XVII	28.05.2005	77° 25.7	41° 02.8	60-70	0.5-1.5
Peak	II	13.07.2003	78° 14.0	27° 18.4	40-60	1-2
Peak	III	15.07.2003	79° 02.4	25° 38.2	50-70	1-1.5
Peak	X	27.07.2004	79° 22.7	28° 41.6	40-50	0.5-1.5
Peak	XI	29.07.2004	79° 49.4	29° 43.6	40-60	1-3
Peak	XIV	20.05.2005	81° 07.6	16° 19.0	50	1-2
Peak	XVI	25.05.2005	77° 08.4	29° 56.7	80-90	1.0
Late	I	10.07.2003	75° 33.4	30° 13.6	40-60	0-1.5
Mixed	XIII	31.07.2004	79° 56.3	30° 56.6	30-40	1.5
Mixed	XVIII	31.05.2005	75° 40.5	31° 47.8	0	-

Table 2: Ratios to chl *a* of light-harvesting carotenoids (LHC), chlorophylls (chl's), photo-protective carotenoids (PPC) and degraded pigments (deg. pig.) isolated from each station and ordered according to early- peak- and late bloom stages. Samples from surface waters (1m) and chl *a*-max were pooled for each station and number of samples is given (n). The ratios of LHP to PPC, and total pigments to chl *a* are given, together with the absolute chl *a* concentration (mg m^{-3}) for the pooled samples. No pigment data were collected at station XIII.

		Early bloom			Peak bloom						Late bloom	
	Station no.	4	7	17	2	3	10	11	14	16	1	18
	No. of samples (n)	6	1	3	3	3	4	2	4	4	4	4
LHC	Peridinin			7.0								
	19`But.-fuco			5.1		0.6					3.6	1.0
	Fuco	10.4	32.6	39.6	32.5	22.6	37.7	45.7	48.3	53.9	23.2	52.0
	19'Hex.-fuco	2.2				0.4					11.7	1.1
	Prasino											0.9
	Viola			1.9								
Chl's	chl *b*	2.6		19.4	0.8	3.4	9.4		2.0		1.8	3.7
	chl *c*1+2	10.0	10.6	21.4	10.1	9.5	10.7		23.5	26.2	12.9	13.3
	chl *c*3	4.1		4.2	2.3	3.9	4.7		5.2	3.5	9.2	
PPC	Diadino + diato	4.7	13.7	10.6	2.5	2.2	6.3	10.9	21.2	19.2	2.4	23.1
Deg.pig.	Fuco-derivat			1.2					0.8			1.3
	cis-peridinin	3.7										
	chlorophyllide *a*											10.2
	phaeophytin *a*				2.9							
	phaeophorbid *a*			3.6					2.7			
	phaeophorbid *a* like			4.6					5.5			2.9
	chl *a*-like	6.1		12.1	17.1	12.6	6.6		6.3	22.9	8.0	29.1
Ratios	LHP/PPC	6.3	3.2	9.3	18.3	18.3	9.9	4.2	3.7	4.3	26.1	3.1
	Total pigment/chl *a*	44	57	131	68	55	75	57	115	126	73	139
	chl *a*, mg m^{-3}	1.8	0.6	5.4	4.5	4.4	2.0	0.5	13.5	9.1	1.6	7.5

* LHP (light-harvesting pigments) is the sum of LHC and chl's

Table 3: Ratios to chl *a* of LHC, chl's, PPC and Deg.pig. from surface waters (1 m) and chl *a*-max, respectively. Samples are ordered after bloom stage and pooled for each stage. Station number and number of samples are given. The ratios of LHP to PPC, and total pigments to chl *a* are given, together with the absolute chl *a* concentration (mg m^{-3}) for the pooled samples. Abbreviations as in Table 2.

		Surface (1 m)			Chl *a*-max		
		Early bloom	Peak bloom	Late bloom	Early bloom	Peak bloom	Late bloom
	Station no.	4,7,17	10,14,16	18	4,17	2,3,10,11,14,16	1,18
	No. of samples (n)	5	6	1	5	14	7
LHC	Peridinin	5.7			4.0		
	19`But.-fuco	4.0		0.7	3.2	0.1	1.9
	Fuco	38.3	50.3	56.5	27.3	40.6	41.3
	19'Hex.-fuco	0.3		0.7	0.6	0.1	4.3
	Prasino			0.6			0.8
	Viola	1.6			1.1		
Chl's	chl *b*	13.2	2.4	3.4	14.7	1.6	3.4
	chl *c*1+2	19.4	24.7		16.7	17.1	20.9
	chl *c*3	4.3	4.9		3.5	3.7	2.6
PPC	Diadino + diato	5.2	20.4	24.6	13.3	12.1	16.4
Deg.pig.	Fuco-derivat	1.7	0.5	1.1		0.2	1.1
	cis-peridinin	0.4			1.2		
	chlorophyllide *a*			11.9			6.4
	phaeophytin *a*					0.6	
	phaeophorbid *a*	5.4	3.3				
	phaeophorbid *a* like	6.8	2.9	3.4		1.9	1.7
	chl *a*-like	7.4	14.5	28.5	11.8	12.1	23.4
Ratios	LHP/PPC	16.7	4.0	2.5	5.3	5.2	4.6
	Total pigment/chl *a*	114	124	131	97	90	124
	chl *a*, mg m^{-3}	3.6	10.9	3.3	4.2	22.9	5.8

Table 4: Incident surface irradiance E_{PAR} in air and immediate sub-surface irradiance $E_{0(PAR)}$ corresponding to the vertical irradiance profiles shown in Fig 2. The depth z (m) for which $E_{z(PAR)}$ equal 10 and 1 % of $E_{0(PAR)}$ (the attenuation depth) is added. E_{PAR} and $E_{0(PAR)}$ were calculated by integrating the spectral irradiance from 400 to 700 nm.

Bloom stage	Station	$E_{(PAR)}$ (µmol photons m^{-2} s^{-1})	$E_{0(PAR)}$ (µmol photons m^{-2} s^{-1})	Depth (m) corresponding to 10 % of $E_{0(PAR)}$	Depth (m) corresponding to 1 % of $E_{0(PAR)}$
Early	IV	379	208	10.5	23.8
Early	VII	124	94	15.9	> 90
Early	XVII	450	309	12	34.8
Peak	II	237	143	26.2	37.0
Peak	III	750	478	25.0	44.6
Peak	X	359	219	14.0	39.0
Peak	XI	-	217	19.6	37.5
Peak	XIV	308	213	6.2	14.5
Peak	XVI	302	237	4.8	12.0
Late	I	435	292	26.0	49.0
Mixed	XIII	184	110	10	32.7
Mixed	XVIII	142	-	12.1*	35*

* calculated from the surface incident irradiance (E_{PAR}), and not $E_{0(PAR)}$

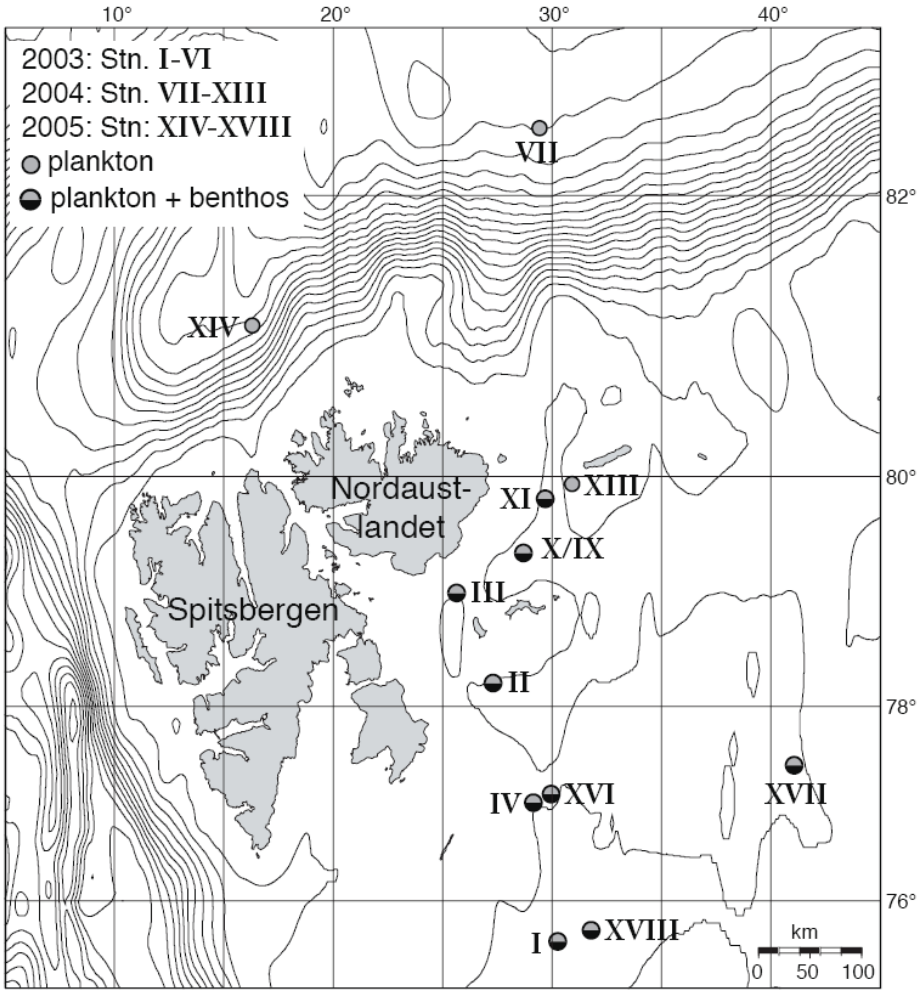

Fig. 1: Map of the study area including the sampling stations, visited in order during 2003 (station I, II, III and IV), 2004 (VII, IX/X, XI and XIII) and 2005 (XIV, XVI, XVII and XVIII). Technical data on the stations are given in Table 1.

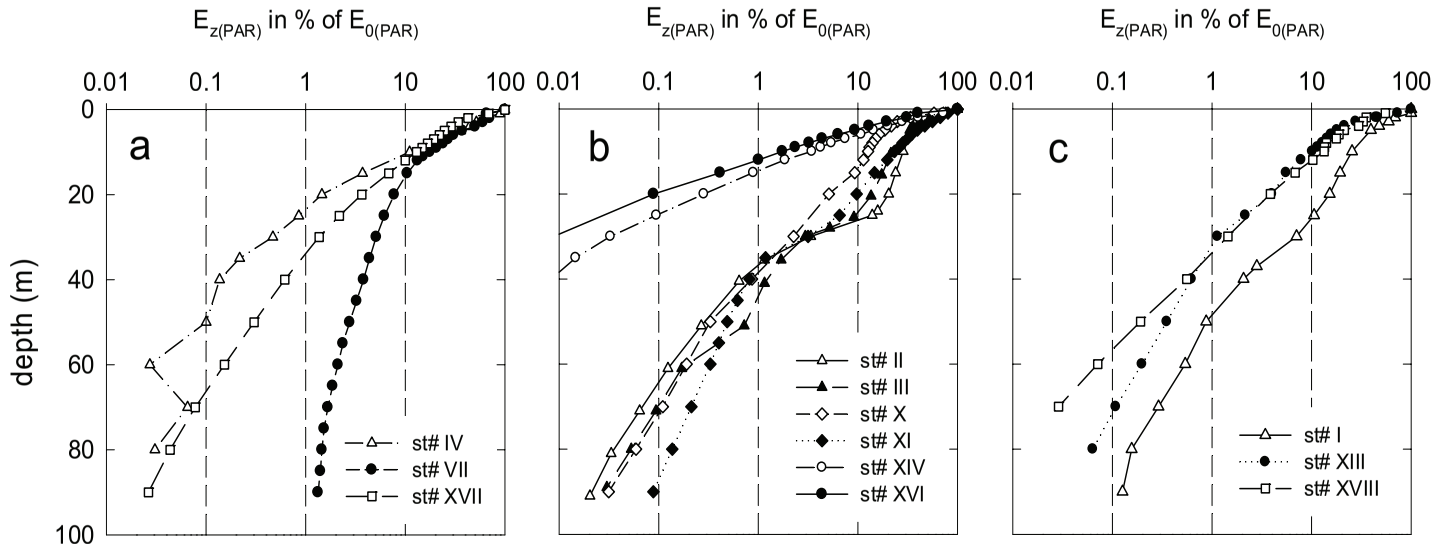

Fig. 2: Vertical profiles of integrated irradiance, PAR, in percent of the sub-surface irradiance, $E_{0(PAR)}$, for all stations, grouped in a) early-, b) peak- and c) late-bloom stages.

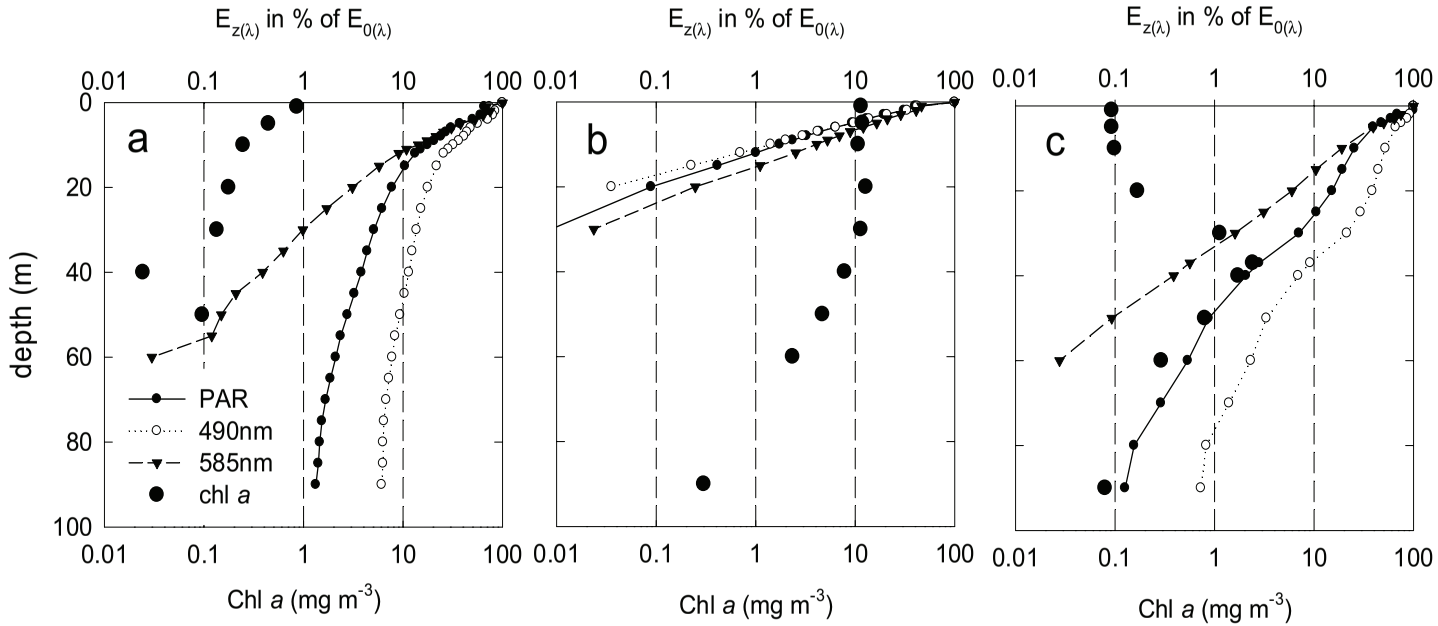

Fig. 3: Vertical profiles of wavelength specific irradiance as function of depth, at 490 and 585 nm, together with PAR, for station a) VII b) XVI and c) I, as typical examples for early- peak- and late-bloom stations, respectively. The chl *a* (mg m^{-3}) are included on log-scale on the same axes as percent irradiance (x-axe).

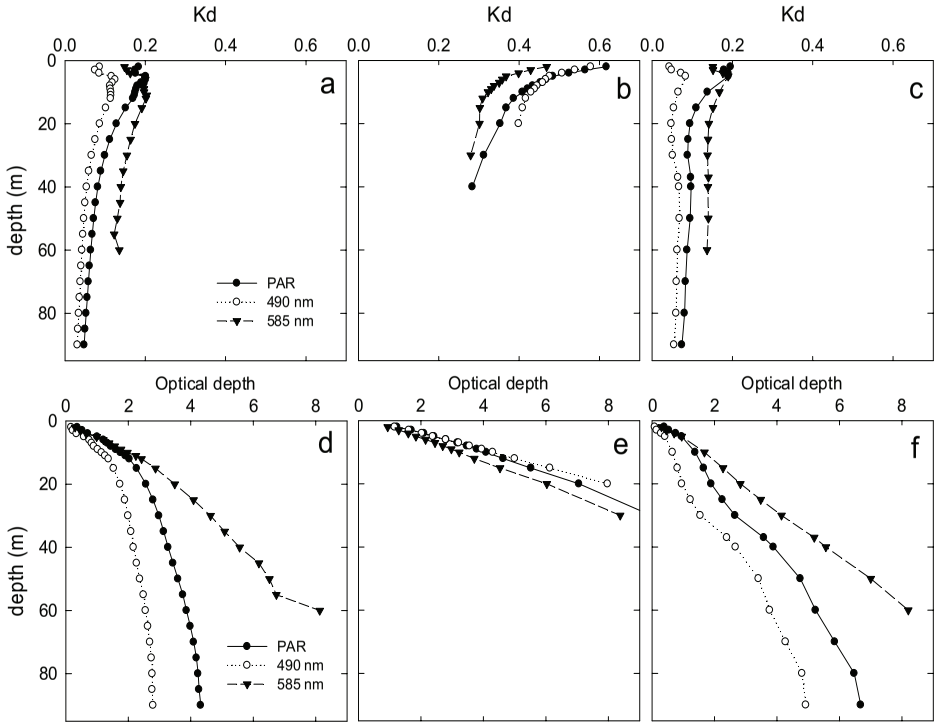

Fig. 4. The spectral attenuation coefficients for downwelling irradiance at 490nm, $K_{d(490)}$, 585 nm, $K_{d(585)}$, and integrated for PAR, $K_{d(PAR)}$, as a function of physical depth (m), for station a) VII, b) XVI and c) I, as typical examples for early- peak- and late-bloom stations, respectively. The lower panel (d-f) shows the relationship between the physical depth and the optical depth at 490 nm, 585 nm and PAR for the same stations as a-c.

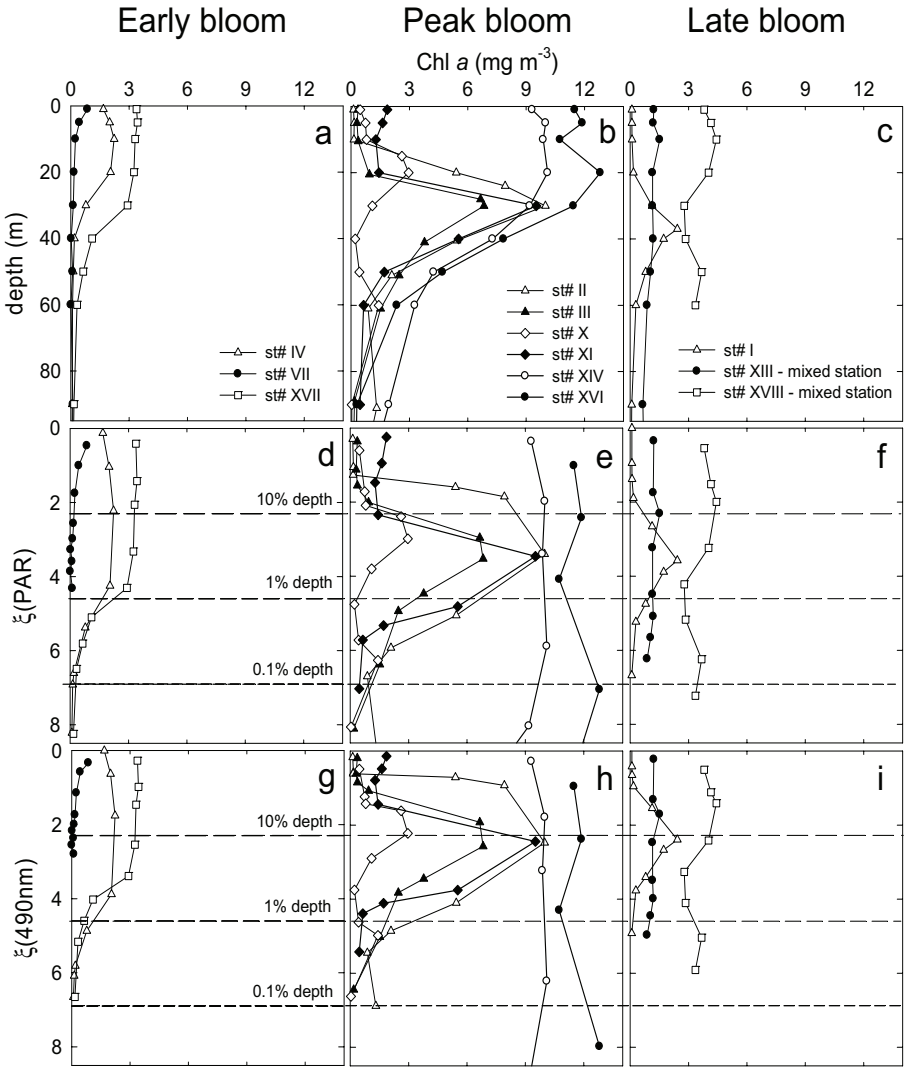

Fig. 5: Chl *a* concentration profiles for the early- (left column), peak- (middle column) and late-bloom (right column) stations plotted as function of physical depth (m, upper panel), optical depth (PAR, middle panel) and optical depth calculated at 490 nm (lower panel). The two mixed stations (XIII and XVIII) are included in the late-bloom panels.

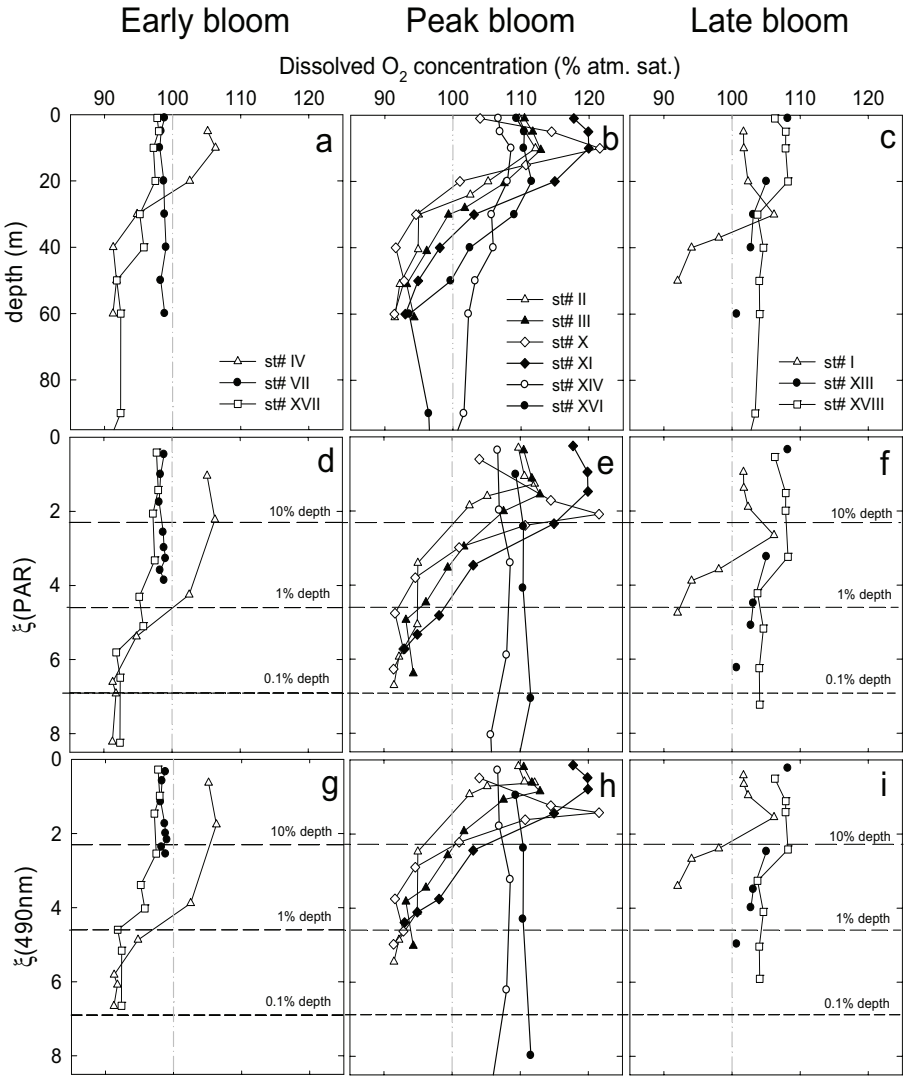

Fig. 6: Dissolved oxygen concentration profiles (in per cent of atmospheric saturation) for the early- (left column), peak- (middle column) and late-bloom (right column) stations plotted as function of physical depth (m, upper panel), optical depth (PAR, middle panel) and optical depth calculated for 490 nm (lower panel). The two mixed stations (XIII and XVIII) are included in the late-bloom panels.

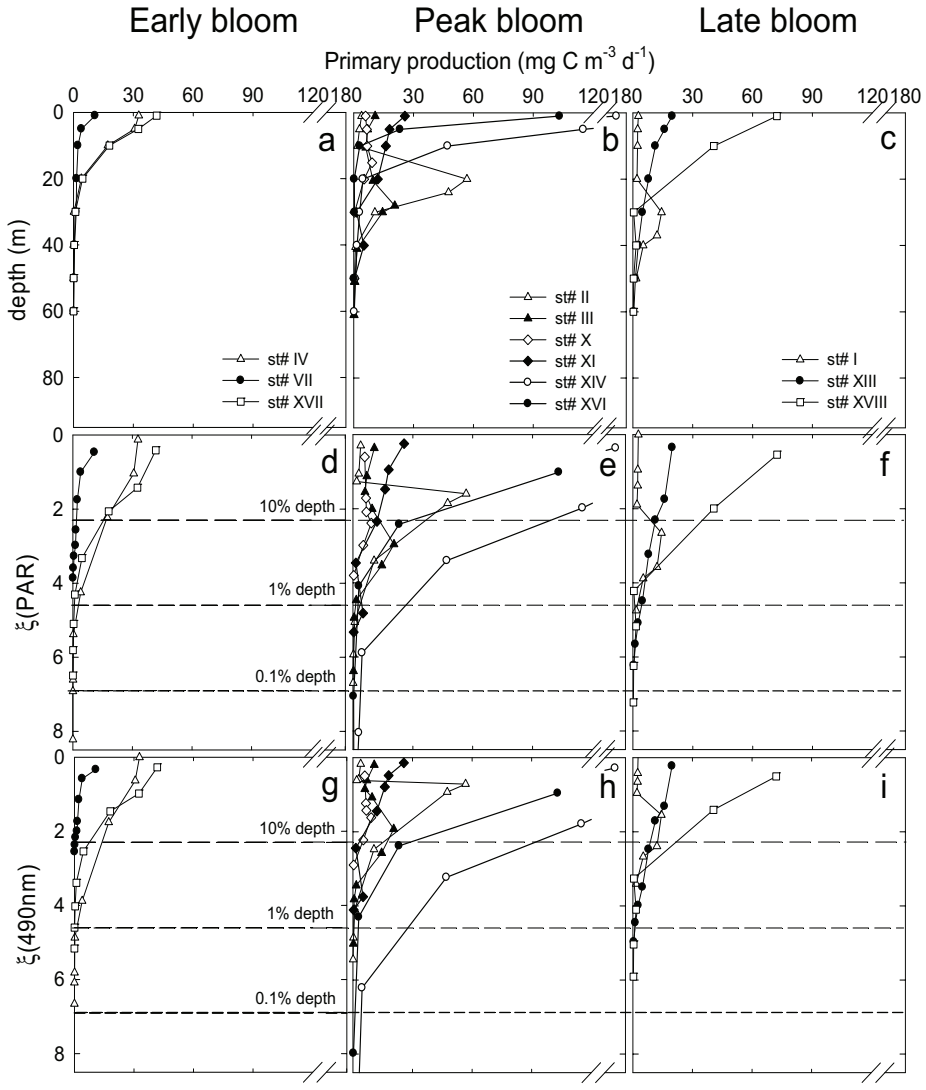

Fig. 7: Primary production profiles for the early- (left column), peak- (middle column) and late-bloom (right column) stations plotted as function of physical depth (m, upper panel), optical depth (PAR, middle panel) and optical depth calculated for 490 nm (lower panel). The two mixed stations (XIII and XVIII) are included in the late-bloom panels. Primary production data from Hodal et al. submitted.

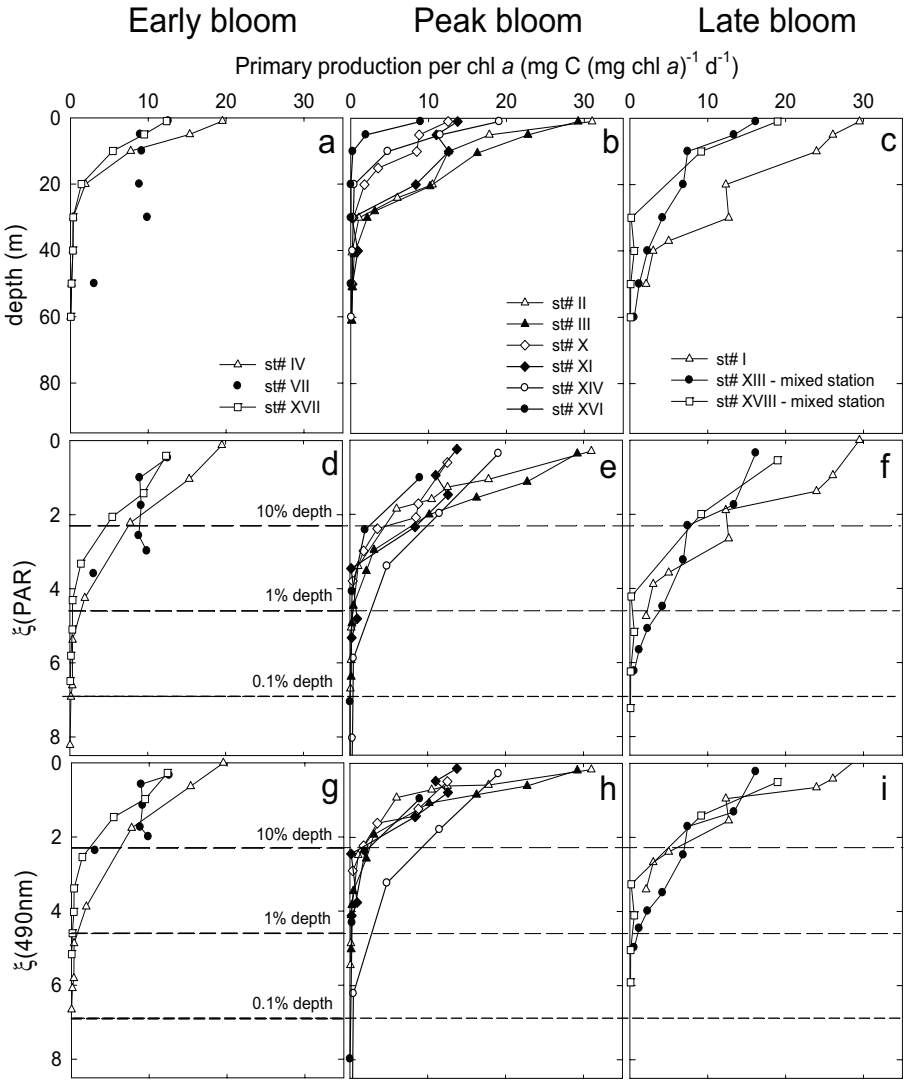

Fig. 8: Profiles of the chl *a*-normalised primary production for the early- (left column), peak- (middle column) and late-bloom (right column) stations plotted as function of physical depth (m, upper panel), optical depth (PAR, middle panel) and optical depth calculated for 490 nm (lower panel). The two mixed stations (XIII and XVIII) are included in the late-bloom panels. Primary production data from Hodal et al. submitted.

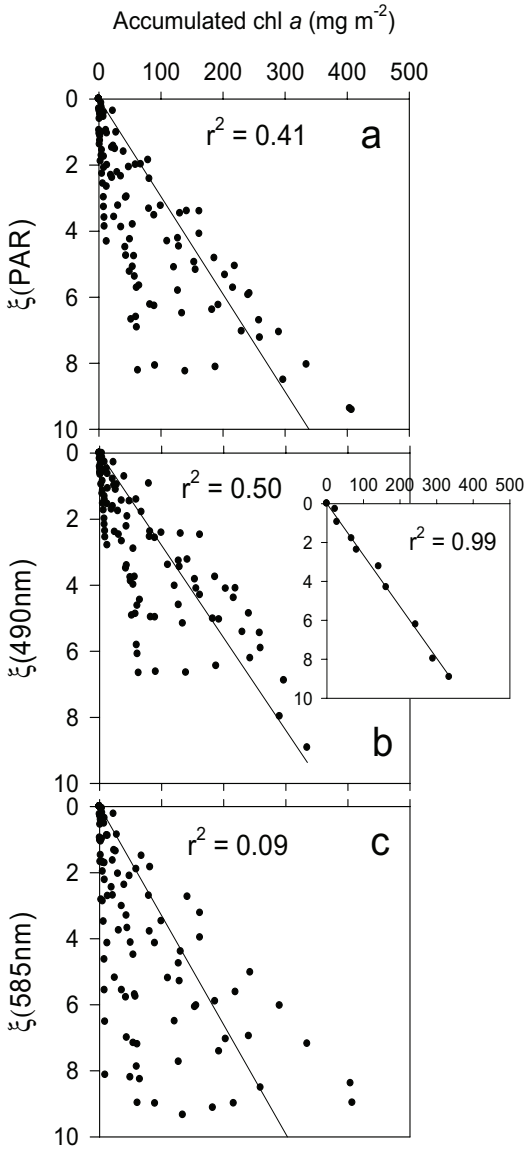

Fig. 9: Accumulated chl *a* concentration down through the water column, collected at all visited stations, as a function of a) optical depth for PAR, $\xi_{(PAR)}$, b) optical depth at 490nm, $\xi_{(490)}$, and optical depth at 585nm, $\xi_{(585)}$. The inlet in b) shows data exclusively calculated for the two chl *a*-rich peak-bloom stations XIV and XVI, with [chl *a*] >9mg m^{-3}. Lines are linearly regressions and the coefficient of determination (r^2) is given.

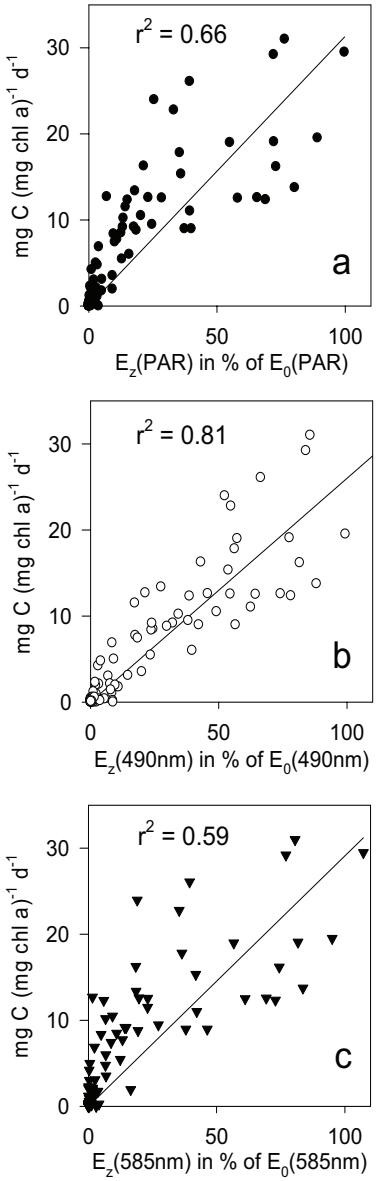

Fig. 10: Chl *a* normalised primary production rates as a function of a) $E_{z(PAR)}$ in per cent of $E_{0(PAR)}$, b) $E_{z(490)}$ in per cent of $E_{0(490)}$, and c) $E_{z(585nm)}$ in per cent of $E_{0(585nm)}$ for the entire dataset. Lines are linearly regressions and the coefficient of determination (r^2) is given. Regression lines were forced through origo.

Paper 2

Hancke TB, Hancke K, Johnsen G, Sakshaug E (submitted) Rate of O_2 production derived from PAM fluorescence: Testing three bio-optical approaches against measured O_2 production rate.

Journal of Phycology

RATE OF O_2 PRODUCTION DERIVED FROM PAM FLUORESCENCE: TESTING THREE BIO-OPTICAL APPROACHES AGAINST MEASURED O_2 PRODUCTION RATE

Torunn B. Hancke, Kasper Hancke, Geir Johnsen and Egil Sakshaug
Department of Biology, Trondhjem Biological Station, Norwegian University of Science and Technology, N-7491 Trondheim

Running title: PAM fluorescence and bio-optics

Author for correspondence: e-mail: torunn.hancke@bio.ntnu.no

ABSTRACT

Light absorption by phytoplankton is both species-specific and affected by photo-acclimational status. To estimate oxygenic photosynthesis from Pulse-Amplitude-Modulated (PAM and Fast repetition rate, FRR) fluorescence, the amount of quanta absorbed by PSII needs to be quantified. We present here three different bio-optical approaches to estimate the fraction of light absorbed by PSII: 1) the factor 0.5 which implies that absorbed light is equally distributed among PSI and PSII, 2) the fraction of chl *a* in PSII determined as the ratio between the scaled red-peak fluorescence excitation and the red absorption peak and 3) the measure of light absorbed by PSII, determined from the scaling of the fluorescence excitation spectra to the absorption spectra by the 'no-overshoot' procedure. Three marine phytoplankton species were used as test organisms: *Prorocentrum minimum* (Pavillard) Schiller (Dinophyceae), *Prymnesium parvum* cf. *patelliferum* Green et al. (Coccolithophyceae in Haptophyceae), and *Phaeodactylum tricornutum* Bohlin (Bacillariophyceae). Photosynthesis *vs.* irradiance (P *vs.* E) parameters calculated using the three approaches were compared with P *vs.* E parameters obtained from simultaneously measured rates of oxygen production. Generally, approach 1) underestimated while approach 2) overestimated the gross O_2 production rate calculated from PAM fluorescence. Approach 3, in principle the best approach to estimate quanta absorbed by PSII, also was superior according data. We, hence, recommend approach 3) for estimation of gross O_2 production rates based on PAM fluorescence measurements.

Key words: Bio-optics, chl *a* fluorescence, PAM, photosynthetic oxygen production, PSII-scaled fluorescence excitation

Abbreviations: AQ_{PSII} - Absorbed quanta by PSII, E – Irradiance, ETR - Electron transfer rate, rETR - Relative electron transfer rate, RC - Reaction centres in PSI or PSII, LHC - Light harvesting complexes associated with PSI and PSII, P – Photosynthesis, PAM – Pulse Amplitude Modulated fluorescence, Q_A - Quinone A, QR – Quantum requirement,

INTRODUCTION

In the past decades, there has been a growing worldwide demand for efficient measuring and monitoring of primary production of phytoplankton. Traditionally, photosynthesis in aquatic systems is measured as carbon fixation using the ^{14}C method (Steemann-Nielsen 1952). This method, however, is labour-intensive; besides, the quantum yield of carbon fixation varies according to changes in the rate constants for the intermediate steps in photosynthesis, variability in environmental conditions and the growth phase of the cells (Kroon et al. 1993). As a consequence, models of primary production based on the ^{14}C method are inaccurate (Prézelin et al. 1991, Falkowski and Woodhead 1992, Schofield et al. 1993, Kroon et al. 1993).

Pulse Amplitude Modulated (PAM) fluorescence in combination with bio-optical measurements offers a technique to estimate gross photosynthetic oxygen production rate. The technique which is based on *in vivo* variable fluorescence, estimates the photochemical efficiency of PSII (Schreiber et al. 1986); it is fast and non-invasive, and provides information of chl *a* fluorescence kinetics (Govindjee 1995). The quantum yield of charge separation in PSII (Φ_{PSII}), which can be calculated (Genty et al. 1989), depends on the red-ox state of the first stable electron acceptor in PSII (Q_A). When all the Q_A are oxidised in dark-acclimated cells, the reaction centres (RC) are open, photochemistry can proceed, and fluorescence emission is low. When all Q_A are reduced under actinic light, the RCs are closed and photosynthesis is saturated. The energy that hits a closed RC is dissipated as heat and fluorescence emission (Owens 1991).

Using the PAM technique, dark-acclimated cells are excited with a red probe light that is not sufficient enough to induce photosynthesis, ensuring that the detected fluorescence is derived only from the light-harvesting antenna pigments. The initial fluorescence (F_0) can only be measured in dark-acclimated cells, which possess the maximum fraction of open RCs. To determine the maximum fluorescence (F_m), a saturation pulse of white light is applied to the dark-acclimated cells in order to close all RCs in PSII. The pulse induces a primary stable charge separation of the first electron (e^-) acceptor of PSII (Q_A). Measured under actinic light, the initial and maximum

fluorescence are denoted F_0' and F_m', respectively. Kroon et al. (1993) modelled the oxygen production rate (P_{PSII}) by quantifying the relationship between light absorbed by PSII (AQ_{PSII}), the quantum yield of charge separation in PSII (Φ_{PSII}), and the stoichiometric ratio of oxygen evolved per electron generated in PSII (Γ). To estimate AQ_{PSII}, bio-optical measurements are required. The *in vivo* chl *a*-specific absorption coefficient ($a^*_\varphi(\lambda)$, m^2(mg Chl *a*)$^{-1}$) (Morel et al. 1987) yields information on total absorption of photosynthetic and photo-protective pigments and reflects the photo-acclimation status of the phytoplankton (Johnsen and Sakshaug 1993). The *in vivo* fluorescence excitation spectrum represents the fraction of light received by PSII (Haxo 1985, Neori et al. 1988). If scaled to $a^*_\varphi(\lambda)$ by the 'no-overshoot' procedure described by Johnsen et al. (1997), assuming 100 % conversion efficiency at the wavelength of maximum fluorescence the scaled fluorescence excitation spectrum, $F^*_{PSII}(\lambda)$, m^2(mg Chl *a*)$^{-1}$ is obtained. In contrast to $a^*_\varphi(\lambda)$, the $F^*_{PSII}(\lambda)$ does not include the signatures from photo-protective carotenoids and PSI (Johnsen and Sakshaug 1993, Johnsen et al. 1997).By spectral weighting, the fraction of absorbed light received by LHCII and transferred to PSII, can be calculated ($\bar{a}^*_{PSII}$, Fig 1, Johnsen and Sakshaug submitted).

Usually, the PAM technique is used to determine photosynthetic variables on a relative scale, such as the quantum yield of charge separation (Φ_{PSII}) or the rate of PSII electron transport (rETR). These variables can be used to determine, on a relative scale, the production of algae in aquatic systems. Investigations as to how and if the relative fluorescence measurements provided by PAM (or the Fast Repetition Rate Fluorometer, FRRF) can be related to photosynthetic oxygen production (P_{PSII}) have been attempted by Kolber and Falkowski 1993, Schreiber et al. 1995, Gilbert et al. 2000, Kromkamp et al. 2001, Longstaff et al. 2002 but, to our knowledge, no attempt has been made to differentiate between absorption of light by PSII and PSI and their respective LHCs to obtain P_{PSII}. So far it has been assumed that PSII and PSI absorb light in equal proportions irrespective of the species in question (Schreiber et al. 1986, Kolber and Falkowski 1993, Gilbert et al. 2000, Kromkamp and Forster 2003).

This paper focuses on methods for determining photosynthetic oxygen production rate based on *in vivo* variable fluorescence. We have tested three different approaches to estimate the fraction of light absorbed by PSII to find out if the PAM-based technique can be used in combination with bio-optics to determine photosynthetic parameters in terms of oxygen production. The results are derived from experiments during which the oxygen evolution and the *in vivo* fluorescence measurements were conducted simultaneously in the PAM cuvette.

MATERIALS AND METHODS

Algal cultures

Unialgal cultures originating from the culture collection of Trondhjem Biological Station, *Prorocentrum minimum* (Pavillard) Schiller (Dinophyceae), *Prymnesium parvum* cf. *patelliferum* Green et al. (Coccolithophyceae in Haptophyceae), and *Phaeodactylum tricornutum* Bohlin (Bacillariophyceae) were grown in semi-continuous cultures in 5-L flasks with f/2 medium (Guillard and Ryther 1962), pre-filtered (0.2 µm sterile filters pasteurised at 80°C in 3h), and enriched with silicate (*P. tricornutum* only), were grown at 15 ± 1°C, salinity of 33, and constantly bubbled with filtered air. The illumination was continuous "white" fluorescent light (Philips TLD 36W/96) providing 80 µmol $\cdot m^{-2} \cdot s^{-1}$. The growth rate and the chl *a* concentration were maintained in a semi-constant state by diluting the cultures once per day, corresponding to a specific growth rate at 0.2 $\mu \cdot d^{-1}$ for *P. minimum* and *P. parvum*, and 0.7-0.8 $\mu \cdot d^{-1}$ for *P. tricornutum,* both prior to and during the experiments. The stock cultures were enriched with 1 g $NaHCO_3$ L^{-1} to avoid depletion of inorganic carbon.

While growing, the physiological state of the cultures was monitored daily by measuring the ratio of *in vivo* chl *a* fluorescence before and after addition of DCMU (3(3,4 dichlorophenyl)–1, 1-dimethylurea, 50 µM final concentration) in a Turner Designs fluorometer. A ratio of DCMU-fluorescence to fluorescence of >2.5 indicates a healthy state of the culture (Sakshaug and Holm-Hansen 1977). In our study the ratio generally ranged from 2.7-3.5.

Experimental set-up

PAM fluorescence measurements and oxygen evolution rate were made simultaneously in a temperature-controlled plastic cuvette (Fig. 2). Prior to incubations, a sub-sample of 100 mL was placed in a temperature-controlled water bath at 10 or 20°C for 30 min, keeping the irradiance. Subsequently, 2.7 mL of the sample was inserted into the cuvette, which was sealed with no headspace of air, using a lid housing a Peltier cell in which the temperature was kept constant (± 0.2°C, Walz, Germany, US-T/S). The algae were

kept suspended inside the cuvette by a slowly circulating water flow driven by the cooling of the Peltier cell and heating of the incubator light.

Sub-samples were kept in the dark for 15 min prior to generating photosynthesis *vs.* irradiance (P *vs*. E) curves. Both P *vs.* E data for oxygen production and PAM fluorescence were measured during 10 min incubations followed by step-wise increasing of the irradiance, from (1-500 µmol photons·m^{-2}·s^{-1}). The incubator light source was a slide projector equipped with a halogen lamp, and the light passed an IR filter (cut off at 695 nm) in front of the PAM detector, and slide frames with different layers of spectrally neutral mosquito netting.

Irradiance measurements

The growth irradiance was measured inside the culture flasks filled with sterile seawater, using a scalar (4π) irradiance sensor (Biospherical Instruments QSL–100, San Diego, USA). The incubation irradiance (PAR) was measured inside the (PAM cuvette) incubation chamber, using a cosine-corrected (2π) light collector on the DIVING-PAM (Walz, Effeltrich, Germany). The spectral distribution of the incubation light was measured using a RAMSES spectroradiometer (TRIOS, Germany) from 400-850 nm with 1 nm resolution. The irradiance and the spectral distribution of the incubation light were used for calculating light absorbed by PSII.

PAM measurements

Fluorescence was measured using a PAM–101 fluorometer with a 102 and 103 module (Walz, Effeltrich, Germany, Schreiber et al. 1986) equipped with a photomultiplier detector (PMT, Walz, Germany, PM–101/N, Fig. 2). A red light-emitting diode (655 nm peak, <0.15 µmol photons·m^{-2}·s^{-1}, at 1.6 kHz) was used as probe light at an intensity too low to induce significant variable fluorescence. In the following we used the nomenclature of van Kooten and Snel (1990). The minimum fluorescence (F_o) and the maximum fluorescence (F_m) was measured at the end of the dark acclimation period (15 min), when approximately all reaction centres (RCs) were closed. F_m was measured during exposure to a saturating light pulse from a halogen lamp (0.6 s at >5000 µmol

photons·m^{-2}·s^{-1}, Scott, Germany, KL1500 electronic) which illuminated the sample via an optical fibre. The maximum quantum yield of PSII charge separation (Φ_{PSII_max}) in the dark-acclimated cells was calculated as

$$\Phi_{PSII\_max} = F_v/F_m = \frac{F_m - F_0}{F_m} \quad (1)$$

Under actinic illumination, the operational quantum yield of PSII (Φ_{PSII}) was calculated from the steady-state fluorescence (F_0') and the maximum fluorescence after a saturation pulse (F_m') at each incubation irradiance (Genty et al. 1989):

$$\Phi_{PSII} = \Delta F/F_m' = \frac{F_m' - F_0'}{F_m'} \quad (2)$$

O_2 measurements

Net O_2 production rate was measured as the O_2 concentration change during incubation for each irradiance by a Clark-type O_2-microsensor (Revsbech 1989) inserted through a tight-fitting miniature pipe in the wall of the incubation cuvette (Fig. 2). The sensor had an external tip diameter of ~100 µm, stirring sensitivity of <1.5%, and a 90% response time of <4 s. Prior to the measurements, the electrode was calibrated by a 2-point calibration both in anoxic and air-saturated seawater at the specific temperature (Glud et al. 2000). The sensor current was measured using a picoammeter (PA 2000, Unisense, Denmark) connected to a strip-chart recorder (Kipp and Zonen, Netherlands) and a PC. The dark respiration rate was measured during the last 10 min of the dark period prior to the light incubations. The photosynthetic O_2 production rate (P_{O2}) was calculated by adding the dark respiration rate to the net O_2 production rate.

Bio-optical measurements

In order to calculate oxygen evolution per biomass and time on basis of measurements of Φ_{PSII}, it is necessary to estimate the light absorbed by PSII in absolute units. Such a calculation requires knowledge of the *in vivo* chl *a*-specific absorption coefficient ($a_\varphi^*(\lambda)$) and the PSII-scaled *in vivo* fluorescence excitation spectrum ($F_{PSII}^*(\lambda)$; Johnsen et al. 1997). We obtained $a_\varphi^*(\lambda)$ and $F_{PSII}^*(\lambda)$ (Fig. 1) by measuring the optical density (OD(λ)) of phytoplankton cells collected on glass fibre filters (Whatman GF/F) in a

dual-beam spectrophotometer (Hitachi 150-20), using a clean filter wetted with filtered sea water as reference (Yentsch 1962, Mitchell and Kiefer 1988). Three replicate spectra were measured from 350 to 800 nm at 1 nm increments, and the average OD from 750-800 nm was subtracted from the whole spectrum to correct for light scattering (Mitchell and Kiefer 1988). OD of the filter with algae (OD_{filt}) was converted to OD in suspension (OD_{susp}) using a second-order polynomial expression (β-correction, Eq. 3, Mitchell 1990).

$$OD_{susp}(\lambda)=m1 \cdot OD_{filt}(\lambda) + m2 \cdot [OD_{filt}(\lambda)]^2 \qquad (3)$$

The parameters 'm1' and 'm2' has been determined on laboratory cultures: m1 = 0.508 and m2 = 0.134 for *P. parvum* (Chauton et al. 2004) and m1 = 0.221 and m2 = 0.577 for *P. minimum* and for *P. tricornutum* values for *Skeletonema costatum* were used; m1 = 0.407 and m2 = 0.602 (R. Sandvik unpublished data) because of their similar pigmentation and size, the parameters for *S. costatum* were used for *P. tricornutum*. Absorption (a, m^{-1}) was calculated from OD_{susp} according to Eq. 4:

$$a = 2.3 \cdot OD_{susp}(\lambda) \cdot (S/V) \qquad (4)$$

S is the clearance rate of GF/F filter (mm^2) and V, the volume (mL) of the filtered sample (Mitchell and Kiefer 1988).

The chl *a* concentration was measured on extracts from the filters that were used for *in vivo* light absorption, using a spectrophotometer (Hitachi 150-20). Immediately after the *in vivo* light absorption measurement, the filters were extracted in pre-cooled 100% methanol (4˚C, 5 mL) for 3 h in glass centrifuge tubes. The tubes were placed in the dark at 4°C and stirred for 10 sec in a Vortex-mixer after 0, 1.5 and 3 h. The extracts were re-filtered (0.2 µm polycarbonate filter) before measuring OD from 350 to 800 nm. The chl *a* concentration ($mg \cdot m^{-3}$) was calculated using the extinction coefficient for chl *a* in methanol at 665 nm, 74.5 $L \cdot g^{-1} \cdot cm^{-1}$ (MacKinney, 1941).

The chl *a*-specific absorption coefficient ($a^*_\varphi(\lambda)$, $m^2(mg\ chl\ a)^{-1}$) was determined by normalising the absorption spectrum (m^{-1}) to the chl *a* concentration ($mg \cdot m^{-3}$, Fig. 1).

In vivo fluorescence excitation spectra were measured using a spectrofluorometer (Hitachi F-3000). An infrared-transmitting glass filter (Schott RG 695 IR) was placed in front of the photomultiplier to prevent direct and scattered light from the light-source and cells. Prior to the measurements, a time scan was recorded with DCMU-treated cells (50 μM final concentration) during 1.5 min (scan time for a full spectrum) avoiding non-variable chl *a* fluorescence signal (Johnsen and Sakshaug 1993). The *in vivo* chl *a* fluorescence excitation spectra were recorded with excitation wavelengths from 400 to 700 nm (5 nm bandwidth), and emission was monitored at 730 nm (5 nm bandwidth, Neori et al. 1988). The data were recorded at 1 nm resolution. All fluorescence excitation measurements were quantum corrected using the dye Basic Blue 3 (Kopf and Heinze 1984, Sakshaug et al. 1991).

Scaling of the fluorescence excitation spectra followed the 'no-overshoot' procedure (Johnsen et al. 1997, Johnsen and Sakshaug submitted) by matching the fluorescence spectra to the corresponding absorption spectra at selected wavelengths, yielding a PSII-scaled fluorescence excitation spectrum, $F^{*}_{PSII}(\lambda)$. The matchpoint preventing 'overshoot' was ~550 nm for *P. minimum* and *P. parvum*, except that for *P. minimum* at 20°C it was ~650 nm (Fig. 3). *P. tricornutum* exhibited matchpoints in the red band, 675-685 nm (Fig. 3). The 'no-overshoot' procedure yields an upper limit for the number of quanta absorbed by PSII (Johnsen and Sakshaug submitted).

Particulate organic carbon

Particulate organic carbon (POC) was measured on filtered subsamples (Whatman GF/F, baked) and analysed after treatment of the samples with fuming hydrochloric acid (Carlo Erba Elemental Analyzer Model Na).

Calculation of the oxygen production rate, P_{PSII}

Oxygen production rate (P_{PSII}) can be calculated as

$$P_{PSII} = \Phi_{PSII} \cdot E \cdot \Gamma \cdot AQ_{PSII} \quad (5)$$

Φ_{PSII} is the quantum yield of charge separations in PSII (mol e^-·mol photon^{-1}, Genty et al. 1989) and E is the irradiance (µmol photons·m^{-2}·s^{-1}), which multiplied by Φ_{PSII} yields the relative electron transfer rate (rETR). Γ is the stoichiometric ratio of oxygen evolved per electron generated at PSII. According to the standard Z-scheme of photosynthesis, four stable charge separations are needed in each PSI and PSII to release one O_2 molecule. Γ, accordingly, is 0.25 O_2·(e^-)$^{-1}$ (Kroon et al. 1993, Gilbert et al. 2000). Empirically, a quantum requirement (QR) higher than eight photons has been observed, caused by different sinks for photosynthetic electron transport; e.g. Mehler-type reactions and photorespiration (Kromkamp et al. 2001; Longstaff et al. 2002). For simplicity, we assumed Γ = 0.25. AQ_{PSII} represents quanta absorbed by PSII (m^2(mg chl *a*)$^{-1}$.

With the aim to quantify the O_2 production rate from PAM fluorescence in absolute units, we tested three different approaches for estimating AQ_{PSII}.

1) $AQ_{PSII} = 0.5 \cdot \bar{a}^*_{\varphi}$. The commonly used correction factor 0.5 implies that absorbed light is equally distributed among PSI and PSII. (Schreiber et al.1986, Kolber and Falkowski 1993, Kroon et al. 1993, Gilbert et al. 2000, Morris and Kromkamp 2003)
2) $AQ_{PSII} = F_{II} \cdot \bar{a}^*_{\varphi}$: F_{II} is the fraction of chl *a* in PSII determined from the ratio between the scaled ('no-overshoot') red-peak fluorescence excitation and the red absorption peak (a^*_{PSII}(red) / a^*_{φ}(red)) (Johnsen et al. 1997, Fig. 1 and 3).
3) $AQ_{PSII} = \bar{a}^*_{PSII}$: This factor represents light absorbed by PSII, determined from the scaling of the fluorescence excitation to the absorption spectra by the 'no-overshoot' procedure (Johnsen et al. 1997, Fig. 1 and 3).

Both $a^*_{\varphi}(\lambda)$ and $F^*_{PSII}(\lambda)$ were spectrally weighted from 400 to 700 nm (Eq. 6)

$$\overline{X} = \frac{\left[\sum_{400}^{700} X(\lambda) \cdot E(\lambda)\, d\lambda\right]}{E(PAR)} \qquad (6)$$

$\overline{X}$ is the spectrally weighted chl *a*-specific absorption coefficient ($\bar{a}^*_{\varphi}$) or the spectrally weighted PSII-absorption ($\bar{a}^*_{PSII}$), X is $a^*_{\varphi}(\lambda)$ or $F^*_{PSII}(\lambda)$, and $E(\lambda)$ is the incubation irradiance.

Curve fitting

The P *vs.* E curves were fitted to data using a non-linear least squares procedure (SigmaPlot 9.0, SYSTAT Sotfware inc. US) using the equation by Webb et al. (1974, Eq. 7). The photosynthetic parameters; the maximum photosynthetic rate (P_{max}) and the maximum light utilisation coefficient (α) were calculated for each curve. The light saturation parameter (E_k) was calculated as P_{max}/α. Notation of the photosynthetic parameters follows Sakshaug et al. (1997), Table 1.

$$P = P_{max}\left(1 - \exp\left(\frac{-\alpha \cdot E}{P_{max}}\right)\right) \qquad (7)$$

RESULTS

The total amount of absorbed light ($\bar{a}^*_{\varphi}$) ranged from 0.0068 to 0.0164 m^2(mg chl *a*)$^{-1}$, *P. parvum* exhibiting the highest and *P. minimum*, the lowest absorption coefficients (Table 2).

The fraction of chl *a* in PSII (F_{II}) ranged from 70 - 98% (Table 2). For *P. tricornutum,* F_{II} was 97% and 98% for the 10°C and 20°C incubations, respectively. *P. minimum* exhibited the lowest coefficients, 80% and 70% for 10ºC and 20ºC, respectively. The fraction of light absorbed by PSII ($\bar{a}^*_{PSII}$) ranged from 0.0054-0.0132 m^2(mg chl *a*)$^{-1}$ with *P. parvum* and *P. minimum* exhibiting the highest and lowest fractions, respectively (Table 2).

P *vs.* E curves for the O_2 production rate, measured with O_2-microsensors (P_{O2}) and calculated from the operational quantum yield of PSII (Φ_{PSII}) in combination with the three bio-optical approaches (P_{PSII}), showed the typical P *vs.* E shape with a nearly linear initial slope (α) and increasing saturation (P_{max}) with increasing irradiance. None of the curves showed a decrease in P at high irradiances; thus, photo-inhibition was not observed.

PAM-derived photosynthetic parameters were compared to parameters derived from direct O_2 measurements (Fig. 4). The photosynthetic parameters derived from PAM measurements are gross O_2 production, since it measures the relative electron transport rate in PSII and are not influenced by O_2 respiration. From the O_2-microsensor technique, net O_2 production was measured. By adding the O_2 respiration in the dark, gross O_2 production was estimated. However, this underestimates the gross O_2 production due to an enhanced O_2 respiration under illumination compared to the dark respiration (Canfield and DesMarais 1993, Glud et al. 1992, Ludden et al. 1985). Consequently, rates of P_{PSII} (based on PAM fluorescence) should theoretically be higher than P_{O2} rates (measured by O_2-microsensors).

The maximum production rate for P_{O2} (P_{O2_max}) was ~2 times higher (1.5 – 2.4) in cultures incubated at 20°C than at 10°C (Fig. 4, Table 3), as expected according to a Q_{10} of ~2 normally observed for phytoplankton (Davison 1991, Hancke et al. submitted). For P_{PSII}, the maximum O_2 production rate (P_{PSII_max}) was normally highest when based on $F_{II} \cdot \bar{a}^*_{\varphi}$ (approach 2), followed by $\bar{a}^*_{PSII}$ (approach 3), and lowest when based on $0.5 \cdot \bar{a}^*_{\varphi}$ (approach 1, Fig. 4, Table 3). Overall, P_{PSII} exhibited the same trend as P_{O2}, except for *P. minimum* at 20°C which yielded P_{PSII_max} ~2 times lower than P_{O2_max}, and for *P. parvum* 20ºC where P_{PSII_max} were ~2 times higher. For the other incubations the range of values for P_{PSII_max} was in the same area as the value of P_{O2_max} (Fig. 4, Table 3).

The light saturation parameter (E_k) showed a pattern opposite of that for P_{max}, implying that E_k was higher when calculated on basis of P_{PSII} than on basis of P_{O2} for *P. minimum* and *P. tricornutum*, and lower for *P. parvum* (Fig. 4, Table 3).

To find the best linear fit between calculated and measured maximum oxygen production, P_{PSII_max}, estimates based on three bio-optical approaches were plotted as a function of P_{O2_max} (Fig. 5a). Approach 1, 2 and 3 gave slope coefficients of 0.6 (R^2 = 0.50), 1.2 (R^2 = 0.51) and 1.0 (R^2 = 0.51), respectively. Approach 3 ($\bar{a}^*_{PSII}$) resulted in the slope coefficient closest to unity, implying that $\bar{a}^*_{PSII}$ provides the best fit for P_{PSII_max} to P_{O2_max}.

The relationship between the maximum light utilisation coefficient (α) for P_{O2} and calculated values of α was tested by plotting α for P_{O2} against α for P_{PSII}, again using the three bio-optical approaches (Fig. 5b). The linear regressions exhibited slopes of 0.12 (R^2 = 0.22), 0.26 (R^2 = 0.27) and 0.19 (R^2 = 0.23) for the three approaches, respectively (Fig. 5b), indicating a weak relationship.

Since P_{O2_max} and P_{PSII_max} calculated from $\bar{a}^*_{PSII}$ matched well, we analysed the relationship between P_{O2} and P_{PSII}, using $\bar{a}^*_{PSII}$, for the entire irradiance range for the three species in question (Fig. 6). The relationship between P_{O2} and P_{PSII} was adequately described by a linear regression (R^2 = 0.7-0.97). The slope differed between the species and in two cases, with the incubation temperature. *P. minimum* incubated at 10°C exhibited a slope of 0.86 (R^2 = 0.94) and at 20°C, 0.59 (R^2 = 0.92) (Fig. 6a), indicating that P_{O2} is closely related to P_{PSII} estimates derived on basis of the $\bar{a}^*_{PSII}$; moreover, that the two are linearly related. The slopes for *P. parvum* were 1.23 (R^2 = 0.70) and 2.5 (R^2 = 0.87) for 10 and 20°C, respectively, suggesting that P_{PSII} overestimates P_{O2} by a factor of 1.2 at 10ºC and 2.5 at 20ºC (Fig. 6b). The slopes for P_{O2} against P_{PSII} of *P. tricornutum* were 1.3 at 10ºC (R^2 = 0.89) and 1.0 at 20ºC (R^2 = 0.97); thus, not significantly different from unity (Fig. 6c). Consequently, the relationship between P_{O2}

and P_{PSII} did not differ between the two incubation temperatures, predicting a linear relationship near unity for the entire P *vs*. E curve.

DISCUSSION

We have tested three bio-optical approaches to determine the fraction of light absorbed by PSII. In combination with PAM fluorescence, they were subsequently evaluated against measured rates of oxygen production. This made it possible to improve the quality of estimates for the O_2 production rate in absolute units from PAM based fluorescence. Johnsen and Sakshaug (submitted) suggested that $\bar{a}^*_{PSII}$ is the most accurate and direct measure of light absorbed by PSII, whereas F_{II} only corrects for light absorbed by PSII and not the photoprotective carotenoids. F_{II} therefore overestimates the light absorbed by PSII and consequently, the O_2 production rate. In addition, presupposing that light is equally absorbed by PSII and PSI, underestimates the absorption by PSII and the O_2 production rate; in chromophytes by ~20%.

The fraction of chl *a* in PSII calculated from of F_{II} (Table 2) was high compared to approach 1. High compared to those suggested by Johnsen and Sakshaug (submitted), our F_{II} might be associated with our high OD_{filt} readings in the 550-600 nm bands, where OD otherwise is typically low. In the same context, uncoupling of LHC from PSII will enhance state II-I transitions (Mullineuax and Allen 1988, Kroon et al. 1993) which may cause high F_{II} values.

Representing total absorbed by PSII, $F_{II} \cdot \bar{a}^*_{\varphi}$ can yield too high values for P_{PSII}. On the other hand, $0.5 \cdot \bar{a}^*_{\varphi}$ usually underestimates P_{O2} because the PSII:PSI ratio is higher for nearly all chromophyte phytoplankton; Johnsen and Sakshaug (submitted) suggest an average F_{II} of 0.72 for this group. In principle, $\bar{a}^*_{PSII}$ yields the most accurate estimate for light absorbed by PSII because it corrects for absorption by photoprotective carotenoids and PSI (Johnsen et al. 1997) and is therefore most suitable for calculating P_{PSII} on basis of PAM data.

The PAM and the O_2-microsensor techniques have their limitations and strengths in terms of sensitivity and noise. In weak light ($E < E_k$), Φ_{PSII} is relatively high compared

to E, yielding a robust measure of the relative electron transfer rate (rETR), thus, the estimation of α based on the PAM technique is reliable. Conversely, the microsensor technique is working near the detection limit, in weak light and with a low signal to noise ratio; thus, yielding low accuracy for α.

During light-saturated photosynthesis ($E > E_k$), the accuracy of the results from PAM and O_2-microsensor techniques, respectively, are opposite that for estimates of α. P_{max} based on PAM yields a small Φ_{PSII} : E ratio because Φ_{PSII} decreases with increasing E, causing low accuracy of rETR at high irradiance. In contrast, the signal to noise ratio of the O_2-microsensor increases with increasing irradiance, turning the method more reliable in the light-saturated part of the P *vs*. E curve.

The operational quantum yield of oxygen production (Φ_{O2}) can be calculated (Flameling and Kromkamp 1998):

$$\Phi_{O2} = \frac{P_{O2}}{115 \cdot E \cdot \bar{a}^{*}_{PSII}} \qquad (8)$$

115 is a correction factor providing uniform dimensions and P_{O2}, the chl *a* specific oxygen production at each irradiance. Comparing Φ_{PSII} from PAM measurements and Φ_{O2} from O_2 measurements show a positive correlation at high irradiance independent of species or temperature (Fig. 7). The exception is data at low light measured with O_2 electrodes. As described, the signal to noise ratio at weak light is low, yielding uncertain data. The 4:1 line in Fig. 7 indicates the relationship between Φ_{PSII} and Φ_{O2}, which illustrates the assumption of four photons in PSII yielding one oxygen molecule; thus, Γ = 0.25. For *P. minimum,* however, the ratio <4:1, indicates a quantum requirement (QR) lower than 4 to produce one oxygen molecule. In contrast, *P. parvum* exhibited QR >4:1. The Φ_{PSII} : Φ_{O2} ratio for *P. tricornutum* fits the 4:1 relationship well. Both Kromkamp et al. (2001) and Longstaff et al. (2002) observed QR different from 4. The difference in QR in our material might cause the divergence between P_{O2} and P_{PSII} for *P. minimum* and *P. parvum* (P *vs.* E curves in Fig. 4 and Fig. 6).

Because our data in principle were conducted simultaneously in the same experimental set-up, they can be used to calculate the maximum quantum yield ${}^{PSII}\Phi_{O2\_max}$ (Hancke et al. submitted) from the initial slope of the P *vs.* E curve based on the O_2 measurements (α) and the fraction of light absorbed by PSII ($\bar{a}^{*}_{PSII}$):

$$ {}^{PSII}\Phi_{O2\_max} = \frac{\alpha^{*}_{P_{O2}}}{\bar{a}^{*}_{PSII} \cdot 115} \tag{9} $$

115 is a correction factor ensuring uniform dimensions. On basis of ${}^{PSII}\Phi_{O2\_max}$, we can in turn calculate the minimum quantum requirement (QR), which is the inverse of ${}^{PSII}\Phi_{O2\_max}$;

$$ QR = \frac{1}{{}^{PSII}\Phi_{O2\_max}} \tag{10} $$

Because of the questionable reliability of ${}^{PSII}\Phi_{O2\_max}$ and QR, they are not used in the calculations of P_{PSII}.

From our tests, $\bar{a}^{*}_{PSII}$ (approach 3) seems to provide the best input variable for calculating the oxygen production rate from PAM measurements. This implies that $\bar{a}^{*}_{PSII}$ is the most relevant for light absorbed by PSII. The other two approaches overestimate ($F_{II} \cdot \bar{a}^{*}_{\varphi}$, approach 2) or underestimate ($0.5 \cdot \bar{a}^{*}_{\varphi}$, approach 1) the measured oxygen production, respectively.
Our results support the theory-based conclusions of Johnsen and Sakshaug (submitted). We, hence, recommend $\bar{a}^{*}_{PSII}$ to estimate gross oxygen production from PAM fluorescence measurements.

Acknowledgements
We thank the European Union financed programme SISCAL (IST 2000-28187), the Norwegian research council financed Strategic University Programme, MODTEQ (NFR # 128726/420) and the NORDKLIMA programme, CABANERA (NFR # 155936/700)

for financial support. In addition we thank the Strategic University Program BIOROV (NTNU # 81111400) for PhD-research fellowship to TBH.

References

Canfield, D. E. & DesMarais, D. J. 1993. Biochemical cycles of carbon, sulphur, and free oxygen in microbial mat. *Geochim. Cosmochim. Acta.* 57:3971-84.

Chauton, M. S., Tilstone, G. H., Legrand, C. & Johnsen, G. 2004. Changes in pigmentation, bio-optical characteristics and photophysiology, during phytoflagellate succession in mesocosms. *Photosynth. Res.* 26:315-24.

Davison, I. R. 1991. Environmental Effects on Algal Photosynthesis - Temperature. *J. Phycol.* 27:2-8.

Falkowski, P. G. & Woodhead, A. D. 1992. Primary Productivity and Biochemical Cycles in the Sea. Plenum Press, New York, 550 pp.

Flameling, I. A. & Kromkamp, J. 1998. Light dependence of quantum yields for PSII charge separation and oxygen evolution in eucaryotic algae. *Limnol. Oceanogr.* 43:284-97.

Genty, B., Briantais, J. M. & Baker, N. R. 1989. The Relationship between the Quantum Yield of Photosynthetic Electron-Transport and Quenching of Chlorophyll Fluorescence. *Biochim. Biophys. Acta* 990:87-92.

Gilbert, M., Domin, A., Becker, A. & Wilhelm, C. 2000. Estimation of primary productivity by chlorophyll a in vivo fluorescence in freshwater phytoplankton. *Photosynthetica* 38:111-26.

Glud, R. N., Gundersen, J. K. & Ramsing, N. B. 2000. Electrochemical and optical oxygen microsensors for in situ measurements. *In* Buffle, J. & Horvai, G. [Eds.] *In situ monitoring of aquatic systems: Chemical analysis and speciation*. John Wiley & Sons Ltd., pp. 20-73.

Glud, R. N., Ramsing, N. B. & Revsbech, N. P. 1992 Photosynthesis and photosynthesis coupled respiration in natural biofilms quantified with oxygen microelectrodes. *J. Phycol.* 28:51-60.

Govindjee 1995. Sixty-three years since Kautsky: Chlorophyll *a* fluorescence. *Aust. J. Plant. Physiol.* 22:131-60.

Guillard, R. R. & Ryther, J. H. 1962. Studies of Marine Planktonic Diatoms .1. Cyclotella Nana Hustedt, and Detonula Confervacea (Cleve) Gran. *Can. J. Microbiol.* 8:229-39.

Hancke, K., Hancke, T. B., Mork, L., Johnsen, G. & Glud, R. 2006. Temperature effects on microalgae photosynthesis-light responses measured by O_2-evolution, pulse amplitude modulated (PAM) fluorescence and ^{14}C-assimilation. Submitted *J. Phycol.*

Haxo, F. T. 1985. Photosynthetic action spectrum of the coccolithophorid, *Emiliania huxleyi* (Haptophyceae): 19'Hexanoyloxyfucoxanthin as antenna pigment. *J. Phycol.* 21:282-7.

Johnsen, G., Prézelin, B. B. & Jovine, R. V. M. 1997. Fluorescence excitation spectra and light utilization in two red tide dinoflagellates. *Limnol. Oceanogr.* 42:1166-77.

Johnsen, G. & Sakshaug, E. 1993. Bio-optical characteristics and photoadaptive responses in toxic and bloomforming dinoflagellates *Gyrodinium aureolum, Gymnodinium galatheanum*, and two strains of *Prorocentrium minimum*. *J. Phycol.* 29:627-42.

Johnsen, G. & Sakshaug, E. 2006. Bio-optical characteristics of PSII and PSI in 33 species (13 pigment groups) of marine phytoplankton, and the relevance for PAM and FRR fluorometry. Submitted *J. Phycol*.

Kolber, Z. & Falkowski, P. G. 1993. Use of active fluorescence to estimate phytoplankton photosynthesis in situ. *Limnol. Oceanogr.* 38:1646-65.

Kopf, U. & Heinze, J. 1984. 2,7-Bis(Diethylamino)Phenazoxonium Chloride as a Quantum Counter for Emission Measurements between 240 and 700 Nm. *Anal. Chem.* 56:1931-5.

Kromkamp, J. C., Domin, A., Dubinsky, Z., Lehmann, C. & Schanz, F. 2001. Changes in photosynthetic properties measured by oxygen evolution and variable chlorophyll fluorescence in a simulated entrainment experiment with the cyanobacterium Planktothrix rubescens. *Aqua. Sci.* 63:363-82.

Kromkamp, J. C. & Forster, R. M. 2003. The use of variable fluorescence measurements in aquatic ecosystems: difference between multiple and single turnover measuring protocols and suggested terminology. *Eur. J. Phycol.* 38:103–12

Kroon, B., Prezelin, B. B. & Schofield, O. 1993. Chromatic regulation of quantum yield for photosystem II charge separation, oxygenevolution and carbon fixation in *Heterocapsa pygmaea* (Pyrrophyta). *J. Phycol.* 29:453-62.

Longstaff, B. J., Kildea, T., Runcie, J. W., Cheshire, A., Dennison, W. C., Hurd, C., Kana, T., Raven, J. A. & Larkum, A. W. D. 2002. An in situ study of photosynthetic oxygen exchange and electron transport rate in the marine macroalga *Ulva lactuca* (Chlorophyta). *Photosynth. Res.* 74:281-93.

Ludden, E., Admiraal, W. & Colijn, F. 1985. Cycling of carbon and oxygen in layers of marine microphytes: a simulation model and its eco-physiological implications. *Oceologia* 66:50-9.

MacKinney, G. 1941 Absorption of light by chlorophyll solutions. *J. Biol. Chem.* 140:315- 22.

Mitchell, B. G. 1990. Algorithms for determining the absorption coefficient for aquatic particulates using the quantitative filter technique (QFT). *Proc. SPIE Ocean Opt. X* 1302:137-48.

Mitchell, B. G. & Kiefer, D. A. 1988. Chlorophyll *a* specific absorption and fluorescence excitation spectra for light-limited phytoplankton. *Deep-Sea Res.* 35:639-63.

Morel, A., Lazzara, L. & Gostan, J. 1987. Growth rate and quantum yield timerespense for a diatome to changing irradiances (energy and color). *Limnol. Oceanogr.* 32:1066-84.

Morris, E. P. & Kromkamp, J. C. 2003. Influence of temperature on the relationship between oxygen- and fluorescence-based estimates of photosynthetic parameters in a marine benthic diatom (Cylindrotheca closterium). *Eur. J. Phycol.* 38:133-42.

Mullineuax, C. W. & Allen, J. F. 1988. Fluorescence induction transients indicate dissociation of photosystem II from the bilisome during the state-2 transition in the cyanobacterium *Synechococcus* 6301. *Biochim. Biophys. Acta.* 934:96–107.

Neori, A., Vernet, M., Holmhansen, O. & Haxo, F. T. 1988. Comparison of Chlorophyll far-red fluorescence excitation spectra with photosynthetic oxygen action spectra for photosystem II in algae. *Mar. Ecol. Prog. Ser.* 44:297-302.

Owens, T. G. 1991. Energy transformation and fluorescence in photosynthesis. *In* Demers, S. [ed] Particle analysis in oceanography. NATO ASI series G, Springer Verlag, Berlin, 27: pp. 101-37.

Prézelin, B. B., Tilzer, M. M., Schofield, O. & Haese, C. 1991. The control of the production process of phytoplankton by the physical structure of the aquatic environment with special reference to its optical properties. *Aquatic Sci.* 53:136-86.

Revsbech, N. P. 1989. An oxygen microelectrode with guard cathode. *Limnol. Oceanogr.* 34:474-8.

Sakshaug, E. & Andresen, K. 1986. Effect of light regime upon growth rate and chemical composition of a clone of Skeletonema costatum from the Trondheimsfjord, Norway. *J. Plankton Res.* 8:619-37.

Sakshaug, E., Andresen, K. & Kiefer, D. A. 1989. A steady-state description of growth and light-absorption in the marine planktonic diatom *Skeletonema-Costatum. Limnol. Oceanogr.* 34:198-205.

Sakshaug, E., Bricaud, A., Dandonneau, Y., Falkowski, P. G., Kiefer, D. A., Legendre, L., Morel, A., Parslow, J. & Takahashi, M. 1997. Parameters of photosynthesis: definitions, theory and interpretation of results. *J. Plankton. Res.* 19:1637-70.

Sakshaug, E. & Holm-Hansen, O. 1977. Chemical Composition of Skeletonema-Costatum (Grev) Cleve and Pavlova (Monochrysis) Lutheri (Droop) Green as a Function of Nitrate-Limited, Phosphate-Limited, and Iron-Limited Growth. *J. Exp. Mar. Biol. Ecol.* 29:1-34.

Sakshaug, E., Johnsen, G., Andresen, K. & Vernet, M. 1991. Modeling of light-dependent algal photosynthesis and growth: Experiments with the Barents Sea diatoms *Thalassiosira nordenskioeldii* and *Chaetoceros furcellatus*. *Deep-Sea Res.* 38:415-30.

Schofield, O., Prézelin, B. B., Bidigare, R. R. & Smith, R. C. 1993. In situ photosynthetic quantum yield. Correspondance to hydrographic and optical variability within the Southern California bight. *Mar. Ecol. Prog. Ser.* 93:25-37.

Schreiber, U., Hormann, H., Neubauer, C. & Klughammer, C. 1995. Assessment of photosystem II photochemical quantum yield by chlorophyll fluorescence quenching analysis. *Aust. J. Plant. Physiol.* 22:103-9.

Schreiber, U., Schliwa, U. & Bilger, W. 1986. Continuous recording of photochemical and non-photochemical chlorophyll fluorescence quenching with a new type of modulation fluorometer. *Photosyn. Res.* 10:51-62.

Steeman-Nielsen, E. 1952. The use of radio-carbon (14C) for measuring organic production in the sea. *J. Cons. Int. Explor. Mer.* 18:117-40.

van Kooten, O. & Snel, J. F. H. 1990. The Use of Chlorophyll Fluorescence Nomenclature in Plant Stress Physiology. *Photosynt. Res.* 25:147-50.

Webb, W. L., Newton, M., & Starr, D. 1974. Carbon exchange of *Alnus rubra*: A mathematical model. *Oecologia* 17:281-91.

Yentsch, C. S. 1962. Measurement of visible light absorption by particulate matter in the ocean. *Limnol. Oceanogr.* 7:207–17.

Table 1. Significant symbols

Symbol	Explanation	Dimension
$a^*_\varphi(\lambda)$	chl *a*-specific absorption coefficient, 400-700 nm	$m^2(mg\ chl\ a)^{-1}$
$F^*_{PSII}(\lambda)$	PSII-scaled fluorescence excitation spectrum, 400-700 nm	$m^2(mg\ chl\ a)^{-1}$
$\bar{a}^*_\varphi$	Total amount of spectrally weighted light absorbed normalised to chl *a*	$m^2(mg\ chl\ a)^{-1}$
$\bar{a}^*_{PSII}$	Spectrally weighted PSII-absorption normalised to chl *a*	$m^2(mg\ chl\ a)^{-1}$
F_{II}	Fraction of chl *a* in PSII and its associated LHC, (F^*_{PSII} (red)/ a^*_φ (red))	
P_{PSII}	Calculated O_2 production rate at a given E	mg O_2(mg POC)$^{-1}\cdot h^{-1}$
P_{PSII_max}	Calculated O_2 production rate at light saturation	mg O_2(mg POC)$^{-1}\cdot h^{-1}$
P_{O2}	Oxygen production rate at a given irradiance	mg O_2(mg POC)$^{-1}\cdot h^{-1}$
P_{O2_max}	Maximum oxygen production rate at light saturation	mg O_2(mg POC)$^{-1}\cdot h^{-1}$
α	Maximum light utilisation coefficient	mg O_2(mg POC)$^{-1}\cdot h^{-1}$(µmol photons$\cdot m^{-2}\cdot s^{-1})^{-1}$
E_k	Light saturation parameter, (P_{max}/α)	µmol photons$\cdot m^{-2}\cdot s^{-1}$
Γ	Stoichiometric ratio of oxygen evolved per electron generated at PSII	$O_2\cdot(e^-)^{-1}$
F_0	Initial fluorescence in dark acclimated cells	
F_0'	Initial fluorescence in cells incubated in actinic light	
F_m	Maximum fluorescence in dark acclimated cells	
F_m'	Maximum fluorescence in cells incubated in actinic light	
F_v	Variable fluorescence in dark acclimated cells	
F_v'	Variable fluorescence in cells incubated in actinic light	
$\Phi_{PSII\ max}$	Maximum quantum yield of charge separation in PSII	mol $e^-\cdot$mol photons^{-1}
Φ_{PSII}	Operational quantum yield of charge separation in PSII	mol $e^-\cdot$mol photons^{-1}
${}^{PSII}\Phi_{O2\ max}$	Maximum quantum yield of O_2 production rate, using $\bar{a}^*_{PSII}$	mol $e^-\cdot$mol photons^{-1}

Table 2. chl *a* concentration (µg L^{-1}), carbon content (POC, µg L^{-1}) and chl *a* C^{-1} ratio (w:w) in the cultures during each experiment. Fraction of chl *a* in PSII calculated from red-peak scaling (F_{II}), spectrally weighted PSII absorption normalised to chl *a* ($\bar{a}^{*}_{PSII}$; m^2 (mg chl *a*)$^{-1}$ or (mg chl *a*)$^{-1}$·h^{-1}) and the spectrally weighted light absorption coefficient normalised to chl *a* ($\bar{a}^{*}_{\varphi}$; m^2 (mg chl *a*)$^{-1}$) for each incubation.

Species	Incubation temperature	[chl *a*]	POC	chl *a* C^{-1}	F_{II}	$\bar{a}^{*}_{PSII}$	$\bar{a}^{*}_{\varphi}$
P. minimum	10 °C	312.3	37396.5	0.0084	0.801	0.0054	0.0068
	20 °C	281.0	29060.6	0.0097	0.702	0.0062	0.0082
P. parvum	10 °C	711.4	36887.2	0.0193	0.873	0.0084	0.0108
	20 °C	689.0	36319.6	0.0190	0.922	0.0132	0.0164
P. tricornutum	10 °C	135.0	6323.2	0.0213	0.966	0.0076	0.0095
	20 °C	205.8	8319.5	0.0247	0.975	0.0068	0.0083

Table 3. Photosynthetic parameters calculated from the P *vs*. E curves in Fig. 4 for $P_{PSII,}$ using $\bar{a}^{*}_{PSII}$, $F_{II}\cdot\bar{a}^{*}_{\varphi}$ and $0.5\cdot\bar{a}^{*}_{\varphi}$, and P_{O2}.

Units: P_{max} (µmol O_2 (mg POC)$^{-1}\cdot h^{-1}$); α (µmol O_2 (mg POC)$^{-1}\cdot h^{-1}$ (µmol photons$\cdot m^{-2}\cdot s^{-1})^{-1}$) and E_k (µmol photons$\cdot m^{-2}\cdot s^{-1}$).

		P_{PSII}							P_{O2}		
	Incubation temperature	P_{max}			α			E_k	P_{max}	α	E_k
Species		$\bar{a}^{*}_{PSII}$	$F_{II}\cdot\bar{a}^{*}_{\varphi}$	$0.5\cdot\bar{a}^{*}_{\varphi}$	$\bar{a}^{*}_{PSII}$	$F_{II}\cdot\bar{a}^{*}_{\varphi}$	$0.5\cdot\bar{a}^{*}_{\varphi}$	-	O_2-meas.	O_2-meas.	O_2-meas.
P. minimum	10 °C	1.839	1.857	1.158	0.030	0.030	0.019	61.0	2.285	0.046	49.8
	20 °C	2.802	2.585	1.843	0.047	0.043	0.031	59.8	5.418	0.084	64.2
P. parvum	10 °C	3.953	4.426	2.538	0.108	0.121	0.069	36.6	3.161	0.048	66.0
	20 °C	8.728	10.040	5.440	0.150	0.173	0.094	58.1	5.020	0.059	84.7
P. tricornutum	10 °C	4.636	5.638	2.915	0.142	0.171	0.089	32.8	5.698	0.362	15.7
	20 °C	9.025	10.725	5.502	0.123	0.146	0.075	73.3	8.597	0.171	50.3

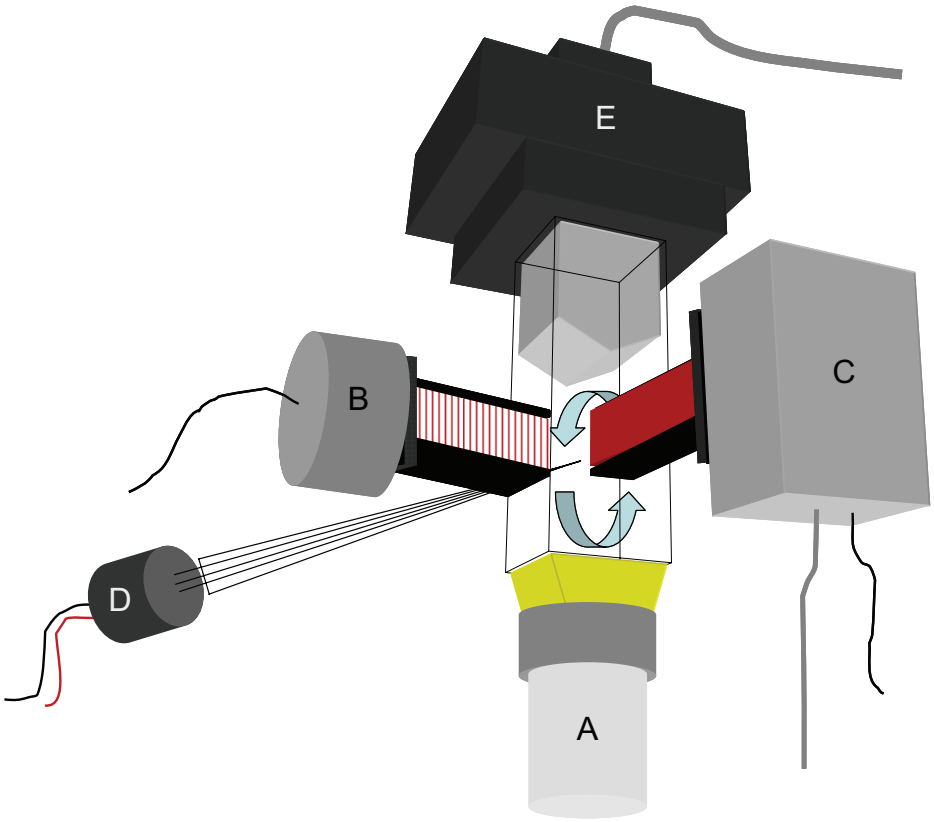

Fig. 1. Schematic drawing of the steps involved in the bio-optical determination of the fraction of light absorbed by PSII according to Johnsen and Sakshaug 1996; Johnsen et al. 1997. The incubation light source is given in PAR, 400-700 nm. F_{II} and $\bar{a}^{*}_{PSII}$ are evaluated as new input parameters to estimate light absorbed by PSII using PAM to estimate oxygenic photosynthesis.

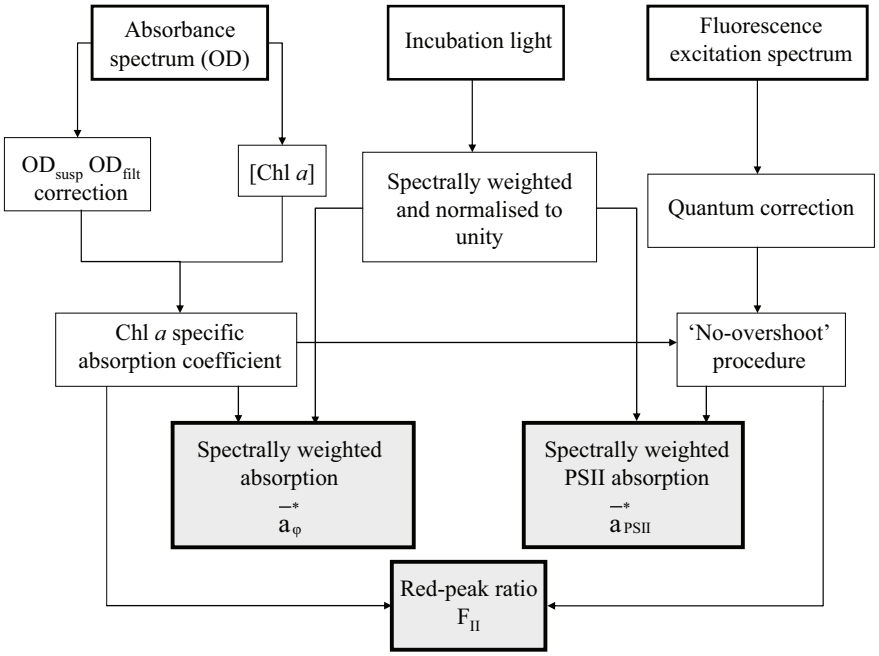

Fig. 2. A schematic drawing of the experimental set-up. A: Fiber optics to lead incubator light and flash light through a short pass filter (SP 695 nm) to the sample in the cuvette. B: Probe light, a red light emitting diode (LED, <0.15 µmol photons·m^{-2}·s^{-1}, 655 nm, 1.6 kHz and 100 kHz) with an excitation filter (SP 695 nm). C: Photomultiplier detector (PMT, Walz, Germany, PM–101/N) with emission filter (LP 695 nm). D: O_2-microsensor inserted through a tight-fitting miniature pipe in the wall of the incubation cuvette. E: A Peltier cell in which the temperature was kept constant (± 0.2°C, Walz, Germany, US-T/S). The algae were kept suspended inside the cuvette by a slowly circulating water flow driven by the cooling of the Peltier cell and heating from the incubator light.

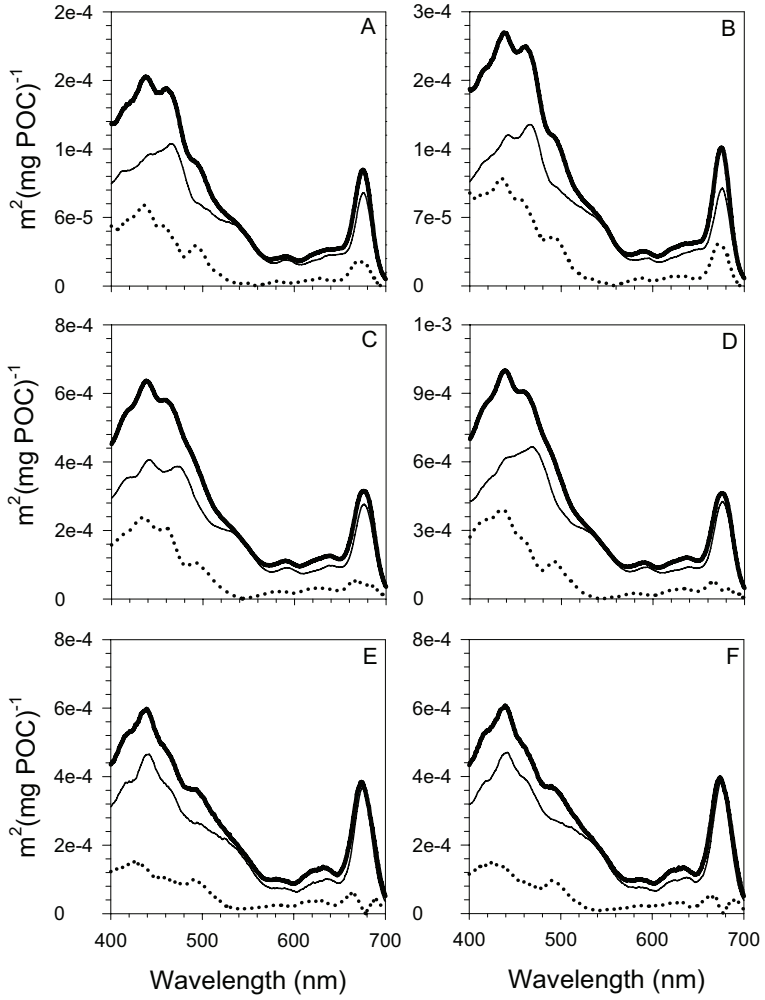

Fig. 3. *In vivo* POC-specific absorption coefficients, $a^*_\varphi(\lambda)$ (thick black line), the PSII-scaled fluorescence excitation spectra, $F^*_{PSII}(\lambda)$ (thin black line) and the corresponding difference spectra, ($a^*_\varphi(\lambda)$- $F^*_{PSII}(\lambda)$, dotted black line) for *P. minimum* (A-B), *P. parvum* (C-D) and *P. tricornutum* (E-F), at 10°C (left column) and 20°C (right column). The difference spectra denote the non-fluorescent fraction indicating absorption of PSI and photoprotective pigments (diadinoxanthin and diatoxanthin).

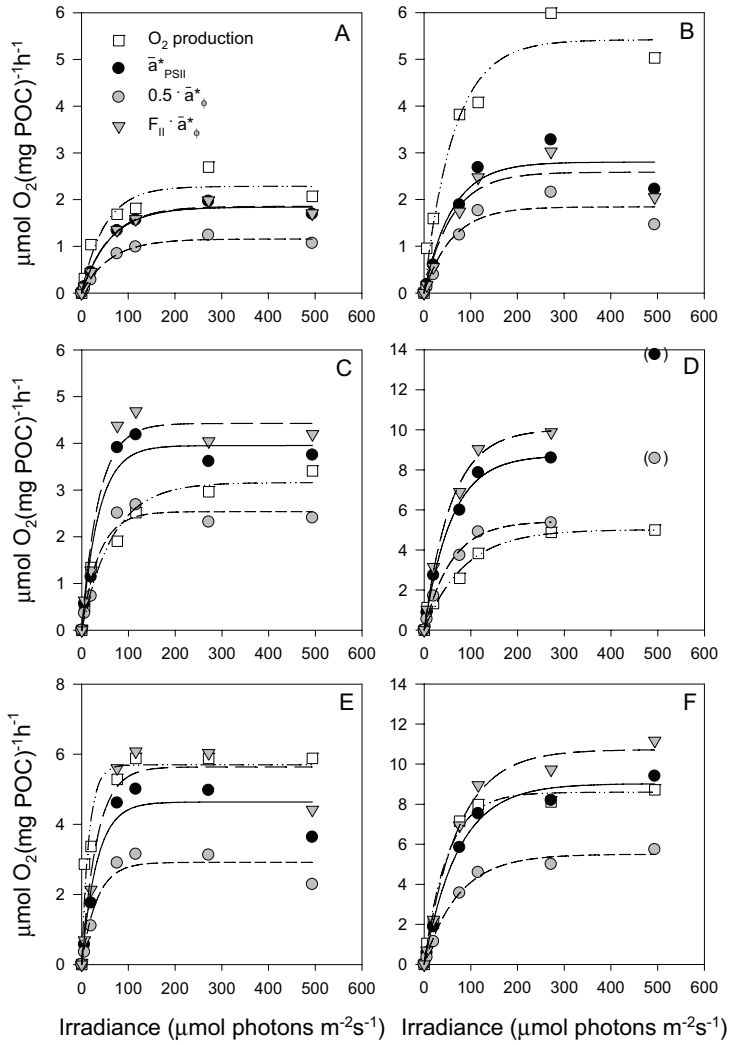

Fig. 4. Photosynthesis *vs.* irradiance curves calculated from PAM fluorescence measurements (P_{PSII}) based on three bio-optical approaches for estimation of light absorbed by PSII, AQ_{PSII}: $0.5 \cdot \bar{a}^*_{\varphi}$ (approach 1), $F_{II} \cdot \bar{a}^*_{\varphi}$ (approach 2) and $\bar{a}^*_{PSII}$ (approach 3) and simultaneously measured photosynthetic O_2 evolution (P_{O2}) for *P. minimum* (A-B), *P. parvum* (C-D) and *P. tricornutum* (E-F), at 10°C (left column) and 20°C (right column). Parenthesis in Fig. 4D denotes outliers. Note different y-axes.

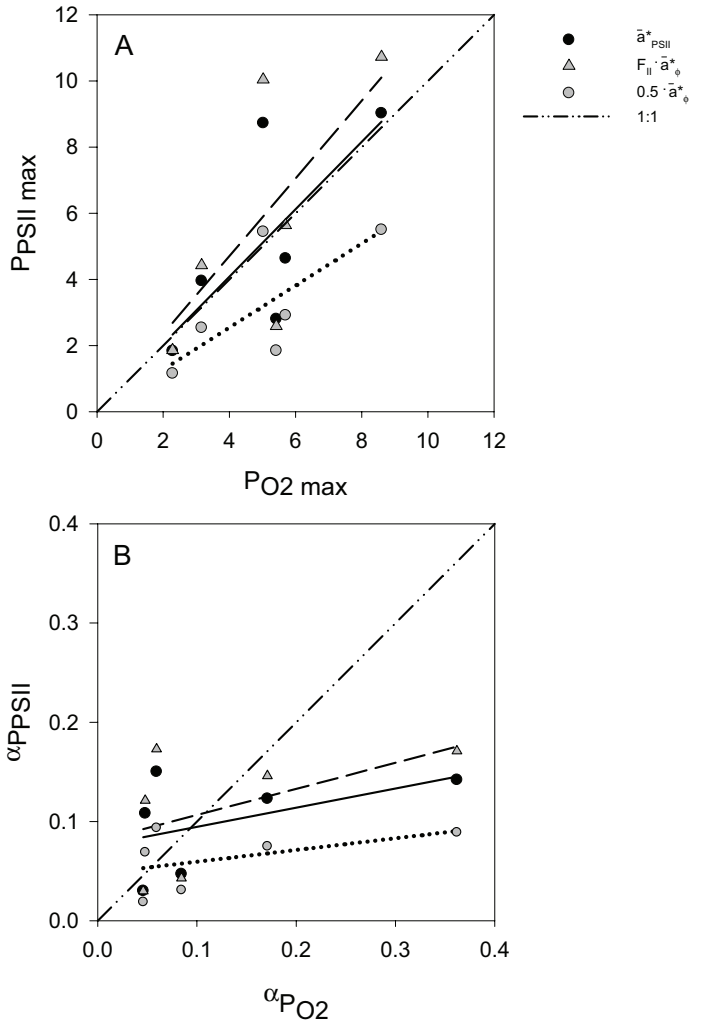

Fig. 5. A) Maximum photosynthetic rate, P_{PSII_max}, based on $\bar{a}^*_{PSII}$, $F_{II} \cdot \bar{a}^*_{\varphi}$ and $0.5 \cdot \bar{a}^*_{\varphi}$, as function of P_{O2_max}, for the six incubations (three species; *P. minimum*, *P. parvum* and *P. tricornutum*, and two temperatures; 10 and 20 °C). Units on both axes are µmol O_2(mg POC)$^{-1}$·h^{-1}. B) α_{PPSII} calculated from $\bar{a}^*_{PSII}$, $F_{II} \cdot \bar{a}^*_{\varphi}$ and $0.5 \cdot \bar{a}^*_{\varphi}$, as function of α_{PO2}, for the same six incubations. Units on both axes are µmol O_2(mg POC)$^{-1}$·h^{-1} (µmol photons·m^{-2}·s^{-1})$^{-1}$. The dashed line represents x = y.

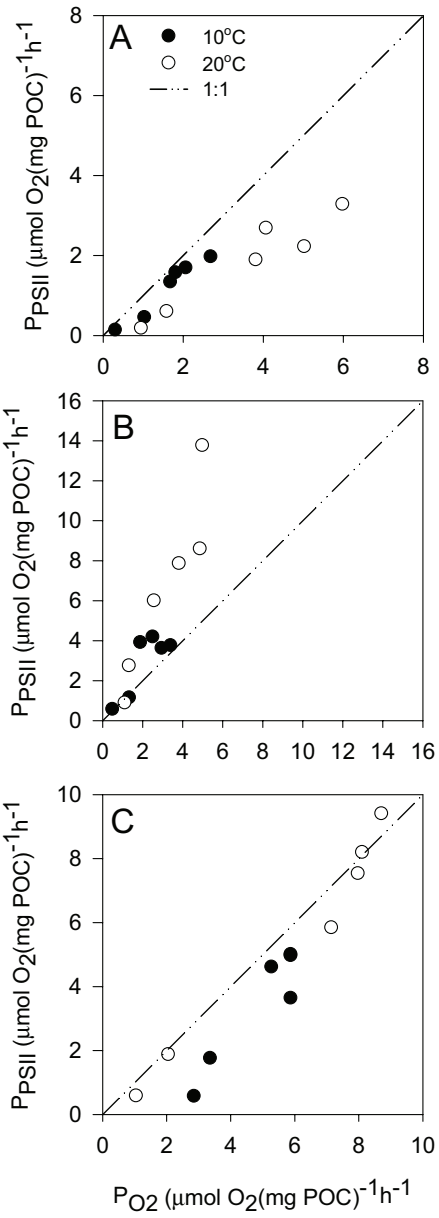

Fig. 6. P_{PSII} based on $\vec{a}^{*}_{PSII}$ as function of P_{O2} incubated at 10 and 20 °C, for A) *P. minimum*, B) *P. parvum* and C) *P. tricornutum*. The dashed line represents x = y.

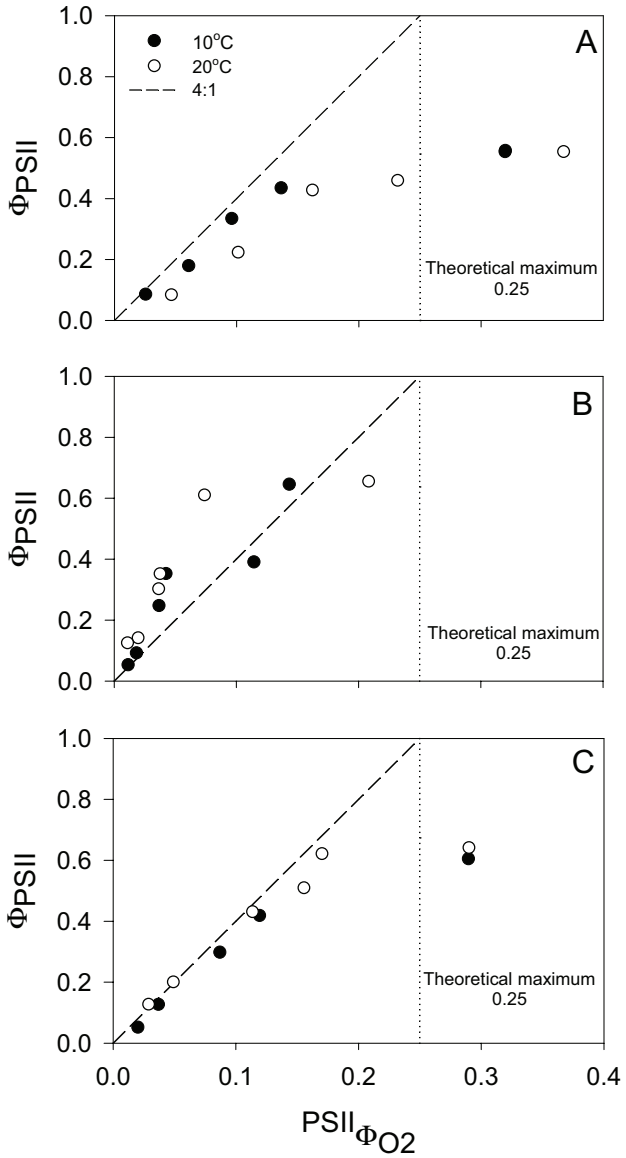

Fig. 7. Φ_{PSII} as a function of $^{PSII}\Phi_{O2}$ incubated at 10 and 20°C, for A) *P. minimum*, B) *P. parvum* and C) *P. tricornutum*. The dashed line represents the theoretical 4:1 relationship between Φ_{PSII} and $^{PSII}\Phi_{O2}$ indicating a maximum quantum yield of oxygen at 0.25.

Paper 3

Hancke K, Hancke TB, Olsen LM, Johnsen G, Glud RN (submitted)

Temperature effects on microalgae photosynthesis-light responses measured by O_2-production, Pulse Amplitude Modulated (PAM) fluorescence and ^{14}C-assimilation.

Journal of Phycology

TEMPERATURE EFFECTS ON MICROALGAE PHOTOSYNTHESIS-LIGHT RESPONSES MEASURED BY O_2-PRODUCTION, PULSE AMPLITUDE MODULATED (PAM) FLUORESCENCE AND ^{14}C-ASSIMILATION[1]

Kasper Hancke[1]*, Torunn B. Hancke, Lasse M. Olsen, Geir Johnsen*

Department of Biology, Norwegian University of Science and Technology, N-7491 Trondheim, Norway

and

Ronnie N. Glud

Marine Biological Laboratory, University of Copenhagen, Strandpromenaden 5, DK-3000 Helsingør, Denmark

Running title: Photosynthesis *versus* temperature

[1] Author for correspondence: email kasper.hancke@bio.ntnu.no, phone: +4773591580, fax: +4773591597

ABSTRACT

Short-term temperature effects on photosynthesis were investigated by measuring O_2-production, Photosystem II (PSII) fluorescence kinetics and ^{14}C-incorporation rates in monocultures of the marine phytoplankton species *Prorocentrum minimum* (Dinophyceae), *Prymnesium parvum* (Coccolithophyceae), and *Phaeodactylum tricornutum* (Bacillariophyceae), grown at 15°C and 80 µmol photons·m^{-2}·s^{-1}. Photosynthesis *versus* irradiance curves were measured at seven temperatures (0 to 30°C) by all three approaches. The maximum photosynthetic rate (P^C_{max}) was strongly stimulated by temperature, reached an optimum for *P. minimum* only (20 - 25°C), and showed a similar relative temperature response for the three applied methods, with Q_{10} ranging from 1.7 to 3.5. The maximum light utilisation coefficient (α^C) was insensitive or decreased slightly with increasing temperature. Absolute rates of O_2-production were calculated from PAM based fluorescence measurements in combination with bio-optical determination of absorbed quanta in PSII. The relationship between PAM based O_2-production and measured O_2-production and ^{14}C-assimilation showed a species-specific correlation with 1.2 to 3.3 times higher absolute values of P^C_{max} and α^C, when calculated from PAM data for *P. parvum* and *P. tricornutum* but equivalent for *P. minimum*. The off-set seemed to be temperature insensitive and could be explained by a lower quantum yield for O_2-production than the theoretical maximum (due to Mehler-type reactions). Conclusively, the PAM technique can be used to study temperature responses of photosynthesis in microalgae when paying attention to the absorption properties in PSII.

Key index words: ^{14}C-assimilation, O_2-production, microalgae, PAM-fluorescence, phi-max, photosynthetic parameters, quantum yield, temperature

Abbreviations: ETR, electron transport rate; PAM, pulse amplitude modulated fluorescence; P-E, photosynthesis-irradiance; POC, particular organic carbon; PQ, photosynthetic quotient; Q_{10}, temperature coefficient; See also Table 1.

INTRODUCTION

Pelagic photosynthesis can be estimated by measuring O_2-evolution, Photosystem II (PSII) fluorescence kinetics or ^{14}C-assimilation. Each of the methods has their advantages and disadvantages and have all been applied to assess the ecosystem primary production in various environments. The techniques, however, measure different products of the photosynthetic pathway and reflect different physiological processes with potential different responses to environmental variables like temperature or salinity (Geider and Osborne 1992, Geel et al. 1997, Morris and Kromkamp 2003).

O_2-evolution measurements using O_2-electrodes allows for net O_2-production measurements in light and O_2-respiration in the dark (Glud et al. 2000). Gross O_2-production can then be estimated as the net production added the respiration (assuming constant respiration in light and dark). As such the approach quantifies the O_2-production rate from the water-splitting complex in PSII. PSII fluorescence can be measured by Pulse Amplitude Modulated (PAM) fluorometry and can be used to measure the operational quantum yield of PSII (Φ_{PSII}, Schreiber et al. 1986). From multiplying Φ_{PSII} with the quanta absorbed in PSII the electron transfer rate in PSII can be calculated (Genty et al. 1989). The electron transfer rate (ETR) is a proxy for the gross photosynthetic rate (Kroon et al. 1993). The electrons generated in PSII are closely coupled to the O_2-evolution , but follows several pathways, among those reduction of CO_2 via NAD(P)H production (Falkowski and Raven 1997). ^{14}C-assimilation rate measurements quantifies the amount of DIC (dissolved inorganic carbon) converted into cell biomass and reflect an activity intermediate to net and gross photosynthesis, dependent on the incubation time (Falkowski and Raven 1997). For 1 hour incubations the technique is for convenience commonly assumed to indicate gross rates.

Photosynthetic O_2-production, Φ_{PSII} and/or ^{14}C-assimilation have been compared in a number of studies of vascular plants (e.g. Demmig and Bjorkman 1987, Seaton and

Walker 1990), macroalgae (e.g. Hanelt and Nultsch 1995, Longstaff et al. 2002), microphytobenthos (Hartig et al. 1998, Barranguet and Kromkamp 2000, Glud et al. 2002a) and marine phytoplankton (Falkowski et al. 1986, Kroon et al. 1993, Geel et al. 1997, Flameling and Kromkamp 1998, Rysgaard et al. 2001, Morris and Kromkamp 2003). Although the investigations have been conducted under a variety of experimental conditions, an overweight of the studies on microalgae find a linear relationship between O_2-evolution and Φ_{PSII} under moderate irradiance (e.g. Falkowski et al. 1986, Genty et al. 1989, Geel et al. 1997), sometimes with deviation at very low (Schreiber et al. 1995, Flameling and Kromkamp 1998, Masojidek et al. 2001) or very high irradiance conditions (Falkowski et al. 1986, Flameling and Kromkamp 1998). Different explanations for the deviation have been proposed; spectral difference in PAR sources, changes in O_2-consumption in the light, cyclic electron transport around PSII and Mehler-type reactions, see Flameling and Kromkamp (1998) for an overview. The relationship between O_2-production and Φ_{PSII} is far from universal and apparently there exist inter-species variance in the shape of the relationship and of the slope-coefficient (Barranguet and Kromkamp 2000, Masojidek et al. 2001). Additionally, it must be expected that environmental variables, such as temperature, can affect established relations for a given species. Even so, detailed comparison studies accounting for environmental variables, such as temperature, are still very limited (Barranguet and Kromkamp 2000, Morris and Kromkamp 2003). If fluorescence measurements are to be applied successfully for quantifying photosynthetic production, more careful and detailed studies of the temperature effect on the relationship between O_2-evolution, Φ_{PSII} and ^{14}C-assimilation are required (e.g. Schofield et al. 1998, Kuhl et al. 2001, Glud et al. 2002b, Morris and Kromkamp 2003)

The aim of the present study was to investigate the relationship between temperature and photosynthetic parameters derived from measurements of O_2-production, Φ_{PSII} and ^{14}C-assimilation, using three culture-grown phytoplankton species; *Prorocentrum minimum* (Pavillard) Schiller (Dinophyceae)*, Prymnesium parvum* cf. *patelliferum* Green (Coccolithophyceae in Haptophyceae), and *Phaeodactylum*

tricornutum Bohlin (Bacillariophyceae), selected to represent typical species of Scandinavian waters. Photosynthetic activity was quantified from 1) measured rates of O_2-production by O_2-microsensors (P^C_{O2}, µmol O_2·(mg POC)$^{-1}$·h^{-1}), 2) calculated rates of O_2-production based on Φ_{PSII} in combination with bio-optical determination of quanta absorbed in PSII (P^C_{PSII}, µmol O_2·(mg POC)$^{-1}$·h^{-1}), and 3) measured rates of ^{14}C-assimilation (P^C_{14C}, µmol ^{14}C·(mg POC)$^{-1}$·h^{-1}). The temperature influence on photosynthetic parameters is discussed in a physiological context.

MATERIALS AND METHODS

Algal cultures

Unialgal cultures of *Prorocentrum minimum* (strain 79A, Oslofjord, isolated by K.Tangen, culture at TBS), *Prymnesium parvum* (isolated in Ryfylke, S- Norway, culture from University of Oslo), and *Phaeodactylum tricornutum* (unknown origin, TBS culture collection) were grown in semi-continuous cultures in f/2 medium (Guillard and Ryther 1962), pre-filtered (0.2 µm sterile filters, and pasteurised at 80°C in 3h) and enriched with silicate (*P. tricornutum* only). All cultures were sub sampled from the culture collection of Trondhjem Biological Station, and grown at 15 ± 1°C, 33 ppt salinity seawater, and constantly bubbled with filtered air. The illumination was continuous "white" fluorescent light (Philips TL 40W/55 tubes) providing 80 µmol photons·m^{-2}·s^{-1} as measured by means of a QSL-100 quantum sensor (Biospherical Instruments, USA) placed inside the culture flasks. The growth rate and the chlorophyll *a* (chl *a*) concentration were maintained semi constant by diluting the cultures once per day corresponding to a specific growth rate of 0.2 µ·d^{-1} for *P. minimum* and *P. parvum*, and 0.7 - 0.8 µ·d^{-1} for *P. tricornutum* both prior to and during the time of the experiments. The cultures were enriched with 1 g $NaHCO_3$ L^{-1} to avoid depletion of inorganic carbon due to photosynthesis.

While growing, the physiological state of the cultures were monitored daily by measuring the ratio of *in vivo* chl *a* fluorescence before and after addition of DCMU (3(3,4 dichlorophenyl)-1, 1-dimethylurea, 50 µM final concentration) in a Turner Designs fluorometer. DCMU blocks the electron transport in PSII and result in a maximal fluorescence. The ratio of fluorescence measured after and before the addition of DCMU >2.5 indicates a healthy state of the cell (Sakshaug and Holm-Hansen 1977). In our study the ratio generally ranged from 2.7 to 3.5.

Experimental conditions

Cultures were sub sampled every morning, in order to perform parallel measurements of photosynthesis versus irradiance (P-E curves) from O_2-evolution, PAM and ^{14}C-assimilation measurements. The sub samples were placed in a water

bath set at one of the seven experimental temperatures (0, 5, 10, 15, 20, 25 and 30°C) and the experiment started after the respective temperatures had stabilised within the sample (<30 min). Incident irradiance was maintained. Subsequently, the sample was simultaneously introduced to each of the experimental setups.

O_2-evolution and ^{14}C-assimilation rates were measured in parallel after placing samples in a photosynthetron (Lewis and Smith 1983) in the dark and at 10 levels of irradiance from 3 to 570 µmol photons·m^{-2}·s^{-1} (PAR), determined by the QSL-100 quantum sensor. The photosynthetron was placed in a temperature controlled laboratory at the respective temperature. The samples were illuminated from below with an adjustable xenon light source (Osram 250W) while a water-flow-through system prevented radiation heat. Correct temperature was ensured by continuous (1 s frequency) temperature measurements using small water-proof data loggers (TidbiT, Onset Computer Cooperation) installed in dummy samples.

Triplicate samples were incubated in 20 mL polyethylene scintillation vials for 1 h. Vials for O_2 evolution measurements were filled completely and closed with a lid mounted with a miniature pipe (i.d. = 0.8 mm, length = 5 mm). The miniature pipe excluded head space of air, avoided potential pressure to accumulate from photosynthetic O_2-production and allowed for insertion of an O_2-microsensor. 2 mL of sample was incubated for carbon assimilation measurements.

O_2-microsensor measurements

All oxygen measurements were carried out using Clark-type O_2-microelectrodes with a guard cathode (Revsbech 1989), having an external tip diameter of ~100 µm, stirring sensitivity of <1.5%, and a 90% response time of <4 s. The electrodes were calibrated using anoxic and air-saturated solutions at the specific temperature setting, as oxygen electrode signals are sensitive to temperature (Gundersen et al. 1998, Glud et al. 2000). The sensor current was measured using a picoammeter (Unisense, Denmark) connected to a strip-chart recorder (Kipp & Zonen, The Netherlands) and a PC (Revsbech and Jørgensen 1986). The gross O_2-production rate (P^C_{O2}) was estimated by adding the dark respiration to the net O_2-evolution rate (both measured at each temperature), determined from the O_2-concentration change corrected for

incubation time. All samples were mixed gently with a Pasteur pipette introduced through the miniature pipe prior to measuring, ensuring a homogeneous O_2-concentration within the vial. In several cases the concentration of O_2 was monitored continuously during incubation, by an electrode installed in a randomly selected sample, confirming linear O_2-evolution.

PAM measurements

Fluorescence was measured using a PAM-101 fluorometer with a 102 and 103 module (Walz, Effeltrich, Germany) (Schreiber et al. 1986) equipped with a photomultiplier detector (PMT, Walz, Germany, PM-101/N). A red light-emitting diode (655 nm peak, <0.15 µmol photons·m^{-2}·s^{-1}, at 1.6 kHz) was used as probe light at an intensity too low to induce variable fluorescence. In the following we used the nomenclature of van Kooten and Snel (1990). The minimum fluorescence (F_o) and the maximum fluorescence (F_m) was measured at the end of a dark acclimation period (15 min), when approximately all reaction centres were closed. F_m was measured during a saturating light pulse from a halogen lamp (0.6 s, at >5000 µmol photons·m^{-2}·s^{-1}, Scott, Germany, KL1500 electronic) exposed to the sample via an optical fibre. The maximum quantum yield of PSII charge separation (Φ_{PSII_max}) in the dark acclimated cells was calculated as:

$$\Phi_{PSII\_max} = F_v/F_m = \frac{F_m - F_0}{F_m} \quad (1)$$

Under actinic illumination, the operational quantum yield of PSII (Φ_{PSII}) was calculated from the steady-state fluorescence (F_s) and the maximum fluorescence after a saturation pulse (F_m') at each incubation irradiance (Genty et al. 1989):

$$\Phi_{PSII} = \Delta F/F_m' = \frac{F_m' - F_s}{F_m'} \quad (2)$$

The incubation light was provided by a slide projector equipped with a halogen lamp and slide frames with different layers of neutral filters. After F_o and F_m were measured, the samples were exposed for 5 min at each of the irradiances (1 - 500 µmol photons·m^{-2}·s^{-1}), before measuring F_s and F_m'. The incubation irradiance (E, PAR) was measured inside the incubation chamber using a cosine-corrected (2π)

light collector of the DIVING-PAM (Walz, Effeltrich, Germany). The spectral distribution of the incubation light was measured using a RAMSES spectroradiometer (TRIOS, Germany) from 400 to 700 nm (E(λ), 1 nm resolution). The irradiance and the spectral distribution of the incubation light were used for further calculations of the amount of light absorbed by PSII. A Peltier cell (US-T/S Walz) kept the temperature constant (± 0.2°C) during incubations.

Bio-optics

To calculate O_2-evolution per biomass and time from Φ_{PSII}, the light absorbed by PSII were quantified in absolute units from the *in vivo* chl *a*-specific absorption coefficient, $a^*_\varphi(\lambda)$, ($m^2 \cdot (\text{chl } a)^{-1}$), and the PSII-scaled *in vivo* fluorescence excitation spectrum $F^*_{PSII}(\lambda)$ ($m^2 \cdot (\text{chl } a)^{-1}$). The optical density (OD) was measured on glass fibre filters according to Yentsch (1962) and Mitchell and Kiefer (1988), and converted to OD in suspension (Mitchell 1990). Absorption was calculated according to Mitchell and Kiefer (1988) and normalised to chl *a* to give $a^*_\varphi(\lambda)$. *In vivo* fluorescence excitation spectra were measured according to Neori et al. (1988) and Johnsen and Sakshaug (1993) and quantum corrected using the dye Basic Blue 3 (Kopf and Heinze 1984). $F^*_{PSII}(\lambda)$ was obtained from scaling the fluorescence excitation spectrum to the corresponding $a^*_\varphi(\lambda)$ using the 'no-overshoot' procedure by matching the two spectra at wavelengths between 540 and 650 (Bidigare et al. 1989, Johnsen et al. 1997). The light absorption in PSII ($\bar{a}^*_{PSII}$, $m^2 \cdot (\text{chl } a)^{-1}$) was obtained by spectrally weighting $F^*_{PSII}(\lambda)$ against the incubator light source according to Eq. 3

$$\bar{a}^*_{PSII} = \frac{\left[\sum_{400}^{700} F^*_{PSII}(\lambda) \cdot E(\lambda)\, d\lambda\right]}{E(PAR)} \qquad (3)$$

where $E(\lambda)$ is the spectral irradiance of the incubator light source and E(PAR) is the integrated irradiance from 400 to 700 nm. The applied bio-optical procedure above is described in details in Hancke et al. (Rate of O_2 production derived from PAM

fluorescence: Testing three bio-optical approaches against measured O_2 production rate, submitted to J. Phycology, hereafter referred to as Hancke et al. submitted). Definitions of bio-optical parameters used are given in Table 1.

Calculation of O_2-evolution from PAM measurements in combination with bio-optics

ETR is equal to the product of Φ_{PSII} and the amount of quanta absorbed by PSII ($\bar{a}^{*}_{PSII}$). By knowing the stoichiometric ratio of oxygen evolved per electron generated in PSII the rate of O_2 evolution (P^{C}_{PSII}) can be quantified (Kroon et al. 1993). Instead of calculating ETR we directly calculated the O_2-production rate in absolute units (P^{C}_{PSII}, μmol O_2·(mg POC)$^{-1}$·h^{-1}), from Eq. 4. (See Hancke et al. (submitted) for a discussion on different approaches for quantifying the amount of quanta absorbed by PSII)

$$P_{PSII} = \Phi_{PSII} \cdot E \cdot \Gamma \cdot \bar{a}^{*}_{PSII} \qquad (4)$$

where Γ is the stoichiometric ratio of oxygen evolved per electron generated at PSII. According to the standard Z-scheme of photosynthesis, four stable charge separations take place in both PSI and PSII, to evolve one O_2 molecule, *i.e.* 8 electrons to yield one molecule of oxygen. Γ will according to this assumption be 0.25 O_2 electrons^{-1} (Kroon et al. 1993, Gilbert et al. 2000). Empirically, a higher number than 8 electrons have been found which may be due to alternative electron "loss", e.g. Mehler-type reactions (Kromkamp et al. 2001, Longstaff et al. 2002, Hancke et al. submitted). For simplicity, we assumed Γ to be 0.25 in the present study.

Most papers that use PAM-estimated Φ_{PSII} to calculate O_2 evolution rates assume that that absorbed irradiance is distributed between PSII and PSI with a ratio of 0.5 (Gilbert et al. 2000). This is a rough estimate and the ratio is higher for most phytoplankton classes with the consequence of underestimating the O_2 evolution from PSII (Johnsen and Sakshaug, Bio-optical characteristics of PSII and PSI in 33 species (13 pigment groups) of marine phytoplankton, and the relevance for PAM and FRR fluorometry, submitted to J. Phycology, hereafter refereed to as Johnsen

and Sakshaug submitted). In the present paper we have applied a bio-optical procedure to measure the PSII-specific absorption directly.

Photosynthetic O_2-production rates obtained in the photosynthetron and in the PAM cuvette was compared in a pilot-study by measuring P-E curves of O_2-evolution in both experimental setups. An O_2-microsensor was inserted directly in the PAM cuvette (Hancke et al. submitted), and measured rates were compared to the O_2-production rates measured in the photosynthetron. The P-E curves calculated from the two experimental set-ups shown equivalent shapes and similar rates and had an average difference and a standard deviation for P^C_{max} and α^C of 2.2 ± 21.3 % and 22.7 ± 23.8 %, respectively. Simultaneous measurements of Φ_{PSII} verified reproducible photosynthetic responses between the pilot-study and the present study.

^{14}Carbon assimilation

Carbon assimilation rate (P^C_{14C}) was calculated from Eq. 5 (Geider and Osborne 1992)

$$P^C_{14C} = f\left(\frac{dpm_{org}}{dpm_{tot}}\right)\cdot[TCO_2]\left(\frac{1}{dt}\right) \qquad (5)$$

where f is the isotope discrimination factor assumed to be 1.06, dpm_{org} is the ^{14}C activity in organic matter (disintegrations per minute), dpm_{tot} is the total ^{14}C activity added to the sample, $[TCO_2]$ is the total inorganic carbon concentration and dt is the incubation time.

After incubation, the samples were acidified with HCl to pH between 1.5 and 2 and left overnight in a fume hood without caps to remove all inorganic C (Geider and Osborne 1992). Samples were back-titrated with NaOH to pH ~8 before scintillation cocktail (Ultima Gold) was added and the activity was measured in a scintillation counter (Packard Tri-Carb 1900). $[TCO_2]$ was estimated from measured pH and total alkalinity (AT). AT was calculated after titration with HCl (Wedborg et al. 1999) and total inorganic carbon from (Andersson et al. 1999). The dark-incubated uptake was generally <20% (<10% at temperature >15°C) of the light-incubated uptake and was

subtracted in the rate calculations. We observed no temperature influence on the dark-incubated ^{14}C-uptake.

Curve fit regression and calculations of Q_{10}

The P-E curves were fitted from Eq. 6 (Webb et al. 1974), as no tendency of reduction of P at irradiance >E_k (photoinhibition) was observed for the applied range of irradiance (0 - 566 µmol photons·m^{-2}·s^{-1}).

$$P^C = P^C_{max}\left(1-\exp\left\{\frac{-\alpha^C \cdot E}{P^C_{max}}\right\}\right) \quad (6)$$

The maximum photosynthetic rate (P^C_{max}; µmol O_2 or ^{14}C·(mg POC)$^{-1}$·h^{-1}), the maximum light utilisation coefficient (α^C; µmol O_2 or ^{14}C·(mg POC)$^{-1}$·h^{-1}·(µmol photons·m^{-2}·s^{-1})$^{-1}$), and the light saturation index ($E_k = P^C_{max}/\alpha^C$; µmol photons·m^{-1}·s^{-1}) were calculated from fit of the P-E curves. All curve fitting was carried out using ordinary least-squares criterion in SigmaPlot 9.0 (SYSTAT Software Inc. USA, 2002).

For α^C or P^C_{max} (response variables) the relationship with temperature and the covariance with method was analyzes using the statistical tool ANCOVA, with method as the test factor. Calculations were computed using S-Plus 6.2 (Insightful Corporation, US).

The temperature response of P^C_{max} was quantified by calculating the apparent activation energy (E_a, kJ·mol^{-1}) and the corresponding Q_{10} from each method and species. E_a was calculated as the slope of the data between 5 to 20°C in an Arrhenius plot (Eq. 7), where ln(k) was plotted as a function of temperature $(R\cdot T)^{-1}$, according to Raven and Geider (1988) as:

$$\ln(k) = \ln(A) + \left(\frac{-E_a}{R\cdot T}\right) \quad (7)$$

where k is the rate of the reaction, A is the Arrhenius constant, R is the gas constant (8.3144 J^{-1}·mol^{-1}) and T is the absolute temperature (K). Q_{10} was calculated from Eq. 8, for the temperature interval of 10°C to 20°C (Isaksen and Jørgensen 1996).

$$Q_{10} = \exp\left\{\frac{Ea \cdot 10}{R \cdot T(T+10)}\right\} \quad (8)$$

The maximum quantum yield for O_2 production ($^{PSII}\Phi_{O2\_max}$; mol O_2·(mol quanta)$^{-1}$) was calculated from the PSII-specific light absorption ($\bar{a}^{*}_{PSII}$) and was calculated for each temperature as:

$$^{PSII}\phi_{O2\_max} = \frac{\alpha^{*}}{115 \cdot \bar{a}^{*}_{PSII}} \quad (9)$$

where 115 is a constant required to obtain consistent dimensions.

RESULTS

P-E data

P-E curves were fitted to POC normalised production rates derived from O_2-microsensor measurements (P^C_{O2}, µmol O_2·(mg POC)$^{-1}$·h^{-1}), quantum yield of charge separation in PSII (Φ_{PSII}) by PAM fluorescence (P^C_{PSII}, µmol O_2·(mg POC)$^{-1}$·h^{-1}) and ^{14}C-assimilation (P^C_{14C}, µmol ^{14}C·(mg POC)$^{-1}$·h^{-1}) at temperatures from 0 to 30°C, at 5°C interval. P-E curves at 5 and 20°C are shown for *P. minimum*, *P. parvum*, and *P. tricornutum* (Fig. 1). O_2-microsensor and ^{14}C-assimilation rates were measured in triplicates and error bars are shown (Fig. 1a-c, g-i). Evident for all three species and three methods, the maximum production rates were clearly higher (2.2 - 6.0 times) at 20°C than at 5°C. We observed no sign of photoinhibition for the applied irradiance range (0 - 566 µmol photons·m^{-2}·s^{-1}). The relationship between temperature and the photosynthetic parameters, calculated from O_2 evolution, Φ_{PSII} and ^{14}C-assimilation, was first investigated for relative values (excluding the significance of the light absorption) normalised at 5°C, being the lowest temperature with minimal scatter (Fig. 2), then for absolute values (calculated by the use of $\bar{a}^*_{PSII}$, Fig. 3).

Temperature effects on relative P-E parameters

The relative response of the maximum photosynthetic rate (P^C_{max}) increased 2.5 to 6.0 times relative to the rate at 5°C, with increasing temperature, for all of the three investigated algal species, and varied overall little between species and method (Fig. 2a-c). P^C_{max} showed a temperature optimum at 20 - 25°C for *P. minimum* followed by a decrease (Fig. 2a), whereas no clear sign of a temperature optimum was observed for *P. parvum* or *P. tricornutum* within the investigated temperature range (Fig. 2b+c). The relative values for $P^C_{14C\_max}$ increased more with temperature than $P^C_{O2\_max}$ indicating a slightly stronger temperature response for ^{14}C-assimilation than for O_2-production, most apparent for *P. minimum*. The relative response of $P^C_{PSII\_max}$ with increasing temperature laid in-between $P^C_{14C\_max}$ and $P^C_{O2\_max}$ for *P. parvum*, and showed slightly lower temperature responses for *P. minimum* and *P. tricornutum*.

The temperature response on P^C_{max} was quantified by the Q_{10} factor (Table 2) calculated from Arrhenius plots (not shown). The average Q_{10} was 2.1 ± 0.2 (mean ± S.E.) and Q_{10} showed only small variance between methods and species, with an exception of $P^C_{14C\_max}$ for *P. minimum*. Apparently, Q_{10} for $P^C_{14C\_max}$ were higher than for $P^C_{O2\_max}$ and $P^C_{PSII\_max}$, supporting the observation of a stronger temperature response for C-assimilation than for the two other methods.

Temperature had no, or only little, effect on relative values of α^C showing similar temperature responses for each of the three species and an average Q_{10} of 1.0 ± 0.2 (mean ± S.E.). Q_{10} values of 0.9 for *P. parvum* and *P. tricornutum* indicated a slight decrease of α^C for this species. No difference was observed between the three methods as function of temperature for any of the species, arguing for an equivalent temperature response on photosynthetic O_2-production, Φ_{PSII} and ^{14}C-assimilation in the light limited part of the photosynthesis *versus* irradiance curve.

Relative values of E_k showed a strong temperature response (Fig. 2g-i) and increased 2.6 to 6.5 times (relative to the rate at 5 °C). As α^C generally was insensitive to temperature the temperature response of E_k mirrored P^C_{max}. Similarly, as α^C did not differ between methods the temperature response of E_k tended to be stronger for ^{14}C-assimilation than for O_2 and Φ_{PSII} based production rates.

Temperature effects on absolute values of P-E parameters

Increased temperature significantly increased the absolute values of P^C_{max} for the three investigated species (Fig. 3a-c), in accordance with the relative response, but varied more between species and in some cases between methods. The absolute values of P^C_{max} supported the observation of a temperature optimum for *P. minimum* at 20 - 25°C and no temperature optimum for *P. parvum* and *P. tricornutum* within the investigated temperature range. The absolute values of P^C_{max} were overall lowest for *P. minimum* (Fig. 3a) and highest for *P. tricornutum* (Fig. 3c). P^C_{max} for the latter decreased slightly at 30°C giving a weak indication of a temperature optimum at 25°C for $P^C_{O2\_max}$ and $P^C_{14C\_max}$. As P^C_{max} are carbon-specific, the rates do correlate

directly to maximum growth rates and reflect the productivity of the studied species (MacIntyre et al. 2002).

Between methods, the absolute values showed some inter-species variation of P^C_{max} as a function of temperature. The method used had a significant effect on P^C_{max} for all the three species ($p < 0.05$), however, the interaction between temperature and method (temperature × method) was significant for *P. parvum* only, as $P^C_{PSII\_max}$ showed 1.8 to 2.9 times higher absolute values than for the two other methods as function of temperature ($p << 0.05$, Fig. 3b). The response of $P^C_{O2\_max}$ and $P^C_{14C\_max}$ was not significantly different. The temperature × method interaction was non-significant for *P. minimum* ($p = 0.43$, Fig. 3a) nor for *P. tricornutum* ($p = 0.07$, Fig. 3c) emphasizing that there was no difference of P^C_{max} between the three methodological approaches. Despite the statistical insignificance, $P^C_{PSII\_max}$ for *P. tricornutum* (seemed to) show slightly higher absolute values than $P^C_{O2\_max}$ and $P^C_{14C\_max}$ (p-values are shown in Table 3).

The temperature effect on absolute values of α^C was non-significant (*P. minimum*, Fig. 3d) or slightly decreasing with increasing temperature (*P. parvum* and *P. tricornutum*, Fig. 3e-f). The slight decrease of α^C was observed as α^C_{O2} (*P. parvum*) and α^C_{O2} and α^C_{PSII} (*P. tricornutum*) decreased marginally. The additional values of α^C did not change with increasing temperature (p-values are shown in Table 3). The temperature × method interaction was non-significant for all of the species demonstrating no difference between the slopes for the three methods applied. Consequently, was the temperature response on the three methods the same. The method, however, had a significant effect on α^C resulting in significantly higher absolute values of α^C_{PSII} compared to α^C_{O2} and $\alpha^C_{14C,}$ for all of the three species. This off-set was especially clear for *P. parvum* as α^C_{PSII} was 1.7 to 3.3 times higher than α^C_{O2} and α^C_{14C} (Fig. 3e). The two latter were not significantly different. For *P. tricornutum* α^C_{PSII} was 1.1 to 1.7 times higher than values for α^C_{O2} and α^C_{14C} (Fig. 3f). Two outliers of α for *P. tricornutum* (α^C_{O2} at 0°C, and α^C_{14C} at 15°C) have been eliminated from the data set due to unrealistic values caused by high scatter at low irradiances.

As α^C was constant or slightly decreasing with increasing temperature, the light saturation index (E_k) vaguely increased or mirrored the P^C_{max} temperature response (Fig. 3g-i). E_k for *P. minimum* increased linearly to a temperature optimum at 20 to 25°C followed by a subsequent decrease. For *P. parvum* and *P. tricornutum*, E_k increased continuously with increasing temperature for all of the three methods. The relative higher values of α^C_{PSII} and $P^C_{PSII\_max}$ compared to the two other methods, for *P. parvum* and *P. tricornutum*, counteracted each other resulting in very similar values of E_k for the three methods, as a function of temperature.

Temperature effects on the maximum quantum yield

The temperature effects on the maximum quantum yield (Φ_{max}) seemed to be neglectable (*P. minimum*) or lead to a minor decrease with increasing temperature (*P. parvum* and *P. tricornutum*) (Fig. 4). Φ_{PSII_max} were in the range of 0.6 to 0.75 and lowest for *P. minimum*. $^{PSII}\Phi_{O2\_max}$ was lowest for *P. parvum* (0.06 to 0.13), but within the same range for *P. minimum* and *P. tricornutum* (0.08 to 0.15), respectively. The lower $^{PSII}\Phi_{O2\_max}$ lead to a higher minimum quantum requirement (QR, the inverse of the maximum quantum yield; $1/\Phi_{max}$) for *P. parvum* than for the two other species; 0.8 to 2.7 times higher than for *P. minimum* (1.9 ± 0.7 times, mean ± S.D.) and 1.7 to 3.1 times higher than for *P. tricornutum* (2.2 ± 0.5 times, mean ± S.D.). The QR for *P. minimum* and *P. tricornutum* was similar.

The calculated $^{PSII}\Phi_{14C\_max}$ was lower than $^{PSII}\Phi_{O2\_max}$ for *P. minimum*, however, slightly higher for the two other species, in contradiction to established theory. We have no obvious explanation for this other than it is likely that α^C_{14C} was overestimated because of few measuring points and high scatter within the light limited part of the P-E curve, which would lead to an overestimation of Φ_{14C_max}. Data for Φ_{14C_max} are not shown.

DISCUSSION

The relationship between P-E parameters calculated from rates of O_2-production, Φ_{PSII} and ^{14}C-assimilation was investigated as a function of short-term changes in temperature. The results demonstrated that P^C_{max} increased and α^C was more or less insensitive to increasing temperature for all of the three species, as typical for most eukaryote algae (Davison 1991). Generally, this is not surprising as α^C represents light-limited photosynthesis and, as such, primarily is a function of photochemical light reactions (not enzyme dependent) and P^C_{max} describes the light-saturated processes of photosynthesis and appears to be limited by enzyme activity associated with the carbon metabolism of the dark reactions (assuming excess nutrients) (Davison 1991, Sakshaug et al. 1997).

Temperature effects on P^C_{max}

The relative values for $P^C_{14C\_max}$ tended to increase more with temperature than $P^C_{O2\_max}$ indicating a slightly stronger temperature response for ^{14}C-assimilation than for O_2-production, most apparent for *P. minimum* (Fig. 2). This observation was supported by the Q_{10} values (Table 2). Theoretically, this was expected as P^C_{14C} expresses gross carbon uptake rates excluding respiratory activity (Sakshaug et al. 1997) whereas P^C_{O2} probably underestimated the gross O_2-production rate, due to an enhanced O_2-consumption in the light compared to the dark, which P^C_{O2} did not account for. Enhanced O_2 consumption in the light is well documented for in marine microalgae, as both intercellular (photorespiration and mitochondrial activity) and extracellular (e.g. bacterial metabolism) O_2-consumption is stimulated by photosynthesis (Weger et al. 1989, Lewitus and Kana 1995, Xue et al. 1996). All the above processes are stimulated by temperature and hence will the discrepancy between the dark and the light O_2-consumption rate increase with increasing temperature (Davison 1991, Morris and Kromkamp 2003). This can explain the relatively stronger temperature response for $P^C_{14C\_max}$ than for $P^C_{O2\_max}$, which will be further enhanced if the temperature response (Q_{10}) on the O_2-consumption

processes exceeds the response of photosynthesis, as found for benthic microphytes (Hancke and Glud 2004).

The potential for photorespiration increase with increasing temperature, as the affinity of Rubisco for O_2 is reduced relatively to the affinity for CO_2 with increase temperature (Berry and Raison 1981). However, the importance of photorespiration in microalgae might be suppressed by the occurrence of a CO_2 concentrating mechanism (Lewitus and Kana 1995).
Although the maximum photosynthetic rate is related only to the number of photosynthetic units (n) and the minimum turnover time for electrons (τ); $P_{max} = n \cdot \tau^{-1}$ (Dubinsky et al. 1986), the rate-limiting step of the photosynthetic pathway has been widely debated (Sakshaug et al. 1997). The relative temperature response of $P^C_{PSII\_max}$ followed the temperature response of the two other techniques. This demonstrated that Φ_{PSII} from intact algae cells responded similarly to the rate of O_2-evolution and ^{14}C-assimilation, to a short-term temperature change. This is consistent with the hypothesis that the overall rate-limiting reaction for light-saturated photosynthesis is carbon fixation rather than electron transport, as suggested by Sukenik et al. (1987). For our data, this implies that Φ_{PSII} as well as the O_2-production must be limited by carbon-fixing enzymes, i.e. the Rubisco-complex, and stress that Φ_{PSII} and O_2-production rates were not separated from the ^{14}C-fixation rate, as a function of short-term temperature changes. This is consistent with the observation of a linear relationship between P^B (chl *a* normalised rates of P^C_{O2}) and ETR as function of temperature, for temperatures between 10 and 30°C (Morris and Kromkamp 2003). However, their data deviated from linearity at the extremes of the investigated temperature range (5 and 35°C).

For absolute values of the maximum photosynthetic rate, the relationship between rates of O_2-production and ^{14}C-assimilation is known as the photosynthetic quotient, PQ (Laws 1991). Calculating PQ as the ratio between $P^C_{O2\_max}$ and $P^C_{14C\_max}$ resulted in values between 1.2 and 3.6 (average for all data = 1.8 ± 0.7), which is consistent with a general PQ of ~1.4 (Laws 1991, Sakshaug et al. 1997). As mention above,

$P^C_{O2\_max}$ might be an underestimate of the gross O_2-production rate. However, $P^C_{14C\_max}$ may underestimate the gross carbon uptake, as 15 min incubations have shown to result in higher carbon uptake rates than 60 min incubations, which are used in the present study (Lewis and Smith 1983, MacIntyre et al. 2002). PQ tended to decrease with increasing temperature for all of the three species (with a slope coefficient of –0.03 to –0.05 (~ Q_{10} of 0.81 to 0.90), data not shown) and showed thus to be temperature sensitive. This could be explained by a more pronounced increase of $P^C_{14C\_max}$ compared to $P^C_{O2\_max}$ as seen from the Q_{10} (Table 2). An alternative explanation for the decrease of PQ with temperature, to a light enhanced O_2 consumption, is a potential electron cost for N uptake with increasing temperature (Laws 1991).

In this paper we quantified the PSII electron flow and calculated the absolute rate of O_2-production in PSII (μmol O_2·(mg POC)$^{-1}$·h^{-1}) by combining Φ_{PSII} (from PAM measurements) with the bio-optically determined quanta absorbed in PSII, $\bar{a}^*_{PSII}$ (Genty et al. 1989, Johnsen et al., Hancke et al. submitted). The aim was to compare absolute rates of calculated O_2-production from PSII with measured rates of O_2-production and ^{14}C-assimilation, where most studies relate only to relative rates of PSII efficiency, e.g. relative ETR, due to the challenge of measuring the light absorption in PSII. The results demonstrated a species-specific correlation between the three methods with P^C_{PSII} showing higher absolute values of P^C_{max} and α^C than those determined from measured O_2-production (P^C_{O2}) and ^{14}C-asssimilation (P^C_{14C}) in most cases (Fig. 3).

The absolute values of P^C_{PSII} showed a species specific off-set compared to P^C_{O2} and P^C_{14C}, what might origin in the assumption of $\Gamma = 0.25$ (Eq. 5) proving it wrong. Assuming that Φ_{PSII} is accurately measured by the PAM technique, which is reasonable (Hancke et al. submitted), the divergence between measured O_2-production and calculated O_2-production (from PSII fluorescence) can only be caused by two parameters; the absorption properties ($\bar{a}^*_{PSII}$) or the amount of O_2 evolved per electron generated in PSII (Γ). As we believe that $\bar{a}^*_{PSII}$ is a good

measure of the PSII absorption (Falkowski and Raven 1997, Johnsen et al. 1997, Johnsen and Sakshaug submitted) we suggest that the electrons needed per O_2 evolved is the major source for the difference between measured and calculated rates of O_2-production. (See Johnsen and Sakshaug (submitted) for a discussion on the absorption by non-photosynthetic *versus* photosynthetic efficient pigments and the relation to PSII and light-harvesting complexes).

The calculated ${}^{PSII}\Phi_{O2\_max}$ for *P. parvum* was in the range of 0.06 to 0.13 (Fig. 4) corresponding to a QR of 8.0 to 17.3 mol photons·(mol O_2 produced)$^{-1}$. This is 1.1 to 2.5 times higher than the theoretical minimum (see below) and was on average 1.9 and 2.2 times higher than the QR for *P. minimum* and *P. tricornutum*, respectively. For the two latter species the QR was in the range of 5.7 to 10.4 and 5.1 to 9.4, respectively. As Φ_{PSII_max} did not differ markedly between the three species, the higher ${}^{PSII}\Phi_{O2\_max}$ for *P. parvum* (of 1.1 to 2.5 times) is likely the explanation for the off-set of P^C_{PSII} compared to P^C_{O2} and P^C_{14C} for this species. The off-set was apparently temperature insensitive, which is consistent with the above explanation and is further supported by the equivalent Q_{10} values of the three methods.

The theoretical maximum quantum yield for O_2 when calculated from total absorption ($\bar{a}^*$, not the PSII-specific absorption) is 0.125 O_2 electron^{-1} (equivalent to a QR = 8 electrons O_2^{-1}). To correct for light absorption by PSI and photo-protective pigments we based the quantum yield calculation on the light absorption in PSII ($\bar{a}^*_{PSII}$) only. Consequently, the theoretical maximum quantum yield must be between 0.125 and 0.25, and we propose that it can be calculated from Eq. 10:

$$theoretical^{PSII}\phi_{O2\_max} = 0.125 \cdot \left(\frac{\bar{a}^*}{\bar{a}^*_{PSII}} \right) \qquad (10)$$

Applying this equation on our data gave theoretical maximum quantum yields for O_2 in the range of 0.155 - 0.165, 0.141 - 0.157 and 0.151 - 0.170 mol O_2·(mol photons)$^{-1}$ for *P. minimum*, *P. parvum* and *P. tricornutum*, respectively (Fig. 4, small open circles). The theoretical maximum quantum yield for O_2 was temperature insensitive,

as $\bar{a}^{*}_{PSII}$ (Table 4). The average of the corresponding theoretical minimum QR was then 6.3 ± 0.2, 6.8 ± 0.2 and 6.3 ± 0.3 for the three species, respectively.
Values for the QR for O_2-production well higher than the theoretical minimum have commonly been published (Myers 1980, e.g. Gilbert et al. 2000). For freshwater phytoplankton Gilbert et al. (1996) found that absolute electron transport rates obtained from PSII fluorescence tends to overestimate primary production rates of ^{14}C-fixation. They ascribe the discrepancy to the package effect of pigments in phytoplankton cells and to a non-carbon related electron flow, e.g. nitrogen fixation, photorespiration and the Mehler reaction. They assumed a PSII:PSI ratio of 0.5 but corrected the absorbance spectra for non-photosynthetic pigments according to Schofield et al. (1997).

Dividing Φ_{PSII_max} with $^{PSII}\Phi_{O2\_max}$ yield the exact amount of electrons generated in PSII needed to produce one O_2 molecule. However, since Φ_{PSII_max} and $^{PSII}\Phi_{O2\_max}$ were measured in two different experimental set-ups, our data do not support such a calculation. However, as Φ_{PSII_max} differed only little the result would follow the trend of $^{PSII}\Phi_{O2\_max}$. The higher QR for *P. parvum* than for *P. minimum* and *P. tricornutum* would influence both P^{C}_{max} and α^{C}. The temperature effect on Φ_{max} is discussed below.

The lower quantum yield for O_2-production than the theoretical maximum can be caused by several pathways of electron 'loss' leading to the off-set between P^{C}_{PSII} and P^{C}_{O2}, e.g. cyclic electron transport is PSII, pseudo cyclic transport in the Mehler reaction, and light dependent mitochondrial respiration (Flameling and Kromkamp 1998, Longstaff et al. 2002). Our data do not offer a separation between these processes but it seems likely that cyclic electron transport around PSII or a Mehler-type of reaction (where the O_2 produced at PSII is reduced again at PSI) could contribute to the off-set.

Nutrient-enriched treatments have shown to lower the quantum requirement from ~ 8 to 5 (mol electrons absorbed per mol O_2) in experiments with the marine macroalga

Ulva lactuca (Chlorophyta, Davison 1991). In our experiments, all of the cultures were grown in f/2 medium and hence we assumed that the nutrients were not limited and that no reduction of the quantum yield was caused by this reason.

Temperature acclimation of light-harvesting properties in form of pigment complexes involves adjustment in both number and ratio of several photosynthetic pigments (Johnsen and Sakshaug submitted). However, it is unlikely that the light-harvesting properties changed in our short-term temperature incubations, as all the cultures were grown at a constant temperature (15°C) and irradiance regime (80 μmol photons·m^{-2}·s^{-1}). Besides, either $\bar{a}^{*}$ or $\bar{a}^{*}_{PSII}$ showed any correlation with temperature nor did the relationship between them. Additionally, $\bar{a}^{*}_{PSII}$ exclude the absorption by PSI and photo-protective pigments (Johnsen et al. 1997, Hancke et al. submitted) hence a potential acclimation changing the absorption properties of these components would not influence the rate of P^{C}_{PSII}.

Temperature effects on α^{C} and E_k

The relative and absolute values of α^{C} showed an analogous response to a short-term temperature change and demonstrated to be insensitive (*P. minimum*) or slightly decreasing (*P. parvum* and *P. tricornutum*) with increasing temperature. This was tested using a statistical test of covariance (Table 3). As the slope of α^{C} as a function of temperature were similar for the three methods and the interaction of temperature × method was non-significant (p = 0.5 – 0.96) we concluded that the temperature response for the three methods was the same, for all three species. This is visually evident as seen from the plot of the relative values, as normalised at 5 °C (Fig. 2d-f). The absolute values of α^{C} demonstrated an off-set of α^{C}_{PSII} compared to α^{C}_{O2} and α^{C}_{14C} which was constant for the entire temperature range, arguing for a linear temperature-insensitive relationship between rates obtained from the three methods, in the light limited part of the P-E curve. The off-set of α^{C}_{PSII} was similar to the off-set of $P^{C}_{PSII\_max}$ and we hence conclude that the off-set was general for the Φ_{PSII} based O_2-production rates (P^{C}_{PSII}), for the entire irradiance range.

A linear off-set of P^C_{PSII} compared to P^C_{O2} argues for a linear relation between the PSII electron transport and the measured O_2-production, however, our experimental setup did not support a direct comparison, as P^C_{PSII} and P^C_{O2} were measured at different irradiance levels (but within the same range). However, in a previous study we found a linear relationship between P^C_{PSII} and P^C_{O2} (as well for Φ_{PSII} and $^{PSII}\Phi_{O2}$) for the same species when measured simultaneously in the same incubation chamber, under equivalent growth conditions (Geel et al. 1997).

A linear relation between P^C_{PSII} and P^C_{O2} aligns with Geel et al. (1986) who also found a linear relation between PSII electron transport rates and O_2-production rates at light-limited conditions in several marine phytoplankton species including *P. tricornutum*. The relation between electron transport rate (ETR) and photosynthetic oxygen evolution has been investigated in a range of studies. Although the investigations were conducted under a variety of experimental conditions, an overweight of these studies describe a linear relationship between O_2-production and Φ_{PSII} under moderate irradiances (e.g. Genty et al. 1989, Schreiber et al. 1995, Geel et al. 1997). Non-linear or curvilinear correlations is described at high irradiance conditions (Falkowski et al. 1986, Flameling and Kromkamp 1998, Masojidek et al. 2001), with an excess of electron transport compared to O_2-production, or at very low irradiance presumably due to light-enhanced dark respiration (Kroon et al. 1993). A close coupling between the quantum yield for O_2-production and of charge separation in PSII, but not between the quantum yield for O_2-production and ^{14}C-fixation has also been reported (MacIntyre et al. 2002). For the deviations, explanations such as spectral difference in PAR source, changes in O_2-consumption in the light, cyclic electron transport around PSII and Mehler-type reactions have been proposed.

The slight decrease of α^C with temperature for *P. tricornutum* could be explained by an apparent decrease of the chl *a* to C ratio, as α^C (carbon-specific) often is correlated with the chl *a* to C ratio, since light absorption is correlated with chl *a* .

The chl *a* to C ratio for *P. minimum* and *P. parvum* was constant across the temperature range (except for a drop at 30°C for P. parvum, Table 5).

A mathematical consequence of the similar off-set of P^C_{PSII} compared to P^C_{O2} and P^C_{14C}, for both P^C_{max} and α^C, resulted in similar values for E_k for the three methods. Hence, did E_k for the three applied methods respond in parallel across the entire range of temperature, and we conclude that temperature responses on E_k can be studied quantitatively by the PAM technique, applying the present procedure to calculate O_2-production rates from Φ_{PSII}. This is in contrast to Gilbert et al. (2000), who found that Φ_{PSII} based O_2-production rates most often overestimated the measured O_2-production rates during light saturation, while the rates were similar during light-limited photosynthesis. This led Gilbert et al. (2000) to conclude that fluorescence-based E_k often showed a shift to higher irradiances compared to that of O_2 based P-E curves, for the green alga *Chlorella vulgaris*.

Conclusions

- Both calculated and measured O_2-production rates along with ^{14}C-assimilation rates showed the same relative response to a short-term temperature change, for the three studied microalgae species. This implies that the PAM technique analogous to O_2-production and ^{14}C-assimilation measurements can be applied to study relative temperature responses of photosynthesis *versus* irradiance relations.
- Absolute rates of calculated O_2-production based on Φ_{PSII} showed a species-specific correlation and overestimated the measured O_2-production rates of ~1 to 3 times during both light-limited (α^C) and light-saturated (P^C_{max}) photosynthesis. The off-set of the Φ_{PSII} based measurements were due to a lower quantum yield for O_2-production than the theoretical maximum and seemed to be insensitive to temperature. The lower quantum yield for O_2-production can possibly be ascribed to irradiance induced Mehler-type reactions.

- The maximum quantum yield for both PSII and O_2-production decreased with increasing temperature, the latter considerable stronger than the first.
- Φ_{PSII} obtained with the PAM technique in combination with bio-optical determined light absorption in PSII can be used as a valuable tool for studying temperature dependence of photo-physiological processes in combination with O_2 and ^{14}C studies.

Acknowledgements

We would like to acknowledge E. Sakshaug for constructive comments and criticism on the manuscript and C. Pelabon for statistical advice. Financial support from the Norwegian Research Council for KH (project no. 155936/700 for 'CABANERA') and LMO (contract: 143511/213) is acknowledged. RG acknowledge the financial support by the Danish National Research Council (# 21-04-039).

References

Andersson, L. G., Turner, D. R., Wedborg, M. & Dyrssen, D. 1999. Determination of total alkalinity and total dissolved inorganic carbon. *In* Grasshoff, K., Kremling, K. & Ehrhardt, M. [Eds.] *Methods of Seawater Analysis*. Wiley-VCH, Weinheim, pp. 127-48.

Barranguet, C. & Kromkamp, J. 2000. Estimating primary production rates from photosynthetic electron transport in estuarine microphytobenthos. *Marine Ecology-Progress Series*. 204:39-52.

Berry, J. & Raison, J. 1981. Responses of macrophytes to temperature. *In* Lange, O., Noble, P., Osmond, C. B. & Ziegler, H. [Eds.] *Physiological PlantEcology*. Springer-Verlag, Berlin, pp. 277-338.

Bidigare, R. R., Schofield, O. & Prezelin, B. B. 1989. Influence of zeaxanthin on quantum yield of photosynthesis of *Synechococcus* clone WH7803 (DC2). *Marine Ecology-Progress Series*. 56:177-88.

Davison, I. R. 1991. Environmental Effects on Algal Photosynthesis - Temperature. *Journal of Phycology*. 27:2-8.

Demmig, B. & Bjorkman, O. 1987. Comparison of the Effect of Excessive Light on Chlorophyll Fluorescence (77k) and Photon Yield of O-2 Evolution in Leaves of Higher-Plants. *Planta*. 171:171-84.

Dubinsky, Z., Falkowski, P. G. & Wyman, K. 1986. Light Harvesting and Utilization by Phytoplankton. *Plant and Cell Physiology*. 27:1335-49.

Falkowski, P. G. & Raven, J. A. 1997. *Aquatic photosynthesis*. Blackwell Science.

Falkowski, P. G., Wyman, K., Ley, A. C. & Mauzerall, D. C. 1986. Relationship of Steady-State Photosynthesis to Fluorescence in Eukaryotic Algae. *Biochimica Et Biophysica Acta*. 849:183-92.

Flameling, I. A. & Kromkamp, J. 1998. Light dependence of quantum yields for PSII charge separation and oxygen evolution in eucaryotic algae. *Limnology and Oceanography*. 43:284-97.

Geel, C., Versluis, W. & Snel, J. F. H. 1997. Estimation of oxygen evolution by marine phytoplankton from measurement of the efficiency of Photosystem II electron flow. *Photosynthesis Research*. 51:61-70.

Geider, R. J. & Osborne, B. A. 1992. *Algal Photosynthesis*. Chapman & Hall, New York.

Genty, B., Briantais, J. M. & Baker, N. R. 1989. The Relationship between the Quantum Yield of Photosynthetic Electron-Transport and Quenching of Chlorophyll Fluorescence. *Biochimica Et Biophysica Acta*. 990:87-92.

Gilbert, M., Domin, A., Becker, A. & Wilhelm, C. 2000. Estimation of primary productivity by chlorophyll a in vivo fluorescence in freshwater phytoplankton. *Photosynthetica*. 38:111-26.

Glud, R. N., Gundersen, J. K. & Ramsing, N. B. 2000. Electrochemical and optical oxygen microsensors for in situ measurements. *In* Buffle, J. & Horvai, G. [Eds.] *In situ monitoring of aquatic systems: Chemical analysis and speciation*. John Wiley & Sons Ltd., pp. 20-73.

Glud, R. N., Kuhl, M., Wenzhofer, F. & Rysgaard, S. 2002a. Benthic diatoms of a high Arctic fjord (Young Sound, NE Greenland): importance for ecosystem primary production. *Marine Ecology-Progress Series*. 238:15-29.

Glud, R. N., Rysgaard, S. & Kuhl, M. 2002b. A laboratory study on O-2 dynamics and photosynthesis in ice algal communities: quantification by microsensors,O-2 exchange rates, C-14 incubations and a PAM fluorometer. *Aquatic Microbial Ecology*. 27:301-11.

Guillard, R. R. & Ryther, J. H. 1962. Studies of Marine Planktonic Diatoms .1. Cyclotella Nana Hustedt, and Detonula Confervacea (Cleve) Gran. *Canadian Journal of Microbiology*. 8:229-&.

Gundersen, J. K., Ramsing, N. B. & Glud, R. N. 1998. Predicting the signal of O-2 microsensors from physical dimensions, temperature, salinity, and O-2 concentration. *Limnology and Oceanography*. 43:1932-7.

Hancke, K. & Glud, R. N. 2004. Temperature effects on respiration and photosynthesis in three diatom-dominated benthic communities. *Aquatic Microbial Ecology*. 37:265-81.

Hancke, T. B., Hancke, K., Johnsen, G. & Sakshaug, E. submitted. Rate of O2 production derived from PAM fluorescence: Testing three bio-optical approaches against measured O2 production rate. *Journal of Phycology*.

Hanelt, D. & Nultsch, W. 1995. Field Studies of Photoinhibition Show Non-Correlations between Oxygen and Fluorescence Measurements in the Arctic Red-Alga Palmaria-Palmata. *Journal of Plant Physiology*. 145:31-8.

Hartig, P., Wolfstein, K., Lippemeier, S. & Colijn, F. 1998. Photosynthetic activity of natural microphytobenthos populations measured by fluorescence (PAM) and C-14-tracer methods: a comparison. *Marine Ecology-Progress Series*. 166:53-62.

Isaksen, M. F. & Jørgensen, B. B. 1996. Adaptation of psychrophilic and psychrotrophic sulfate-reducing bacteria to permanently cold marine environments. *Applied and Environmental Microbiology*. 62:408-14.

Johnsen, G., Prezelin, B. B. & Jovine, R. V. M. 1997. Fluorescence excitation spectra and light utilization in two red tide dinoflagellates. *Limnology and Oceanography*. 42:1166-77.

Johnsen, G. & Sakshaug, E. 1993. Biooptical Characteristics and Photoadaptive Responses in the Toxic and Bloom-Forming Dinoflagellates *Gyrodinium-Aureolum*, *Gymnodinium-Galatheanum*, and two strains on *Prorocentrum minimum*. *Journal of Phycology*. 29:627-42.

Johnsen, G. & Sakshaug, E. submitted. Bio-optical characteristics of PSII and PSI in 33 species (13 pigment groups) of marine phytoplankton, and the relevance for PAM and FRR fluorometry. *Journal of Phycology*.

Kopf, U. & Heinze, J. 1984. 2,7-Bis(Diethylamino)Phenazoxonium Chloride as a Quantum Counter for Emission Measurements between 240 and 700 nm. *Analytical Chemistry*. 56:1931-5.

Kromkamp, J. C., Domin, A., Dubinsky, Z., Lehmann, C. & Schanz, F. 2001. Changes in photosynthetic properties measured by oxygen evolution and variable chlorophyll fluorescence in a simulated entrainment experiment with the cyanobacterium Planktothrix rubescens. *Aquatic Sciences*. 63:363-82.

Kroon, B., Prezelin, B. B. & Schofield, O. 1993. Chromatic Regulation of Quantum Yields for Photosystem-Ii Charge Separation, Oxygen Evolution, and Carbon Fixation in Heterocapsa-Pygmaea (Pyrrophyta). *Journal of Phycology*. 29:453-62.

Kuhl, M., Glud, R. N., Borum, J., Roberts, R. & Rysgaard, S. 2001. Photosynthetic performance of surface-associated algae below sea ice as measured with a pulse-amplitude-modulated (PAM) fluorometer and O-2 microsensors. *Marine Ecology-Progress Series*. 223:1-14.

Laws, E. A. 1991. Photosynthetic Quotients, New Production and Net Community Production in the Open Ocean. *Deep-Sea Research Part a-Oceanographic Research Papers*. 38:143-67.

Lewis, M. R. & Smith, J. C. 1983. A Small Volume, Short-Incubation-Time Method for Measurement of Photosynthesis as a Function of Incident Irradiance. *Marine Ecology-Progress Series*. 13:99-102.

Lewitus, A. J. & Kana, T. M. 1995. Light Respiration in 6 Estuarine Phytoplankton Species - Contrasts under Photoautotrophic and Mixotrophic Growth-Conditions. *Journal of Phycology*. 31:754-61.

Longstaff, B. J., Kildea, T., Runcie, J. W., Cheshire, A., Dennison, W. C., Hurd, C., Kana, T., Raven, J. A. & Larkum, A. W. D. 2002. An *in situ* study of photosynthetic oxygen exchange and electron transport rate in the marine macroalga *Ulva lactuca* (Chlorophyta). *Photosynthesis Research*. 74:281-93.

MacIntyre, H. L., Kana, T. M., Anning, T. & Geider, R. J. 2002. Photoacclimation of photosynthesis irradiance response curves and photosynthetic pigments in microalgae and cyanobacteria. *Journal of Phycology*. 38:17-38.

Masojidek, J., Grobbelaar, J. U., Pechar, L. & Koblizek, M. 2001. Photosystem II electron transport rates and oxygen production in natural waterblooms of freshwater cyanobacteria during a diel cycle. *Journal of Plankton Research*. 23:57-66.

Mitchell, B. G. 1990. Algorithms for determining the absorption coefficient for aquatic particulates using the quantitative filter technique (QFT). *Proc. SPIE Ocean Opt. X*. 1302:137-48.

Mitchell, B. G. & Kiefer, D. A. 1988. Chlorophyll *a* specific absorption and fluorescence excitation spectra for light-limited phytoplankton. *Deep-Sea Research Part I*. 35:639-63.

Morris, E. P. & Kromkamp, J. C. 2003. Influence of temperature on the relationship between oxygen- and fluorescence-based estimates of photosynthetic parameters in a marine benthic diatom (*Cylindrotheca closterium*). *European Journal of Phycology*. 38:133-42.

Myers, J. 1980. *On the algae: thoughts about physiology and measurements of efficiency*. Plenum Press, New York, 1-16 pp.

Neori, A., Vernet, M., Holmhansen, O. & Haxo, F. T. 1988. Comparison of chlorophyll far-red and red fluorescence excitation-spectra with photosynthetic oxygen action spectra for Photosystem-II in algae. *Marine Ecology-Progress Series*. 44:297-302.

Raven, J. A. & Geider, R. J. 1988. Temperature and Algal Growth. *New Phytologist*. 110:441-61.

Revsbech, N. P. 1989. An Oxygen Microsensor with a Guard Cathode. *Limnology and Oceanography*. 34:474-8.

Revsbech, N. P. & Jørgensen, B. B. 1986. Microelectrodes - Their Use in Microbial Ecology. *Advances in Microbial Ecology*. 9:293-352.

Rysgaard, S., Kuhl, M., Glud, R. N. & Hansen, J. W. 2001. Biomass, production and horizontal patchiness of sea ice algae in a high-Arctic fjord (Young Sound, NE Greenland). *Marine Ecology-Progress Series*. 223:15-26.

Sakshaug, E., Bricaud, A., Dandonneau, Y., Falkowski, P. G., Kiefer, D. A., Legendre, L., Morel, A., Parslow, J. & Takahashi, M. 1997. Parameters of photosynthesis: definitions, theory and interpretation of results. *Journal of Plankton Research*. 19:1637-70.

Sakshaug, E. & Holm-Hansen, O. 1977. Chemical Composition of *Skeletonema-Costatum* (Grev) Cleve and Pavlova (Monochrysis) Lutheri (Droop) Green as a

Function of Nitrate-Limited, Phosphate-Limited, and Iron-Limited Growth. *Journal of Experimental Marine Biology and Ecology*. 29:1-34.

Schofield, O., Grzymski, J., Moline, M. M. A. & Jovine, R. V. M. 1998. Impact of temperature acclimation on photosynthesis in the toxic red-tide dinoflagellate *Alexandrium fundyense* (Ca28). *Journal of Plankton Research*. 20:1241-58.

Schofield, O., Prezelin, B. B. & Johnsen, G. 1996. Wavelength dependency of the maximum quantum yield of carbon fixation for two red tide dinoflagellates, *Heterocapsa pygmaea* and *Prorocentrum minimum* (Pyrrophyta). *J. Phycol*. 32:574-83.

Schreiber, U., Hormann, H., Neubauer, C. & Klughammer, C. 1995. Assessment of Photosystem-II Photochemical Quantum Yield by Chlorophyll Fluorescence Quenching Analysis. *Australian Journal of Plant Physiology*. 22:209-20.

Schreiber, U., Schliwa, U. & Bilger, W. 1986. Continuous Recording of Photochemical and Nonphotochemical Chlorophyll Fluorescence Quenching with a New Type of Modulation Fluorometer. *Photosynthesis Research*. 10:51-62.

Seaton, G. G. R. & Walker, D. A. 1990. Chlorophyll Fluorescence as a Measure of Photosynthetic Carbon Assimilation. *Proceedings of the Royal Society of London Series B-Biological Sciences*. 242:29-35.

Sukenik, A., Bennett, J. & Falkowski, P. 1987. Light-Saturated Photosynthesis - Limitation by Electron-Transport or Carbon Fixation. *Biochimica Et Biophysica Acta*. 891:205-15.

van Kooten, O. & Snel, J. F. H. 1990. The Use of Chlorophyll Fluorescence Nomenclature in Plant Stress Physiology. *Photosynthesis Research*. 25:147-50.

Webb, W. L., Newton, M. & Starr, D. 1974. Carbon-Dioxide Exchange of Alnus-Rubra - Mathematical-Model. *Oecologia*. 17:281-91.

Wedborg, M., Turner, D. R., Anderson, L. G. & Dyrssen, D. 1999. Determination of pH. *In* Grasshoff, K., Kremling, K. & Ehrhardt, M. [Eds.] *Methods of Seawater Analysis*. Wiley-VCH, Weinheim, pp. 109-25.

Weger, H. G., Herzig, R., Falkowski, P. G. & Turpin, D. H. 1989. Respiratory Losses in the Light in a Marine Diatom - Measurements by Short-Term Mass-Spectrometry. *Limnology and Oceanography*. 34:1153-61.

Xue, X. P., Gauthier, D. A., Turpin, D. H. & Weger, H. G. 1996. Interactions between photosynthesis and respiration in the green alga *Chlamydomonas reinhardtii* - Characterization of light-enhanced dark respiration. *Plant Physiology*. 112:1005-14.

Yentsch, C. S. 1962. Measurement of Visible Light Absorption by Particulate Matter in the Ocean. *Limnology and Oceanography*. 7:207-17.

Table 1. Definitions of the productivity, photosynthetic and bio-optical parameters used in the text. Photosynthetic parameters according to Sakshaug et al. (1997).

P^{C}_{O2}	Carbon specific measured O_2-production (net production + dark respiration) (µmol O_2·(mg POC)$^{-1}$·h^{-1})
P^{C}_{PSII}	Carbon specific O_2-production calculated from Φ_{PSII} and $\bar{a}^{*}_{PSII}$ in absolute units (µmol O_2·(mg POC)$^{-1}$·h^{-1})
P^{C}_{14C}	Carbon specific ^{14}C-assimilation (µmol ^{14}C·(mg POC)$^{-1}$·h^{-1})
α^{C}	Maximum light utilization coefficient normalized to carbon (µmol O_2 or ^{14}C·(mg POC)$^{-1}$·h^{-1}·(µmol·m^{-2}·s^{-1})$^{-1}$)
P^{C}_{max}	Maximum photosynthetic rate normalized to carbon (µmol O_2·(mg POC)$^{-1}$·h^{-1})
E_k	Light saturation index (µmol photons·m^{-2}·s^{-1})
Φ_{PSII}	Operational quantum yield for PSII charge separation (Eq. 2, mol electrons·(mol quanta)$^{-1}$)
$\Phi_{O2,\ PSII,\ 14C\_max}$	Maximum quantum yield for O_2, PSII or ^{14}C, respectively (mol product·(mol quanta)$^{-1}$)
${}^{PSII}\phi_{O2\_max}$	Maximum quantum yield for O_2 calculated from $\bar{a}^{*}_{PSII}$ (Eq. 10, mol O_2·(mol quanta)$^{-1}$)
$\bar{a}^{*}$	Spectrally weighted *in vivo* chl *a*-specific absorption (m^2·(mg chl *a*)$^{-1}$)
$\bar{a}^{*}_{PSII}$	Spectrally weighted *in vivo* PSII-specific absorption (m^2·(mg chl *a*)$^{-1}$)

Table 2. The temperature effect expressed as Q_{10} for the maximum photosynthetic rate of P^C_{O2}, P^C_{PSII} and P^C_{14C} for *P. minimum*, *P. Parvum* and *P. tricornutum*, respectively. Q_{10} was calculated from the slope of P^C_{max} as a function of temperature, from 5 to 20°C, in an Arrhenius plot. The maximum photosynthetic rate of P^C_{O2}, P^C_{PSII} and P^C_{14C} were calculated from measured rates of O_2-production, Φ_{PSII} and ^{14}C-assimilation, respectively.

	P. minimum	*P. parvum*	*P. tricornutum*
$P^C_{O2\_max}$	2.1	1.8	1.8
$P^C_{PSII\_max}$	1.7	2.1	1.9
$P^C_{14C\_max}$	3.5	2.3	2.1

Table 3. p-values of statistical tested variance and covariance (ANCOVA) for the significance of temperature, method and the interaction between temperature and method (temperature × method). A significance of temperature × method indicates that the relationship between the response variable (α^C or P^C_{max}) and temperature depended on the method used.

		P. minimum (0 - 20°C)	*P. minimum* (0 - 30°C)	*P. parvum* (0 - 30°C)	*P. tricornutum* (0 - 30°C)
P^C_{max}	temperature	*** ($p < 0.001$)	-	*** ($p < 0.001$)	*** ($p < 0.001$)
	method	*** ($p < 0.001$)	-	*** ($p < 0.001$)	*** ($p < 0.001$)
	temperature × method	N.S. ($p = 0.43$)	-	*** ($p < 0.001$)	N.S. ($p = 0.07$)
α^C	temperature	-	N.S. ($p = 0.23$)	*** ($p < 0.001$)	*** ($p = 0.001$)
	method	-	*** ($p < 0.001$)	*** ($p < 0.001$)	*** ($p < 0.001$)
	temperature × method	-	N.S. ($p = 0.71$)	N.S. ($p = 0.96$)	N.S. ($p = 0.50$)

*** indicate a significant effect ($p < 0.05$)

N.S. means non-significant ($p > 0.05$)

Table 4. Measured $\bar{a}^*$ and $\bar{a}^*_{PSII}$ for each sub sample incubated in the PAM setup (Halogen light source) and O_2-production/^{14}C-assimilation setup (Xenon light source) for each experimental temperature, for *P. minimum*, *P. parvum* and *P. tricornutum*. Growth conditions as in Table 2.

	Temp (°C)	PAM incub. setup (Halogen lamp)			O_2, ^{14}C incub. setup (Xenon lamp)		
		$\bar{a}^*$	$\bar{a}^*_{PSII}$	$\bar{a}^*/\bar{a}^*_{PSII}$	$\bar{a}^*$	$\bar{a}^*_{PSII}$	$\bar{a}^*/\bar{a}^*_{PSII}$
P. minimum	0	0.0075	0.0058	1.29	0.0067	0.0054	1.24
	5	0.0065	0.0047	1.38	0.0058	0.0044	1.32
	10	0.0071	0.0053	1.34	0.0063	0.0050	1.26
	15	0.0073	0.0056	1.30	0.0065	0.0050	1.30
	20	0.0068	0.0055	1.24	0.0060	0.0049	1.22
	25	0.0074	0.0057	1.30	0.0066	0.0052	1.27
	30	0.0062	0.0049	1.27	0.0057	0.0043	1.33
P. parvum	0	0.0087	0.0074	1.18	0.0078	0.0068	1.15
	5	0.0085	0.0073	1.16	0.0077	0.0066	1.17
	10	0.0093	0.0076	1.22	0.0083	0.0070	1.19
	15	0.0092	0.0077	1.19	0.0083	0.0070	1.19
	20	0.0093	0.0080	1.16	0.0083	0.0072	1.15
	25	0.0098	0.0087	1.13	0.0088	0.0078	1.13
	30	0.0131	0.0109	1.20	0.0121	0.0096	1.26
P. tricornutum	0	0.0075	0.0062	1.21	0.0070	0.0057	1.23
	5	0.0075	0.0059	1.27	0.0072	0.0054	1.33
	10	0.0073	0.0057	1.28	0.0071	0.0053	1.34
	15	0.0074	0.0057	1.30	0.0072	0.0053	1.36
	20	0.0094	0.0076	1.24	0.0088	0.0071	1.24
	25	0.0099	0.0083	1.19	0.0092	0.0076	1.21
	30	0.0101	0.0078	1.29	0.0094	0.0073	1.29

Table 5. Chl *a* to C ratios (w/w) for *P. minimum*, *P. parvum* and *P. tricornutum* for each sub sample incubated at one of the experimental temperatures (see M&M). All cultures were grown at 80 µmol photons·m^{-2}·s^{-1} at 15°C.

Temperature (°C)	*P. minimum*	*P. parvum*	*P. tricornutum*
0	0.0113	0.0252	0.0324
5	0.0124	0.0262	0.0294
10	0.0127	0.0258	0.0317
15	0.0117	0.0285	0.0304
20	0.0115	0.0275	0.0244
25	0.0117	0.0265	0.0238
30	0.0115	0.0192	0.0232
Mean	0.0118	0.0256	0.0279
S.D. (C.V.)	0.0005 (4.4%)	0.0030 (11%)	0.0040 (14%)

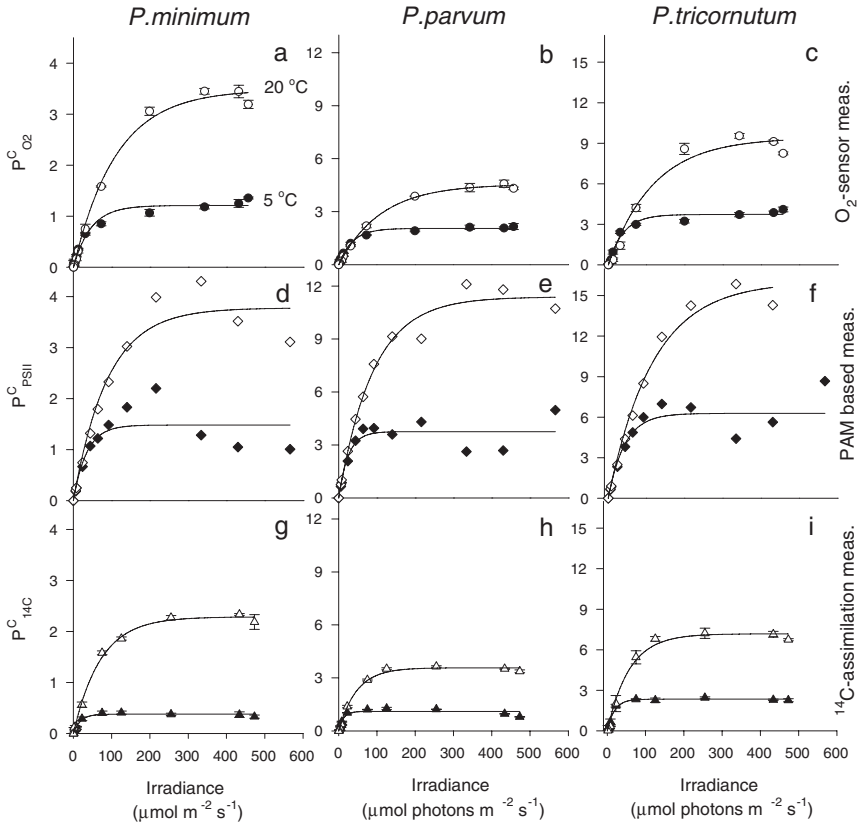

Fig. 1. Photosynthesis *versus* irradiance (P-E) curves measured by a-c) O_2-microsensors (P^C_{O2}), d-f) calculated from Φ_{PSII} (based on PAM measurements) in combination with bio-optical measurements (P^C_{PSII}) and g-i) measured ^{14}C-assimilation (P^C_{14C}), at 5°C (filled symbols) and 20°C (open symbols), respectively. The study was conducted on three unialgal cultures of *P. minimum* (left column), *P. parvum* (middle column) and *P. tricornutum* (right column). Units for P^C_{O2} and P^C_{PSII} are in µmol O_2·(mg POC) $^{-1}$·h^{-1} and for P^C_{14C} in µmol ^{14}C·(mg POC)$^{-1}$·h^{-1}.

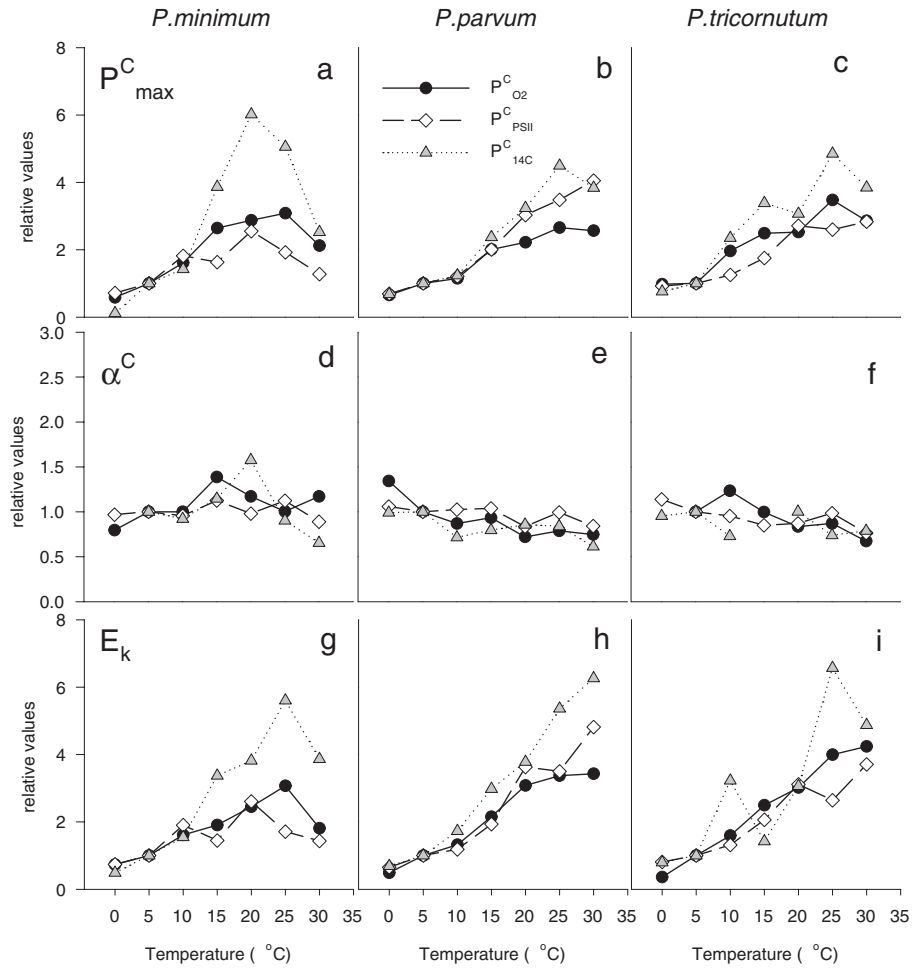

Fig. 2. Relative effect of temperature on the maximum photosynthetic rate (P^C_{max}, upper panel), the maximum light utilization coefficient (α^C, middle panel), and the light saturation index (E_k, lower panel) for *P. minimum* (left), *P. parvum* (middle) and *P. tricornutum* (right). The photosynthetic parameters were calculated from rates of measured O_2-production (P^C_{O2}, filled circles), Φ_{PSII} (P^C_{PSII}, open diamonds), and ^{14}C-assimilation (P^C_{14C}, grey triangles). All parameters were normalised to 1.0 at 5 °C. All cultures were grown at 15°C and 80 µmol photons·m^{-2}·s^{-1}.

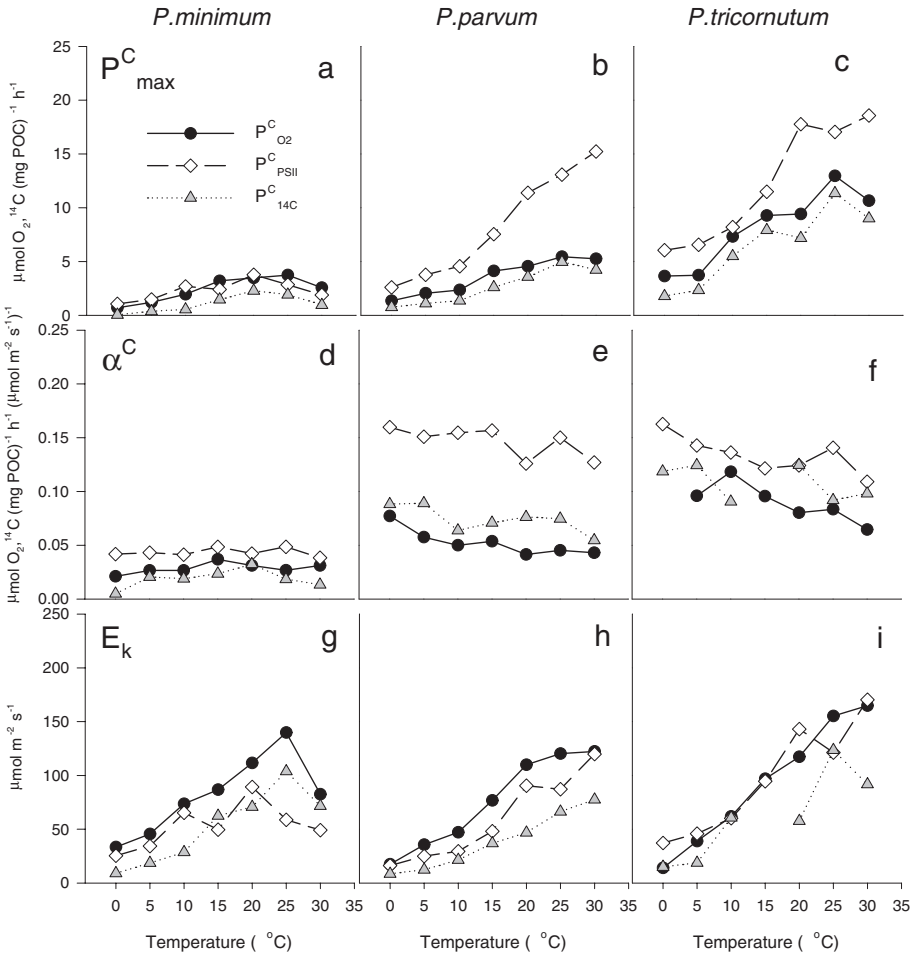

Fig. 3. Effect of temperature on the absolute values for the maximum photosynthetic rate (P^C_{max}, upper panel), the maximum light utilization coefficient (α^C, middle), and the light saturation index (E_k, lower panel) for *P. minimum* (left), *P. parvum* (middle) and *P. tricornutum* (right). Calculation of photosynthetic parameters and growth conditions as in Fig. 2.

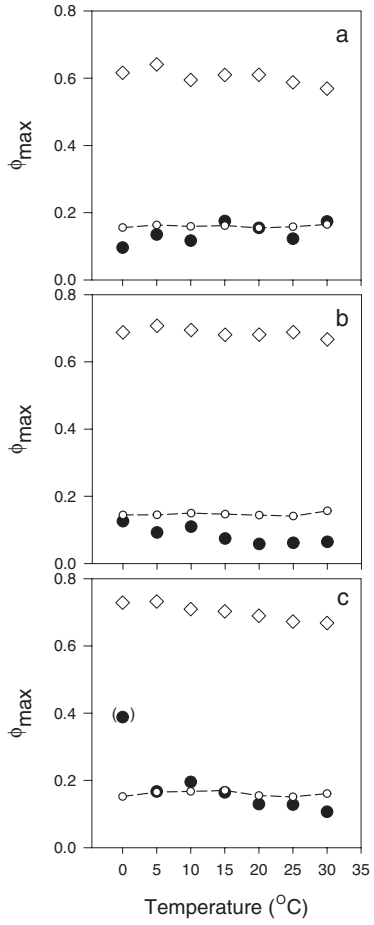

Fig. 4. Maximum quantum yield for O_2 ($^{PSII}\Phi_{O2\_max}$, filled circles) and PSII (Φ_{PSII_max}, open diamonds) as function of temperature for (a) *P. minimum*, (b) *P. parvum* and (c) *P. tricornutum*. $^{PSII}\Phi_{O2\_max}$ was calculated based on the light absorption in PSII ($\bar{a}^{*}_{PSII}$) and similar was the theoretical maximum quantum yield for O_2 production (small open circles), which was calculated for each temperature (Eq. 9, details in text).

Paper 4

Hancke K, Glud RN (2004) Temperature effects on respiration and photosynthesis in three diatom-dominated benthic communities. *Aquatic Microbial Ecology 37:265-281*

Vol. 37: 265–281, 2004 | AQUATIC MICROBIAL ECOLOGY
Aquat Microb Ecol | Published December 15

Temperature effects on respiration and photosynthesis in three diatom-dominated benthic communities

Kasper Hancke[1, 2,*], Ronnie N. Glud[1]

[1]Marine Biological Laboratory, University of Copenhagen, Strandpromenaden 5, 3000 Helsingør, Denmark

[2]*Present address:* Trondhjem Biological Station, Norwegian University of Science and Technology, 7491 Trondheim, Norway

ABSTRACT: Short-term temperature effects on respiration and photosynthesis were investigated in intact diatom-dominated benthic communities, collected at 2 temperate and 1 high-arctic subtidal sites. Areal rates of total (TOE) and diffusive (DOE) O_2 exchange were determined from O_2-microsensor measurements in intact sediment cores in the temperature range from 0 to 24°C in darkness and at 140 µmol photons m^{-2} s^{-1}. In darkness, the O_2 consumption increased exponentially with increasing temperature for both TOE and DOE, and no optimum temperature was observed within the applied temperature range. Q_{10} was calculated from the linear slope in Arrhenius plots and ranged between 1.7 and 3.3 at the respective sites. The volume-specific rate ($R_{dark,vol}$) solely representing the biological temperature response was somewhat stronger, with Q_{10} values of 2.6 to 5.2. The Q_{10} values were overall not correlated to the *in situ* water temperature or geographical position. Accordingly, no difference in the temperature acclimation or adaptation strategy of the microbial community was observed. Slurred oxic sediment samples showed a Q_{10} of 1.7 and were, hence, lower than estimates based on intact sediment core measurements. This can be ascribed to changes in physical and biological controls during resuspension. Gross photosynthesis was measured with the light-dark shift method at the 2 temperate sites. Both areal (P_{gross}) and volumetric ($P_{gross,vol}$) rates increased with temperature to an optimum temperature at 12 and 15°C, with a Q_{10} for P_{gross} of 2.2 and 2.6 for the 2 sites, respectively. The gross photosynthesis response could be categorised as psychrotrophic for both sites and no temperature adaptation was observed between the 2 sites. Our measurements document that temperature stimulates heterotrophic activity more than gross photosynthesis, and that the benthic communities gradually become heterotrophic with increasing temperature. This has implications for C-cycling in shallow water communities experiencing seasonal and diel temperature fluctuations.

KEY WORDS: Temperature · Adaptation · Benthic microphytes · Photosynthesis · Respiration · Q_{10} · Microelectrodes · Oxygen

INTRODUCTION

Temperature and irradiance are important environmental controls on photosynthesis and respiration in marine sediments (e.g. Hartwig 1978, Rasmussen et al. 1983, Grant 1986, MacIntyre & Cullen 1995). In shallow waters, both variables change on a seasonal and a diel basis superimposed by tidal and weather-driven variations, all having an impact on the benthic microbial activity (Grant 1986, Cahoon 1999, Glud et al. 2002). Studies at subtidal and intertidal sites have shown that temperature can exert tight control on benthic photosynthetic rates, and can lead to seasonal acclimation and/or change in the microphytobenthic community composition (Rasmussen et al. 1983, Grant 1986, Blanchard et al. 1996, Barranguet et al. 1998). Temperature acclimation usually describes phenotypic changes in a community as a response to short-term

*Email: kasper.hancke@bio.ntnu.no

temperature change, whereas temperature adaptation involves genetic differences in metabolism between communities from different thermal environments (Berry & Bjorkman 1980, Davison 1991). Temperature adaptation in microorganisms has typically been studied in cultures or in sediment slurries placed in benches at well-defined temperatures (Blanchard et al. 1996, Isaksen & Jørgensen 1996, Thamdrup & Fleischer 1998). Based on data for minimum, optimum and maximum temperatures of the activity, the organisms are divided into groups, such as psychrophile, mesophile and thermophile, that tolerate low, medium and high temperatures, respectively (Davison 1991).

Temperature-changed activity is often quantified by the so-called Q_{10} factor (the relative rate of increase at a temperature increase of 10°C). Such studies have shown an insignificant difference in temperature adaptation of aerobic respiration between arctic and temperate communities (Thamdrup & Fleischer 1998). In contrast, lower Q_{10} values have been reported for benthic sulphate reduction in Antarctic sediments compared to measurements performed at temperate latitudes (Isaksen & Jørgensen 1996). However, most benthic temperature studies have been performed on highly manipulated samples or inferred from seasonal rates at *in situ* temperature, which may be confounded by changes in other environmental controls. To our knowledge, only 2 detailed temperature studies on intact benthic communities exist, both performed in hyper-saline mat systems (Epping & Kühl 2000, Wieland & Kühl 2000). No detailed studies have been performed on subtidal microphytic communities.

Studying the temperature response of intact benthic microbial communities is complicated by the simultaneous impact on physical and chemical controls, and by the fact that benthic microbial communities host a complex phototrophic and heterotrophic diversity (Revsbech et al. 1981, Epping & Jørgensen 1996, Fenchel & Glud 2000). Temperature studies of aerobic activity based on traditional bell jar approaches can easily be misinterpreted, as they do not account for changes in O_2 penetration depth (Epping & Jørgensen 1996). Further, it is to be expected that data from slurry samples can be biased due to changes in the benthic community structure and in the environmental controls. Application of O_2 microsensors allows a detailed and unconfounded evaluation of the biological temperature effects on both photosynthesis and respiration with a high spatial resolution (Revsbech & Jørgensen 1986, Glud et al. 2000).

The aim of the present study was to evaluate possible differences in the temperature adaptation strategy between arctic and temperate benthic microphyte communities, during short-term temperature variations. The study includes rate measurements of sediment community respiration, gross photosynthesis and net photosynthesis as determined from O_2 microsensor measurements in intact sediments, sampled at 3 different sites.

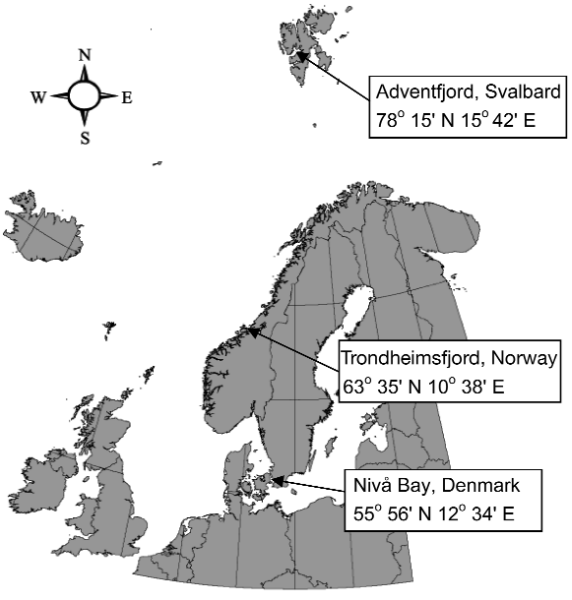

Fig. 1. Map including the sampling sites, Nivå Bay, Denmark, the Trondheimsfjord, Norway, and the Adventfjord, Svalbard, Norway

MATERIALS AND METHODS

Study site and conditions. Sediment samples were collected from a temperate site (Nivå Bay, Denmark), a northern-temperate site (Trondheimsfjord, Norway) and a high-arctic site (Adventfjord, Svalbard, Norway) (Fig. 1). The 3 sites were located in the subtidal zone (water depth <4 m, Table 1) and characterised by fine-grained sandy sediments, without onsite-growing macroalgae or vascular plants. Median grain size was not determined but microscopic investigations suggested that the mean grain size was around 200 to 500 µm at all the investigated sites. All sites were located in partly protected semi-enclosed bays, and the benthic microphytes were apparent as a golden-brownish colouring of the sediment surface. Microscopic analyses of fresh and Lugol-fixed samples verified that the benthic microphytes were dominated by the pennate diatom genera *Nitzschia* and *Navicula*. Few specimens of *Fragilaria*, *Surirella* and *Amphora* were observed. There was no apparent difference in the genera present at the different sites.

Table 1. Time of sampling, geographical position, and *in situ* water temperature, irradiance, salinity, water depth, and chlorophyll *a* concentration for the 3 investigated sites. n: number of samples

Parameter/site	Nivå Bay (Denmark)	Trondheimsfjord (Norway)	Adventfjord (Svalbard, Norway)
Time of sampling	February 2001	March 2002	May 2000[d]
Temperature (°C)[a]	2.5 ± 1.3 (0–30)	4.2 ± 0.7 (0–18)	–1.6 ± 0.2 (–1.8–7.0)
Irradiance (µmol photons m^{-2} s^{-1})[b]	68 ± 46 (380)	35 ± 20 (83)	46 ± 35 (195)
Salinity (‰)[c]	18 ± 7	29 ± 3	34 ± 0.4
Water depth (m)	0.4 ± 0.2	3.0 ± 1.5	1.3 ± 0.6
Chlorophyll *a* (mg m^{-2})	22.9 ± 6.5 (n = 4)	23.8 ± 5.6 (n = 10)	2.7 ± 0.7 (n = 4)

[a]*In situ* temperature at day of sampling, annual temperature range shown in parentheses
[b]Average incident irradiance (during light hours) measured on sediment surface at day of sampling; maximum measured irradiance at month of sampling shown in parentheses
[c]Measured across a 30 d interval
[d]Sampled beneath 40 to 50 cm of sea ice cover

Sediment porosity (ϕ) was determined by core slicing and subsequent drying, but resulted in underestimated values due to an unavoidable loss of water in the relatively sandy sediment (data not shown). Therefore, porosity was instead estimated from the ratio between the O_2 concentration gradient measured immediately above and below the sediment surface (Glud et al. 1995, Epping & Jørgensen 1996). In addition, porosity was estimated from resistivity measurements according to Klinkenberg (1951) and Ullman & Aller (1982). The average porosity applying these 2 approaches amounted to 0.60 ± 0.11 (n = 19). No significant difference in porosity was observed between the investigated sites and the same value was therefore used for all calculations.

All samples were collected during the winter months and consequently the temperature at the time of sampling was close to the minimum of the annual range (Table 1). Irradiance and salinity during the sampling periods are shown in Table 1. Incident irradiance and temperature at the sediment surface were measured using small-submerged data loggers (HOBO, Onset Computer Cooperation), intercalibrated to a cosine-corrected quantum sensor (LiCor LI-190SA connected to a LiCor LI-1000 data logger). The chlorophyll *a* (chl *a*) concentration of the surficial sediment (0 to 1 cm) was determined from at least 4 sediment cores at each site. Samples were initially frozen at –80°C and subsequently extracted in 96% ethanol for 24 h. The chl *a* concentration was determined spectrophotometrically (Parsons & Strickland 1963) using the extinction coefficient suggested by Wintermans & DeMots (1965) (Table 1).

Sampling and experimental set-up. Samples were collected by hand in Nivå Bay, by SCUBA divers in the Trondheimsfjord, and by a 'kayak'-like home-made sampler in the Adventfjord. During sampling in the Adventfjord 40 to 50 cm of sea ice covered the fjord and holes were drilled prior to sampling. All samples were collected directly in Plexiglas core liners (inner diameter = 52 mm; length ≈ 150 mm). Intact, undisturbed sediment cores with clear overlying water and without larger stones were selected. For each site, 6 to 12 cores were sampled, placed in an insulated box and transported within a couple of hours and with minimum disturbance to the laboratory. In the laboratory, cores were placed in bottom water from the sampling site kept at *in situ* temperature. The cores were exposed to a 12:12 h light:dark cycle (140:0 µmol photons m^{-2} s^{-1}, respectively) by a halogen lamp (Schott KL 1500). Even though the daylight period was longer at the more northern sites, irradiance at the 3 sites was comparable as a consequence of lower zenith angle of the sun at higher latitude. Data from the Trondheimsfjord were based on 3 individual sampling sessions, whereas data from Nivå Bay and the Adventfjord were based on a single set of samples from each site.

To enable temperature manipulation of the sediment cores, a microcosm was constructed (Fig. 2). By combinating a heating plate and a cooling coil, water temperature in the microcosms was changed in steps of 3 ± 0.2°C. A halogen lamp equipped with an optical fiber served as light source (Schott KL 1500) and incident irradiance was measured at the sediment surface using a cosine-corrected quantum sensor (LiCor LI-190SA). A stable water flow above the sediment surface was secured using an internal rotating magnet, which caused a diffusive boundary layer (DBL) of 300 to 500 µm at the measuring spots. Flushing by an air pump kept the water of the microcosm at atmospheric oxygen saturation at all times.

Microsensor measurements. All oxygen measurements were carried out using Clark-type O_2 microelectrodes with a guard cathode (Revsbech 1989). Total oxygen exchange (TOE) rates were measured using electrodes with external tip diameters of ~1000 µm,

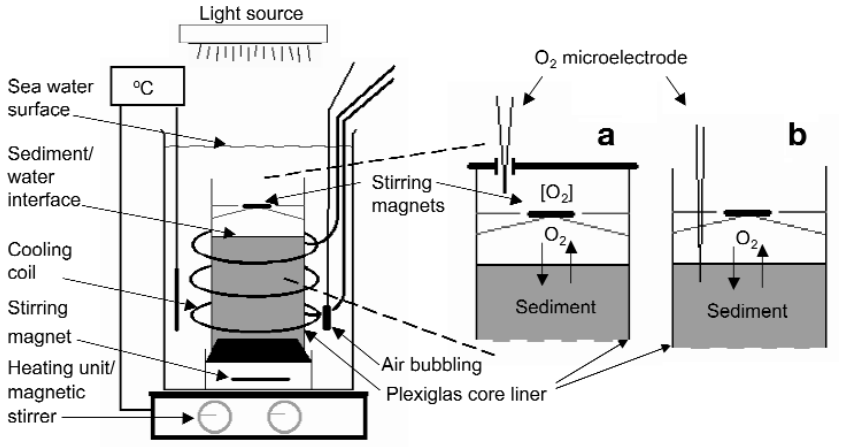

Fig. 2. Microcosms in which samples were installed prior to and during measurements. Sample temperature was controlled by a cooling coil and a heating plate connected to a digital temperature sensor. Two Teflon-coated magnets were installed and driven by a magnetic stirrer in the heating plate (65 to 70 rpm). The upper magnet (20 mm length) was mounted inside the core liner, 30 mm above the sediment surface, by a thin metal wire. The lower magnet provided stirring of the water in the microcosm, together with the air bubbling. (a) Close-up of the upper sediment core closed by a transparent lid mounted with an O_2 microelectrode and stirring magnet. (b) Close-up of the upper sediment core open to the surrounding water, with a positioned O_2 microelectrode for measuring O_2 microprofiles

stirring sensitivity of <3%, and a 90% response time of <40 s (Glud et al. 2000). Gross photosynthesis and microprofiles were measured using electrodes with external tip diameters <15 µm, stirring sensitivity <1% and a 90% response time <0.5 s. All electrodes were calibrated at the individual temperature settings by a 2-point calibration performed in both anoxic and air-saturated samples (Glud et al. 2000). This is essential because the Clark-type microelectrode responds to the partial pressure of O_2, thus the signal is sensitive to ambient temperature (Gundersen et al. 1998). The sensors were positioned either manually or by motor-driven micromanipulators. The sensor current was measured using a picoammeter (Unisense) connected to a strip chart recorder and a PC using the software 'Profix' (Unisense) (Revsbech & Jørgensen 1986).

Total oxygen exchange measurements. TOE rates were calculated from the change in the O_2 concentration of the overlying water, accounting for the enclosed water volume (Fig. 2a). Net O_2 consumption by the benthic community was apparent from a decrease in the O_2 concentration, while net production was seen as an increase in O_2 concentration. Oxygen microprofiles were measured in the same set-up after removal of the transparent lid and ensuring 100% air saturation of the overlying water phase (Fig. 2b).

Each core was incubated in darkness and at 140 µmol photons m^{-2} s^{-1} at each temperature. After changing the irradiance, cores were pre-incubated for 45 min prior to any measurements to ensure quasi steady state (this was confirmed by repeated microsensor measurements). To study impacts of temperatures, the ambient temperature was increased stepwise by 3°C. All cores were initially incubated at the lowest temperature. After a temperature change, the cores were pre-incubated for 60 min to obtain quasi steady state. At each temperature level, the measuring period lasted for approximately 3 h. Consequently, all cores experienced the same 'temperature history'.

The time required to ensure quasi steady state was determined by repeated microprofiling (every 5 to 10 min). Further, preliminary investigations confirmed that the order of temperature change had no effect on the community response in the interval from −1 to 18°C. However, after exposure to temperatures >18°C, the community rates were not always re-established when temperatures were subsequently lowered (data not shown).

Diffusive oxygen exchange (DOE) measurements. DOE rate was estimated from the diffusive flux of O_2 between the sediment and the water (J_{up}) as calculated from steady-state O_2 concentration profiles (Figs. 2b & 3). J_{up} was determined from the linear concentration gradient within the DBL, using Fick's first law of diffusion (Eq. 1 in Fig. 3a) (Jørgensen & Revsbech 1985, Crank 1989). Symbols and abbreviations used throughout the paper are listed in Table 2.

Oxygen profiles across the benthic interface were obtained with a vertical resolution of 50 to 100 µm. The thickness of the oxic zone (O_2-pd) was directly deter-

mined from the measured profiles accounting for the observed thickness of DBL. The sediment dark respiration (R_{dark}) was estimated as the flux of O_2 into the sediment ($-J_{up}$) from the overlying water (Eq. 1 in Fig. 3a). The average specific sediment respiration ($R_{dark,vol}$), defined as the integrated average volumetric respiration of the oxic zone, was calculated by dividing R_{dark} with O_2-pd (Eq. 2 in Fig. 3a).

Net photosynthesis (P_n) in light equalled the flux of O_2 out of the sediment (J_{up}) towards the overlying water (Eq. 6 in Fig. 3b). The specific net photosynthesis of the production zone ($P_{n,vol}$) was calculated as the total flux of O_2 out of the production zone, i.e. the sum of the flux to the overlying water (J_{up}) and the downward flux to the non-production zone (J_{down}) (Eq. 7 in Fig. 3b) divided by the thickness of the production zone (Eq. 8 in Fig. 3b) (Glud et al. 1992, Kühl et al. 1996). J_{down} was determined from the turning tangent to the O_2 profile at the boundary between the production and the non-production zones. The production zone was defined as the upper oxic zone delimited downward by the horizon of the compensation point, i.e. where the gross O_2 production equalled the O_2 consumption at incident surface irradiance of 140 µmol photons m^{-2} s^{-1} (Fig. 3b). The production zone is not identical to the photic sediment zone; however, in the present study the actual production zone is in focus. The light attenuation within the investigated sediments was not determined but supposed similar to the light attenuation measured by Kühl & Jørgensen (1994) in similar coastal sandy sediments. The non-production zone was defined as the oxic zone beneath the production zone.

In addition to R_{dark} and $R_{dark,vol}$, the specific respiration of the separated production and non-production zones was calculated. The specific dark respiration rate of the production zone ($R_{dark,vol,prod}$) was calculated as the O_2 flux into the production zone ($-J_{up}$) minus the O_2 flux down to the non-production zone (J_{down}), accounting for the thickness of the production zone (Eq. 4 in Fig. 3a). Consequently, the dark respiration rate of the non-production zone ($R_{dark,vol,nprod}$) was calculated as the downward flux to the non-production zone (J_{down}) accounting for the thickness of the oxic non-production zone (Eq. 5 in Fig. 3a). The oxygen profiles were measured at spots with high microphytic biomass in order to study the temperature response of respiration and photosynthesis. For this reason, the measured DOE rates were not always representative for the entire core area.

For O_2 flux calculation in the sediment, the effective diffusion coefficient of O_2 (D_s) was derived from the molecular diffusion coefficient of O_2 (D_o) and the sediment porosity (ϕ), according to Ullmann & Aller (1982) (Eq. 9). The D_o was from Broecker & Peng (1974) and corrected for temperature and salinity as described by Li & Gregory (1974).

$$D_s = \phi \cdot D_o \quad (9)$$

Table 2. Definition of abbreviations

Abbreviation	Definition
DBL	Diffusive boundary layer
TOE	Total oxygen exchange (whole core consumption/production rates)
DOE	Diffusive oxygen exchange (diffusive consumption/production rates)
$C(z)$	Oxygen concentration at depth z (nmol cm^{-3})
D_o	Molecular diffusion coefficient of oxygen in water (cm^2 s^{-1})
D_s	Effective diffusion coefficient of oxygen in sediment (cm^2 s^{-1})
$depth_{prod}$	Thickness of production zone
$depth_{nprod}$	Thickness of non-production zone
E_a	Apparent activation energy (kJ mol^{-1})
J_{down}	Flux of O_2 from the production zone to the non-production zone (nmol O_2 cm^{-2} s^{-1})
J_{up}, $-J_{up}$	Flux of O_2 across the DBL (nmol O_2 cm^{-2} s^{-1})
R_{dark} (DOE)	Areal sediment respiration in darkness (nmol O_2 cm^{-2} s^{-1})
$R_{dark,vol}$	Specific sediment respiration in darkness (nmol O_2 cm^{-3} s^{-1})
$R_{dark,vol,prod}$	Specific respiration of the production zone[a] in darkness (nmol O_2 cm^{-3} s^{-1})
$R_{dark,vol,nprod}$	Specific respiration of the non-production zone[b] in darkness (nmol O_2 cm^{-3} s^{-1})
P_n (DOE)	Areal net photosynthesis of the sediment in light (nmol O_2 cm^{-2} s^{-1})
$P_{n,vol}$	Specific net photosynthesis of the production zone (nmol O_2 cm^{-3} s^{-1})
P_{gross}	Areal gross photosynthesis of the production zone (nmol O_2 cm^{-2} s^{-1})
$P_{gross,vol}$	Volumetric gross photosynthesis (nmol O_2 cm^{-3} s^{-1})
$P_{(z)}$	Volumetric gross photosynthesis at depth z (nmol O_2 cm^{-3} s^{-1})
O_2-pd	Oxygen penetration depth in the sediment

[a]The production zone was defined as the upper 1.0 to 1.2 mm of the sediment having a net O_2 production in light
[b]The non-production zone was defined as the oxic zone immediately beneath the production zone. The oxic zone was defined as the upper sediment zone with a $[O_2] > 1$ nmol O_2 cm^{-3}

Diffusive O_2 exchange calculations

Dark:

$$R_{dark} = -J_{up} = -D_o \frac{dC(z)}{dz} \quad (1)$$

$$R_{dark,vol} = \frac{-J_{up}}{O_2\text{-pd}} \quad (2)$$

$$J_{down} = D_s \frac{dC(z)}{dz} \quad (3)$$

$$R_{dark,vol,prod} = \frac{(-J_{up}) + J_{down}}{depth_{prod}} \quad (4)$$

$$R_{dark,vol,nprod} = \frac{J_{down}}{depth_{nprod}} \quad (5)$$

Light:

$$P_n = J_{up} = D_s \frac{dC(z)}{dz} \quad (6)$$

$$J_{down} = D_s \frac{dC(z)}{dz} \quad (7)$$

$$P_{n,vol} = \frac{J_{up} + J_{down}}{depth_{prod}} \quad (8)$$

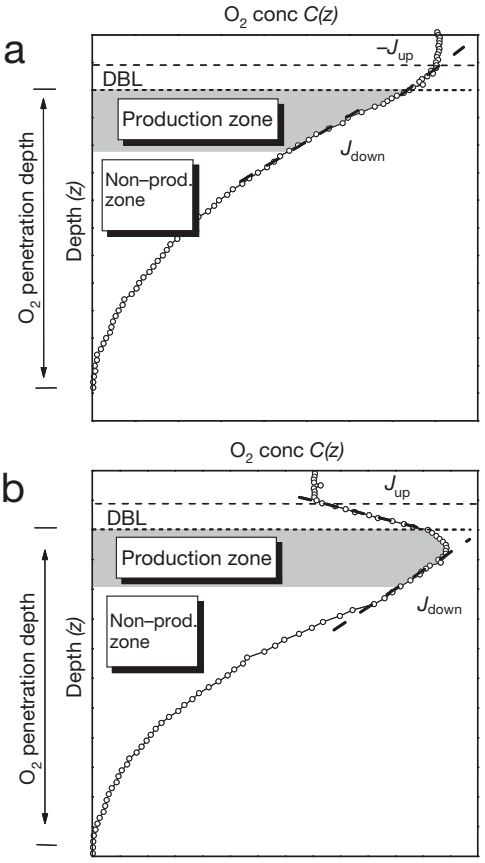

Fig. 3. Eqs. (1) to (8) for calculating diffusive O_2 consumption and production rates from steady-state O_2 concentration profiles in (a) darkness and (b) light, respectively. See Table 2 for definition of abbreviations. For calculations performed in the DBL, D_o was applied, but for calculations in the sediment, D_o was replaced by D_s (see text). The DBL and the production and the non-production zones of the sediment are shown in each panel. All flux measurements were performed under steady-state conditions and calculations were based on Fick's 1st law of diffusion. Inspired by Kühl et al. (1996)

Steady-state oxygen profiles were confirmed in each experiment by comparing 2 or more profiles measured within a time interval of 5 to 20 min.

Gross photosynthesis. Gross photosynthesis at depth z, $P(z)$, was measured by the light-dark shift method. This approach estimates the gross O_2 production from the initial decrease of O_2 after a sudden eclipse of light (Revsbech & Jørgensen 1983, Glud et al. 1992). The O_2 concentration was recorded continuously for 4 s during a light-dark shift. Repetitive measurements at 5 min intervals were performed at the same position. A photoelectrical cell connected to the flatbed recorder was used to obtain the exact timing for the onset of darkness.

Two practical approaches were applied to obtain the gross photosynthetic rate as a function of temperature. In Approach 1, we depth-integrated the gross photosynthesis of the entire production zone (P_{gross}). In this approach, an electrode sensor tip was placed at the very surface of the sediment and then moved downward in steps of 100 µm. $P(z)$ was measured at each depth, using the light-dark shift method, until the measured rates approached zero at the bottom of the production zone. Temperature was kept constant until a complete vertical gross photosynthesis profile was obtained (Glud et al. 1992, Kühl et al. 1996).

Approach 2 did not include profiling, and gross photosynthesis was solely obtained at the depth of the maximum activity within the production zone ($P_{gross,vol}$). In this approach, the microsensor tip was carefully placed at the given position, and subsequently temperature was changed <6°C h^{-1} while performing light-dark shifts every 10 to 20 min. P_{gross} rates were calculated using Fick's second law of diffusion simplified according to Revsbech et al. (1986):

$$P(z) = -\frac{dC(z,t)}{dt} \quad (10)$$

The gross O_2 production $P(z)$ equals the initial linear decrease of the O_2 concentration $C(z,t)$ at a specific

depth (z) over time (t). For a more detailed discussion of the technique and the required assumptions, see Glud et al. (1992).

Slurry experiments. Apart from the measurements in intact benthic communities, slurry experiments on re-suspended samples from the Trondheimsfjord were performed in darkness. The oxic, production and non-production zones of the sediment were incubated in parallel by resuspending sediment samples (equivalent to ~100 g dry matter l^{-1}) in seawater from the sampling site. The boundaries of the production and the oxic zones were determined from O_2 microprofiles measured prior to core slicing. Before suspension of the sediments, fauna visual to the naked eye was carefully removed from the slurries. The sediment slurries were placed in the thermo-regulated water bath (Fig. 2) and air-flushed for 30 min prior to the experiment to ensure air-saturation and oxidation of reduced inorganic substances. All slurries were stirred with a magnetic stirrer in the time period prior to and during the measurements. Any potential O_2 consumption by bacteria in the added seawater was assumed minor and ignored (Thamdrup et al. 1998). Oxygen consumption was measured after closing the samples, avoiding bubbles and placing a microelectrode in the chamber lid. The O_2 consumption was measured continuously for each incubation and was in all cases linear. The temperature was kept constant during each incubation, and the incubations were performed at temperature steps between 0 and 48°C. Each incubation period was adjusted to ensure a total O_2 concentration change of 10 to 30%.

Arrhenius plot and Q_{10} calculations. The effect of temperature on respiration rates, net photosynthetic and gross photosynthetic rates was quantified by calculating the apparent activation energy (E_a, in kJ mol^{-1}) and the corresponding Q_{10} value for each type of data set. E_a was calculated as the slope of the available data point from the initial linear part of an Arrhenius plot (temperature < optimum), where $\ln(k)$ was plotted as a function of temperature $(RT)^{-1}$, according to Raven & Geider (1988) and Isaksen & Jørgensen (1996) as:

$$\ln(k) = \ln(A) + [-E_a(RT)^{-1}] \quad (11)$$

where k is the rate of the reaction, A is the Arrhenius constant, R is the gas constant (8.3144 J K^{-1} mol^{-1}) and T is the absolute temperature (K). E_a is not the chemical activation energy but the overall temperature response of respiration or photosynthesis within the entire sediment community. The Q_{10} value was calculated from Eq. (12), where E_a quantifies the increase of the reaction rate. In all cases, a temperature interval from 0 to 10°C was used in the calculation of Q_{10}. Standard errors (SE) were obtained for E_a based on the linear regressions ($p = 0.05$).

$$Q_{10} = \exp\{E_a \cdot 10[RT(T+10)]^{-1}\} \quad (12)$$

Measured rates of respiration, as well as gross and net photosynthesis, were compared between sites. A statistical analysis of covariance (ANCOVA) was performed to test for insignificance of the Q_{10} values between sites, as the rate × site interaction computed by S-PLUS 6.2. ANCOVA assumes statistically independent values. The experimental design of the present study, however, does not offer completely independent data due to the repeated measurements on the incubated cores. We, however, judged that this had little effect on the obtained statistical results and we found no superior statistical model to fit the present study.

RESULTS

Total O_2 exchange rates

TOE rates were measured in darkness and at 140 µmol photons m^{-2} s^{-1} as a function of temperature (Fig. 4). The negative TOE rates in darkness reflect sediment O_2 consumption (influx of O_2), whereas the positive TOE rates in light reflect net O_2 production (efflux of O_2). In darkness, the O_2 consumption increased exponentially with increasing temperature at all the investigated sites. No optimum temperature was observed between −1 and 21°C. To compare the temperature response between sites, $Q_{10(0-10°C)}$ values were calculated from the apparent E_a based on the linear slope of the Arrhenius plots (Fig. 4d). The calculated Q_{10} values for the dark-incubated cores were 3.3, 2.4 and 2.4 for Nivå Bay, the Trondheimsfjord, and the Adventfjord, respectively. E_a ± SE and Q_{10} values are presented in Table 3.

In light, the TOE rates increased gradually with increasing temperature to a maximum at temperatures between 6 and 12°C, followed by a decrease (Fig. 4). The Q_{10} values for TOE in light were 1.7, 2.4 and 1.5 for Nivå Bay, the Trondheimsfjord, and the Adventfjord, respectively (Fig. 4e, Table 3).

For TOE in the dark, no significant difference of the Q_{10} was observed between the Trondheimsfjord and the Adventfjord ($p > 0.05$); however, a significant difference ($p = 0.01$) between the 3 sites was observed, as E_a for Nivå Bay was higher than for the 2 other sites. For TOE in light, there was no significant difference of the Q_{10} between the 3 sites ($p = 0.59$). In all cases, increasing temperature stimulated heterotrophic activity more than photosynthesis, gradually shifting the otherwise net autotrophic sediment community towards a greater predominance of heterotrophic activity. Temperature effects on total oxygen exchange rates, however, essentially represent a 'black box'

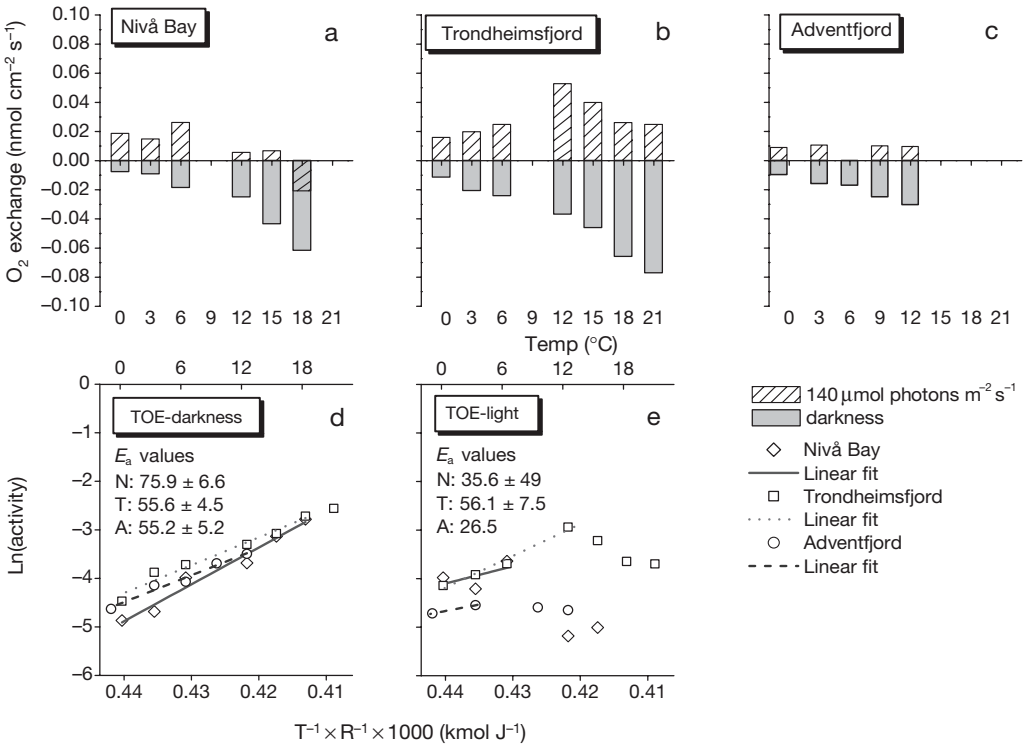

Fig. 4. Areal rates of total oxygen exchange (TOE) as a function of temperature, measured from whole core incubations in darkness and at 140 µmol photons m^{-2} s^{-1} in (a) Nivå Bay, (b) the Trondheimsfjord and (c) the Adventfjord. Negative values indicate net O_2 consumption and positive values net O_2 production. Rates from each site were plotted in Arrhenius plots in (d) darkness and (e) light. The activation energy (E_a ± SE; kJ mol^{-1}) was calculated from the initial linear fit (d, e), labelled N (Nivå Bay), T (Trondheimsfjord) and A (Adventfjord). Corresponding Q_{10} values are shown in Table 3

approach confounded by changes in the O_2 penetration depth, DBL thickness, diffusion coefficients, etc., and yields limited information on the actual microbial temperature response. This, however, can be derived from micro-profile measurements.

Diffusive O_2 exchange rates in darkness

With increasing temperature, the O_2 solubility decreases while the molecular diffusion coefficient increases. In order to extract the biological response of the intact community, detailed microsensor measurements at the different experimental settings are required. Steady-state O_2 microprofiles were measured at temperatures from –1 to 21°C, and the corresponding DOE rates were calculated. In darkness, DOE rates increased exponentially with increasing temperature while the O_2-pd decreased (Fig. 5). The $Q_{10(0–10°C)}$ values for DOE in darkness were 2.2, 1.7 and 2.4 for Nivå Bay, Trondheimsfjord and Adventfjord, respectively (E_a ± SE and Q_{10} are presented in Fig. 5d & Table 3), and were not significantly different between the 3 sites ($p = 0.19$). The Q_{10} values in darkness, at the selected spots that were dominated by phototrophs, tended to be lower than for the TOE, which integrates the response of the entire sediment area. This supports the observation of lower Q_{10} values for the autotrophic activity compared to the heterotrophic activity. Q_{10} for O_2-pd were 0.42, 0.64 and 0.73 for Nivå Bay, the Trondheimsfjord and the Adventfjord, respectively (Fig. 5e, Table 3). The decrease in O_2-pd with decreasing temperature led to a lower volume of oxic sediment. The specific respiration rates ($R_{dark,vol}$) (for method see Fig. 3) were thereby strongly stimulated by increasing temperature, with Q_{10} values of 5.2, 2.6 and 3.2 for Nivå Bay, the Trondheimsfjord and the Adventfjord, respectively (E_a ± SE and Q_{10} are presented in Fig. 5f & Table 3). However, the Q_{10} for Nivå Bay was slightly higher than for the 2 other sites; the difference was not significant ($p = 0.06$). The biological temperature response for the community

was, hence, significantly stronger than was obtained from simple flux measurements.

Production and non-production zone respiration

The oxic zone of the sediment was divided into an upper production zone and a lower non-production zone, to some extent reflecting the natural zonation of microbes (Fig. 3) (e.g. MacIntyre & Cullen 1995, Epping & Jørgensen 1996). Based on measured O_2 profiles in darkness, specific consumption rates were calculated for each zone, as $R_{dark,vol,prod}$ and $R_{dark,vol,nprod}$, respectively. The O_2 consumption rates were overall higher (1 to 6 times) for the production zone than for the non-production zone (Fig. 6). However, the Q_{10} values tended to be higher for the non-production than for the production zone, the exception being the Adventfjord, which exhibited very low microphytic biomass (Table 4). The higher Q_{10} response in Nivå Bay and the Trondheimsfjord for non-production zone respiration supports the previous observation of heterotrophs being more sensitive to temperature changes compared to the autotroph organisms.

Gross photosynthesis

Due to the relatively low biomass of microphytes at the Adventfjord (Table 1), it was not possible to make robust gross photosynthetic measurements at that location. Depth-integrated rates of gross photosynthesis (P_{gross}) (Approach 1, see 'Materials and methods') were determined as a function of temperature only for the Trondheimsfjord, whereas point measurements ($P_{gross,vol}$) (Approach 2) were carried out in both Nivå Bay and the Trondheimsfjord.

P_{gross} rates were obtained from integrating vertical profiles of gross photosynthesis across the production zone, for each temperature (Fig. 7). The shape of the profiles was similar during changing temperature, demonstrating a constant activity distribution with depth and, hence, no vertical shift in the photosynthetic activity was observed. The P_{gross} rate showed a linear response with increasing temperature from 0°C to the optimum temperature (T_{opt}) at 12°C, with a Q_{10} value of 3.1 (Fig. 8d, Table 3). The $P_{gross,vol}$ rate, based on point measurements, showed a response similar to P_{gross} obtained both in the Trondheimsfjord and in Nivå Bay. For the Trondheimsfjord, T_{opt} was 12°C and Q_{10} for $P_{gross,vol}$ was 2.6 (Fig. 8b,d, Q_{10} and E_a in Table 3). For Nivå Bay, T_{opt} was 15°C and Q_{10} 2.2 (Fig. 8a,c, Q_{10} and E_a in Table 3). Conclusively, the point measurements confirmed the same trend as the depth-integrated approach.

Table 3. Q_{10} values (upper values) of respiration, net production and gross photosynthesis, calculated from the activation energies (E_a) (lower values) from Figs. 4, 5, 8 & 9. $E_a \pm$ SE (kJ mol^{-1}) is given below the Q_{10}, n is number of regression points

	Nivå Bay	Trondheimsfjord	Adventfjord
Darkness			
TOE	3.3 (n = 6) 75.9 ± 6.6	2.4 (n = 15) 55.6 ± 4.5	2.4 (n = 5) 55.2 ± 5.2
DOE (R_{dark})	2.2 (n = 6) 50.0 ± 10	1.7 (n = 12) 33.5 ± 6.2	2.4 (n = 5) 56.0 ± 12
O_2-pd	0.42 (n = 6) −55.9 ± 3.4	0.64 (n = 12) −27.1 ± 4.9	0.73 (n = 5) −20.0 ± 7.3
$R_{dark,vol}$	5.2 (n = 6) 105 ± 13	2.6 (n = 12) 61.8 ± 10	3.2 (n = 5) 75.0 ± 17
Slurry respiration	–	1.7 (n = 7) 35.7 ± 9.3	–
Light			
TOE	1.7 (n = 3) 35.6 ± 49	2.4 (n = 7) 56.1 ± 7.5	1.5 (n = 2) 26.5
DOE (P_n)	1.4 (n = 3) 23.5 ± 7.3	2.2 (n = 4) 50.2 ± 11	1.6 (n = 5) 31.1 ± 13
O_2-pd	0.78 (n = 4) −16.0 ± 12	0.82 (n = 4) −12.4 ± 3.3	0.78 (n = 5) −15.7 ± 6.4
$P_{n,vol}$	1.5 (n = 3) 24.6 ± 2.2	2.1 (n = 4) 46.3 ± 11	1.6 (n = 5) 30.4 ± 6.8
P_{gross}	–	3.1 (n = 4) 73.6 ± 11	–
$P_{gross,vol}$	2.2 (n = 10) 50.9 ± 7.0	2.6 (n = 13) 62.5 ± 11	–

Diffusive O_2 exchange rates in light

The net photosynthetic rate integrates the gross O_2 production (production zone) and the O_2 consumption (in light) of the entire oxic zone. Net photosynthetic rates (P_n) were calculated from O_2 microprofiles in light (140 µmol m^{-2} s^{-1}) (Fig. 9a–c). The light-induced response was highest in Nivå Bay and lowest in the Adventfjord, reflecting the microphytic biomass at the respective sites. Generally, the O_2 concentration and the O_2-pd of the benthic community decreased with increasing temperature. Calculated rates of P_n increased continuously with temperature from 0°C to T_{opt}, at all sites (Fig. 9d). Rates for Nivå Bay and the Trondheimsfjord showed a subsequent decrease above T_{opt}, which was 12°C for the Trondheimsfjord and the Adventfjord and 15°C for Nivå Bay. Calculated Q_{10} values for P_n, derived from the Arrhenius plot, were 1.4, 2.2 and 1.6 for Nivå Bay, the Trondheimsfjord and the Adventfjord, respectively (E_a in Fig. 9d, including Q_{10} in Table 3), and were not significantly different ($p = 0.47$). The Adventfjord showed lower absolute rates than for the 2 other sites. No rates were obtained for the Adventfjord at temperatures >12°C.

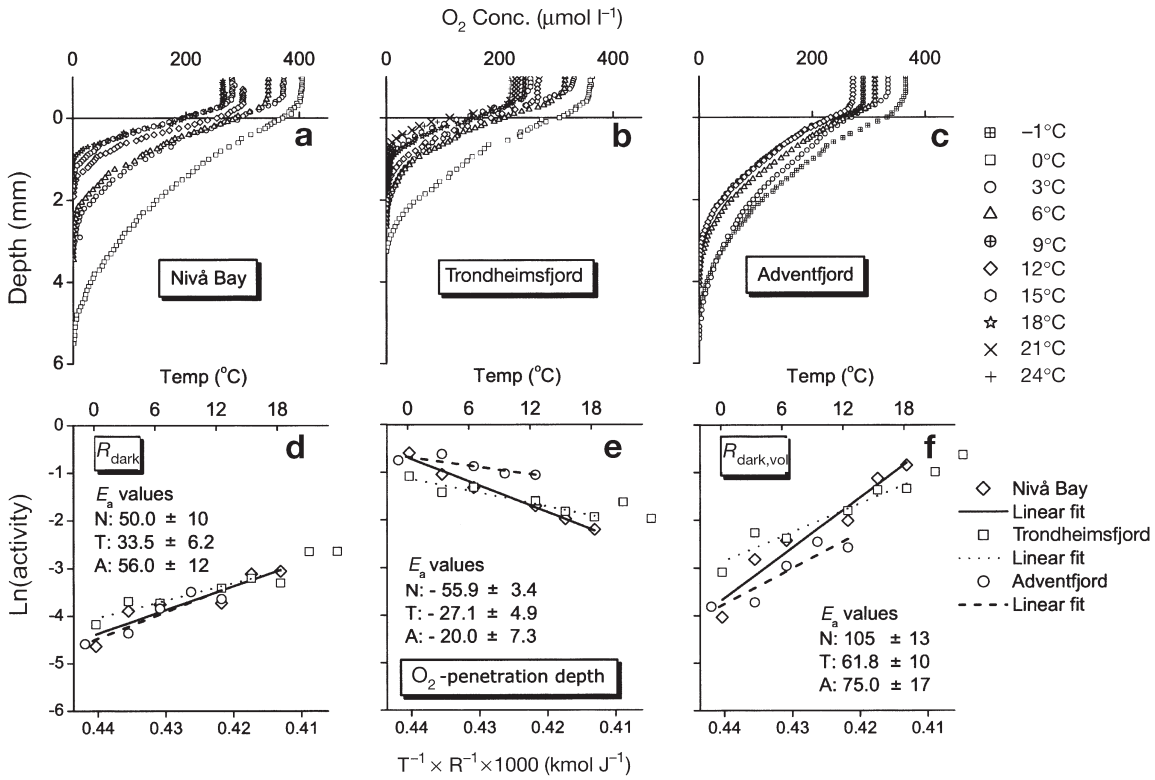

Fig. 5. Steady-state O_2 microprofiles in intact sediment cores in darkness at various temperatures (–1 to 24°C) from (a) Nivå Bay, (b) the Trondheimsfjord and (c) the Adventfjord. Arrhenius plots of (d) diffusive O_2 consumption (R_{dark}) calculated from the slope of the profile in DBL, (e) the oxygen penetration depth and (f) the specific respiration as a function of temperature are shown. Activation energies (E_a ± SE; kJ mol^{-1}) are included (d–f), labelled N (Nivå Bay), T (Trondheimsfjord) and A (Adventfjord). Corresponding Q_{10} values are shown in Table 3

Table 4. Q_{10} values (upper values) of the production and non-production zone-specific respiration based on the activation energies (E_a) (lower values) calculated from intact sediment cores and slurry samples in darkness (Figs. 6 & 10). E_a ± SE (kJ mol^{-1}) is given below the Q_{10}, n is number of regression points

	Nivå Bay	Trondheimsfjord	Adventfjord
Intact sediment core respiration			
Prod. zone	3.5 (n = 6)	2.2 (n = 12)	3.5 (n = 5)
	80.5 ± 19	49.5 ± 11	81.4 ± 20
Non-prod. zone	6.1 (n = 6)	2.4 (n = 12)	2.1 (n = 5)
	116 ± 8.9	56.1 ± 11	46.6 ± 13
Slurred sample respiration			
Prod. zone	–	1.9 (n = 6)	–
		42.0 ± 10	
Non-prod. zone	–	1.6 (n = 5)	–
		31.0 ± 9.4	

O_2-pd decreased with increasing temperature for all 3 sites (Fig. 9e), and calculated values of Q_{10} were 0.78, 0.82 and 0.78 in Nivå Bay, the Trondheimsfjord and the Adventfjord, respectively (Table 3). Conclusively, O_2-pd in the light showed a similar temperature response as in darkness but with Q_{10} values closer to 1.0.

The specific net photosynthesis ($P_{n,vol}$) integrates the sum of the gross O_2 production and the O_2 consumption (in light) in the production zone. The $P_{n,vol}$ rates generally showed the same trend as P_n but with higher rates (Fig. 9f). The Q_{10} of $P_{n,vol}$ was 1.5, 2.1 and 1.6 for Nivå Bay, the Trondheimsfjord and the Adventfjord, respectively (Table 3), and there was no significant difference between the sites (p = 0.34). The $P_{n,vol}$ data indicate that the temperature response of the production zone was similar to the entire oxic zone of the sediment exposed to light.

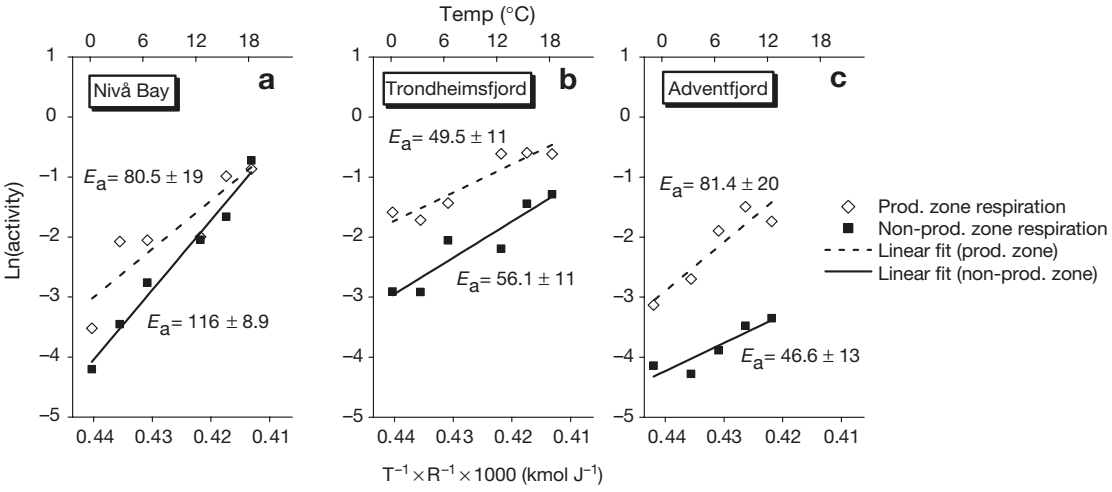

Fig. 6. Arrhenius plot of production and non-production zone. O_2 consumption rates in darkness as function of temperature for (a) Nivå Bay, (b) the Trondheimsfjord and (c) the Adventfjord. Specific respiration rates for the separated zones are calculated from oxygen profiles. Lines represent linear fits and activation energies (E_a) are included. Corresponding Q_{10} valuesare shown in Table 4

Slurry experiments

For the Trondheimsfjord, the oxygen consumption in darkness was additionally measured in sediment slurries from the oxic, production and non-production zones (Fig. 10). The experiment was performed partly to elucidate to what extent resuspension affects the biological response and to allow for comparison with previous studies of temperature effects on O_2 consumption rates, which mainly have been conducted on slurred samples. Oxygen consumption of the entire oxic zone increased with temperature from 0°C to T_{opt} at 21°C followed by a decrease, and Q_{10} was 1.7 ± 0.5 (Fig. 10, Table 3). Oxygen consumption of the separated production and non-production zones showed similarly increasing rates with increasing temperature towards T_{opt} at 24 and 39°C, respectively (Fig. 10a). For both sediment zones, a clear decrease in the consumption rate was observed at temperatures higher than T_{opt}. $Q_{10(6–16°C)}$ for the initial O_2 consumption increase (6 to 18°C) was 1.9 and 1.6 for the production and non-production zones, respectively (Fig. 10b, Table 4). Q_{10} of the sediment slurries showed a generally weaker temperature response than the $R_{dark,vol}$ rates for intact sediment cores. The higher T_{opt} for the non-production than for the production zone indicates a higher temperature optimum for the heterotrophic community than for the phototrophic-dominated part of the sediment, presumably due to the overall vertical zonation of phototrophs and heterotrophs. The Q_{10} value, however, was not significantly different for the 2 zones.

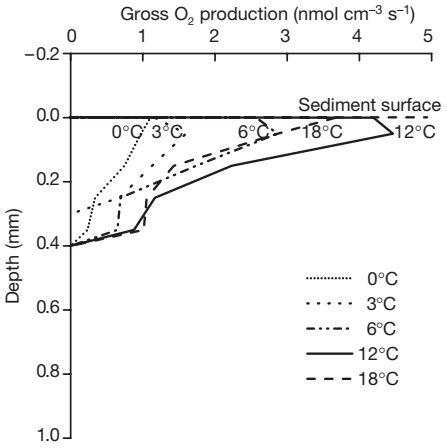

Fig. 7. Gross O_2 production profiles as a function of temperature in the Trondheimsfjord. Areal rates of gross photosynthesis were calculated from the integrated area of each profile (Fig. 8)

DISCUSSION

Heterotrophic temperature response

Despite differences in water temperature and geographical position, the Q_{10} for the short-term temperature response of the dark respiration showed no signif-

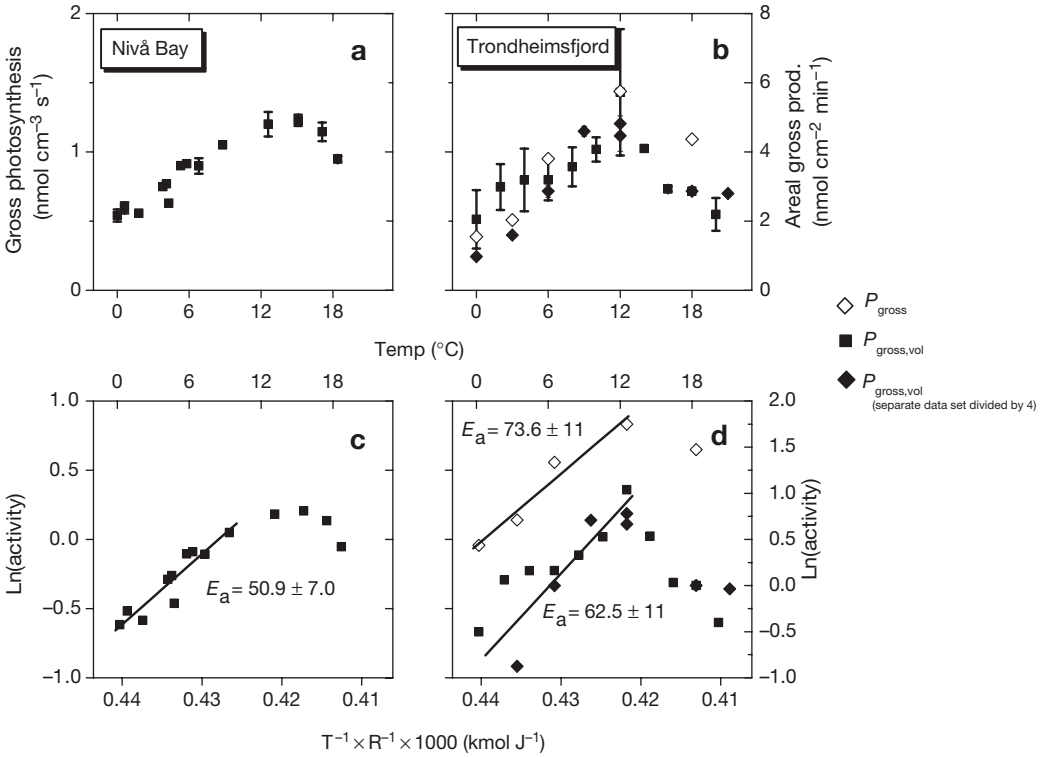

Fig. 8. Gross photosynthesis rates as a function of temperature in (a) Nivå Bay and (b) the Trondheimsfjord. Closed symbols indicate volumetric spot measurements, whereas open symbols represent depth-integrated areal gross photosynthesis rates (note different *y*-axis scales). (◆) Separate data set obtained data divided by 4. Arrhenius plots of the rates shown in (a) and (b) are presented in (c) and (d), respectively. Activation energies (E_a ± SE; kJ mol^{-1}) are included: corresponding Q_{10} values are shown in Table 3

icant difference ($p > 0.05$) between the 3 sites. This was true for both TOE and DOE rates, with one exception for TOE in Nivå Bay showing a higher Q_{10} than for the 2 other sites ($p < 0.05$); we have no good explanation for this exception. In general, we conclude that the temperature acclimation response was similar for the 3 investigated sites. The lack of any distinct latitude related temperature adaptation strategy could be due to the relatively moderate temperature difference between the investigated sites during sampling. In fact, the seasonal temperature amplitude at each site was larger than the temperature difference between the sites at the time of sampling (Table 1). Moreover, the diel temperature amplitude for the 2 temperate sites, in summer, exceeded the temperature difference between the 3 sites at sampling (in winter), with Nivå Bay demonstrating a diel temperature amplitude of up to 10°C during summer (data not shown). It can be speculated that a seasonal temperature acclimation at each site could be more pronounced than any latitude related response.

A comparative study on short-term temperature effects of aerobic respiration in slurred coastal sediments also concluded that Arctic and temperate sediments had similar Q_{10} values (Thamdrup & Fleischer 1998). However, a seasonal temperature acclimation was observed for the temperate site, with $Q_{10(0–10°C)}$ of 2.0 and 3.0 for winter (1 to 3°C) and summer (13 to 15°C), respectively (Thamdrup et al. 1998). The seasonal Q_{10} response was ascribed to a physiological acclimation or a change in the genotypic composition of the aerobic community. These findings contrast conclusions of sulphate reduction measurements, obtained in intact sediment incubations, having $Q_{10(2–12°C)}$ of 1.5 and 3.0 to 3.9 for Antarctic and temperate sediments, respectively (Isaksen & Jørgensen 1996). However, E_a in the range of 40 to 75 kJ mol^{-1} (corresponding to a $Q_{10(0–10°C)}$ of 1.8 to 3.2) for sulphate reduction have been published from the permanently cold areas around Svalbard (Sagemann et al. 1998), also pointing to a non-consistent latitude dependence of Q_{10} on sulphate reduction rates.

Q_{10} for the area based dark heterotrophic response varied from 1.7 to 3.3. Published Q_{10} values of areal O_2 consumption rates from comparable experiments range between 2.0 and 3.0 for subtidal and intertidal sites (Duff & Teal 1965, Davis & McIntire 1983). A broader range of Q_{10} values are published derived from correlations between seasonal rates and water temperatures and from manipulated samples (e.g. Grant 1986, Therkildsen & Lomstein 1993). The latter findings are, however, not directly comparable to our short-term incubations.

Q_{10} for TOE tended to be higher than for DOE. As previously mentioned, this supports a stronger temperature response for the heterotrophs compared to the phototrophs in the dark, as DOE is measured at spots with high biomass of phototrophs, compared to TOE integrating the entire core surface. TOE data potentially include the infauna response, which can lead to a relatively higher Q_{10} due to infaunal respiration. Q_{10} for fauna respiration is typically published to be ~2.5 and it cannot be excluded that it affected the Q_{10} based on the TOE rates (Caron et al. 1990).

The Q_{10} values for the specific rate ($R_{dark,vol}$) were higher than the area based values (2.6 to 5.2, Table 3). As previously described, the $R_{dark,vol}$ is corrected for the O_2-pd and solely represents the microbial response, where the temperature effects on the areal rates are biased by the decreasing thickness of the oxic zone, with increasing temperature. In the literature, there are only very few measurements of benthic volume-specific temperature responses from similar settings and these were not performed on intact communities but on slurred samples. Our measurements show that the temperature response in slurred sediments is lower than in undisturbed sediment cores, with a Q_{10} of 1.7 (E_a = 35.7 ± 9.3) versus 2.6 (E_a = 61.8 ± 10), respectively (Table 3). The lower temperature response following resuspension must be ascribed to a radical change in the community structure and the micro-environmental controls of the community. Our data show that Q_{10}

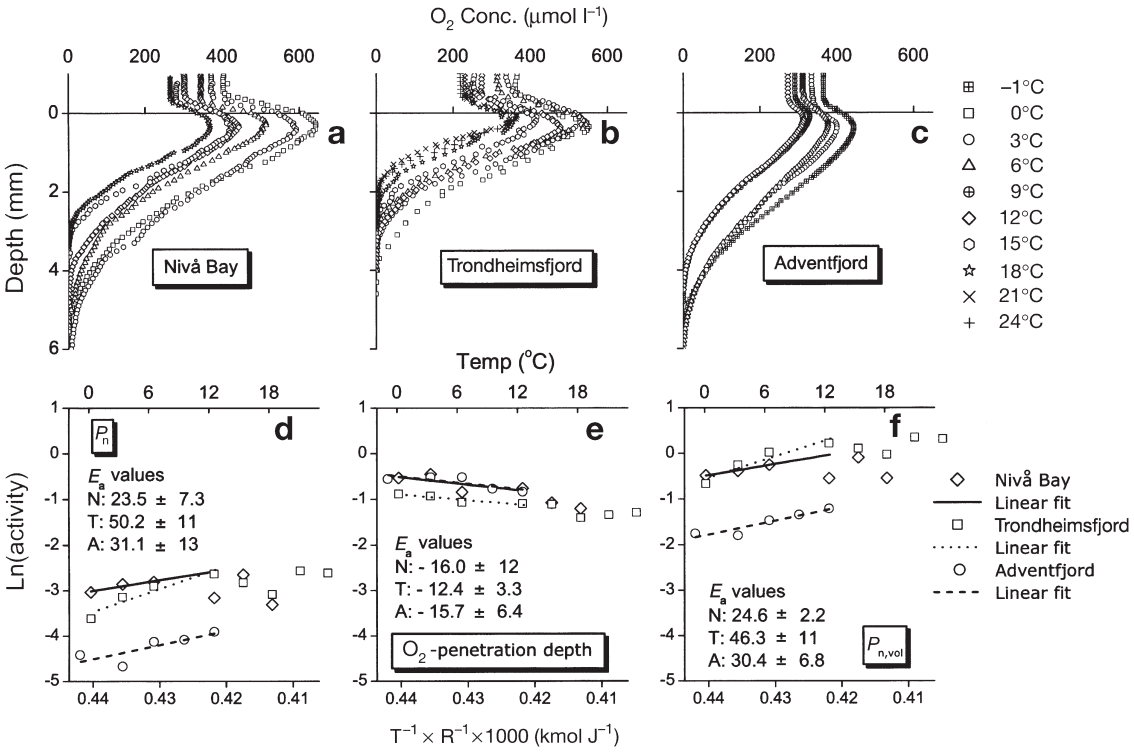

Fig. 9. Steady-state O_2 microprofiles in intact sediment cores at 140 µmol photons m^{-2} s^{-1} at various temperatures (–1 to 24°C) from (a) Nivå Bay, (b) the Trondheimsfjord and (c) the Adventfjord. Arrhenius plots of (d) diffusive oxygen exchange (DOE) equivalent to the areal net photosynthesis (P_n), (e) the oxygen penetration depth and (f) the specific net photosynthesis of the production zone ($P_{n,vol}$) as a function of temperature are shown. Activation energies (E_a ± SE; kJ mol^{-1}) are included, labelled N (Nivå Bay), T (Trondheimsfjord) and A (Adventfjord) (d–f). Corresponding Q_{10} values are shown in Table 3

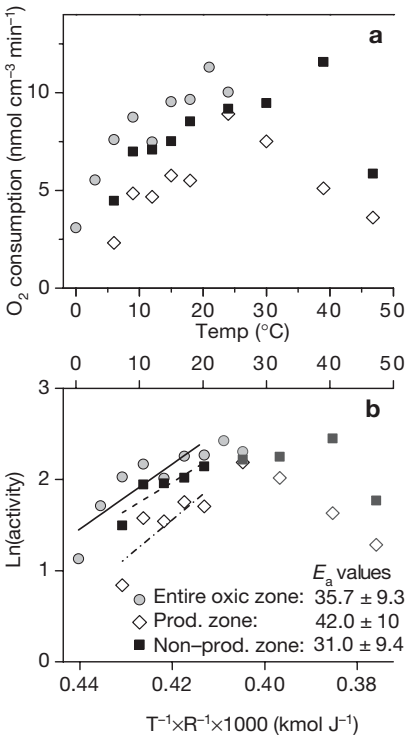

Fig. 10. (a) O_2 consumption of sediment slurries in darkness from the Trondheimsfjord as a function of temperature. (b) Arrhenius plot of rates in (a). Data were fitted linearly in the temperature interval 0 to 18°C for the oxic zone and 6 to 18°C for the production and non-production zones, corresponding to available data. Activation energies (E_a ± SE; kJ mol^{-1}) are included (b). Corresponding Q_{10} values are shown in Tables 3 & 4

values from sediment O_2 consumption studies, estimated from areal rates and slurred samples, generally underestimate the temperature response of intact sediment microbial communities.

Phototrophic temperature response

The temperature response of the gross photosynthesis from the 2 investigated sites was very similar (Table 3). At both sites, P_{gross} and $P_{gross,vol}$ increased almost linearly until reaching T_{opt} of 12 to 15°C, whereafter it gradually decreased. The curve expresses a classical metabolic temperature response, thus the following criteria for cardinal temperatures were used for categorisation: for psychrophiles, $T_{min} < 0$°C, $T_{opt} \leq 15$°C and $T_{max} \leq 20$°C; for psychrotrophs, $T_{min} \leq 0$°C, $T_{opt} \leq 25$°C and $T_{max} \leq 35$°C; and for mesophiles, T_{opt} is ~25 to 40°C and $T_{max} \approx 35$ to 45°C (Isaksen & Jørgensen 1996). Even though cardinal temperature ranges traditionally refer to thermal classes of growth, with narrower limits and lower optimums, they have also been used to describe metabolic activity (Isaksen & Jørgensen 1996, Thamdrup & Fleischer 1998). This generally accepted scheme categorises the gross photosynthetic response for both Nivå Bay and the Trondheimsfjord as psychrotrophic. Studies from the Danish and Dutch Wadden Seas, applying other techniques, have shown lower-end mesophile temperature responses of gross photosynthesis, with T_{opt} of 15 to 30°C (Colijn & van Buurt 1975, Rasmussen et al. 1983, Blanchard et al. 1996).

In the literature, Q_{10} values of benthic photosynthesis have been based on a variety of different laboratory and *in situ* techniques, which grossly hamper any direct comparison. The majority of published Q_{10} values, however, are within the range of 1.5 to 2.5 (e.g. Colijn & van Buurt 1975, Davis & McIntire 1983, Grant 1986), with a few outliers representing air-exposed intertidal sediments (Rasmussen et al. 1983). In general, a Q_{10} of ~2 for the gross photosynthetic rate is commonly accepted (Davison 1991). Our data are at the high end (2.2 to 3.1) of any comparable studies; however, all previous measurements were performed by ^{14}C incubation techniques, which are known to poorly represent the *in situ* rates (e.g. Revsbech et al. 1981). To our knowledge, no previous studies have compared the benthic temperature response of gross photosynthesis at different geographic settings.

Several intertidal studies have shown diatom migration on both diel and seasonal scales, and suggested temperature and light to be controlling factors (e.g. Barranguet et al. 1998, Saburova & Polikarpov 2003). However, migration of diatoms (or physical mixing) can occur without any measurable effect on the overall photosynthetic activity of the benthic community (Blanchard & Gall 1994). In the present study, the benthic activity distribution was unaffected by changes in temperature and the conclusions on activity changes were thus not confounded by any vertical migration. We can, however, not exclude the possibility that migration took place but had no effect on the overall activity distribution.

Heterotroph versus phototroph temperature response

The present study shows that increasing temperature stimulates the heterotrophic activity more than gross photosynthesis. Consequently, the typically mixed benthic community of heterotrophic and phototrophic microbes gradually turns heterotrophic at increasing temperature. A gradual transition from a phototrophic- to a heterotrophic-dominated community with increasing

temperature has previously been reported for intertidal sediments, with Q_{10} values of 2.05 and 2.70 for gross photosynthesis and respiration, respectively (Davis & McIntire 1983). The authors hypothesize that a high Q_{10} can be seen as a response to high water-temperature variability and, hence, the authors ascribe the higher Q_{10} for the respiration to a more efficient acclimation of heterotrophic compared to phototrophic organisms. Similar observations have been made in temperate planktonic communities (Lefèvre et al. 1994, Robinson 2000) and for Antarctic macroalgae (Wiencke et al. 1993). The observations have generally been explained by a stronger and more rapid physiological acclimation of heterotrophic metabolism compared to photosynthesis during short-term temperature variations. In the present study, however, the diel temperature variability was low at the time of sampling and the data do not support the idea of a more rapid acclimation of heterotrophic metabolism. The stronger heterotrophic temperature response, as observed in this study, seems to be a general phenomenon rather than being exceptional. This was supported by Robinson (2000) with data from a pelagic study carried out in the relatively temperature-stable Aegean Sea.

A comparable detailed microsensor study on temperature responses of a cyanobacterial mats in Solar Lake (Egypt) (*in situ* temperatures of 25 to 45°C) has been performed. The study indicated a relatively low temperature response of the O_2 consumption in the dark (1.3) compared to the gross photosynthesis (3.1) (Wieland & Kühl 2000). The authors ascribed the low Q_{10} for respiration to a limitation of the O_2 transport across the DBL at such high temperatures (>40°C). However, the Q_{10} values were calculated from areal rates and, hence, they do not represent the true microbial response. In accordance with our observations, the authors also concluded that at a moderate irradiance (as for the present study), temperature clearly increased the percentage of O_2 which was consumed within the cyanobacterial mat. Thus, elevated temperature increased the light requirement for a net phototrophic community and, hence, at constant irradiance, the mat turned into a net heterotroph community at increasing temperature. Recalculating the data from Wieland & Kühl (2000), correcting the areal rates for the O_2-pd, led to a $Q_{10(25–35°C)}$ for the volume-specific O_2 consumption of 2.7. This 2-fold higher Q_{10} for the specific rate is in agreement with our study and supports that Q_{10} values estimated from areal rates underestimate the microbial community temperature response.

All Q_{10} values in the present study of O_2 consumption were calculated from dark consumption rates. In light, phototrophic as well as heterotrophic organisms consume O_2, and besides the metabolic respiration, elevated O_2 consumption can be caused by photorespiration and the turn-over of excreted photosynthate by heterotrophic organisms. Several studies have documented a higher (10 to 30%) O_2 consumption in light compared to that in the dark, due to photorespiration and associated processes (Glud et al. 1992, 1999, Epping & Jørgensen 1996, Wieland & Kühl 2000). The present study does not allow for detailed calculation of O_2 consumption in light, nor was it possible to calculate the Q_{10} for the O_2 consumption in light from the data of Wieland & Kühl (2000).

In general, substrate limitation is not considered rate limiting in coastal shallow water sediments, as a net flux of nutrients and DOC from the sediment to the water column is typical (Dalsgaard 2003). However, due to the tight spatial and temporal coupling between production and consumption of organic matter (e.g. Epping & Jørgensen 1996) and the light-dependent excretion of photosynthates by microphytes, it is possible that improved substrate availability will fuel an increased respiration in light. No sign of rate-suppressing substrate limitation was observed in the present study.

In conclusion, no difference in the temperature acclimation response between the sites was observed, suggesting that the temperature adaptation strategic for the benthic microbial community was the same for the arctic and the temperate community. The biological temperature response for the sediment O_2 consumption, as derived from the volume-specific O_2 consumption rate ($R_{dark,vol}$) showed higher Q_{10} values than derived from areal flux measurements. Thus, Q_{10} calculated from areal rates of sediment O_2 consumption will underestimate the Q_{10} for the microbial temperature response. Similarly, we suggest that slurred sediment samples for estimation of metabolic activity and responses to changes of environmental factors, i.e. temperature or irradiance, will underestimate the response due to significantly altered microenvironments. The present study shows that increasing temperature stimulates heterotrophic activity more than gross photosynthesis, and consequently, the sediment gradually turns heterotrophic with increasing temperature.

Acknowledgements. O. J. Lønne and the staff at The University Centre on Svalbard (UNIS) are gratefully acknowledged for the help with logistics and providing field equipment and laboratory facilities. A. Glud deserves a special thanks for providing excellent microelectrodes and technical assistance. N. O. G. Jørgensen is greatly acknowledged for constructive criticism of the work. G. Johnsen, the staff at Trondheim Biological Station and the crew at Harry Borthen II are greatly thanked for their efforts in assisting the fieldwork in the Trondheimsfjord and at the Biological Station. T. Johansen and J. Evertsen provided indispensable assistance and a cheerful working climate during all diving operations. Finally, we thank 3 anonymous reviewers for constructive criticism that improved the manuscript. The research was supported by the Danish Natural Research Council and by the Improving Human Potential — Transnational Access to Research Infrastructures Programme of the European Commission.

LITERATURE CITED

Barranguet CJ, Kromkamp J, Peene J (1998) Factors controlling primary production and photosynthetic characteristics of intertidal microphytobenthos. Mar Ecol Prog Ser 173:117–126

Berry JA, Bjorkman O (1980) Photosynthetic response and adaptation to temperature in higher-plants. Annu Rev Plant Physiol 31:491–543

Blanchard GF, Gall VC (1994) Photosynthetic characteristics of microphytobenthos in Marennes-Oléron Bay, France: preliminary results. J Exp Mar Biol Ecol 182:1–14

Blanchard GF, Guarini JM, Richard P, Gros P, Mornet F (1996) Quantifying the short-term temperature effect on light-saturated photosynthesis on intertidal microphytobenthos. Mar Ecol Prog Ser 134:309–313

Broecker WS, Peng TH (1974) Gas exchange rates between air and sea. Tellus 26:21–35

Cahoon LB (1999) The role of benthic microalgae in neritic ecosystems. Oceanogr Mar Biol Annu Rev 37:47–86

Caron DA, Goldman JC, Fenchel T (1990) Protozoan respiration and metabolism. In: Capriulo GM (ed) Ecology of marine protozoa. Oxford University Press, New York, p 307–322

Colijn G, van Buurt G (1975) Influence of light and temperature on the photosynthetic rate of marine benthic diatoms. Mar Biol 31:209–214

Crank J (1989) The mathematics of diffusion. Clarendon Press, Oxford

Dalsgaard T (2003) Benthic primary production and nutrient cycling in sediments with benthic microalgae and transient accumulation of macroalgae. Limnol Oceanogr 48: 2138–2150

Davis MW, McIntire CD (1983) Effects of physical gradients on the production dynamics of sediment-associated algae. Mar Ecol Prog Ser 13:103–114

Davison IR (1991) Environmental effects on alga photosynthesis: temperature. J Phycol 27:2–8

Duff S, Teal JM (1965) Temperature change and gas exchange in Nova Scotia and Georgia salt-marsh muds. Limnol Oceanogr 10:67–73

Epping EHC, Jørgensen BB (1996) Light enhanced oxygen respiration in benthic phototrophic communities. Mar Ecol Prog Ser 139:193–203

Epping EHC, Kühl M (2000) The responses of photosynthesis and oxygen consumption to short-term changes in temperature and irradiance in a cyanobacterial mat (Ebro Delta, Spain). Environ Microbiol 2:465–474

Fenchel T, Glud RN (2000) Benthic primary production and O_2-CO_2 dynamics in a shallow-water sediment: spatial and temporal heterogeneity. Ophelia 53:159–171

Glud RN, Ramsing NB, Revsbech NP (1992) Photosynthesis and photosynthesis-coupled respiration in natural biofilms measured by use of oxygen microsensors. J Phycol 28: 51–60

Glud RN, Jensen K, Revsbech NP (1995) Diffusivity in surficial sediments and benthic mats determined by use of a combined N_2O-O_2 microsensor. Geochim Cosmochim Acta 59:231–237

Glud RN, Kühl M, Kohls O, Ramsing NB (1999) Heterogeneity of oxygen production and consumption in a photosynthetic microbial mat as studied by planar optodes. J Phycol 35:270–279

Glud RN, Gundersen JK, Ramsing NB (2000) Electrochemical and optical oxygen microsensors for *in situ* measurements. In: Buffle J, Horvai G (eds) *In situ* monitoring of aquatic systems — chemical analysis and speciation. J Wiley & Sons, Chichester, p 19–75

Glud RN, Kühl M, Wenzhöfer F, Rysgaard S (2002) Benthic diatoms of a high arctic fjord (Young Sound NE Greenland): importance for ecosystem primary production. Mar Ecol Prog Ser 238:15–29

Grant J (1986) Sensitivity of benthic community respiration and primary production to changes in temperature and light. Mar Biol 90:299–306

Gundersen JK, Glud RN, Ramsing NB (1998) Predicting the signal of O_2 microsensors from physical dimensions, salinity and O_2 concentration. Limnol Oceanogr 43:1932–1937

Hartwig EO (1978) Factors affecting respiration and photosynthesis by the benthic community of a subtidal siliceous sediment. Mar Biol 46:283–293

Isaksen MF, Jørgensen BB (1996) Adaptation of psychrophilic and psychrotrophic sulfate-reducing bacteria to permanently cold marine sediments. Appl Environ Microbiol 62: 408–414

Jørgensen BB, Revsbech NP (1985) Diffusive boundary layers and the oxygen uptake of sediments and detritus. Limnol Oceanogr 30:111–122

Klinkenberg LJ (1951) Analogy between diffusion and electrical conductivity in porous rocks. Bull Geol Soc Am 62: 559–564

Kühl M, Jørgensen BB (1994) The light-field of microbenthic communities — radiance distribution and microscale optics of sandy coastal sediments. Limnol Oceanogr 39: 1368–1398

Kühl M, Glud RN, Ploug H, Ramsing NB (1996) Microenvironmental control of photosynthesis and photosynthesis-coupled respiration in an epilithic cyanobacterial biofilm. J Phycol 32:799–812

Lefèvre D, Bentley TL, Robinson C, Blight SP, Williams PJL (1994) The temperature response of gross and net community production and respiration in time-varying assemblages of temperate marine micro-plankton. J Exp Mar Biol Ecol 184:201–215

Li YH, Gregory S (1974) Diffusion of ions sea water and in deep-sea sediments. Geochim Cosmochim Acta 38:703–714

MacIntyre HL, Cullen JJ (1995) Fine-scale vertical resolution of chlorophyll and photosynthetic parameters in shallow-water benthos. Mar Ecol Prog Ser 122:227–237

Parsons TR, Strickland JHD (1963) Discussion of spectrophotometric determination of marine-plant pigments with revised equations for ascertaining chlorophylls and carotenoids. J Mar Res 21:155–163

Rasmussen MB, Henriksen K, Jensen A (1983) Possible causes of temporal fluctuations in primary production of the microphytobenthos in the Danish Wadden Sea. Mar Biol 73:109–114

Raven JA, Geider RJ (1988) Temperature and algae growth. New Phycol 110:441–461

Revsbech NP (1989) An oxygen microelectrode with a guard cathode. Limnol Oceanogr 34:474–478

Revsbech NP, Jørgensen BB (1983) Photosynthesis of benthic microflora measured by the oxygen microprofile method: capabilities and limitations of the method. Limnol Oceanogr 28:749–56

Revsbech NP, Jørgensen BB (1986) Microelectrodes — their use in microbial ecology. Adv Microb Ecol 9:293–352

Revsbech NP, Jørgensen BB, Brix O (1981) Primary production of microalgae in sediments measured by oxygen microprofile, $H^{14}CO_3^-$ fixation, and oxygen exchange methods. Limnol Oceanogr 26:717–730

Revsbech NP, Madsen B, Jørgensen BB (1986) Oxygen production and consumption in sediments determined at high spatial resolution by computer simulation of oxygen microelectrode data. Limnol Oceanogr 31:293–304

Robinson C (2000) Plankton gross production and respiration in the shallow water hydrothermal systems of Milos, Aegean Sea. J Plankton Res 22:887–906

Saburova MA, Polikarpov IG (2003) Diatom activity within soft sediments: behavioural and physiological processes. Mar Ecol Prog Ser 251:115–126

Sagemann J, Jørgensen BB, Greeff O (1998) Temperature dependence and rates of sulfate reduction in cold sediments of Svalbard, Arctic Ocean. Geomicrobiol J 15: 85–100

Thamdrup B, Fleischer S (1998) Temperature dependence of oxygen respiration, nitrogen, mineralization, and nitrification in Arctic sediments. Aquat Microb Ecol 15: 191–199

Thamdrup B, Hansen JW, Jørgensen BB (1998) Temperature dependence of aerobic respiration in a coastal sediment. FEMS Microbiol Ecol 25:189–200

Therkildsen MS, Lomstein BA (1993) Seasonal-variation in net benthic C-mineralization in a shallow estuary. FEMS Microbiol Ecol 12:131–142

Ullmann WJ, Aller RC (1982) Diffusion coefficients in nearshore marine sediments. Limnol Oceanogr 27:552–556

Wieland A, Kühl M (2000) Irradiance and temperature regulation of oxygenic photosynthesis and O_2 consumption in a hypersaline cyanobacterial mat (Solar Lake, Egypt). Mar Biol 137:71–85

Wiencke C, Rahmel J, Karsten U, Weykam G, Kirst GO (1993) Photosynthesis of marine macroalgae from Antarctica—light and temperature requirements. Bot Acta 106:78–87

Wintermans JFGM, DeMots A (1965) Spectrophotometric characteristics of chlorophylls *a* and *b* and their pheophytins in ethanol. Biochim Biophys Acta 109:448–453

Editorial responsibility: John Dolan, Villefranche-sur-Mer, France

Submitted: January 25, 2004; Accepted: August 23, 2004
Proofs received from author(s): November 5, 2004

Doctoral theses in Biology
Norwegian University of Science and Technology
Department of Biology

Year	Name	Degree	Title
1974	Tor-Henning Iversen	Dr. philos Botany	The roles of statholiths, auxin transport, and auxin metabolism in root gravitropism
1978	Tore Slagsvold	Dr. philos. Zoology	Breeding events of birds in relation to spring temperature and environmental phenology.
1978	Egil Sakshaug	Dr.philos Botany	"The influence of environmental factors on the chemical composition of cultivated and natural populations of marine phytoplankton"
1980	Arnfinn Langeland	Dr. philos. Zoology	Interaction between fish and zooplankton populations and their effects on the material utilization in a freshwater lake.
1980	Helge Reinertsen	Dr. philos Botany	The effect of lake fertilization on the dynamics and stability of a limnetic ecosystem with special reference to the phytoplankton
1982	Gunn Mari Olsen	Dr. scient Botany	Gravitropism in roots of *Pisum sativum* and *Arabidopsis thaliana*
1982	Dag Dolmen	Dr. philos. Zoology	Life aspects of two sympartic species of newts (*Triturus, Amphibia*) in Norway, with special emphasis on their ecological niche segregation.
1984	Eivin Røskaft	Dr. philos. Zoology	Sociobiological studies of the rook *Corvus frugilegus.*
1984	Anne Margrethe Cameron	Dr. scient Botany	Effects of alcohol inhalation on levels of circulating testosterone, follicle stimulating hormone and luteinzing hormone in male mature rats
1984	Asbjørn Magne Nilsen	Dr. scient Botany	Alveolar macrophages from expectorates – Biological monitoring of workers exosed to occupational air pollution. An evaluation of the AM-test
1985	Jarle Mork	Dr. philos. Zoology	Biochemical genetic studies in fish.
1985	John Solem	Dr. philos. Zoology	Taxonomy, distribution and ecology of caddisflies (*Trichoptera*) in the Dovrefjell mountains.
1985	Randi E. Reinertsen	Dr. philos. Zoology	Energy strategies in the cold: Metabolic and thermoregulatory adaptations in small northern birds.
1986	Bernt-Erik Sæther	Dr. philos. Zoology	Ecological and evolutionary basis for variation in reproductive traits of some vertebrates: A comparative approach.
1986	Torleif Holthe	Dr. philos. Zoology	Evolution, systematics, nomenclature, and zoogeography in the polychaete orders *Oweniimorpha* and *Terebellomorpha*, with special reference to the Arctic and Scandinavian fauna.
1987	Helene Lampe	Dr. scient. Zoology	The function of bird song in mate attraction and territorial defence, and the importance of song repertoires.

1987	Olav Hogstad	Dr. philos. Zoology	Winter survival strategies of the Willow tit *Parus montanus*.
1987	Jarle Inge Holten	Dr. philos Bothany	Autecological investigations along a coust-inland transect at Nord-Møre, Central Norway
1987	Rita Kumar	Dr. scient Botany	Somaclonal variation in plants regenerated from cell cultures of *Nicotiana sanderae* and *Chrysanthemum morifolium*
1987	Bjørn Åge Tømmerås	Dr. scient. Zoology	Olfaction in bark beetle communities: Interspecific interactions in regulation of colonization density, predator - prey relationship and host attraction.
1988	Hans Christian Pedersen	Dr. philos. Zoology	Reproductive behaviour in willow ptarmigan with special emphasis on territoriality and parental care.
1988	Tor G. Heggberget	Dr. philos. Zoology	Reproduction in Atlantic Salmon (*Salmo salar*): Aspects of spawning, incubation, early life history and population structure.
1988	Marianne V. Nielsen	Dr. scient. Zoology	The effects of selected environmental factors on carbon allocation/growth of larval and juvenile mussels (*Mytilus edulis*).
1988	Ole Kristian Berg	Dr. scient. Zoology	The formation of landlocked Atlantic salmon (*Salmo salar* L.).
1989	John W. Jensen	Dr. philos. Zoology	Crustacean plankton and fish during the first decade of the manmade Nesjø reservoir, with special emphasis on the effects of gill nets and salmonid growth.
1989	Helga J. Vivås	Dr. scient. Zoology	Theoretical models of activity pattern and optimal foraging: Predictions for the Moose *Alces alces*.
1989	Reidar Andersen	Dr. scient. Zoology	Interactions between a generalist herbivore, the moose *Alces alces*, and its winter food resources: a study of behavioural variation.
1989	Kurt Ingar Draget	Dr. scient Botany	Alginate gel media for plant tissue culture,
1990	Bengt Finstad	Dr. scient. Zoology	Osmotic and ionic regulation in Atlantic salmon, rainbow trout and Arctic charr: Effect of temperature, salinity and season.
1990	Hege Johannesen	Dr. scient. Zoology	Respiration and temperature regulation in birds with special emphasis on the oxygen extraction by the lung.
1990	Åse Krøkje	Dr. scient Botany	The mutagenic load from air pollution at two work-places with PAH-exposure measured with Ames Salmonella/microsome test
1990	Arne Johan Jensen	Dr. philos. Zoology	Effects of water temperature on early life history, juvenile growth and prespawning migrations of Atlantic salmion (*Salmo salar*) and brown trout (*Salmo trutta*): A summary of studies in Norwegian streams.
1990	Tor Jørgen Almaas	Dr. scient. Zoology	Pheromone reception in moths: Response characteristics of olfactory receptor neurons to intra- and interspecific chemical cues.
1990	Magne Husby	Dr. scient. Zoology	Breeding strategies in birds: Experiments with the Magpie *Pica pica*.
1991	Tor Kvam	Dr. scient. Zoology	Population biology of the European lynx (*Lynx lynx*) in Norway.

1991	Jan Henning L'Abêe Lund	Dr. philos. Zoology	Reproductive biology in freshwater fish, brown trout *Salmo trutta* and roach *Rutilus rutilus* in particular.
1991	Asbjørn Moen	Dr. philos Botany	The plant cover of the boreal uplands of Central Norway. I. Vegetation ecology of Sølendet nature reserve; haymaking fens and birch woodlands
1991	Else Marie Løbersli	Dr. scient Botany	Soil acidification and metal uptake in plants
1991	Trond Nordtug	Dr. scient. Zoology	Reflctometric studies of photomechanical adaptation in superposition eyes of arthropods.
1991	Thyra Solem	Dr. scient Botany	Age, origin and development of blanket mires in Central Norway
1991	Odd Terje Sandlund	Dr. philos. Zoology	The dynamics of habitat use in the salmonid genera *Coregonus* and *Salvelinus*: Ontogenic niche shifts and polymorphism.
1991	Nina Jonsson	Dr. philos.	Aspects of migration and spawning in salmonids.
1991	Atle Bones	Dr. scient Botany	Compartmentation and molecular properties of thioglucoside glucohydrolase (myrosinase)
1992	Torgrim Breiehagen	Dr. scient. Zoology	Mating behaviour and evolutionary aspects of the breeding system of two bird species: the Temminck's stint and the Pied flycatcher.
1992	Anne Kjersti Bakken	Dr. scient Botany	The influence of photoperiod on nitrate assimilation and nitrogen status in timothy (*Phleum pratense* L.)
1992	Tycho Anker-Nilssen	Dr. scient. Zoology	Food supply as a determinant of reproduction and population development in Norwegian Puffins *Fratercula arctica*
1992	Bjørn Munro Jenssen	Dr. philos. Zoology	Thermoregulation in aquatic birds in air and water: With special emphasis on the effects of crude oil, chemically treated oil and cleaning on the thermal balance of ducks.
1992	Arne Vollan Aarset	Dr. philos. Zoology	The ecophysiology of under-ice fauna: Osmotic regulation, low temperature tolerance and metabolism in polar crustaceans.
1993	Geir Slupphaug	Dr. scient Botany	Regulation and expression of uracil-DNA glycosylase and O^6-methylguanine-DNA methyltransferase in mammalian cells
1993	Tor Fredrik Næsje	Dr. scient. Zoology	Habitat shifts in coregonids.
1993	Yngvar Asbjørn Olsen	Dr. scient. Zoology	Cortisol dynamics in Atlantic salmon, *Salmo salar* L.: Basal and stressor-induced variations in plasma levels ans some secondary effects.
1993	Bård Pedersen	Dr. scient Botany	Theoretical studies of life history evolution in modular and clonal organisms
1993	Ole Petter Thangstad	Dr. scient Botany	Molecular studies of myrosinase in Brassicaceae
1993	Thrine L. M. Heggberget	Dr. scient. Zoology	Reproductive strategy and feeding ecology of the Eurasian otter *Lutra lutra*.
1993	Kjetil Bevanger	Dr. scient. Zoology	Avian interactions with utility structures, a biological approach.
1993	Kåre Haugan	Dr. scient Bothany	Mutations in the replication control gene trfA of the broad host-range plasmid RK2

1994	Peder Fiske	Dr. scient. Zoology	Sexual selection in the lekking great snipe (*Gallinago media*): Male mating success and female behaviour at the lek.
1994	Kjell Inge Reitan	Dr. scient Botany	Nutritional effects of algae in first-feeding of marine fish larvae
1994	Nils Røv	Dr. scient. Zoology	Breeding distribution, population status and regulation of breeding numbers in the northeast-Atlantic Great Cormorant *Phalacrocorax carbo carbo*.
1994	Annette-Susanne Hoepfner	Dr. scient Botany	Tissue culture techniques in propagation and breeding of Red Raspberry (*Rubus idaeus* L.)
1994	Inga Elise Bruteig	Dr. scient Bothany	Distribution, ecology and biomonitoring studies of epiphytic lichens on conifers
1994	Geir Johnsen	Dr. scient Botany	Light harvesting and utilization in marine phytoplankton: Species-specific and photoadaptive responses
1994	Morten Bakken	Dr. scient. Zoology	Infanticidal behaviour and reproductive performance in relation to competition capacity among farmed silver fox vixens, *Vulpes vulpes*.
1994	Arne Moksnes	Dr. philos. Zoology	Host adaptations towards brood parasitism by the Cockoo.
1994	Solveig Bakken	Dr. scient Bothany	Growth and nitrogen status in the moss *Dicranum majus* Sm. as influenced by nitrogen supply
1995	Olav Vadstein	Dr. philos Botany	The role of heterotrophic planktonic bacteria in the cycling of phosphorus in lakes: Phosphorus requirement, competitive ability and food web interactions.
1995	Hanne Christensen	Dr. scient. Zoology	Determinants of Otter *Lutra lutra* distribution in Norway: Effects of harvest, polychlorinated biphenyls (PCBs), human population density and competition with mink *Mustela vision*.
1995	Svein Håkon Lorentsen	Dr. scient. Zoology	Reproductive effort in the Antarctic Petrel *Thalassoica antarctica*; the effect of parental body size and condition.
1995	Chris Jørgen Jensen	Dr. scient. Zoology	The surface electromyographic (EMG) amplitude as an estimate of upper trapezius muscle activity
1995	Martha Kold Bakkevig	Dr. scient. Zoology	The impact of clothing textiles and construction in a clothing system on thermoregulatory responses, sweat accumulation and heat transport.
1995	Vidar Moen	Dr. scient. Zoology	Distribution patterns and adaptations to light in newly introduced populations of *Mysis relicta* and constraints on Cladoceran and Char populations.
1995	Hans Haavardsholm Blom	Dr. philos Bothany	A revision of the *Schistidium apocarpum* complex in Norway and Sweden.
1996	Jorun Skjærmo	Dr. scient Botany	Microbial ecology of early stages of cultivated marine fish; inpact fish-bacterial interactions on growth and survival of larvae.
1996	Ola Ugedal	Dr. scient. Zoology	Radiocesium turnover in freshwater fishes
1996	Ingibjørg Einarsdottir	Dr. scient. Zoology	Production of Atlantic salmon (*Salmo salar*) and Arctic charr (*Salvelinus alpinus*): A study of some physiological and immunological responses to rearing routines.

1996 Christina M. S. Pereira	Dr. scient. Zoology	Glucose metabolism in salmonids: Dietary effects and hormonal regulation.
1996 Jan Fredrik Børseth	Dr. scient. Zoology	The sodium energy gradients in muscle cells of *Mytilus edulis* and the effects of organic xenobiotics.
1996 Gunnar Henriksen	Dr. scient. Zoology	Status of Grey seal *Halichoerus grypus* and Harbour seal *Phoca vitulina* in the Barents sea region.
1997 Gunvor Øie	Dr. scient Bothany	Eevalution of rotifer *Brachionus plicatilis* quality in early first feeding of turbot *Scophtalmus maximus* L. larvae.
1997 Håkon Holien	Dr. scient Botany	Studies of lichens in spurce forest of Central Norway. Diversity, old growth species and the relationship to site and stand parameters.
1997 Ole Reitan	Dr. scient. Zoology	Responses of birds to habitat disturbance due to damming.
1997 Jon Arne Grøttum	Dr. scient. Zoology	Physiological effects of reduced water quality on fish in aquaculture.
1997 Per Gustav Thingstad	Dr. scient. Zoology	Birds as indicators for studying natural and human-induced variations in the environment, with special emphasis on the suitability of the Pied Flycatcher.
1997 Torgeir Nygård	Dr. scient. Zoology	Temporal and spatial trends of pollutants in birds in Norway: Birds of prey and Willow Grouse used as Biomonitors.
1997 Signe Nybø	Dr. scient. Zoology	Impacts of long-range transported air pollution on birds with particular reference to the dipper *Cinclus cinclus* in southern Norway.
1997 Atle Wibe	Dr. scient. Zoology	Identification of conifer volatiles detected by receptor neurons in the pine weevil (*Hylobius abietis*), analysed by gas chromatography linked to electrophysiology and to mass spectrometry.
1997 Rolv Lundheim	Dr. scient. Zoology	Adaptive and incidental biological ice nucleators.
1997 Arild Magne Landa	Dr. scient. Zoology	Wolverines in Scandinavia: ecology, sheep depredation and conservation.
1997 Kåre Magne Nielsen	Dr. scient Botany	An evolution of possible horizontal gene transfer from plants to sail bacteria by studies of natural transformation in *Acinetobacter calcoacetius*.
1997 Jarle Tufto	Dr. scient. Zoology	Gene flow and genetic drift in geographically structured populations: Ecological, population genetic, and statistical models
1997 Trygve Hesthagen	Dr. philos. Zoology	Population responces of Arctic charr (*Salvelinus alpinus* (L.)) and brown trout (*Salmo trutta* L.) to acidification in Norwegian inland waters
1997 Trygve Sigholt	Dr. philos. Zoology	Control of Parr-smolt transformation and seawater tolerance in farmed Atlantic Salmon (*Salmo salar*) Effects of photoperiod, temperature, gradual seawater acclimation, NaCl and betaine in the diet
1997 Jan Østnes	Dr. scient. Zoology	Cold sensation in adult and neonate birds
1998 Seethaledsumy Visvalingam	Dr. scient Botany	Influence of environmental factors on myrosinases and myrosinase-binding proteins.

1998	Thor Harald Ringsby	Dr. scient. Zoology	Variation in space and time: The biology of a House sparrow metapopulation
1998	Erling Johan Solberg	Dr. scient. Zoology	Variation in population dynamics and life history in a Norwegian moose (*Alces alces*) population: consequences of harvesting in a variable environment
1998	Sigurd Mjøen Saastad	Dr. scient Botany	Species delimitation and phylogenetic relationships between the Sphagnum recurvum complex (Bryophyta): genetic variation and phenotypic plasticity.
1998	Bjarte Mortensen	Dr. scient Botany	Metabolism of volatile organic chemicals (VOCs) in a head liver S9 vial equilibration system in vitro.
1998	Gunnar Austrheim	Dr. scient Botany	Plant biodiversity and land use in subalpine grasslands. – A conservtaion biological approach.
1998	Bente Gunnveig Berg	Dr. scient. Zoology	Encoding of pheromone information in two related moth species
1999	Kristian Overskaug	Dr. scient. Zoology	Behavioural and morphological characteristics in Northern Tawny Owls *Strix aluco*: An intra- and interspecific comparative approach
1999	Hans Kristen Stenøien	Dr. scient Bothany	Genetic studies of evolutionary processes in various populations of nonvascular plants (mosses, liverworts and hornworts)
1999	Trond Arnesen	Dr. scient Botany	Vegetation dynamics following trampling and burning in the outlying haylands at Sølendet, Central Norway.
1999	Ingvar Stenberg	Dr. scient. Zoology	Habitat selection, reproduction and survival in the White-backed Woodpecker *Dendrocopos leucotos*
1999	Stein Olle Johansen	Dr. scient Botany	A study of driftwood dispersal to the Nordic Seas by dendrochronology and wood anatomical analysis.
1999	Trina Falck Galloway	Dr. scient. Zoology	Muscle development and growth in early life stages of the Atlantic cod (*Gadus morhua* L.) and Halibut (*Hippoglossus hippoglossus* L.)
1999	Torbjørn Forseth	Dr. scient. Zoology	Bioenergetics in ecological and life history studies of fishes.
1999	Marianne Giæver	Dr. scient. Zoology	Population genetic studies in three gadoid species: blue whiting (*Micromisistius poutassou*), haddock (*Melanogrammus aeglefinus*) and cod (*Gradus morhua*) in the North-East Atlantic
1999	Hans Martin Hanslin	Dr. scient Botany	The impact of environmental conditions of density dependent performance in the boreal forest bryophytes *Dicranum majus*, *Hylocomium splendens*, *Plagiochila asplenigides*, *Ptilium crista-castrensis* and *Rhytidiadelphus lokeus*.
1999	Ingrid Bysveen Mjølnerød	Dr. scient. Zoology	Aspects of population genetics, behaviour and performance of wild and farmed Atlantic salmon (*Salmo salar*) revealed by molecular genetic techniques
1999	Else Berit Skagen	Dr. scient Botany	The early regeneration process in protoplasts from *Brassica napus* hypocotyls cultivated under various g-forces
1999	Stein-Are Sæther	Dr. philos. Zoology	Mate choice, competition for mates, and conflicts of interest in the Lekking Great Snipe
1999	Katrine Wangen Rustad	Dr. scient. Zoology	Modulation of glutamatergic neurotransmission related to cognitive dysfunctions and Alzheimer's disease

1999 Per Terje Smiseth	Dr. scient. Zoology	Social evolution in monogamous families: mate choice and conflicts over parental care in the Bluethroat (*Luscinia s. svecica*)
1999 Gunnbjørn Bremset	Dr. scient. Zoology	Young Atlantic salmon (*Salmo salar* L.) and Brown trout (*Salmo trutta* L.) inhabiting the deep pool habitat, with special reference to their habitat use, habitat preferences and competitive interactions
1999 Frode Ødegaard	Dr. scient. Zoology	Host spesificity as parameter in estimates of arhrophod species richness
1999 Sonja Andersen	Dr. scient Bothany	Expressional and functional analyses of human, secretory phospholipase A2
2000 Ingrid Salvesen, I	Dr. scient Botany	Microbial ecology in early stages of marine fish: Development and evaluation of methods for microbial management in intensive larviculture
2000 Ingar Jostein Øien	Dr. scient. Zoology	The Cuckoo (*Cuculus canorus*) and its host: adaptions and counteradaptions in a coevolutionary arms race
2000 Pavlos Makridis	Dr. scient Botany	Methods for the microbial econtrol of live food used for the rearing of marine fish larvae
2000 Sigbjørn Stokke	Dr. scient. Zoology	Sexual segregation in the African elephant (*Loxodonta africana*)
2000 Odd A. Gulseth	Dr. philos. Zoology	Seawater tolerance, migratory behaviour and growth of Charr, (*Salvelinus alpinus*), with emphasis on the high Arctic Dieset charr on Spitsbergen, Svalbard
2000 Pål A. Olsvik	Dr. scient. Zoology	Biochemical impacts of Cd, Cu and Zn on brown trout (*Salmo trutta*) in two mining-contaminated rivers in Central Norway
2000 Sigurd Einum	Dr. scient. Zoology	Maternal effects in fish: Implications for the evolution of breeding time and egg size
2001 Jan Ove Evjemo	Dr. scient. Zoology	Production and nutritional adaptation of the brine shrimp *Artemia* sp. as live food organism for larvae of marine cold water fish species
2001 Olga Hilmo	Dr. scient Botany	Lichen response to environmental changes in the managed boreal forset systems
2001 Ingebrigt Uglem	Dr. scient. Zoology	Male dimorphism and reproductive biology in corkwing wrasse (*Symphodus melops* L.)
2001 Bård Gunnar Stokke	Dr. scient. Zoology	Coevolutionary adaptations in avian brood parasites and their hosts
2002 Ronny Aanes	Dr. scient	Spatio-temporal dynamics in Svalbard reindeer (*Rangifer tarandus platyrhynchus*)
2002 Mariann Sandsund	Dr. scient. Zoology	Exercise- and cold-induced asthma. Respiratory and thermoregulatory responses
2002 Dag-Inge Øien	Dr. scient Botany	Dynamics of plant communities and populations in boreal vegetation influenced by scything at Sølendet, Central Norway
2002 Frank Rosell	Dr. scient. Zoology	The function of scent marking in beaver (*Castor fiber*)
2002 Janne Østvang	Dr. scient Botany	The Role and Regulation of Phospholipase A_2 in Monocytes During Atherosclerosis Development
2002 Terje Thun	Dr.philos Biology	Dendrochronological constructions of Norwegian conifer chronologies providing dating of historical material

2002	Birgit Hafjeld Borgen	Dr. scient Biology	Functional analysis of plant idioblasts (Myrosin cells) and their role in defense, development and growth
2002	Bård Øyvind Solberg	Dr. scient Biology	Effects of climatic change on the growth of dominating tree species along major environmental gradients
2002	Per Winge	Dr. scient Biology	The evolution of small GTP binding proteins in cellular organisms. Studies of RAC GTPases in *Arabidopsis thaliana* and
2002	Henrik Jensen	Dr. scient Biology	Causes and consequenses of individual variation in fitness-related traits in house sparrows
2003	Jens Rohloff	Dr. philos Biology	Cultivation of herbs and medicinal plants in Norway – Essential oil production and quality control
2003	Åsa Maria O. Espmark Wibe	Dr. scient Biology	Behavioural effects of environmental pollution in threespine stickleback *Gasterosteus aculeatur* L.
2003	Dagmar Hagen	Dr. scient Biology	Assisted recovery of disturbed arctic and alpine vegetation – an integrated approach
2003	Bjørn Dahle	Dr. scient Biology	Reproductive strategies in Scandinavian brown bears
2003	Cyril Lebogang Taolo	Dr. scient Biology	Population ecology, seasonal movement and habitat use of the African buffalo (*Syncerus caffer*) in Chobe National Park, Botswana
2003	Marit Stranden	Dr.scient Biology	Olfactory receptor neurones specified for the same odorants in three related Heliothine species (*Helicoverpa armigera, Helicoverpa assulta* and *Heliothis virescens*)
2003	Kristian Hassel	Dr.scient Biology	Life history characteristics and genetic variation in an expanding species, *Pogonatum dentatum*
2003	David Alexander Rae	Dr.scient Biology	Plant- and invertebrate-community responses to species interaction and microclimatic gradients in alpine and Artic environments
2003	Åsa A Borg	Dr.scient Biology	Sex roles and reproductive behaviour in gobies and guppies: a female perspective
2003	Eldar Åsgard Bendiksen	Dr.scient Biology	Environmental effects on lipid nutrition of farmed Atlantic salmon (*Salmo Salar* L.) parr and smolt
2004	Torkild Bakken	Dr.scient Biology	A revision of Nereidinae (Polychaeta, Nereididae)
2004	Ingar Pareliussen	Dr.scient Biology	Natural and Experimental Tree Establishment in a Fragmented Forest, Ambohitantely Forest Reserve, Madagascar
2004	Tore Brembu	Dr.scient Biology	Genetic, molecular and functional studies of RAC GTPases and the WAVE-like regulatory protein complex in *Arabidopsis thaliana*
2004	Liv S. Nilsen	Dr.scient Biology	Coastal heath vegetation on central Norway; recent past, present state and future possibilities
2004	Hanne T. Skiri	Dr.scient Biology	Olfactory coding and olfactory learning of plant odours in heliothine moths. An anatomical, physiological and behavioural study of three related species (*Heliothis virescens, Helicoverpa armigera* and *Helicoverpa assulta*).

2004	Lene Østby	Dr.scient Biology	Cytochrome P4501A (CYP1A) induction and DNA adducts as biomarkers for organic pollution in the natural environment
2004	Emmanuel J. Gerreta	Dr. philos Biology	The Importance of Water Quality and Quantity in the Tropical Ecosystems, Tanzania
2004	Linda Dalen	Dr.scient Biology	Dynamics of Mountain Birch Treelines in the Scandes Mountain Chain, and Effects of Climate Warming
2004	Lisbeth Mehli	Dr.scient Biology	Polygalacturonase-inhibiting protein (PGIP) in cultivated strawberry (*Fragaria* x *ananassa*): characterisation and induction of the gene following fruit infection by *Botrytis cinerea*
2004	Børge Moe	Dr.scient Biology	Energy-Allocation in Avian Nestlings Facing Short-Term Food Shortage
2005	Matilde Skogen Chauton	Dr.scient Biology	Metabolic profiling and species discrimination from High-Resolution Magic Angle Spinning NMR analysis of whole-cell samples
2005	Sten Karlsson	Dr.scient Biology	Dynamics of Genetic Polymorphisms
2005	Terje Bongard	Dr.scient Biology	Life History strategies, mate choice, and parental investment among Norwegians over a 300-year period
2005	Tonette Røstelien	PhD Biology	Functional characterisation of olfactory receptor neurone types in heliothine moths
2005	Erlend Kristiansen	Dr.scient Biology	Studies on antifreeze proteins
2005	Eugen G. Sørmo	Dr.scient Biology	Organochlorine pollutants in grey seal (*Halichoerus grypus*) pups and their impact on plasma thyrid hormone and vitamin A concentrations.
2005	Christian Westad	Dr.scient Biology	Motor control of the upper trapezius
2005	Lasse Mork Olsen	PhD Biology	Interactions between marine osmo- and phagotrophs in different physicochemical environments
2005	Åslaug Viken	PhD Biology	Implications of mate choice for the management of small populations
2005	Ariaya Hymete Sahle Dingle	PhD Biology	Investigation of the biological activities and chemical constituents of selected *Echinops* spp. growing in Ethiopia
2005	Ander Gravbrøt Finstad	PhD Biology	Salmonid fishes in a changing climate: The winter challenge
2005	Shimane Washington Makabu	PhD Biology	Interactions between woody plants, elephants and other browsers in the Chobe Riverfront, Botswana
2005	Kjartan Østbye	Dr.scient Biology	The European whitefish *Coregonus lavaretus* (L.) species complex: historical contingency and adaptive radiation
2006	Kari Mette Murvoll	PhD Biology	Levels and effects of persistent organic pollutans (POPs) in seabirds Retinoids and α-tocopherol – potential biomakers of POPs in birds?
2006	Ivar Herfindal	Dr.scient Biology	Life history consequences of environmental variation along ecological gradients in northern ungulates

2006 Nils Egil Tokle	PhD Biology	Are the ubiquitous marine copepods limited by food or predation? Experimental and field-based studies with main focus on *Calanus finmarchicus*
2006 Jan Ove Gjershaug	Dr.philos Biology	Taxonomy and conservation status of some booted eagles in south-east Asia
2006 Jon Kristian Skei	Dr.scient Biology	Conservation biology and acidification problems in the breeding habitat of amphibians in Norway
2006 Johanna Järnegren	PhD Biology	Acesta Oophaga and Acesta Excavata – a study of hidden biodiversity
2006 Bjørn Henrik Hansen	PhD Biology	Metal-mediated oxidative stress responses in brown trout (*Salmo trutta*) from mining contaminated rivers in Central Norway
2006 Vidar Grøtan	PhD Biology	Temporal and spatial effects of climate fluctuations on population dynamics of vertebrates
2006 Jafari R Kideghesho	PhD Biology	Wildlife conservation and local land use conflicts in western Serengeti, Corridor Tanzania
2006 Anna Maria Billing	PhD Biology	Reproductive decisions in the sex role reversed pipefish *Syngnathus typhle*: when and how to invest in reproduction
2006 Henrik Pärn	PhD Biology	Female ornaments and reproductive biology in the bluethroat
2006 Anders J. Fjellheim	PhD Biology	Selection and administration of probiotic bacteria to marine fish larvae
2006 P. Andreas Svensson	PhD Biology	Female coloration, egg carotenoids and reproductive success: gobies as a model system
2007 Sindre A. Pedersen	PhD Biology	Metal binding proteins and antifreeze proteins in the beetle *Tenebrio molitor* - a study on possible competition for the semi-essential amino acid cysteine